JOURNAL OF CAVE AND KARST STUDIES

August 2016
Volume 78, Number 2
ISSN 1090-6924
A Publication of the National Speleological Society

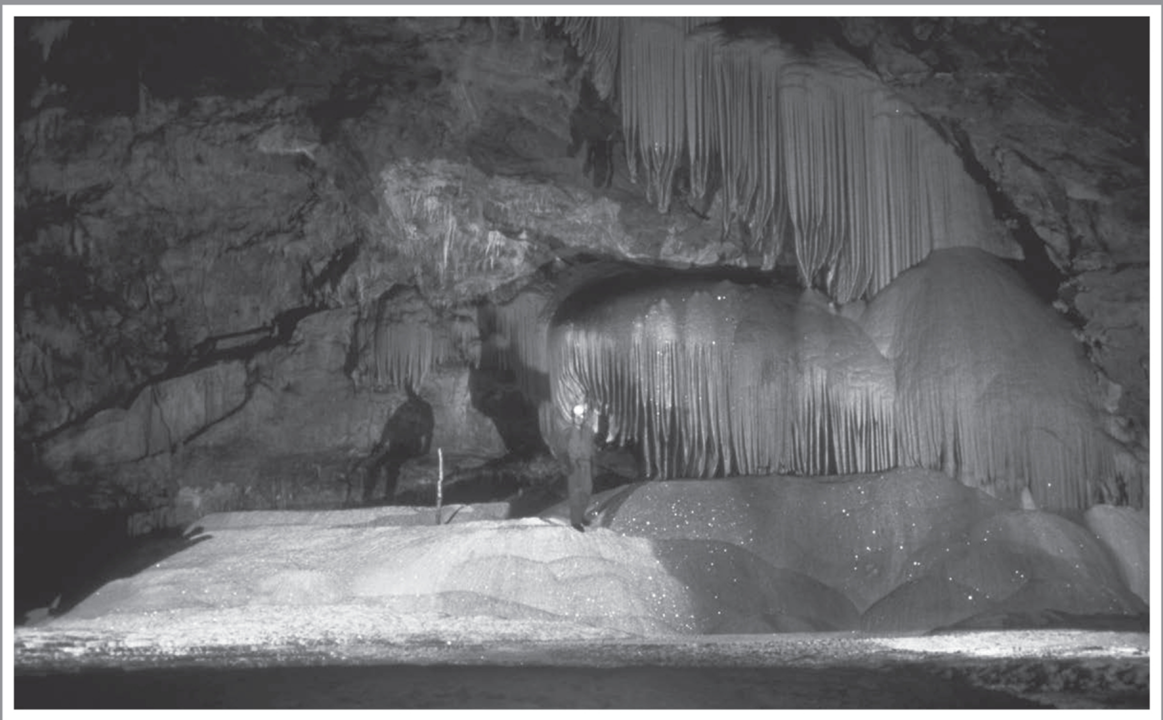

DEDICATED TO THE ADVANCEMENT OF SCIENCE, EDUCATION, AND EXPLORATION

Published By
The National Speleological Society

The *Journal of Cave and Karst Studies* (ISSN 1090-6924, CPM Number #40065056) is a multi-disciplinary, refereed journal published three times a year by the National Speleological Society, 6001 Pulaski Pike NW, Huntsville, AL 35810-4431 USA; Phone (256) 852-1300; Fax (256) 851-9241, email: nss@caves.org; World Wide Web: http://www.caves.org/pub/journal/.
Check the *Journal* website for subscripion rates. Back issues are available from the NSS office.

POSTMASTER: send address changes to the *Journal of Cave and Karst Studies*, 6001 Pulaski Pike NW, Huntsville, AL 35810-4431 USA.

The *Journal of Cave and Karst Studies* is covered by the following ISI Thomson Services Science Citation Index Expanded, ISI Alerting Services, and Current Contents/Physical, Chemical, and Earth Sciences.

Front cover: Pumpkin Palace in Hurricane Crawl Cave, Sequoia National Park. Photo by Dave Bunell.

Y. Aguilar, F. Bautista, M.E. Mendoza, O. Frausto, and T. Ihl – Density of karst depressions in Yucatán state, Mexico. *Journal of Cave and Karst Studies*, v. 78, no. 2, p. 51–60. DOI: 10.4311/2015ES0124

DENSITY OF KARST DEPRESSIONS IN YUCATÁN STATE, MEXICO

Yameli Aguilar[1,2], Francisco Bautista[1,3]*, Manuel E. Mendoza[1], Oscar Frausto[4], and Thomas Ihl[1]

Abstract: The abundance of karst depressions in Yucatán has been widely recognized, but they have not been classified or quantified despite their importance in land-use planning. Our objective was to study the types and areas of the sinkholes, uvalas, and poljes and identify their patterns of spatial distribution. We used 58 topographic maps (1:50,000) from INEGI, from which we extracted the depressions and bodies of water. For typology, we used a circularity index and the shape and area of the depressions. For single-density analysis, we extracted the centroids and added an inventory of karst features (cenotes, caves). We counted 6717 depressions with a total area of 454 km^2 and 750 karst features. We identified 4620 dolines (34 km^2), mainly in plateaus below 30 masl. In number, they are followed by uvalas (2021) and poljes (76), occupying together a similar area (210 km^2) and dominating in elevations higher than 30 masl. Eighty percent of the dolines were automatically labeled. The density of depressions allowed us to identify the "ring of cenotes" and the "field of dolines" according to two main types of factors, structural and climatic. The typology and density of the depressions could be used as geomorphological differentiation criteria in the vast plateaus of central and eastern parts of the state.

Introduction

Morphometric studies of the landforms of karstic systems has become very popular since the 1970s (Williams, 1972; White and White, 1979; Gracia, 1987; Gracia-Prieto, 1991; Brinkmann et al., 2008). In the beginning, most of these studies were limited to a set of measurements obtained from field surveys or topographic maps elaborated at large scales (Lyew-Ayee et al., 2007; Bruno et al., 2008; Basso et al., 2013), so that the studied areas were relatively small. In large areas, geomorphological analysis used to be very general (Lugo-Hubp et al., 1992; Lugo-Hubp and Garcia, 1999).

Recent technological developments, such as geographic information systems (GIS), global positioning system (GPS), digital elevation models (DEM), and high resolution satellite images, allow for faster morphometric analysis of landforms and can generate very robust information, increasing our knowledge about the origin and nature of karstic terrain and the factors that have an influence on it (Denizman and Randazo, 2000; Shofner et al., 2001; Hung et al., 2002; Florea, 2005; Lyew-Ayee et al., 2007; Huang, 2007; Gao and Zhou, 2008; Galve et al., 2009; Siart et al., 2009). The implementation of vector-based GIS in karstic studies is still relatively new, but very versatile and increasingly popular (Szukalski, 2002; Gao, 2008; Siart et al., 2009).

Lyew-Ayee et al., (2007), Gao and Zhou (2008), and Ihl et al. (2007) demonstrated the utility of DEM for the morphometric analysis of landforms, mainly in areas with greater landform relief, but the exclusive use of satellite imagery and digital elevation models is insufficient to characterize and automatically detect karstic depressions, mainly dolines and other smaller features (Shofner et al., 2001; Gutiérrez-Santolalla et al., 2005; Siart et al., 2009; Gutierrez et al., 2014). For this reason, Siart et al., (2009) indicated the need for an alternative approach using a combination of inputs, processing, and spatial analysis, including support and validation by fieldwork.

Several studies have focused on the analysis of the spatial distribution of karstic depressions. Density maps have been among the most common approaches (Denizman, 2003; Angel et al., 2004; Farfán González et al., 2010; Lindsey et al., 2010); there are also some studies on the typology of these landforms, differentiating between dolines, uvalas, and poljes (Plan et al., 2009; Siart et al., 2009; Goeppert et al., 2011; Fragoso-Servón et al., 2014; Pepe and Parise, 2014). These are important in land planning, mainly related to the vulnerability of aquifers to pollution, the risk of ground collapse and subsidence, and potential flooding.

There are previous studies in the Yucatan Peninsula that recognize this diversity of karstic landforms. Cole (1910) and Fich (1965) conducted local studies in some areas of Yucatan and described some examples of the different types of *cenotes,* the local name for collapse dolines containing water, schematically representing their relationship with the aquifer. Subsequently, other studies about landforms

* Corresponding author: leptosol@ciga.unam.mx
[1] Centro de Investigaciones en Geografía Ambiental (CIGA), Universidad Nacional Autónoma de México (UNAM). Antigua Carretera a Pátzcuaro No. 8701, Col. Ex-Hacienda de San José de la Huerta. C.P. 58190. Morelia Michoacán México.
[2] Instituto Nacional de Investigaciones Forestales, Agrícolas y Pecuarias, Centro de Investigación Regional Sureste. Calle 6 No. 398 por 13, Colonia Díaz Ordaz C.P. 97130 Mérida Yucatán México.
[3] Centro de Edafología y Biología Aplicada del Segura, CSIC. Murcia, España.
[4] Universidad de Quintana Roo, Boulevard Bahía s/n colonia del Bosque, Chetumal, C.P. 77019 Quintana Roo, México.

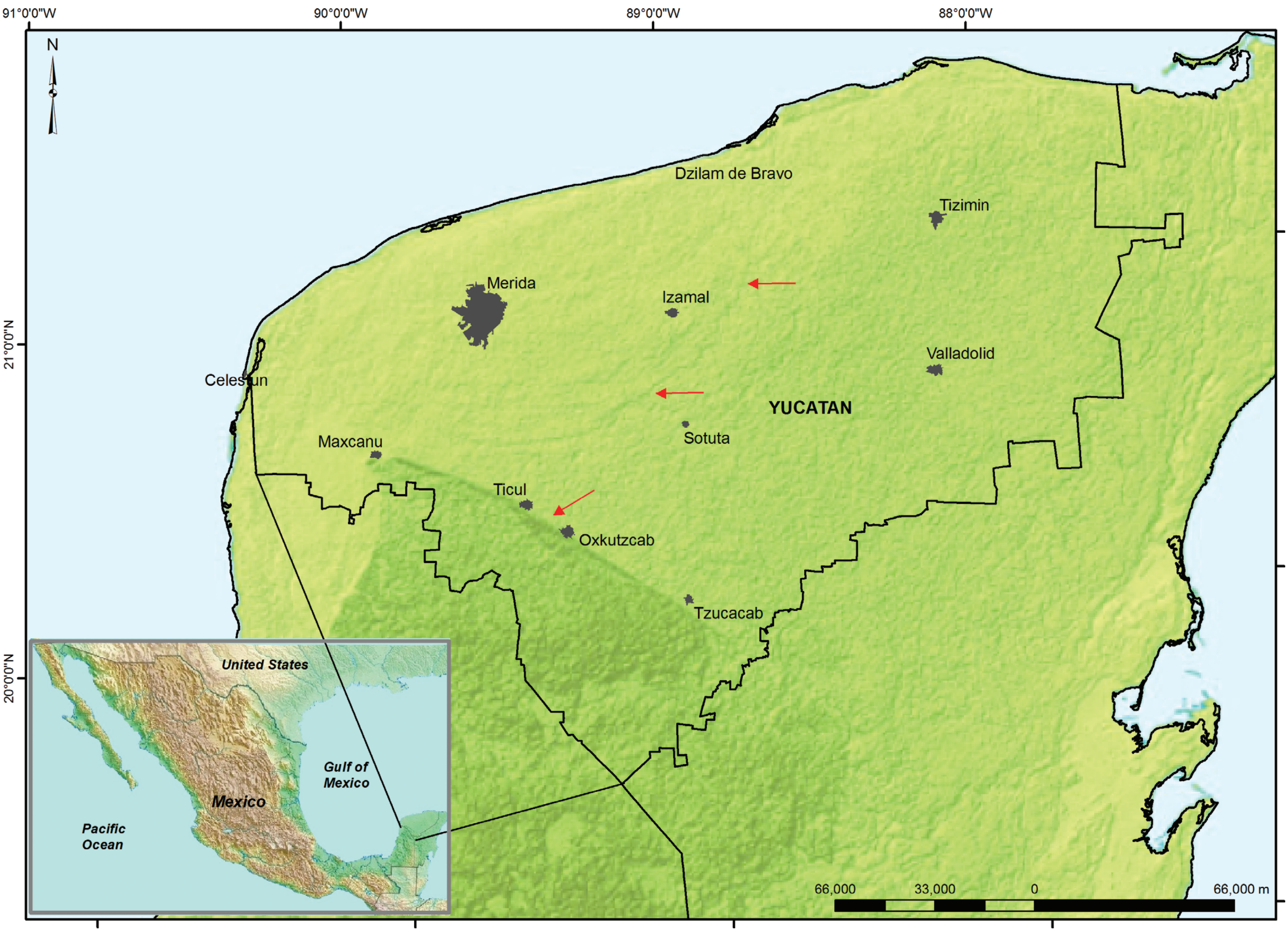

Figure 1. The study area is the state of Yucatán (outlined, modified from NASA/JPL, 2000). Red arrows indicate the ring of cenotes and the aligned hills of Tikul.

of Yucatan were done at small (1:1.2 million; Lugo-Hubp et al., 1992; Lugo-Hubp and Garcia, 1999) and medium scale (1:500,000; Bautista-Zúñiga et al., 2003; Bautista et al., 2005), distinguishing two different geomorphological regions. The first is a large plateau in northeastern Yucatan and the second, in the south, is characterized by a system of plateaus alternating with low hills. Only the south of Yucatan has been described in detail at 1:50,000 scale using DEM and Landsat images (Ihl et al., 2007), but without considering the typology of the different depressions.

Previous studies have recognized that different types of karstic depressions abound in the vast plateaus of the northern and eastern Yucatan Peninsula, named locally as *cenotes*, *aguadas*, *hondonadas*, and *rejolladas*. However, the quantity, spatial distribution, and characterization of Yucatan depressions have not been sufficiently analyzed on geomorphological maps, despite the great importance of these landforms for proper land management, mainly to protect regional groundwater supplies (Marin-Stillman et al., 2004). Our objective was to study the types and area of the dolines, uvalas, and poljes and to identify their patterns of spatial distribution in Yucatán state; this basic geomorphological information is needed for better differentiation of the landscape.

Materials and Methods

The state of Yucatán has an area of 39,340 km^2 and is located in Mexico. The most outstanding structural features of Yucatán are the ring of cenotes and the aligned hills of Ticul (Fig. 1). The hills of Ticul divide Yucatán into two major sub-regions. The north, larger region is where the ring of cenotes is located and continues eastward to where karst plateaus not exceeding 40 m elevation dominate (Lugo-Hubp et al., 1992; Ihl et al., 2007). The second sub-region extends from the aligned hills of Ticul to the south, with topographic elevations higher than 50 m, even reaching 300 m in some places. There are also extensive systems of

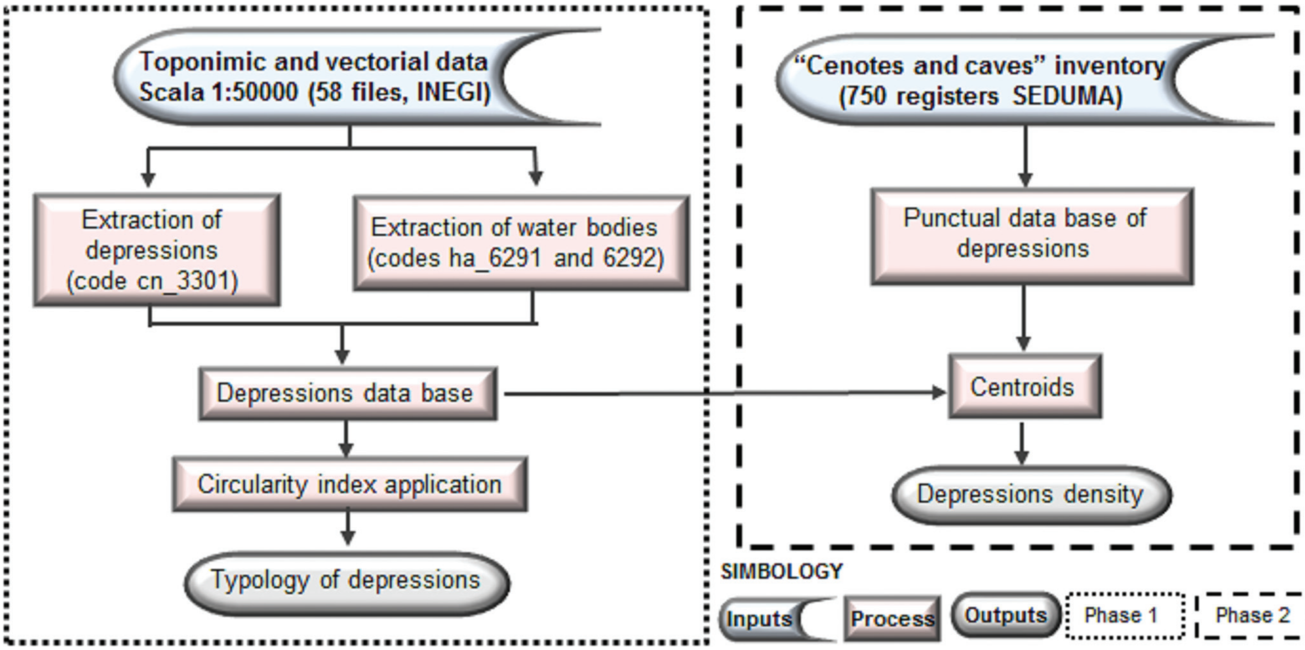

Figure 2. Flow chart of the determination of types of karst depressions and depression density.

caves and caverns in the entire landscape (Finch, 1965; Bonor Villarejo and Sanchez Pinto, 1991).

Climatic subtypes vary from south to north (Aw_0, Aw_1, BS_0, and BS_1; García, 2004); the first is warm and humid with summer rains; the second warm and humid with summer and winter rains; the third dry and semi-arid; and the last is the least dry of the semi-arid subtypes. An agroclimatic index called the length of growing period has been applied to the area of study (Delgado-Carranza, 2010; Delgado-Carranza et al., 2011); this index considers the start of the season when precipitation exceeds half the potential evapotranspiration and ends when precipitation is less than half the potential evapotranspiration. The index indicates the number of months, not only of the duration of the rainy season, but also of the amount and intensity of the rain, which have an ascending tendency from the northwest to the southeast. Our calculations (Fig. 2) includes two main phases, the typology of the depressions and their density, which are described below.

Phase 1. Typology of the Depressions

Our main input was 58 topographic maps at 1:50000 scale, elaborated by the Instituto Nacional de Estadística y Geografía (INEGI, 1999). From these maps, we extracted, in polygon format, the contour lines identified as depressions and the temporary and permanent bodies of water. We assigned a typology to the depressions, differentiating between dolines, uvalas, and poljes. The dolines in the collapsing or collapsing-dissolution region have a shape that resembles a circle, while the uvalas were formed as a result of the coalescence of dolines, and so they have an irregular shape that does not resemble a circle. Finally, poljes have elongated or amorphous shapes with larger area (Pavlopoulos et al., 2009). This was based on an examination of contour lines on the topographic map, which then allowed for calculation the area using ArcGIS 9.3.

To try to automate this typology, we used the Gravelius coefficient (Gc), also called circularity index, given by the formula $Gc = 0.28\,P/\sqrt{A}$, where P is the perimeter and A is the area. The circularity index Gc is a dimensionless number that provides information about circularity; it is based on the ratio between the perimeter of the object and that of a circle with an equal area. This coefficient will tend to one when the object is most similar to a circle, and will deviate from one when the object has a more irregular shape (Fragoso-Servon et al., 2014, 2015). Polygons with Gc equal to 1 and up to 1.04 were automatically classified as dolines. The classifying criteria for uvalas were an irregular shape and area smaller than 1 km^2. The classifying criteria for poljes were an irregular shape and area larger than 1 km^2.

All closed contours defined as depressions that fulfill the criterion of Gc equal to 1 and up to 1.04 and that were not reported as water bodies were reclassified as non-flooding dolines. Water bodies were also evaluated using Gc and labeled according to their flooding regime as dolines with temporary flooding and dolines with permanent flooding. There were also uvalas with some kind of flooding regime. The water bodies of the coastal plateau were considered as coastal lagoons, although, according to Delle Rose and Parise (2002), they may also be derived from dolines and uvales.

Phase 2. Density of Depressions

We extracted the centroids of the polygon in the database generated from information from INEGI (1999) in

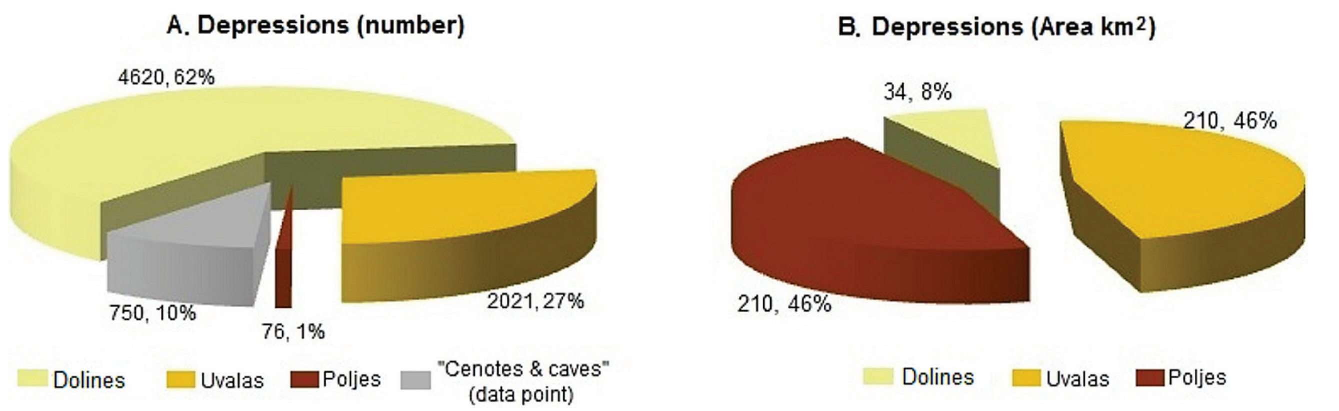

Figure 3. Numbers (A) and total areas (B) of types of karstic depressions in the study area. The SEDUMA dataset of cenotes and caves does not include areas, so they are not included in part B.

Phase 1. This database was complemented with an inventory provided by the Secretaría de Desarrollo Urbano y Medio Ambiente (SEDUMA) of the state of Yucatán that records 750 karst features, mainly cenotes, caves, and grottos; only the name of each location and its geographical coordinates is recorded. It is worth noting that the word *cenote* is a local term derived from the Mayan *dzonot* or *ts'onot* used to designate dolines, natural wells, and caves that hold water either permanently or temporarily. Technically, many of these cenotes, those called open-sky cenotes, correspond to typical collapse dolines (Waltham et al., 2005; Gutierrez et al., 2008, 2014). A cave is a natural cavity in rock large enough to be entered by man. It may be water-filled; if it becomes full of ice or sediment and is impenetrable, the term applies but will need qualification. A grotto is a small cave or a room in a cave of moderate dimensions but richly decorated (Jennings, 1997).

To avoid double-counting the bodies of water recorded by INEGI (1999) and by the inventory of cenotes and caves of SEDUMA, a buffer of 25 m was assigned to each data point recorded by SEDUMA; this buffer corresponded to a length of 1 mm in the topographic map (1:50000) and was the accuracy of the map; only three coincidences were found. The centroids were used for the single-density analysis, with a search radius of 5 km.

RESULTS

We counted a total of 6717 karstic depressions, occupying an area of about 454 km^2; in addition, we recorded 750 karstic features (cenotes, grottos, and caves). Dolines dominate in quantity (4620); however, they occupy a total of only 34 km^2. Poljes and uvalas occupy similar areas of 210 km^2, but there is a greater number of uvalas compared to poljes (2021 and 76, respectively; Fig. 3). Specifically, non-flooding dolines are the most numerous (2892) and with the largest total area (25 km^2), followed by dolines with permanent flooding and dolines with temporary flooding (Fig. 4).

Using our methods, of the total number of depressions in the area, we identified 4620 as dolines, of which 80%, 3699, were classified automatically by having a circularity index of 1 to 1.04; the other 20% showed slightly higher values (Fig. 5A). The most common circularity index values were 1.02, 1.03, 1.04, and 1.01 (Fig. 5B). The 921 dolines that were not automatically classified were displayed on the computer monitor to verify their geometry and area and

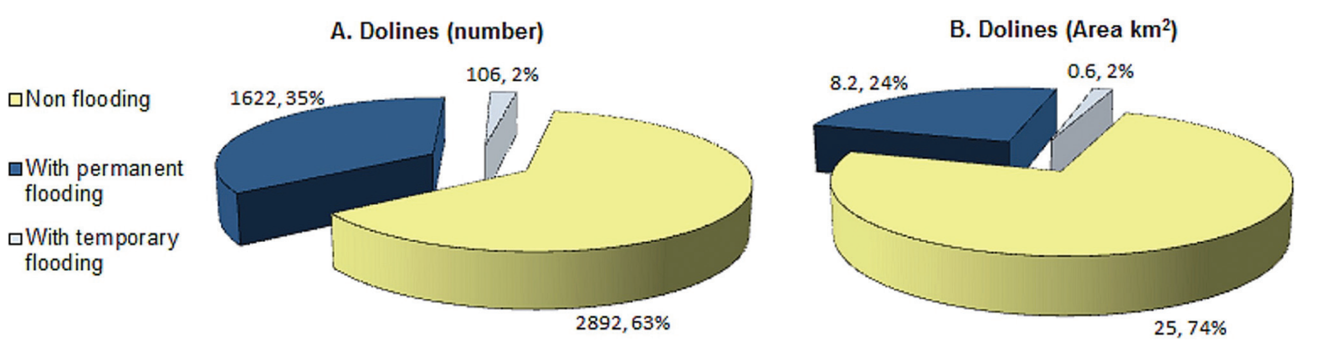

Figure 4. Numbers (A) and total areas (B) of types of dolines found in the study area.

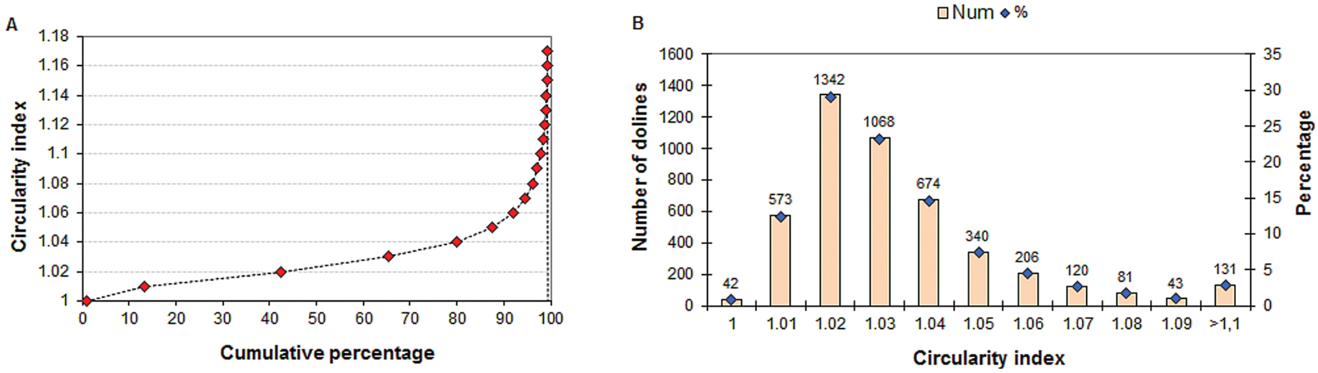

Figure 5. Cumulative plot (A) and frequency distribution by number and percentage (B) of the circularity indexes Gc calculated for the dolines.

were manually labeled. Figure 6 shows the different types of depressions in terms of number (Fig. 6A) and total area (Fig. 6B) differentiated according to elevation intervals from the the digital elevation model.

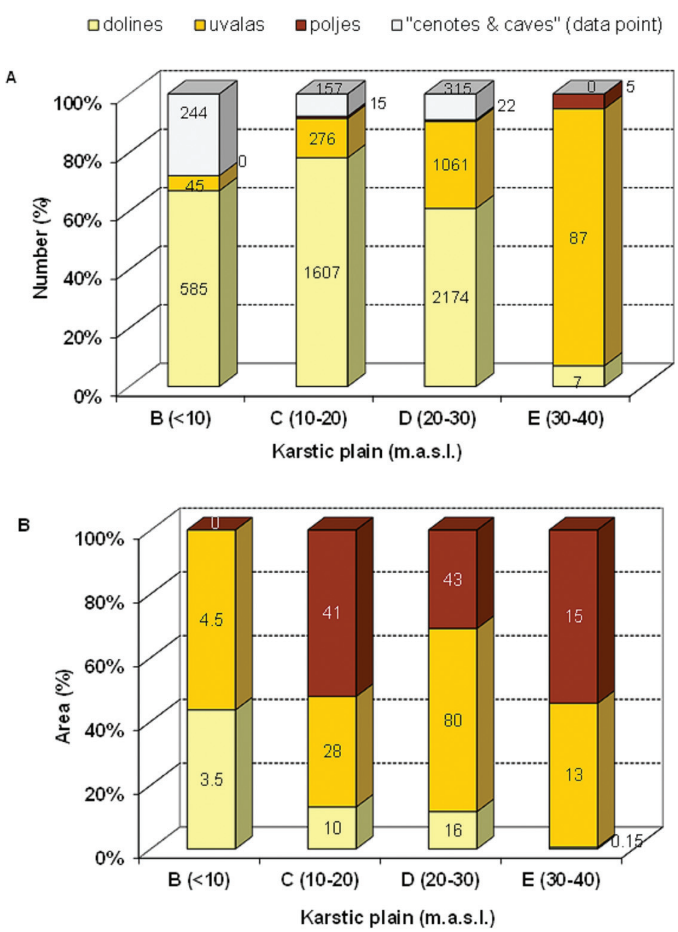

Figure 6. Distributions by number and total area of the various types of karst depressions in each of the indicated elevations ranges. The SEDUMA dataset of cenotes and caves does not include areas, so they are not included in part B.

In areas of the karst plateau lower than 10 m elevation, the dominant forms were dolines and smaller forms (cenotes, grottos and caves) (Fig. 6A); no poljes were found. This region, recently risen, is geologically composed of the Holocene to Pliocene portions of the Carrillo Puerto Formation (Lopez-Ramos, 1973; Lugo-Hubp and Garcia, 1999). Part of this plateau exhibits large areas of bare rock and a micro-relief of the limestone pavement type.

Elevation ranges C and D, 10–20 m and 20–30 m respectively, are similar, even in their lithological composition. They consist of Tertiary limestone from the Miocene-Pliocene part of the Carrillo Puerto Formation and the Oligocene, consisting of marl, lutites, and calcarenites. The lithology of some areas from the Eocene consists of fossiliferous crystalline limestone (Lopez-Ramos, 1973; Lugo-Hubp and Garcia, 1999; Villasuso and Méndez-Ramos, 2000). In terms of number, both these elevations are dominated by dissolution and collapse dolines, followed by uvalas, other features (cenotes and grottos) and finally, poljes (Fig. 6A). However, in terms of total area, dolines occupy the smallest area, while uvalas and poljes occupy the largest (Figure 6B).

The highest elevation range E, 30–40 m, is geologically older; its lithology belongs to the Pisté Member of the Chichén Itzá Formation, consisting of fossiliferous crystalline limestone from the Middle Eocene (López-Ramos, 1973; Lugo-Hubp and Garcia, 1999; Villasuso and Mendez, 2000). It has been more exposed to the dissolution process, which has produced more evolved depressions such as uvalas and poljes. Only seven dolines have been recorded, but no features in the point database, although they could exist.

The typological map of depressions (Fig. 7A) shows the spatial arrangement of their different forms. The pattern of the ring of cenotes, formed by dolines, stands out. The map also shows the numerical dominance of dolines in eastern Yucatan, compared with the numbers of uvalas and poljes. The opposite case occurs in the south of the state, with fewer depressions and less area of both uvalas and poljes.

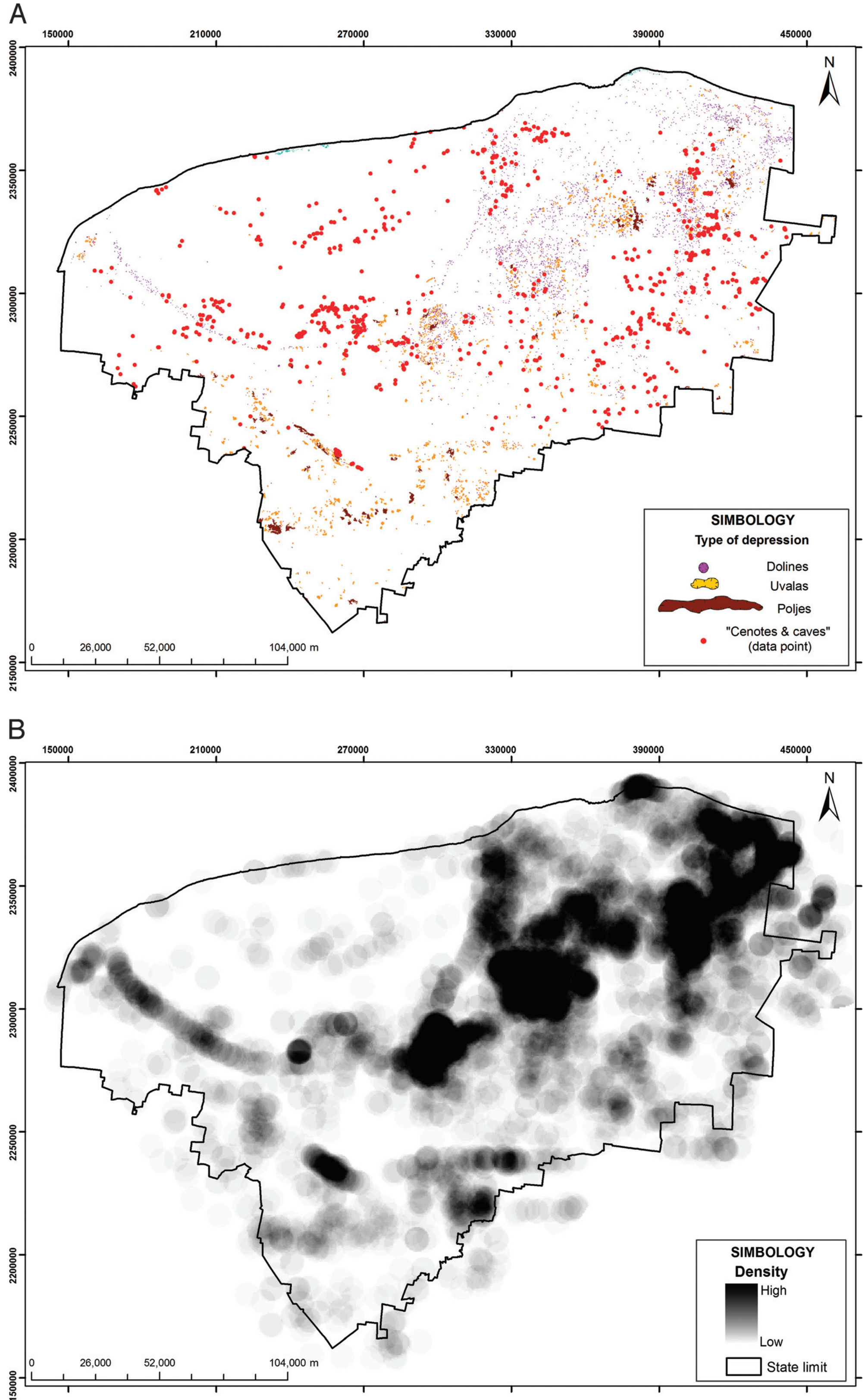

Figure 7. (A) Geographic distribution of types of karstic depressions identified in this study and the karst features in the SEDUMA dataset in the state of Yucatán. (B) Relative density of depressions calculated from the data in part A. The ring of cenotes and the fields of dolines in the eastern part of the state are conspicuous in the figure.

Density analysis showed two main patterns of spatial distribution (Fig. 7Bb). As expected, the first is the ring of cenotes. The second is another important area in the east that can be called fields of dolines. These patterns of depression distribution coincide with the main structural lineaments reported in previous studies (Lugo-Hubp et al., 1992; Pope et al., 1993; Perry et al., 1995; Lugo-Hubp and Garcia, 1999). Thus the higher density of dolines is partially explained by the presence of the structures, as well as by the effect of weather.

Discussion

American and Caribbean countries have extensive karst areas, estimated at about 300,000 km^2, of which the Yucatan Peninsula contains the largest area (Kueny and Day, 2002). These areas do not necessarily show the classic karst development proposed by Cvijic (1918), which is even considered obsolete (Fragoso-Servón et al., 2014). Bosák (2008) proposed a Caribbean model, pointing to certain characteristics shared by American and Caribbean countries that make them differ from the Dinaric karstic system. These characteristics of our study area include short exposure time, unstable mineralogy of shallowly-buried carbonate, fewer tectonic processes, a shallow phreatic zone, tropical and semi-arid environments, and mixing processes in the marine zone.

In general, it is recognized that depressions, particularly dolines, are the most characteristic features in karst systems. The circularity index can be interpreted as an indicator of the intensity of karstification or karst development. According to Brinkmann et al., (2008), more circular dolines indicate a more recent development of the karst landscape. The same authors found that the dolines in an area of Florida are more circular in sites lower than 30 m elevation and more complex and less circular at higher elevations. This is consistent with the patterns found in the karst plateaus of Yucatán; dolines dominate at elevations lower than 30 m that include the geologically younger Pleistocene area. In addition, 80% of the dolines are circular, with circularity index values equal to or lower than 1.04. In areas higher than 30 m, the dominant depressions are the irregular in shape and more developed uvalas and poljes.

However, each karstic region has its particularities, and consequently, its own evolution dynamics (Kohler, 2001). This can be observed when comparing with the types of depressions in Quintana Roo (Fragoso-Servón et al., 2014), where, unlike Yucatán, uvalas are found in greater quantity at the various elevations, as well as poljes, which are located mainly at lower elevations, where the dissolution processes and the proximity to the phreatic zone favor development of these large sunken areas.

In this study, the depression density showed a pattern that goes from lower to higher density in the southwest to northeast direction (Fig. 7B). Significant alignments of karstic depressions can only be controlled by the existence of tectonic features (Siart et al., 2009), but secondary factors such as climate, mainly larger quantities and higher intensities of rain and warm temperatures, favorably influence karstic processes (Gracia, 1987; Gracia-Prieto, 1991), which appears as a similar pattern of low to high humidity (Delgado-Carranza et al., 2011).

In the case of the ring of cenotes, the structural factor is what defines this density pattern, since the ring is the surface expression of a buried crater and marks the boundary between non-fractured limestone inside the ring and fractured limestone outside it (Pope et al., 1993, 2001). Furthermore, the dissolution of limestone has been favored by the various sea-level fluctuations over time, as well as by the chemical processes produced by the mixing of freshwater and seawater (Back et al., 1986; Denizman and Randazzo, 2000).

In non-fractured limestone inside the ring, the density of karst depressions is low (Fig. 7B), with evidence of karst landforms of the limestone pavement type, with pans and some wide-mouth cenotes containing shallow water (Lugo-Hubp et al., 1992); there are also Leptosols, specifically lithic and skeletal LPs in the notation of Bautista et al. (2011). The poor expression of the landforms and poor soil development are also the result of a semi-arid climate, with higher evapotranspiration rates, a rainfall period of less than three months, and no more than 150 mm of rainfall (Delgado-Carranza, 2010; Delgado-Carranza et al., 2011). These climatic conditions favored the formation of the *laja*, a local term for designating consolidated limestone. This area is described as the Chicxulub Sedimentary Basin by Perry et al. (1995, 2002).

Higher density values of karst depressions are found along a gradient to the southeast and east, forming a field of dolines (Fig. 7B) due to the concentration of circular depressions (Gracia-Prieto, 1991); these areas may be surface expressions of structural factors such as the fault zones of Chemax-Catoche (Pope et al., 1993). Gracia-Prieto (1991) mentions that the fields of dolines are also related to the existence of secondary factors conducive to the development of these forms in specific areas of a karst massif. In the study area, climate is the secondary factor contributing to a high density of karst depressions, as the field of dolines coincides with areas with rainy seasons of five or even more than six months, as well as the presence of an additional wet period defined by low evapotranspiration (Delgado-Carranza, 2010; Delgado-Carranza et al., 2011). The presence of edaphic associations Leptosol/Cambisol/Luvisol, that is, of soils with greater depth, also supports the evidence of a larger karstification process (Bautista et al., 2007, 2011). The fields of dolines are the manifestation of a highly developed epikarst with high permeability, and coincides with the area known as pockermarked terrain by Perry et al. (2002).

The karstic plateau with elevations 30–50 m (E in Fig. 6) emerged a longer time ago (Eocene) and also has rainy periods ranging from six to seven months with the presence of wet periods (Delgado-Carranza et al., 2011). Both factors, geological and climatic, may be behind the fact that in this area, though it has fewer depressions compared with area at lower elevations, the depressions occupy a larger area due to the dominance of more developed forms such as uvalas and poljes.

For the purpose of making karst-depression maps that include dolines and other small forms, satellite images and digital elevation models are insufficient inputs (Shofner et al., 2001; Gutiérrez-Santolalla et al., 2005; Siart et al., 2009). Thus Siart et al., (2009) indicated that an alternative methodological approach that combines inputs, processing, and spatial analysis, including the support and validation provided by fieldwork is needed to deal with this complexity. In this sense, the quantitative method proposed in this study allows us to obtain, relatively quickly, a first approximation of the spatial distribution patterns of the karst depressions when the study area is quite large, as in this study. It provides a way to semi-automate the typing of the depressions using a combination of inputs, mainly the semi-detailed topographic maps available in various Latin American countries (Bocco et al., 2001), as well as an inventory of karst features built by government agencies or speleologists (Ordóñez-Crespo and Garcia-Rodriguez, 2010).

Although this approach is useful and could be replicated in karstic geomorphological studies elsewhere in Latin America, it is important to consider that each region has its own particularities (Kohler, 2001) that could require an adaptation of the method. As reported by Fragoso-Servón et al. (2014), who applied the circularity index in Quintana Roo, they were able to identify only 62.1% of the depressions with certainty using the same parameters reported in this study. In that case, the authors used a discriminant analysis to improve the semi-automated criteria for classifying depressions.

Conclusions

Density maps of karst depressions have a wide range of applications. The different densities are indicative of the types of groundwater flow (Lindsey et al., 2010), and these characteristics should be included in models of groundwater flow (Kiraly, 2002; Parise et al., 2015a, b). In addition, density maps can also be used as precursors to tracer studies to identify preferential water flows to locate aquifer limits (Angel et al., 2004).

Lindsey et al. (2010) showed that there are high concentrations of nitrates and pesticides, mainly from agriculture, in places with high density of dolines. In this context, analysis of the depressions can help generate vulnerability assessments to delineate the boundaries of protection areas or for the use of water resources (Angel et al., 2004; Huang, 2007; Frausto and Ihl, 2008; Plan et al., 2009; Farfán González et al., 2009; Farfán et al. 2010; Molerio Leon and Parise, 2009; Lindsey et al., 2010). Depression-density maps are also useful in determining areas with hazard of subsidence and collapse (Angel et al., 2004; Gutiérrez-Santolalla et al., 2005; Ihl et al., 2007; Parise et al., 2008, 2015a; Galve et al., 2009; Simon et al., 2009; Parise and Lollino, 2011; Gutierrez et al., 2014).

The use of morphometric variables such as the index of circularity, area, and irregular shape allowed the semi-automated differentiation of karstic depressions, characterizing them into three main types, dolines, uvalas, and poljes. Dolines dominate in number, especially at elevations lower than 30 m; furthermore, 80% of them tend to a circular shape, with circularity index values between 1 and 1.04. More complex forms (uvalas and poljes) dominate at elevations higher than 30 m. The spatial patterns of karst depressions, such as the ring of cenotes and the field of dolines, depend on both structural and climatic factors. The use of inputs, such as topographic maps at 1:50000 scale and of inventories of karst features (caves, cenotes, grottos), is useful for analyzing extensive karst terrains, as in the study area. This method has a high degree of replicability, adaptability, and simplicity.

Acknowledgments

The authors would like to thank Dr. E. Batllori for the technical support with the karstic depressions database. We also thank the Dirección General de Asuntos del Personal Académico (DGAPA) de la Universidad Nacional Autónoma de México (UNAM) for their financial support to the project PAPIIT IN223110-3. Yameli Aguilar thanks the CONACYT for the Ph.D. fellowship. Francisco Bautista thanks DGAPA-UNAM the financial support for the sabbatical stay in CEBAS-CSIC in Spain.

References

Angel, J.C., Nelson, D.O., and Panno, S.V., 2004, Comparison of a new GIS-based technique and a manual method for determining sinkhole density: An example from Illinois' sinkhole plain: Journal of Cave and Karst Studies, v. 66, p. 9–17.

Back, W., Hanshaw, B.B., Herman, J.S., and Van Driel, J.N., 1986, Differential dissolution of a Pleistocene reef in the ground-water mixing zone of coastal Yucatan, Mexico: Geology, v. 14, no. 2, p. 137–140, doi: 10.1130/0091-7613(1986)14<137:DDOAPR>2.0.CO;2.

Basso, A., Bruno, E., Parise, M., and Pepe, M., 2013, Morphometric analysis of sinkholes in a karst coastal area of southern Apulia (Italy): Environmental Earth Sciences, v. 70, p. 2545–2559, doi: 10.1007/s12665-013-2297-z.

Bautista, F., Aguilar, Y., Rivas, H., and Páez, R., 2007, Los suelos del estado de Yucatán, *in* Sánchez-Monedero, M., and Cabañas, D., eds., Importancia del Binomio Suelo Materia Orgánica en el Desarrollo Sostenible: Murcia, Spain, Consejo Superior de Investigaciones Científicas, Agencia Española de Cooperación Internacional, p. 11–42.

Bautista, F., Batllori-Sampedro, E., Palacio-Aponte, G., Ortiz-Pérez, M., and Castillo-González, M., 2005, Integración del conocimiento actual sobre los paisajes geomorfológicos de la Península de Yucatán, *in*

Bautista Zúñiga, F., and Palacio, Á.G., eds., Caracterización y Manejo de los Suelos de la Península de Yucatán: Implicaciones Agropecuarias, Forestales y Ambientales: Universidad Autónoma de Campeche, Universidad Autónoma de Yucatán, p. 33–58.

Bautista-Zúñiga, F., Batllori-Sampedro, E., Ortiz-Pérez, M.A., Palacio-Aponte, G., and Castillo-González, M., 2003, Geoformas, agua y suelo en la Península de Yucatán, *in* Colunga-GarcíaMarín, P., and Larqué-Saavedra, A., eds., Naturaleza y Sociedad en el Área Maya. Pasado, Presente y Futuro: Academia Mexicana de Ciencias y Centro de Investigación Científica de Yucatán, p. 21–35.

Bautista, F., Palacio-Aponte, G., Quintana, P., and Zinck, A.J., 2011, Spatial distribution and development of soils in tropical karst areas from Peninsula of Yucatan, Mexico: Geomorphology, v. 135, p. 308–321, doi:10.1016/j.geomorph.2011.02.014.

Bocco, G., Mendoza, M.E., and Velásquez, A., 2001, Remote sensing and GIS-based regional geomorphological mapping—a tool for land use planning in developing countries: Geomorphology, v. 39, p. 211–219, doi:10.1016/S0169-555X(01)00027-7.

Bonor Villajero, J.L., and Sánchez Pinto, I., 1991, Cavernas del municipio de Oxkutzcab, Yucatán, México: Nuevas aportaciones: Revista Mayab, n. 7, p. 36–52.

Bosák, P., 2008, Karst processes and time: Geologos, v. 14, p. 19–36.

Brinkmann, R., Parise, M., and Dye, D., 2008, Sinkhole distribution in a rapidly developing urban environment: Hillsborough County, Tampa Bay area, Florida: Engineering Geology, v. 99, p. 169–184. doi:10.1016/j.enggeo.2007.11.020.

Bruno, E., Calcaterra, D., and Parise, M., 2008, Development and morphometry of sinkholes in coastal plains of Apulia, southern Italy. Preliminary sinkhole susceptibility assessment: Engineering Geology, v. 99, p. 198–209. doi: 10.1016/j.enggeo.2007.11.017.

Cole, L. J., 1910, The caverns and people of Northern Yucatan: Bulletin of the American Geographical Society, v. 42, p. 321–336. http://www.jstor.org/stable/199038?seq=2 (accessed October 2010).

Cvijic, M.J., 1918, Hydrographie souterraine et évolution morphologique du Karst: Recueil des Travaux de l'Institut de Géographie Alpine, v. 6, p. 375–426. doi:10.3406/rga.1918.4727. http://www.persee.fr/web/revues/home/prescript/article/rga_0249-6178_1918_num_6_4_4727 (accessed April 2010).

Delgado-Carranza, C., 2010, Zonificación agroecológica del estado de Yucatán con base en índices agroclimáticos y calidad agrícola del agua subterránea (Ph.D. thesis): Centro de Investigación Científica de Yucatán, Mérida, Yucatán, México, 162 p.

Delgado-Carranza, C., Bautista, F., Orellana-Lanza, R., and Reyes-Hernández, H., 2011, Classification and agroclimatic zoning using the relationship between precipitation and evapotranspiration in the state of Yucatán, Mexico: Investigaciones Geográficas, Boletín del Instituto de Geografía, UNAM, no. 75, p. 51–60. doi:10.14350/rig.29795.

Delle Rose, M., and Parise, M., 2002, Karst subsidence in south-central Apulia Italy: International Journal of Speleology, v. 31, p. 181–199. doi: 10.5038/1827-806X.31.1.11.

Denizman, C., 2003, Morphometric and spatial distribution parameters of karstic depressions, Lower Suwannee River Basin, Florida: Journal of Cave and Karst Studies, v. 65, p. 29–35.

Denizman, C., and Randazzo, A.F., 2000, Post-Miocene subtropical karst evolution, lower Suwannee River basin, Florida: Geological Society of American Bulletin, v. 112, p. 1804–1813. doi:10.1130/0016-7606(2000)112<1804:PMSKEL>2.0.CO;2.

Farfán, H., Dias, C., Parise, M., and Aldana, C., 2010, Scenarios of groundwater pollution in a karst watershed: A case study in the Pinar del Rio province at Cuba, *in* Carrasco, F., LaMoreaux, J.W., Durán, J.J., and Andreo, B., eds., Advances in Research in Karst Media: Heidelberg, Springer, Environmental Earth Sciences Series 1, p. 287–292. doi: 10.1007/978-3-642-12486-0_44.

Farfán González, H., Díaz Guanche, C., Parise, M., Aldana Vilas, C., y Corvea Porras, J.L., 2009, Inventario y caracterización de los escenarios de peligros a la contaminación de las aguas en la Cuenca del Arroyo de Santo Tomás, Viñales, Cuba: Mapping, no. 135, p. 66–70.

Farfán González, H., Díaz Guanche, C., and Ramírez, R., 2010, Algunas consideraciones sobre el desarrollo y distribución de las dolinas en el Parque Nacional Viñales, Pinar del Río, Cuba: Mapping, no. 139, p. 46-50.

Finch, W. A., 1965, The Karst Landscape of Yucatan: Washington, D.C., National Research Council, 180 p.

Florea, L., 2005, Using state-wide GIS data to identify the coincidence between sinkholes and geologic structure: Journal of Cave and Karst Studies, v. 67, p. 120–124.

Fragoso-Servón, P., Bautista, F., Frausto, O., and Pereira, A., 2014, Caracterización de las depresiones kársticas (forma, tamaño y densidad) a escala 1:50000 y sus tipos de inundación en el Estado de Quintana Roo, México: Revista Mexicana de Ciencias Geológicas, v. 31, no. 1, p. 127–137.

Fragoso-Servón, P., Pereira, A., Frausto, O., Bautista, F., 2015. Geodiversity of a tropical karst zone in south-east Mexico, *in* Andreo, B., Carrasco, F., Durán, J.J., Jiménez, P., and LaMoreaux J.W., eds., Hydrogeological and Environmental Investigations in Karst Systems: Heidelberg, Springer, vol 1, p. 609–618. doi: 10.1007/978-3-642-17435-3_68.

Frausto, O., and Ihl, T., 2008, Mapa de formas exokársticas del norte de Quintana Roo a escala 1:50000, *in* Gutiérrez-Aguirre, M.A., and Cervantes-Martínez, A., eds., Estudio Geohidrológico del Norte de Quintana Roo, México: Universidad de Quintana Roo, p. 45–58:

Galve, J.P., Gutiérrez, F., Remondo, J., Bonachea, J., Lucha, P., and Cendrero, A., 2009, Evaluating and comparing methods of sinkhole susceptibility mapping in the Ebro Valley evaporite karst (NE Spain): Geomorphology, v. 111, p. 160–172. doi:10.1016/j.geomorph.2009.04.017.

García, E., 2004, Modificaciones al Sistema de Clasificación Climática de Köppen, fifth edition: Universidad Nacional Autónoma de México, Instituto de Geografía, Serie Libros 6, 90 p.

Gao, Yongli, 2008, Spatial operations in a GIS-based karst feature database: Environmental Geology, v. 54, p. 1017–1027. doi: 10.1007/s00254-007-0896-2.

Gao, Yongli, and Zhou, Wanfang, 2008, Advances and challenges of GIS and DBMS applications in karst: Environmental Geology, v. 54, p. 901–904. doi: 10.1007/s00254-007-0894-4.

Goeppert, N., Goldscheider, N., and Scholz, H., 2011, Karst geomorphology of carbonatic conglomerates in the Folded Molasse zone of the Northern Alps (Austria/Germany): Geomorphology, v. 130, p. 289–298. doi:10.1016/j.geomorph.2011.04.011.

Gracia, F.J., 1987, Controles morfométricos de los campos de dolinas en el sector central de la Cordillera Ibérica: Cuaternario y Geomorfología, v. 1, p. 119–134.

Gracia-Prieto, F. J., 1991, Criterios de clasificación morfométrica de campos de dolinas: Cuaternario y Geomorfología, v. 5, p. 65–76.

Gutiérrez, F., Guerrero, J., and Lucha, P., 2008, A genetic classification of sinkholes illustrated from evaporite paleokarst exposures in Spain: Environmental Geology, v. 53, p. 993–1006. doi: 10.1007/s00254-007-0727-5.

Gutierrez, F., Parise, M., De Waele, J., and Jourde, H., 2014, A review on natural and human-induced geohazards and impacts in karst: Earth Science Reviews, v. 138, p. 61–88. doi: 10.1016/j.earscirev.2014.08.002.

Gutiérrez-Santolalla, F., Gutiérrez-Elorza, M., Marín, C., Desir, G., and Maldonado, C., 2005, Spatial distribution, morphometry and activity of La Puebla de Alfindén sinkhole field in the Ebro river valley (NE Spain): Applied aspects for hazard zonation: Environmental Geology, v. 48, p. 360–369. doi: 10.1007/s00254-005-1280-8.

Huang, H.H., 2007, Geomorphologic investigations on karst terrain: a GIS-assisted case study on the island of Barbados (M.S. thesis): Montréal, Québec, McGill University, 108 p.

Hung, L.Q., Dinh, N.Q., Batelaan, O., Tam, V.T., and Lagrou, D., 2002, Remote sensing and GIS-based analysis of cave development in the Suoimuoi catchment (Son La – NW Vietnam): Journal of Cave and Karst Studies, v. 64, p. 23–33.

Ihl, T., Frausto Martínez, O., Rojas López, J., Giese, S., Goldacker, S., Bautista Zúñiga, F., and Bocco Verdinelli, G., 2007, Identification of geodisasters in the state of Yucatan, Mexico: Neues Jahrbuch für Geologie und Paläontologie Abhandlungen, v. 246, p. 299–311. doi: 10.1127/0077-7749/2007/0246-0299.

INEGI (Instituto Nacional de Estadística, Geografía e Informática), 1999, Conjunto de datos vectoriales escala 1:50,000, 58 files, INEGI, México.

Jennings, J.N., 1997, Cave and karst terminology: Australian Speleological Federation Inc. http://home.mira.net/~gnb/caving/papers/jj-cakt.html [accessed November, 2009].

Kiraly, L., 2002, Karstification and groundwater flow, *in* Gabrovšek, F., eds., Evolution of Karst: from Prekarst to Cessation: Postojna-Ljubljana, Zalozba ZRC, pp. 155–190.

Kohler, H.C., 2001, Geomorfología cárstica, *in* Teixeira-Guerra, A.J., and Baptista da Cunha, S., eds., Geomorfologia, uma Atualização de Bases e Conceitos: Rio de Janeiro, Bertrand Brasil, p. 309–334.

Kueny, J.A., and Day, M.J., 2002, Designation of protected karstlands in Central America: A regional assessment: Journal of Cave and Karst Studies, v. 64, p. 165–174.

Lindsey, B.D., Katz, B.G., Berndt, M.P., Ardis, A.F., and Skach, K.A., 2010, Relations between sinkhole density and anthropogenic contaminants in selected carbonate aquifers in the Eastern United States: Environmental Earth Sciences, v. 60, no. 5, p. 1073–1090. doi: 10.1007/s12665-009-0252-9.

López-Ramos, E., 1973, Estudio geológico de la Península de Yucatán: Boletín Asociación Mexicana de Geólogos Petroleros, v. 25, p. 23–76.

Lugo-Hubp, J., Aceves-Quesada, J.F., and Espinasa-Pereña, R., 1992, Rasgos geomorfológicos mayores de la Península de Yucatán: Revista Universidad Autónoma de México Instituto de Geología, v. 10, no. 2, p. 143–150.

Lugo-Hubp, J.I., and García, M.T., 1999, El relieve de la península de Yucatán, *in* García de Fuentes, A., Córdoba, J., and Ponce, Ch., eds., Atlas de Procesos Territoriales del Estado de Yucatán, Facultad de Arquitectura, Universidad Autónoma de Yucatán, México, p. 155–162.

Lyew-Ayee, P., Viles, H.A., and Tucker, G.E., 2007, The use of GIS-based digital morphometric techniques in the study of cockpit karst: Earth Surface Processes and Landforms, v. 32, p. 165–179. doi: 10.1002/esp.1399.

Marín-Stillman, L.E., Pachecho-Ávila, J.G., and Méndez-Ramos, R., 2004, Hidrogeología de la Península de Yucatán, *in* Jiménez, B., and Marín, L., eds., El Agua en México, Vista desde la Academia: México, D.F., Academia Mexicana de Ciencias, p. 159–176.

Molerio León, L., and Parise, M., 2009, Managing environmental problems in Cuban karstic aquifers: Environmental Geology, v. 58, p. 275–283. doi: 10.1007/s00254-008-1612-6.

NASA/JPL, 2000, Shaded Relief with Height as Color, Yucatan Peninsula, Mexico, from Mission Shuttle Radar Topography Mission (SRTM), resolution about 30 meters or 98 feet, http://photojournal.jpl.nasa.gov/catalog/PIA03379 (accessed June, 2008).

Ordoñez-Crespo, I., and García-Rodríguez, M., 2010, Formas kársticas comunes de los *cenotes* del estado de Quintana Roo (México) : M + A, Revista Electrónica de Medio Ambiente, v. 9, p. 15–35. http://revistas.ucm.es/index.php/MARE/article/view/MARE1010220015A [accessed July 2012].

Parise, M., Closson, D., Gutiérrez, F., and Stevanović, Z., 2015a, Anticipating and managing engineering problems in the complex karst environment: Environmental Earth Sciences, 13 p. doi:10.1007/s12665-015-4647-5.

Parise, M., De Waele, J. and Gutierrez, F., 2008, Engineering and environmental problems in karst - An introduction: Engineering Geology, v. 99, p. 91–94. doi: 10.1016/j.enggeo.2007.11.009.

Parise, M., and Lollino, P., 2011, A preliminary analysis of failure mechanisms in karst and manmade underground caves in Southern Italy: Geomorphology, v. 134, p. 132–143. doi: 10.1016/j.geomorph.2011.06.008.

Parise, M., Ravbar, N., Živanović, V., Mikszewski, A., Kresic, N., Mádl-Szőnyi, J., and Kukurić N., 2015b, Hazards in karst and managing water resources quality, *in* Stevanović, Z., ed., Karst Aquifers - Characterization and Engineering: Cham, Switzerland, Springer, Professional Practice in Earth Sciences series, p. 601–687. doi: 10.1007/978-3-319-12850-4_17.

Pavlopoulos, K., Evelpidou, N, and Vassilopoulos, A., 2009, Karstic environments, *in* Mapping Geomorphological Environments: Heidelberg, Springer-Verlag, p. 135–150. doi: 10.1007/978-3-642-01950-0.

Pepe, M., and Parise, M., 2014, Structural control on development of karst landscape in the Salento Peninsula (Apulia, SE Italy): Acta Carsologica, v. 43, p. 101–114. doi: 10.3986/ac.v43i1.643.

Perry, E., Marin, L., McClain, J., and Velazquez, G., 1995, Ring of *Cenotes* (sinkholes), northwest Yucatan, Mexico: Its hydrogeologic characteristics and possible association with the Chicxulub impact crater: Geology, v. 23, p. 17–20. doi: 10.1130/0091-7613(1995)023<0017:ROCSNY>2.3.CO;2.

Perry, E., Velasquez-Oliman, G., and Marin, L., 2002, The hydrogeochemistry of the karst aquifer system of the Northern Yucatan Peninsula, Mexico: International Geology Review, v. 44, p. 191–221. doi: 10.2747/0020-6814.44.3.191.

Plan, L., Decker, K., Faber, R., Wagreich, M., and Grasemann, B., 2009, Karst morphology and groundwater vulnerability of high alpine karst plateaus: Environmental Geology, v. 58, p. 285–297. doi: 10.1007/s00254-008-1605-5.

Pope, K.O., Ocampo, A.C., and Duller, C.E., 1993, Surficial geology of the Chicxulub impact crater, Yucatan, Mexico: Earth, Moon, and Planets, v. 63, p. 93–104. doi: 10.1007/BF00575099.

Pope, K.O., Rejmankova, E., and Paris, J.F., 2001, Spaceborne imaging radar-C (SIR-C) observations of groundwater discharge and wetlands associated with the Chicxulub impact crater, northwestern Yucatan Peninsula, Mexico: Geological Society of America Bulletin, v. 113, p. 403–416. doi: 10.1130/0016-7606(2001)113<0403:SIRCSC>2.0.CO;2.

Shofner, G.A., Mills, H.H., and Duke, J.E., 2001, A simple map index of karstification and its relationship to sinkhole and cave distribution in Tennessee: Journal of Cave and Karst Studies, v. 63, p. 67–75.

Siart, C., Bubanzer, O., and Eitel, B., 2009, Combining digital elevation data (SRTM/ASTER), high resolution satellite imagery (Quickbird) and GIS for geomorphological mapping: A multi-component case study on Mediterranean karst in central Crete: Geomorphology, v. 112, p. 106–121. doi:10.1016/j.geomorph.2009.05.010.

Simón, J.L., Soriano, M.A., Pocoví Juan, A., Arlegui Crespo, L.E., Casas Sáinz, A.M., Liesa Carrera, C.L., Luzón, A., Pérez García, A., Pueyo Anchuela, O., Pueyo Morer, E.L., Mochales, T., Gracia-Abadías, F.J., and Ansón, D., 2009, Riesgo de subsidencia kárstica en áreas urbanas: El caso de Zaragoza: Enseñanza de las Ciencias de la Tierra, v. 17, p. 303–315.

Szukalski, B.W., 2002, Introduction to cave and karst GIS: Journal of Cave and Karst Studies, v. 64, p. 3.

Villasuso, M.J., and Méndez-Ramos, R., 2000, A conceptual model of the aquifer of the Yucatan Peninsula, *in* Lutz, W., Prieto, L., and Sanderson, W., eds., Population, Development, and Environment on the Yucatán Peninsula: From Ancient Maya to 2030: Laxenburg, Austria, International Institute for Applied Systems Analysis, p. 120–139.

Waltham, T., Bell, F., and Culshaw, M., 2005, Sinkholes and Subsidence: Karst and Cavernous Rocks in Engineering and Construction: Berlin, Springer, 382 p.

White, E.L., and White, W.B., 1979, Quantitative morphology of landforms in carbonate rock basins in the Appalachian Highlands: Geological Society of American Bulletin, v. 90, p. 385–396. doi: 10.1130/0016-7606(1979)90<385:QMOLIC>2.0.CO;2.

Williams, P.W., 1972, Morphometric analysis of polygonal karst in New Guinea: Geological Society of American Bulletin, v. 83, p. 761–796. doi: 10.1130/0016-7606(1972)83[761:MAOPKI]2.0.CO;2.

D. de M. Bento, R.L. Ferreira, X. Prous, M. Souza-Silva, B.C. Bellini, and A. Vasconcellos – Seasonal variations in cave invertebrate communities in the semiarid Caatinga, Brazil. *Journal of Cave and Karst Studies*, v. 78, no. 2, p. 61–71. DOI: 10.4311/2015LSC0111

SEASONAL VARIATIONS IN CAVE INVERTEBRATE COMMUNITIES IN THE SEMIARID CAATINGA, BRAZIL

Diego de M. Bento[1]*, Rodrigo L. Ferreira[2], Xavier Prous[2], Marconi Souza-Silva[2], Bruno Cavalcante Bellini[3], and Alexandre Vasconcellos[4]

Abstract: The Brazilian semiarid region has a clear distinction between the dry season, which can last up to nine months, and the rainy season. Caves are connected to different extents to surface ecosystems, although they are idealized as stable environments due to their isolation. Furthermore, little is known about the effects of wet and dry seasonal variations on underground biological assemblages. Invertebrate communities were analyzed during dry and rainy seasons in 24 caves in the semiarid region of northeastern Brazil. We also investigated whether the environmental stability of caves attenuates the effects of seasonality in this particular region. Morphospecies richness and abundance and the diversity indexes of caves were significantly higher during the rainy season. In addition, more stable caves showed less variation in the community composition between seasons. Our data point to a clear influence of the surface ecosystems on the caves in Caatinga. However, the intensity of this influence apparently depends on the environmental stability of the cave, and the most stable caves present smaller changes in the structure of their invertebrate communities during different seasons.

Introduction

The underground environment has distinct features in comparison to adjacent surface ecosystems: a permanent lack of light, except in areas near the entrances, and a higher tendency toward stable environmental conditions such as temperature and moisture (Culver, 1982). The size of the oscillation of these climatic parameters will depend substantially on the morphological complexity of the cave and on the amplitude of climatic variations on the surface (Culver and White, 2005).

The permanent absence of light inside caves prevents the existence of photoautotrophic organisms. Therefore, food sources available for the resident fauna usually have allochthonous origin (Schneider et al., 2011; Souza-Silva et al., 2011a). Such resources are imported from the external environments continuously or temporarily by physical and biological agents (Culver, 1982; Howarth, 1983; Ferreira and Martins, 1999). Hence, cave ecosystems are generally, to a greater or lesser extent, connected to surface ecosystems, whose environmental variations affect the communities of cave invertebrates (Culver, 1982; Culver and White, 2005; Souza-Silva et al., 2011a; Simões et al., 2015). The general features of numbers, positions, distribution, and extents of the entrances and their relation with the length of caves are factors that can act directly on the maintenance of microclimate in underground environments (Ferreira, 2004; Simões et al., 2015).

Caves located in semiarid ecosystems are generally subject to seasonal variations in the external environment with a clear alternation between dry and rainy seasons. The structure of cave communities may suffer alterations due to climate changes on the surface, given that the resource availability may increase during the rainy season for some weeks or months (Culver and White, 2005; Souza-Silva et al., 2011a). The availability may also decrease because of intense leaching that might follow the organic resources importation (Souza-Silva et al., 2007; Souza-Silva et al., 2011a).

The Brazilian semiarid region has a relatively predictable seasonality, with a dry season that may last for more than nine months (Sampaio, 1995). The effects of climatic variables in the ecoregion of Caatinga on several invertebrate taxa in epigean ecosystems have already been investigated. Some of the sampled taxa were Apoidea (Aguiar and Martins, 1997), Sphingidae (Gusmão and Creão-Duarte, 2004), Buprestidae (Iannuzzi et al., 2006), Scarabeidae (Hernández, 2007), Scorpiones (Araújo et al., 2010a), and ants (Medeiros et al., 2012), besides some studies on larger groups like Hexapoda (Vasconcellos et al., 2010) and soil macroarthopods (Araújo et al., 2010b). The vast majority of these studies have shown a positive relation between population size and rainfall.

Other studies of seasonality in caves are scarce and restricted to a few groups such as mites in Belgium

* Corresponding author: diego.bento@icmbio.gov.br
[1] Centro Nacional de Pesquisa e Conservação de Cavernas, Base Avançada Compartilhada no Rio Grande Do Norte, Instituto Chico Mendes de Conservação da Biodiversidade. 59015-350 Natal, Rio Grande do Norte, Brasil.
[2] Centro de Estudos em Biologia Subterrânea, Setor de Zoologia Geral, Departamento de Biologia (DBI), Universidade Federal de Lavras (UFLA), Minas Gerais, CEP: 37200-000, Brasil.
[3] Departamento de Botânica, Ecologia e Zoologia, Centro de Biociências, Universidade Federal do Rio Grande do Norte, CEP 59072-970, Natal, Rio Grande do Norte, Brazil.
[4] Laboratório de Termitologia, Departamento de Sistemática e Ecologia, Universidade Federal da Paraíba, 58051-900, João Pessoa, Paraíba, Brazil.

(Ducarme et al., 2004), crickets in North America (Lavoie et al., 2007), and even a single species of spider in southern Brazil (Ferreira et al., 2005). In caves at Caatinga, most other studies were focused solely on the characterization of invertebrate communities, without regard to season (Trajano, 1987; Ferreira and Martins, 1998; Ferreira et al., 2010).

The present study aimed to evaluate changes in the structure of invertebrate communities between the dry and rainy seasons in limestone caves from five municipalities in the semiarid region of Brazil. In addition, we also investigated if the environmental stability of these caves can mitigate the effects of seasonal variations on invertebrate communities. In this context, due to the strong seasonality on the surface and the connection between epigean and hypogean environments, we expected changes in the structure of the cave invertebrate community between dry and rainy seasons, and that caves with greater environmental stability would have less fluctuation in the composition of the invertebrate community throughout the year.

Material and Methods

The study was conducted in 24 caves in the municipalities of Baraúna, Felipe Guerra, Governador Dix-Sept Rosado, Apodi, and Mossoró, Rio Grande do Norte state, northeastern Brazil (Figure 1; Table 1). These caves are embedded in the limestones of the Jandaíra Formation, which is the most extensive area of carbonate outcrops of Phanerozoic age in Brazil. Deposited between the Meso-Turonian and Eocampanian, the rocks of Jandaíra Formation are a carbonate ramp that crops out in almost all the onshore portion of the Potiguar Basin. This carbonate ramp was submitted, during and after deposition, to various episodes of uplift that led to a subaerial exposure and erosion, resulting in intense epigenetic karstification (Bezerra et al., 2007).

Most caves in the area occur as clusters in limestone outcrops locally called *lajedos*. The sampled caves were randomly selected according to georeferenced data from all the caves of the area in order to cover all these clusters.

The climate is predominantly BSw′h′ according to the Köppen climate classification, characterized as a hot and semiarid climate, in which the rainy season is delayed to the autumn (Kottek et al., 2006). The average long-period annual rainfall is about 670 mm, the potential evaporation is over 1,760 mm, and there is a water deficit of 1,000 mm during nine months. The rainfall is irregular and occurs in the period between February and July, most frequently between March and June. The relative humidity is variable, usually between 59 and 76%, and the annual average temperature is around 28 °C (IDEMA, 2005).

The determination of sampling dates was based on analysis of data from 1999 to 2009 about the water balance (rainfall and water surplus/drought) of the municipalities of the study area (INPE, 2010). Two sampling visits were conducted on each cave between December 2009 and August 2010, one at the end of the dry season and other at the end of the rainy season, with a six-month interval between visits.

We carried out the sampling by visually searching across all the same accessible parts of each cave during both events, prioritizing organic matter such as debris, carcasses, and guano and microhabitats such as humid soil, cracks, speleothems, and spaces under rocks. Manual collections were made with the aid of tweezers, brushes, and entomological nets (Souza-Silva et al., 2011b). Invertebrates were collected from water bodies with the aid of forceps, hand nets, and creels, in accordance with Ferreira et al. (2010).

The collection team was always composed of the same four biologists with experience in caving and manual collection of invertebrates, as recommended by Weinstein and Slaney (1995). This methodology is effective for collections and reduces the impact generated by other kinds of sampling, such as the installation of pitfall traps, which are notorious for causing population disturbances in caves (Weinstein and Slaney, 1995; Sharratt et al., 2000). To ensure that the sampling was as standardized as possible, the sampling time was approximately one hour per 50 m^2 cave area for each biologist.

All invertebrates were identified to the lowest possible taxonomic level and grouped in morphospecies for all statistical analysis (Oliver and Beattie, 1996a; Derraik et al., 2002; Ward and Stanley, 2004; Derraik et al., 2010; Souza-Silva et al. 2011b). Oliver and Beattie (1996a) showed that morphospecies identified by non-specialists can provide estimates of richness and turnover consistent with those generated using species identified by taxonomic specialists. The use of morphospecies or corrected morphospecies inventories in the analyses generally provides results concordant with conventional species inventories (Oliver and Beattie, 1996b).

All the invertebrate morphospecies found on each cave had some specimens collected. The individuals observed during the collections were counted and plotted on schematic maps of each cave according to the methodology proposed by Ferreira (2004). All caves in this study were mapped using a standardized mapping methodology with degree of precision 4D-BCRA (Day, 2002), with additional information related to the area of the cave and the number and area of the entrances.

The general abundance of each morphospecies was acquired through the recording of individuals on each schematic map, thus generating information regarding morphospecies richness, abundance, and spatial distribution of each population. Taxa of small size with large populations concentrated in accumulations of organic matter, such as Collembola in guano deposits, had their abundance estimated from the count of individuals in a square decimeter, extrapolated to the area occupied by the nutrient source. The calculation of diversity was made using the Shannon index (Magurran, 1988).

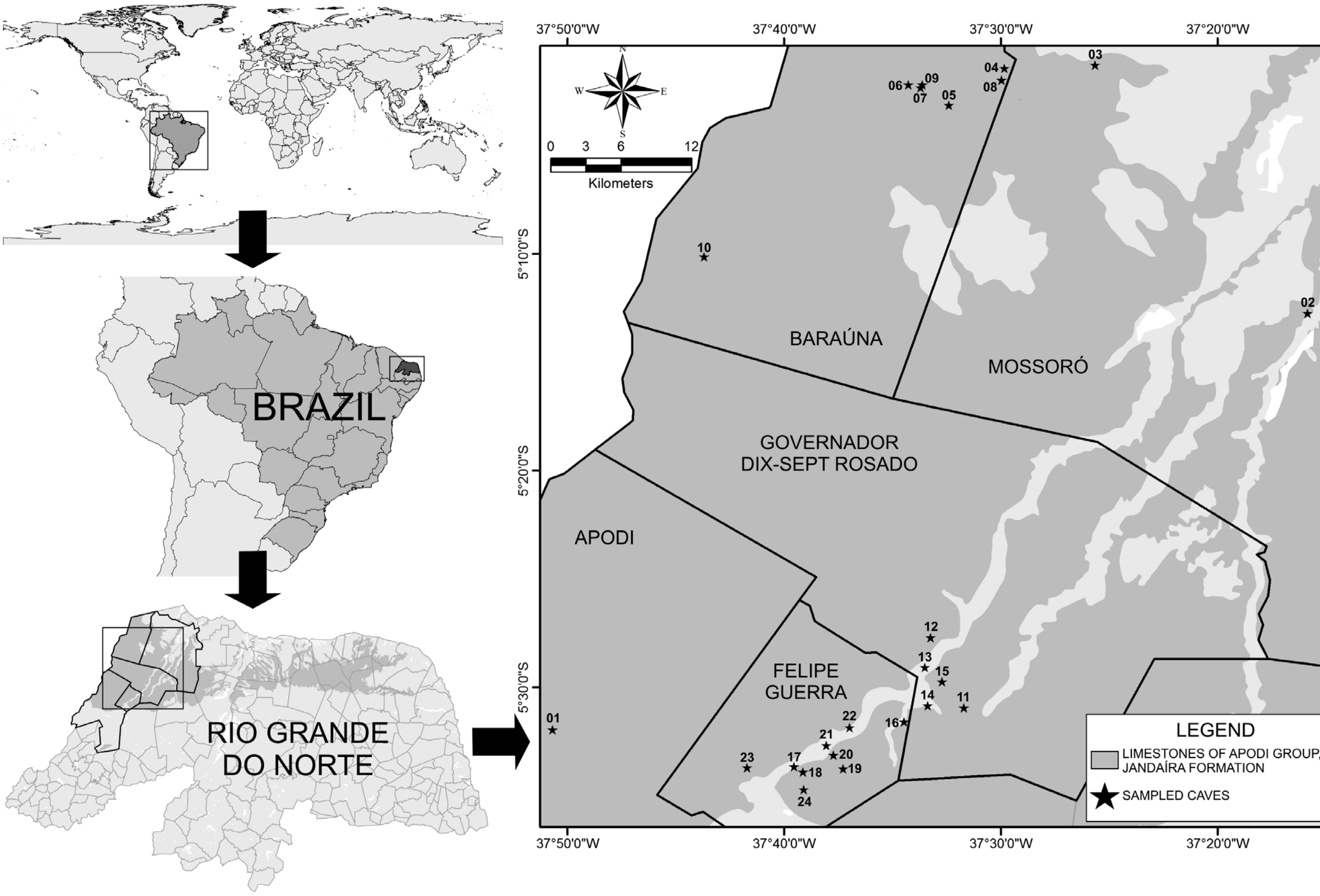

Figure 1. Map with the location of the study area and sampled caves. The numbered caves are identified in Table 1.

The environmental stability of each cavity was determined using the Environmental Stability Index (*ESI*) (Ferreira, 2004), modified to use the area of the cave (in square meters) instead of its linear extent. The index considers the isolation of the cave atmosphere and the external one through a mathematical ratio between the total area of the cave, the area of entrances, and the distance among them according to the following formulas:

For caves having just one entrance

$$ESI = \ln\left(\frac{AT}{AE}\right), \tag{1}$$

where *ESI* is the Environmental Stability Index, AT is the total area of each cave (m^2), and AE is the area of the cave entrance (m^2).

For caves having more than one entrance

$$ESI = \ln\left[\frac{(AT^2/\Sigma AE)}{NE\ DE}\right], \tag{2}$$

where *ESI* is the Environmental Stability Index, AT is the total area of the cavity (m^2), ΣAE is the total area of the cave's entrances (m^2), NE is the number of entrances, and DE is the average distance between entrances, taking the largest of them as reference.

We used the Levene test to verify the homogeneity of variance between seasons of each of the parameters morphospecies richness, abundance, and diversity index. The variables that were not normally distributed (morphospecies richness and abundance of individuals) were normalized with natural log. Then differences between the community parameters' averages for rainy and dry seasons were verified by t-test.

Finally, to verify the similarity between invertebrate communities in the same cave, but from different seasons, a matrix of similarity was built based on presence and absence data using the Bray-Curtis coefficient through the software Primer-5 (Clarke and Warwick, 2001). Subsequently, a Pearson correlation test was applied on the similarity values (dry/rainy) and *ESI* values of the sampled caves to check if the more stable caves have a greater similarity between seasons and showed a lower influence of the epigean ecosystems.

Table 1. Names and data on the sampled caves numbered in Figure 1.

Number	Cave	Municipality	Total Area (m^2)	Number of Entrances	Area of Entrances (m^2)	Environmental Stability Index (*ESI*)	Coordinates Latitude (S)	Coordinates Longitude (W)
1	Buraco da Nega	Apodi	108.51	1	4.6	3.16	05° 31′ 57.16″	37° 50′ 40.73″
2	Trinta	Mossoró	644.65	4	21.31	4.28	05° 12′ 44.36″	37° 15′ 50.95″
3	Javan	Mossoró	92.17	1	9.38	2.29	05° 01′ 17.61″	37° 25′ 39.03″
4	Britador	Baraúna	179.28	3	30.72	4.04	05° 01′ 25.85″	37° 29′ 49.51″
5	Pinga	Baraúna	25.95	1	1.32	2.98	05° 03′ 08.06″	37° 32′ 22.97″
6	Lago	Baraúna	157.1	1	2.73	4.44	05° 02′ 11.40″	37° 34′ 15.24″
7	Macacos/Esquecida	Baraúna	217.25	3	4.14	6.78	05° 02′ 19.80″	37° 33′ 41.30″
8	Cipós	Baraúna	167.86	1	6.28	3.29	05° 01′ 58.99″	37° 29′ 57.51″
9	Furna Feia	Baraúna	5726.85	5	163.12	5.97	05° 02′ 11.54″	37° 33′ 36.69″
10	Escada	Baraúna	124.81	7	21.1	3.2	05° 10′ 07.83″	37° 43′ 40.98″
11	Capoeira de João Carlos	Gov. Dix-Sept Rosado	251.4	2	17.22	4.35	05° 30′ 56.69″	37° 31′ 41.75″
12	Boca de Peixe	Gov. Dix-Sept Rosado	175.6	2	2.38	4.82	05° 29′ 04.45	37° 33′ 29.62″
13	Lajedo Grande	Gov. Dix-Sept Rosado	245.4	2	21.7	3.59	05° 27′ 44.20″	37° 33′ 09.06″
14	Boniteza	Gov. Dix-Sept Rosado	30.39	1	1.68	2.9	05° 30′ 51.02″	37° 33′ 21.54″
15	Marimbondo Caboclo/Água	Gov. Dix-Sept Rosado	284.67	4	18.98	4.45	05° 29′ 44.11″	37° 32′ 42.24″
16	Cote	Felipe Guerra	106.94	2	28.36	3.07	05° 31′ 34.76″	37° 34′ 27.27″
17	Crotes	Felipe Guerra	1402.83	8	99.69	4.65	05° 33′ 38.77″	37° 39′ 31.54″
18	Rumana	Felipe Guerra	917.25	15	139.95	3.48	05° 33′ 54.25″	37° 39′ 07.13″
19	Trapiá	Felipe Guerra	13698.4	2	13.32	12.7	05° 33′ 45.43″	37° 37′ 15.92″
20	Beira-Rio	Felipe Guerra	51.78	1	3.65	2.65	05° 33′ 07.39″	37° 37′ 42.91″
21	Seta	Felipe Guerra	124.5	2	13.25	3.62	05° 32′ 40.23″	37° 38′ 03.10″
22	Arapuá	Felipe Guerra	570	1	3.24	5.17	05° 31′ 48.25″	37° 36′ 58.47″
23	Lapa I/ Engano	Felipe Guerra	192.73	5	12.1	4.11	05° 33′ 41.89″	37° 41′ 42.25″
24	Buraco Redondo	Felipe Guerra	108.76	2	10.56	4.9	05° 34′ 42.98″	37° 39′ 04.99″

Results

The invertebrate communities showed differences in their structure according to the collection season, with the greatest values of richness, abundance, and diversity index occurring during the rainy season (Tables 2 and 3). A total of 24,177 invertebrates were recorded. During the dry season, 9,275 individuals of 225 morphospecies belonging to 32 orders and 104 families were recorded. Collembola was the most abundant group, with 3,509 individuals (37.83 %), followed by Araneae (969 individuals; 10.44 %) and Ensifera (754 individuals; 8.13 %). In the rainy season, 14,902 individuals of 302 morphospecies were found, belonging to 38 orders and 130 families. Again, Collembola was the most abundant group with 4,314 individuals (28.95 %), followed by Araneae with 2,255 individuals (15.13 %), and Ensifera (1,300 individuals; 8.72 %) (Table 2).

Only eight orders showed a decrease in abundance during the rainy season (Opiliones, Scorpiones, Polydesmida, Spirobolida, Diptera, Embioptera, Isoptera, and Neuroptera). Five taxa were not found in the dry season (Scolopendromorpha, Symphyla, Diplura, Odonata and Turbellaria), and only one order was not found in the rainy season (Embioptera) (Table 2).

The average richness observed in the dry season was 27.62 ± 12.1 morphospecies per cave and in the rainy season 40.8 ± 14.3 morphospecies, while the average abundances were 386.46 ± 368.46 individuals in the dry season and 620.92 ± 538.66 individuals in the rainy season. For the diversity index, the values were 2.08 ± 0.56 in the dry season and 2.51 ± 0.42 in the rainy season. Stated uncertainties are standard errors; see Figure 2. All community parameters measured for the invertebrates of caves (morphospecies richness [$t = -3.83$; df.46, $p < 0.01$], abundance [$t = -2.19$; df.46, $p < 0.05$] and diversity index [$t = -2.99$; df.46, $p < 0.01$]) were significantly higher during the rainy season (Table 3; Fig. 2).

The similarity calculated from presence and absence data among communities during the rainy and dry seasons was positively and significantly related to the *ESI* of each cave ($R = 0.45$; $p < 0.05$) (Fig. 3).

Discussion

There is a clear relation between rainfall and the dynamics of invertebrate communities in epigean ecosystems in Caatinga, where the abundance and richness of taxa of soil macrofauna, especially of organisms related to the scavengers chain, increase considerably during the rainy season (Araújo et al., 2010b). Likewise, Vasconcellos et al. (2010) observed that ten of twelve insect orders have greater abundance or breeding and foraging activity at the time of increases in precipitation and relative humidity in Caatinga. Araújo et al. (2010a) reported that about 84% of collected scorpions were obtained in the rainy months, with precipitation and evapotranspiration as the variables most strongly related to the number of collected individuals.

Regarding the effects of seasonality in a cave, Lavoie et al. (2007) reported results similar to those found in the present work, regarding seasonal variations on the populations and the reproductive activity of cave crickets in North America, which affected populations of predators of their eggs, such as cave beetles (Kane and Poulson, 1976). Ferreira et al. (2005) also mentioned the greater availability of prey during the rainy season as the probable cause of the growth of *Loxosceles similis* population at Gruta da Lavoura, Minas Gerais, Brazil.

The majority of invertebrates found in Brazilian caves (Ferreira et al., 2010) are in troglophilic groups typically associated with soil and adjacent epigean habitats (Pinto-da-Rocha, 1995; Trajano and Bichuette, 2009), including those from caves in the present work (Ferreira et al., 2010). Thus the patterns observed for epigean communities may be, to some extent, similar to those observed for subterranean communities.

One of the possible explanations for this fact is the almost complete dependence of organic resources importation from the surface, which makes relative changes in the communities of cave invertebrates something expected (Culver and White, 2005). The increases in morphospecies richness, abundance, and diversity index in the rainy season demonstrate the association between hypogean and epigean ecosystems in the Caatinga, as rainfall causes an increased production of leaves, flowers and fruits, which is reversed in the dry season when there are few plant species producing flowers and leaves (Machado et al., 1997). This increase in organic resources supply for many invertebrates during the rainy season, especially for the herbivores, stimulates guilds of predators (Vasconcellos et al., 2010).

Although forests in limestone areas have well-defined phenophases and produce more leaf litter during dry periods (Brina, 1998), limestone caves tend to experience a greater transport of debris into the hypogean environment during the rainy season (Souza-Silva et al., 2007; Souza-Silva et al., 2011a). Rivers, streams, runoff, and percolation water can carry large amounts of organic matter such as leaves, tree fragments, animal carcasses, and dissolved organic compounds (Gibert et al., 1997; Simon et al., 2007; Souza-Silva et al., 2012).

Except for three caves (Trapiá, Furna Feia, and Lago), the others in the study area have no significant streams even during the rainy season, and even those with streams are not currently subject to flood events. Thus, flooding causing major changes in the invertebrate cave community or nutrient inflow, as reported by Souza Silva et al. (2011a) and Simões et al. (2015), is not expected.

The water from surface runoff and percolation seems to have a considerable influence on the organic resource supply in the studied region (Ferreira et al., 2010). During rainy periods the water enters through skylights and horizontal entrances, carrying organic matter, especially leaves

Table 2. Abundance (N) and relative frequency (%) of different invertebrate taxa sampled from all the studied caves in different seasons.

	Dry Season		Wet Season		Total	
Invertebrate Taxa	N	%	N	%	N	%
Arthropoda	9094	98.05	14646	98.28	23740	98.19
Chelicerata	1710	18.44	3625	24.33	5335	22.07
Arachnida	1710	18.44	3625	24.33	5335	22.07
Acari	132	1.42	521	3.5	653	2.70
Amblypygi	135	1.46	268	1.80	403	1.67
Araneae	969	10.45	2255	15.13	3224	13.33
Opiliones	126	1.36	113	0.76	239	0.99
Palpigradi	1	0.01	10	0.07	11	0.05
Pseudoscorpiones	48	0.52	72	0.48	120	0.50
Schizomida	291	3.14	381	2.56	672	2.78
Scorpiones	8	0.09	5	0.03	13	0.05
Myriapoda	132	1.42	183	1.23	315	1.30
Diplopoda	127	1.37	158	1.06	285	1.18
Polydesmida	60	0.65	51	0.34	111	0.46
Polyxenida	3	0.03	19	0.13	22	0.09
Spirobolida	9	0.10	5	0.03	14	0.06
Spirostreptida	55	0.59	83	0.56	138	0.57
Chilopoda	5	0.05	20	0.13	25	0.10
Geophilomorpha	2	0.02	6	0.04	8	0.03
Scolopendromorpha	0	*	5	0.03	5	0.02
Scutigeromorpha	3	0.03	9	0.06	12	0.05
Symphyla	0	*	5	0.09	5	0.07
Crustacea	484	5.22	1112	7.46	1596	6.60
Amphipoda	5	0.05	42	0.28	47	0.19
Isopoda	479	5.16	1070	7.18	1549	5.41
Hexapoda	6768	72.97	9276	65.27	16494	68.22
Entognatha	3509	37.83	4318	28.98	7827	32.37
Collembola	3509	37.83	4314	28.95	7823	32.36
Diplura	0	*	4	0.03	4	0.02
Insecta	3259	35.14	5408	36.29	8667	35.85
Archaeognatha	2	0.02	9	0.06	11	0.05
Blattodea	150	1.62	406	2.72	556	2.30
Coleoptera	145	1.56	204	1.37	349	1.44
Diptera	931	10.04	661	4.44	1592	6.58
Embioptera	5	0.05	0	*	5	0.02
Ensifera	754	8.13	1300	8.72	2054	8.50
Hemiptera	223	2.40	367	2.46	590	2.44
Hymenoptera	515	5.55	887	5.95	1402	5.80
Isoptera	26	0.28	18	0.12	44	0.18
Lepidoptera	264	2.85	391	2.62	655	2.71
Neuroptera	51	0.55	31	0.21	82	0.34
Odonata	0	*	1	0.01	1	*
Psocoptera	141	1.52	893	5.99	1034	4.28
Zygentoma	52	0.56	240	1.61	292	1.21
Annelida	89	0.96	94	0.63	183	0.76
Oligochaeta	89	0.96	94	0.96	183	0.76
Platyhelminthes	0	*	19	0.13	19	0.08
Turbellaria	0	*	19	0.13	19	0.08
Mollusca	92	0.99	143	0.96	235	0.97
Gastropoda	92	0.99	143	0.96	235	0.97
Total	9275	100	14902	100	24177	100

* means that the frequency was less than 0.1%.

Table 3. Community parameters (S, morphospecies richness; N, abundance; H′, Shannon diversity index) for each cave in different seasons.

	Dry Season			Wet Season		
Cave	S	N	H′	S	N	H′
Buraco da Nega	26	99	2.72	32	324	2.68
Caverna do Trinta	27	259	2.14	49	1235	2.33
Caverna de Javan	14	152	1.81	39	302	2.54
Caverna do Britador	21	211	2.36	50	393	2.49
Gruta do Pinga	13	443	0.76	31	382	2.15
Caverna do Lago	21	353	1.97	33	706	1.58
Cav.Macacos/ Esquecida	36	230	2.75	42	269	3.02
Caverna dos Cipós	17	178	1.59	38	280	2.64
Furna Feia	61	1895	2.40	57	2497	2.47
Gruta da Escada	25	209	2.84	39	236	2.89
Cav. Capoeira de João Carlos	26	559	1.51	69	992	2.47
Gruta Boca de Peixe	13	59	2.22	42	445	2.91
Caverna do Lajedo Grande	17	79	2.52	37	557	2.31
Caverna da Boniteza	26	260	2.15	35	404	2.21
Cav. Marimbondo Caboclo/Água	36	613	2.27	66	580	3.43
Caverna do Cote	16	239	1.98	24	357	2.29
Caverna dos Crotes	50	632	2.49	77	742	3.06
Caverna da Rumana	49	331	3.03	39	473	2.86
Caverna do Trapiá	27	571	1.51	36	1579	2.56
Caverna Beira-Rio	33	591	1.04	33	151	2.80
Caverna da Seta	29	165	2.44	17	177	2.02
Caverna do Arapuá	31	520	1.64	34	972	1.85
Lapa I/ Caverna do Engano	23	211	2.07	37	755	2.03
Caverna do Buraco Redondo	26	416	1.79	24	94	2.66

and branches, into the caves. So in addition to resources such as carcasses and guano provided to the cave fauna by trogloxenes, other agents, such as water, play an important role during the rainy season (Ferreira et al., 2010).

Regarding the organic matter carried by trogloxenes, bat guano plays an important role as a food source for many communities inside the studied caves. Since most of them do not have perennial water, guano becomes one of the main resources available the entire year (Ferreira et al., 2010), and several studies have shown the importance of guano as a source of organic matter for cave communities, especially in permanently dry caves (Ferreira and Martins, 1998; Ferreira and Martins, 1999; Ferreira et al., 2000; Ferreira et al., 2007; Pellegrini and Ferreira, 2013; Pape, 2014; Iskali and Zhang, 2015). Furthermore, in a similar way to what occurs in temperate regions where bat colonies often exhibit annual cycles and add a temporal component to the deposition of guano (Harris, 1970), most species of Neotropical bats tend to synchronize their reproductive periods with periods of increased food availability, which usually occurs during the rainy season (Willig, 1985; Bernard, 2002). This situation leads to a similar cycle in the abundance of invertebrates that depend directly or indirectly on guano.

Another factor contributing to the increase in activity or abundance of invertebrates during the rainy season may be the direct and indirect consequences of rain on decomposition and the invertebrate populations involved in this process. Soil moisture is a key factor for the increase in biomass of edaphic microorganisms, stimulating species of scavenger arthropods and predators that are part of soil micro-, meso-, and macrofauna (Swift et al., 1979, Lavelle et al., 1995). In terrestrial environments of caves, unfavorable conditions such as low humidity may inhibit colonization by animals and decrease the rate of plant debris processing (Souza-Silva et al., 2011a), since high humidity is critical to rapid decomposition because it regulates the metabolism of the decomposer organisms (Souza-Silva et al., 2013).

Therefore, fluctuations in morphospecies richness and abundance during the rainy season are certainly related to variations of the main routes of matter and energy into the caves. Although the details were not assessed directly in this work, they must be related to a greater transport of organic material, especially of vegetable origin, from the surface by rains, increased deposition of guano, and the increase in the rate of decomposition of animal and especially vegetable organic matter in caves.

A significant relationship between the similarity of invertebrate communities in the dry and rainy seasons and the Environmental Stability Index of each cave certainly reflects an interaction between hypogean and epigean ecosystems. However, the degree of interaction between these two systems was not uniform, and the most isolated caves exhibited little variation in the invertebrate fauna between seasons, a consequence of a low interaction with the epigean ecosystem (Poulson and White, 1969; Culver, 1982; Howarth, 1983). This trend indicates that caves with greater *ESI* and more stability tend to maintain the structure of their communities in comparison with less stable caves.

Caves and other subterranean habitats are not fully stable environments as is often assumed, but they exhibit seasonal fluctuations in temperature and humidity that reflect a delayed response to the climate change on the surface (Tobin et al., 2013). In most of the caves, the seasonality on the surface affects the speed, direction, and daily fluctuations in pressure and chimney effect on air flows, resulting in seasonal variations of moisture and temperature (Howarth, 1980; Cigna, 2002). Variable environmental conditions tend to occur in areas next to the entrances, while the most stable

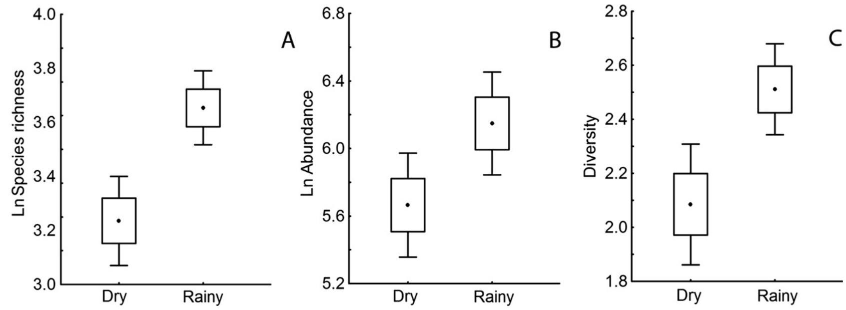

Figure 2. Community parameters of sampled cave invertebrate communities during dry and rainy seasons: a. morphospecies richness (log values); b. abundance (log values); c. Shannon diversity index. Central dots inside box-plots represent mean values, boxes represent standard errors, and bars represent standard deviation.

conditions occur in deeper areas within the caves (Tobin et al., 2013).

As a result, the classical interpretation leads one to expect that trogloxenes are more suited to the entrance zone, troglophiles in the twilight zone, and troglobionts in the totally dark zone, deep inside the cave (Novak et al., 2012). Thus, although this work did not attempt an ecological classification of the sampled groups, which would require more detailed ecological studies, the results suggest some considerations.

Generally, species that are more specialized to the cave environment tend to be restricted to the aphotic areas with more stable temperature and humidity. Troglobiont and troglophile species are commonly stenothermic (adapted to a narrow temperature range) and stenohygrobic (Barr and Kuehne, 1971; Howarth, 1980). Such preferences are probably generated by the presence of thinner exoskeletons and longer appendages, resulting in greater desiccation in relation to surface taxa (Howarth, 1980). Thus, their distribution can be influenced by seasonal changes in temperature and humidity, and, in many cases, such species are restricted to areas with more stable temperature and humidity (Tobin et al., 2013). For these groups, the entrance zone acts as a disturbance, disrupting or limiting their preferred subsurface habitat that range from the shallow subterranean to deep caves (Novak et al., 2012). Such species tend to form communities with stable composition and distribution over time and space.

The entrance and transition twilight areas, in turn, have microhabitats that vary considerably according to changes

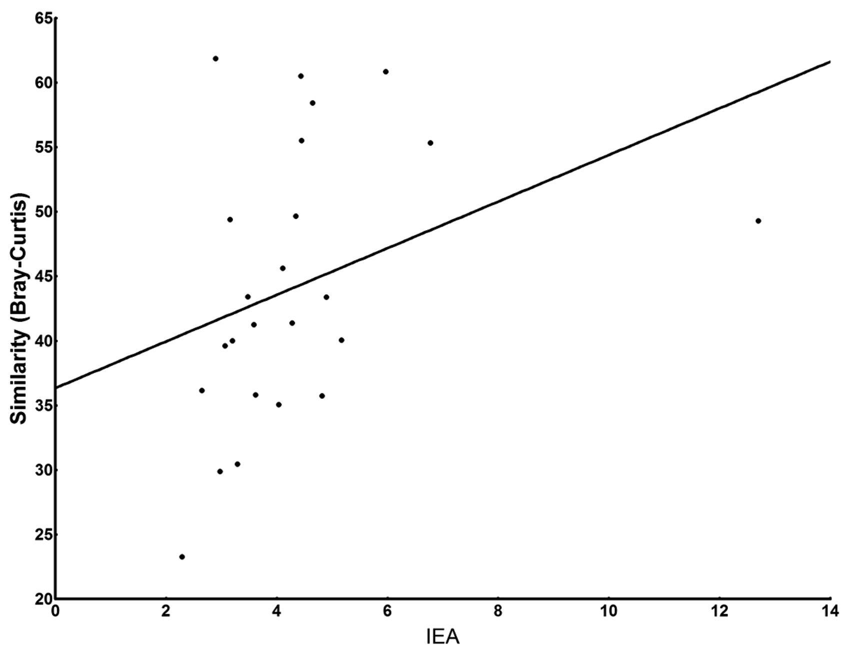

Figure 3. Positive and significant correlation ($R = 0.45$; $p < 0.05$) between the similarity (Bray-Curtis) of invertebrate communities in the dry and wet seasons in the same cave and its Environmental Stability Index (IEA, from Portuguese initials).

in the external environment (Culver, 1982). These habitats are subject to colonization by a wide range of invertebrate species, with or without pre-adaptation to the deep hypogean environments (Ferreira and Martins, 2001; Prous et al., 2004) and generally exhibit a greater species diversity than deep subterranean habitats (Culver and Pipan, 2009). Thus, these communities have much more temporally variable composition.

Conclusions

Morphospecies richness, abundance, and diversity index in caves were significantly higher during the rainy season. There was a difference in the community structure between seasons, showing a clear relationship between hypogean and epigean environments. Nevertheless, this relationship may vary according to the environmental stability of the hypogean ecosystem; greater internal stability will lead to a lower fluctuation in the composition of the invertebrate community throughout the year. Moreover, these seasonal differences in the invertebrate fauna reinforce the need for biological samples during at least two different seasons as required in the current Brazilian environmental legislation dealing with the environmental licensing of projects and activities potentially harmful to caves (MMA, 2009).

Climate change projections for Latin America indicate a slight increase in temperature and increased variability in rainfall for the next decades (Silva, 2004; Sivakumar et al., 2005). For Caatinga, both drastic decreases and significant increases in precipitation are plausible scenarios for the next 50 years (Krol and Bronstert, 2007). According to our results, these climatic changes will probably have effects on cave communities and their directly or indirectly associated ecosystems. Partial loss of biodiversity in these systems would be important not only in a local ecological context, but also because several collected species are undescribed, and probably many of them have distribution restricted to the sampled region.

Acknowledgements

The authors would like to thank Programa de Pós-Graduação em Ciências Biológicas (UFRN), Laboratório de Ecologia e Conservação da Biodiversidade (LECB/UFRN), Centro de Estudos em Biologia Subterrânea (CEBS/UFLA), and Centro Nacional de Pesquisa e Conservação de Cavernas (ICMBio/CECAV) for providing infrastructure for the development of the study. Thanks to Darcy Santos, Iatagan Freitas, Uilson Campos, and Geilson Goes for helping with the collections; to colleagues of CEBS/UFLA and LECB/UFRN for helping with the material analysis and invertebrate identification; and to Dr. Mauro Pichorim for valuable contributions to the text. Funding was provided by the Conselho Nacional de Pesquisa (CNPq), process n. 477712/2006-1, and to R.L.F. (CNPq grant n. 304682/2014-4).

References

Aguiar, C.M.L., and Martins, C.F., 1997, Abundância relativa, diversidade e fenologia de abelhas (Hymenoptera, Apoidea) na Caatinga, São João do Cariri, Paraíba, Brasil: Iheringi, Série Zoologia, v. 83, p. 151–163.

Araújo, C.S, Candido, D.M, Araújo, H.F.P, Dias, S.C, Vasconcellos, A., 2010a, Seasonal variations in scorpion activities (Arachnida: Scorpiones) in an area of Caatinga vegetation in northeastern Brazil: Zoologia, v. 27, no. 3, p. 372–376. doi:10.1590/S1984-46702010000300008.

Araújo, V.F.P, Bandeira, A.G, Vasconcellos, A., 2010b, Abundance and stratification of soil macroarthropods in a Caatinga Forest in Northeast Brazil: Brazilian Journal of Biology, v. 70, no. 3 suppl., p. 737–746. doi:10.1590/S1519-69842010000400006.

Barr, T.C. and Kuehne, R.A., 1971, Ecological studies in the Mammoth Cave system of Kentucky II: the ecosystem: Annales de Spéléologie, v. 26, p. 47–96.

Bernard, E., 2002, Diet, activity and reproduction of bat species (Mammalia, Chiroptera) in Central Amazonia, Brazil: Revista Brasileira de Zoologia, v. 19, no. 1, p. 173–188. doi:10.1590/S0101-81752002000100016.

Bezerra, F.H.R., Takeya, M.K., Sousa, M.O.L., Nascimento, A.F., 2007, Coseismic reactivation of the Samambaia fault, Brazil. Tectonophysics, v. 430, p. 27–39. doi:10.1016/j.tecto.2006.10.007.

Brina, A.E., 1998, Aspectos da dinâmica da vegetação associada a afloramentos calcários na APA Carste de Lagoa Santa, MG [Masters Thesis]: Belo Horizonte, Universidade Federal de Minas Gerais, 105 p.

Cigna, A.A, 2002, Modern trend in cave monitoring: Acta Carsologica, v. 31, p. 35–54.

Clarke, K.R., and Warwick, R.M., 2001, Change in Marine Communities: An Approach to Statistical Analyses and Interpretation 2nd edition: Plymouth, United Kingdom, PRIMER-E Ltd, 176 p.

Culver, D.C, 1982, Cave Life. Evolution and Ecology: Cambridge, Harvard University Press.

Culver, D.C., and Pipan, T., 2009, The Biology of Caves and Other Subterranean Habitats: New York, Oxford University Press, 256 p.

Culver, D.C., and White, W.B., 2005, Encyclopedia of Caves: Amsterdam, Academic/Elsevier Press, 654 p.

Day, A., 2002, Cave Surveying: Buxton: British Cave Research Association, Cave Studies Series 11, 40 p.

Derraik, J.G.B., Closs, G.P., Dickinson, K.J.M., Sirvid, P., Barratt, B.I.P., and Patrick, B.H, 2002, Arthropod morphospecies versus taxonomic species: a case study with Araneae, Coleoptera, and Lepidoptera: Conservation Biology, v. 16, p. 1015–1023. doi:10.1046/j.1523-1739.2002.00358x.

Derraik, J.G.B., Early, J.W., Closs, G.P., and Dickinson, K.J.M., 2010, Morphospecies and taxonomic species comparison for Hymenoptera: Journal of Insect Science. v. 10, article 108, 7 p. doi: 10.1673/031.010.10801.

Ducarme, X., André, H.M., Wauthy, G., and Lebrun, P., 2004, Comparison of endogeic and cave communities: microarthropod density and mite species richness: European Journal of Soil Biology, v. 40, no. 3-4, p. 129–138. doi:10.1016/j.ejsobi.2004.10.003.

Ferreira, R.L., 2004, A medida da complexidade ecológica e suas aplicações na conservação e manejo de ecossistemas subterrâneos [Ph.D. thesis]: Belo Horizonte, Universidade Federal de Minas Gerais, 161 p. [http://pos.icb.ufmg.br/pgecologia/teses/T23_rodrigo_lopes%20.pdf]

Ferreira, R.L., and Martins, R.P., 1998, Diversity and distribution of spiders associated with bat guano piles in Morrinho cave (Bahia State, Brazil): Diversity and Distributions, v. 4, no. 5-6, p. 235–241.

Ferreira, R.L., and Martins, R.P., 1999, Trophic structure and natural history of bat guano invertebrate communities, with special reference to Brazilian caves: Tropical Zoology, v. 12, no. 2, p. 231–252. doi:10.1080/03946975.1999.10539391.

Ferreira, R.L., and Martins, R.P., 2001, Cavernas em risco de 'extinção': Ciência Hoje, v. 29, no. 173, p. 20–28.

Ferreira, R.L., Martins, R.P., and Yanega, D., 2000, Ecology of bat guano arthropod communities in a Brazilian dry cave: Ecotropica, v. 6, no. 2, p. 105–116.

Ferreira, R.L., Prous, X., Machado, S.F., and Martins, R.P., 2005, Population dynamics of *Loxosceles similis* (Moenkhaus, 1898) in a brazilian dry cave: a new method for evaluation of population size: Revista Brasileira de Zoociências, v. 7, p. 129–141.

Ferreira, R.L., Prous, X., and Martins, R.P., 2007, Structure of bat guano communities in a dry Brazilian cave: Tropical Zoology, v. 20, p. 55–74.

Ferreira, R.L, Prous, X., Bernardi, L.F.O., Souza-Silva, M., 2010, Fauna subterrânea do Estado do Rio Grande do Norte: Caracterização e impactos: Revista Brasileira de Espeleologia, v. 1, p. 25–51.

Gibert, J., Mathieu, J., and Fournier F., eds., 1997, Groundwater/ Surface water ecotones: Biological and hydrological interactions and management options: Cambridge, UK, Cambridge University Press, International Hydrobiology Series, Cambridge, 246 p. doi:10.1017/CBO9780511753381.

Gusmão, M.A.B., and Creão-Duarte, A.J., 2004, Diversidade e análise faunística de Sphingidae (Lepidoptera) em área de brejo e caatinga no Estado da Paraíba, Brasil: Revista Brasileira de Zoologia, v. 21, p. 491–498. doi:10.1590/S0101-81752004000300011.

Harris, J.A., 1970, Bat guano cave environment: Science, v. 169, p. 1342–1343. doi:10.1126/science.169.3952.1342-a.

Hernández, M.I.M., 2007, Besouros escarabeíneos (Coleoptera: Scarabaeidae) da caatinga paraibana, Brasil: Oecologia Brasiliensis, v. 11, p. 356–364.

Howarth, F.G., 1980, The zoogeography of specialized cave animals: a bioclimatic model: Evolution, v. 34, p. 394–406. doi:10.2307/2407402.

Howarth, F.G., 1983, Ecology of cave arthropods: Annual Review of Entomology, v. 28, p. 365–389. doi:10.1146/annurev.en.28.010183.002053.

Iannuzzi, L., Maia, A.C.D, Vasconcelos, S.D., 2006, Ocorrência e sazonalidade de coleópteros buprestídeos em uma região de caatinga nordestina: Biociências, v. 14, p. 174–179.

IDEMA, Instituto de Desenvolvinmento Sustentável e Meio Ambiente, 2005, Atlas para o Desenvolvimento Sustentável do RN, www.idema.rn.gov.br/governo/secretarias/idema/atlasdes/atlas.zip, [acessed February 10, 2014].

INPE, Instituto Nacional de Pesquisas Espaciais, 2010, Balanço Hídrico Municipal, www.cptec.inpe.br/proclima, [accessed on February 12, 2014].

Iskali, G., and Zhang, Y., 2015, Guano subsidy and the invertebrate community in Bracken Cave: the world's largest colony of bats: Journal of Cave and Karst Studies, v. 77, no. 1, p. 28–36. doi:10.4311/2013LSC0128.

Kane, T.C., and Poulson, T.L., 1976, Foraging by cave beetles: Spatial and temporal heterogeneity of prey: Ecology, v. 57, p. 793–800. doi:10.2307/1936192.

Kottek, M., Grieser, J., Beck, C., Rudolf, B., and Rubel, F., 2006, World map of the Köppen-Geiger climate classification updated: Meteorologische Zeitschrift, v. 15, no. 3, p. 259–263. doi:10.1127/0941-2948/2006/0130.

Krol, M.S., and Bronstert, A., 2007, Regional integrated modelling of climate change impacts on natural resources and resource usage in semi-arid Northeast Brazil: Environmental Modelling & Software, v. 22, p. 259–268. doi:10.1016/j.envsoft.2005.07.022.

Lavelle, P., Lattaud, D.T., and Barois, I., 1995, Mutualism and biodiversity in soils: Plant and Soil, v. 170, p. 23–33. doi:10.1007/BF02183052.

Lavoie, K.H., Helf, K.L, and Poulson, T.L., 2007, The biology and ecology of North American cave crickets: Journal of Cave and Karst Studies, v. 69, p. 114–134.

Machado, I.C.S., Barros, L.M., and Sampaio, E.V.S.B., 1997, Phenology of caatinga species at Serra Talhada, PE, Northeastern Brazil: Biotropica, v. 29, p. 57–68.

Magurran, A.E., 1988, Ecological Diversity and Its Measurement: London, Cromm Helm, 179 p.

Medeiros, J., Araújo, A., Araújo, H.F.P., Queiroz, J.P.C., and Vasconcellos, A., 2012, Seasonal activity of *Dinoponera quadriceps* Santschi (Formicidae, Ponerinae) in the semi-arid Caatinga of northeastern Brazil: Revista Brasileira de Entomologia, v. 56, no. 1, p. 81–85. doi:10.1590/S0085-56262012000100013.

MMA, Ministério de Meio Ambiente, 2009, Instrução Normativa N° 02, de 20 de agosto de 2009. Diário Oficial da República Federativa do Brasil, Brasil.

Novak, T., Perc, M., Lipovšek, S., and Janžekovič, F., 2012, Duality of terrestrial subterranean fauna: International Journal of Speleology, v. 41, no. 2, p. 181–188. doi:10.5038/1827-806X.41.2.5.

Oliver, I., and Beattie, A.J., 1996a, Invertebrate morphospecies as surrogates for species: a case study: Conservation Biology, v. 1, no. 10, p. 99–109. doi:10.1046/j.1523-1739.1996.10010099.x.

Oliver, I., and Beattie, A.J., 1996b, Designing a cost-effective invertebrate survey: a test of methods for rapid assessment of biodiversity: Ecological Applications, v. 6, no. 2, p. 594–607. doi:10.2307/2269394.

Pape, R.B., 2014, Biology and ecology of Bat Cave, Grand Canyon National Park, Arizona: Journal of Cave and Karst Studies, v. 76, no. 1, p. 1–13. doi:10.4311/2012LSC0266.

Pellegrini, T.G., and Ferreira, R.L., 2013, Structure and interactions in a cave guano-soil continuum community: European Journal of Soil Biology, v. 57, p. 19–26. doi:10.1016/j.ejsobi.2013.03.003.

Pinto-da-Rocha, R., 1995, Sinopse da fauna cavernícola do Brasil (1907–1994): Papéis Avulsos de Zoologia, v. 39, no. 6, p. 61–173.

Poulson, T.L., and White, W.B., 1969, The cave environment: Science, v. 165, p. 971–981. doi:10.1126/science.165.3897.971.

Prous, X., Ferreira, R.L., and Martins, R.P., 2004, Ecotone delimitation: epigean-hypogean transition in cave ecosystems: Austral Ecology, v. 29, p. 374–382. doi:10.1111/j.1442-9993.2004.01373.x.

Sampaio, E.V.S.B., 1995, Overview of the Brazilian caatinga, *in* Bullock, S.H., Mooney, H.A., and Medina, E., eds., Seasonally Dry Tropical Forests: Cambridge, Cambridge University Press, p. 35–58. doi:10.1017/CBO9780511753398.003.

Schneider, K., Christman, M.C., and Fagan, W.F., 2011, The influence of resource subsidies on cave invertebrates: results from an ecosystem-level manipulation experiment: Ecology, v. 92, no. 3, p. 765–776. doi:10.1890/10-0157.1.

Sharratt, N.J., Picker, M.D., and Samways, M.J., 2000, The invertebrate fauna of the sandstone of the caves of the Cape Penisula (South Africa): patterns of endemism and conservation priorities: Biodiversity and Conservation, v. 9, p. 107–143. doi:10.1023/A:1008968518058.

Silva, V.P.R., 2004, On climate variability in northeast of Brazil: Journal of Arid Environments, v. 58, p. 575–596. doi:10.1016/j.jaridenv.2003.12.002.

Simões, M.H., Souza-Silva, M., and Ferreira, R.L., 2015, Cave physical attributes influencing the structure of terrestrial invertebrate communities in Neotropics: Subterranean Biology 16: 103–121. doi:10.3897/subtbiol.16.5470.

Simon, K.S., Pipan, T., and Culver, D.C., 2007, A conceptual model of the flow and distribution of organic carbon in caves: Journal of Cave and Karst Studies, v. 69, p. 279–284.

Sivakumar, M.V.K., Das, H.P., and Brunini, O., 2005, Impacts of present and future climate variability and change on agriculture and forestry in the arid and semi-arid tropics: Climatic Change, v. 70, p. 31–72. doi:10.1007/s10584-005-5937-9.

Souza-Silva, M., Ferreira, R.L., Bernardi, L.F.O., and Martins, R.P., 2007, Importação e processamento de detritos orgânicos em uma caverna calcária: Espeleo-Tema, v. 19, p. 31–46.

Souza-Silva, M., Martins, R.P., and Ferreira, R.L., 2011a, Trophic Dynamics in a Neotropical Limestone Cave: Subterranean Biology, v. 9, p. 127–138. doi:10.3897/subtbiol.9.2515.

Souza-Silva, M., Martins, R.P., and Ferreira, R.L., 2011b, Cave lithology determining the structure of the invertebrate communities in the Brazilian Atlantic Rain Forest: Biodiversity and Conservation, v. 20, no. 8, p. 1713–1729. doi:10.1007/s10531-011-0057-5.

Souza-Silva, M., Bernardi, L.F.O., Martins, R.P., and Ferreira, R.L., 2012, Transport and consumption of organic detritus in a neotropical limestone cave: Acta Carsologica, v. 41, no. 1, p. 139–150.

Souza-Silva, M., Júnior, A.S., and Ferreira, R.L., 2013, Food resource availability in a quartzite cave in the Brazilian montane Atlantic Forest: Journal of Cave and Karst Studies, v. 75, no. 3, p. 177–188. doi:10.4311/2010JCKS0158.

Swift, M.J., Heal, O.W., and Anderson, J.M., 1979, Decomposition in Terrestrial Ecosystems: London, Blackwell Scientific, Studies in Ecology series, 372 p.

Tobin, B.W., Hutchins, B.T., and Schwartz, B.F., 2013, Spatial and temporal changes in invertebrate assemblage structure from the entrance to deep-cave zone of a temperate marble cave: International Journal of Speleology, v. 42, no. 3, p. 203–214. doi:10.5038/1827-806X.42.3.4.

Trajano, E., 1987, Fauna cavernícola brasileira: composição e caracterização preliminar: Revista Brasileira de Zoologia, v. 3, no. 8, p. 533–561. doi:10.1590/S0101-81751986000400004.

Trajano, E., and Bichuette, M.E., 2009, Diversity of Brazilian subterranean invertebrates, with a list of troglomorphic taxa: Subterranean Biology, v. 7, p. 1–16.

Vasconcellos, A., Andreazze, R., Almeida, A.M., Araujo, H.F.P., Oliveira, E.S., and Oliveira, U., 2010, Seasonality of insects in the semi-arid Caatinga of northeastern Brazil: Revista Brasileira de Entomologia, v. 54, no. 3, p. 471–476. doi:10.1590/S0085-56262010000300019.

Ward, D.F., and Stanley, M.C., 2004, The value of RTUs and parataxonomy versus taxonomic species: New Zealand Entomologist: v. 27, p. 3–9. doi:10.1080/00779962.2004.9722118.

Weinstein, P., and Slaney, D., 1995, Invertebrate faunal survey of Rope Ladder Cave, Northern Queensland: a comparative study of sampling methods: Journal of the Australian Entomological Society, v. 34, p. 233–236. doi:10.1111/j.1440-6055.1995.tb01329.x.

Willig, M.R., 1985, Reproductive patterns of bats from caatingas and cerrado biomes in northeast Brazil: Journal of Mammalogy, v. 66, no. 4, p. 668–681. doi:10.2307/1380793.

J.D. Despain, B.W. Tobin, and G.M. Stock – Geomorphology and paleohydrology of Hurricane Crawl Cave, Sequoia National Park, California. *Journal of Cave and Karst Studies*, v. 78, no. 2, p. 72–84. DOI: 10.4311/2013ES0114

GEOMORPHOLOGY AND PALEOHYDROLOGY OF HURRICANE CRAWL CAVE, SEQUOIA NATIONAL PARK, CALIFORNIA

Joel D. Despain[1]*, Benjamin W. Tobin[2], and Greg M. Stock[3]

Abstract: Hurricane Crawl Cave in Sequoia and Kings Canyon National Parks, California, contains adjacent but varied passage morphologies including network and anastomotic mazes, large rooms, narrow canyons, prolific speleothems, and multiple levels that collectively are difficult to explain. We investigated the cave through cartography, geochronology, dye traces, modern discharge measurements, and paleodischarge estimates from scallop and cobble measurements. The cave has strong structural control along vertically oriented beds and subparallel fractures. $^{26}Al/^{10}Be$ burial dating of coarse clastic sediment suggests a minimum cave age of 1.4 Ma, and a time-averaged in-cave incision rate of 0.02 mm y^{-1}. Dye traces proved that an obvious surface stream is the source of the primary stream in the cave, but that other small streams rise from diffuse flow. Modern discharge measurements range from 0.042 to 0.002 m^3 s^{-1}. Paleodischarge and flow velocity values determined from scallops and cobbles vary more in relation to passage morphology than to passage elevation, a proxy for time. Paleodischarges were orders of magnitude larger than modern discharge. We attribute varied morphology and location of mazes to temporally and spatially variable sediment flux and stream discharges. Higher sediment loads and stream discharges promote the development of passages with anastomotic maze morphology. The morphology of Hurricane Crawl Cave differs from that Crystal Cave, which is in the same basin, primarily due to a comparatively lower sediment load.

Introduction

Caves and karst of the Kaweah River basin in Sequoia and Kings Canyon National Parks, California (Fig. 1), have proven ideal locations to study the hydrologic behavior of mountain karst aquifers, the geomorphology of caves and karst in the region, and how these features relate to the overall geomorphic evolution of the Sierra Nevada. Hydrologic research has identified the causes of unique aquifer behavior at Big Spring and Lilburn Cave (Abu-Jaber et al., 2001; Urzendowski, 1993), the relationships between surface and groundwater systems (Tinsley, et al., 1981; Tobin and Schwartz, 2012), and the importance of karst aquifers to river flow (Despain and Stock, 2005; Tobin and Schwartz., Submitted). Geomorphic histories of caves in the basin have provided insight into cave geomorphology (Despain and Stock, 2005; Despain et al., in review), geochronology (Stock et al., 2005b), and the history of regional mountain uplift and canyon incision (Stock et al., 2004; Stock et al, 2005a). These previous works have primarily focused on the two longest cave systems in the river basin, Lilburn Cave and Crystal Cave, with some additional work on large springs not associated with extensive cave passages. To assess the karst hydrologic and geomorphic history of the Kaweah River basin further, this research aims to describe the hydrologic and geomorphologic history that led to the variety of passage forms in the third-longest cave system in the basin, Hurricane Crawl Cave (HCC). HCC developed in very similar hydrologic and geologic conditions to Crystal Cave, the second longest in the basin, yet they have very different morphologies. This research seeks to explain why.

Hurricane Crawl Cave

HCC contains 3132 m of surveyed passage with a vertical extent of 70.5 m in a canyon in the watershed of the North Fork of the Kaweah River, with the lower entrance and the cave resurgence at an elevation of 1220 m amsl. The cave was discovered by national park staff and cavers from the San Francisco Bay area in 1986 (Despain, 1999; Stock 1999). The cave has varied morphologies that imply a varied and complex history. Adjacent passage types in Hurricane include both anastomotic and network mazes (Palmer, 1975; 1991), rooms 35 m across, canyons 20 m deep and 1 m wide, and multiple levels (Fig. 2 and Fig. 3).

The Sierra Nevada has a Mediterranean climate with long dry summers and wet winters with rain at lower elevations and snow generally above 1500 m. Most of the basin for HCC lies within the snow zone, while the cave itself is at an elevation of 1220 m to 1300 m. Surface and cave streams in the Sierra Nevada experience periods of high discharge due to runoff from spring snowmelt and from

* Corresponding author: joeldespaincaves@gmail.com
[1] Joel D. Despain, 27171 State Highway 299 East, Bella Vista, CA 96008, USA.
[2] Benjamin W. Tobin, National Park Service, Grand Canyon National Park, Grand Canyon, AZ 86023, USA.
[3] Greg M. Stock, National Park Service, Yosemite National Park, El Portal, CA 95318, USA.

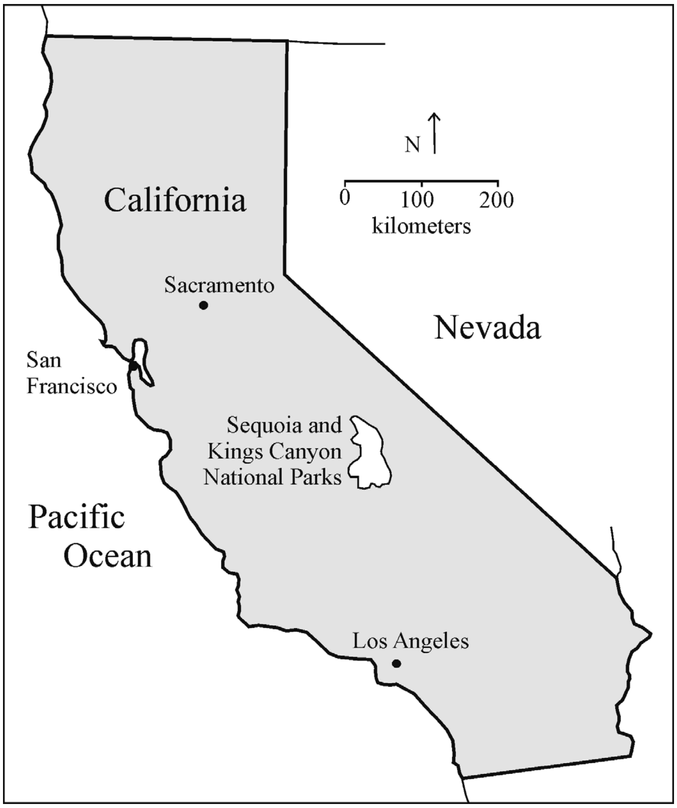

Figure 1. Location map of Sequoia and Kings Canyon National Parks, California, USA.

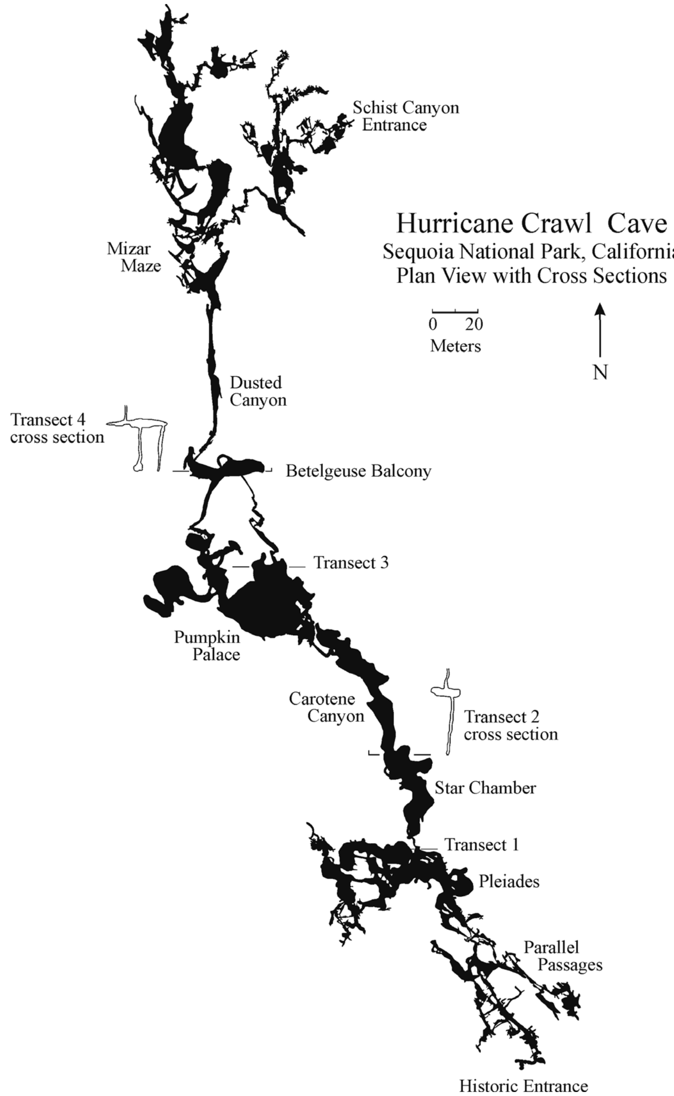

Figure 2. Plan view map of Hurricane Crawl Cave showing locations of vertical transects and locations referenced in the text.

infrequent rain-on-snow events during warm winter storms. This causes flooding within caves of the region (Tinsley, et al., 1981; Despain and Stock, 2005). Floods overwhelm existing stream conduits, promoting the development of network, and much more frequently, anastomotic mazes within caves (Palmer, 1975; 1991).

HCC developed in vertically bedded Mesozoic marble of the Sequoia Pendant of metamorphosed marine rocks assigned to a Triassic to Jurassic timeframe and as a component of the Kings Sequence and Kings Terrane (Bateman and Clark, 1974; Saleeby et al, 1978; Nokleberg, 1983). Multiple marble bodies within the metamorphic pendant are bounded by quartzite schist (Sisson and Moore, 1994) seen in prominent outcrops on the surface and in many caves. These contacts' conformal bedding are within 10 degrees of vertical (Despain and Stock, 2005). Many similar pendants occur in the Sierra Nevada and are generally surrounded by larger granitic plutons. The Sequoia Pendant is approximately 4 km wide and 18 km long and lies parallel to the crest of the Sierra Nevada, trending north-northwest to south-southeast. HCC formed in the central of three parallel marble lenses. This body of marble is 100 to 300 m wide and 3 km long (Sisson and Moore, 1994) (Fig. 4).

Two entrances allow access to the cave through breakdown collapses near the upstream and downstream termini; these collapses likely relate to stress-relief fracturing along the canyon walls (e.g., Sasowsky and White, 1994). The cave has three perennial streams, although two have very low discharge, with base flows of less than 0.001 m^3 s^{-1}. Much of the cave's lowest level is composed of two narrow, tall canyon passages with streams (Fig. 5), although mazes are found at the upstream and downstream margins. A large room, Pumpkin Palace, is in the central portion of the cave (Fig. 6).

The cave stream emerges as a series of small springs on the banks of the local base-level stream, a major tributary to the North Fork of the Kaweah River. Inside the cave are many small knickpoint waterfalls up to 2 m in height, particularly near the downstream cave terminus and the spring. The surface base-level stream to which the cave drains lies in a steep canyon with many knickpoints and waterfalls 5 to 30 m tall. The headward migration of knickpoints past the cave very likely drove vadose cave stream

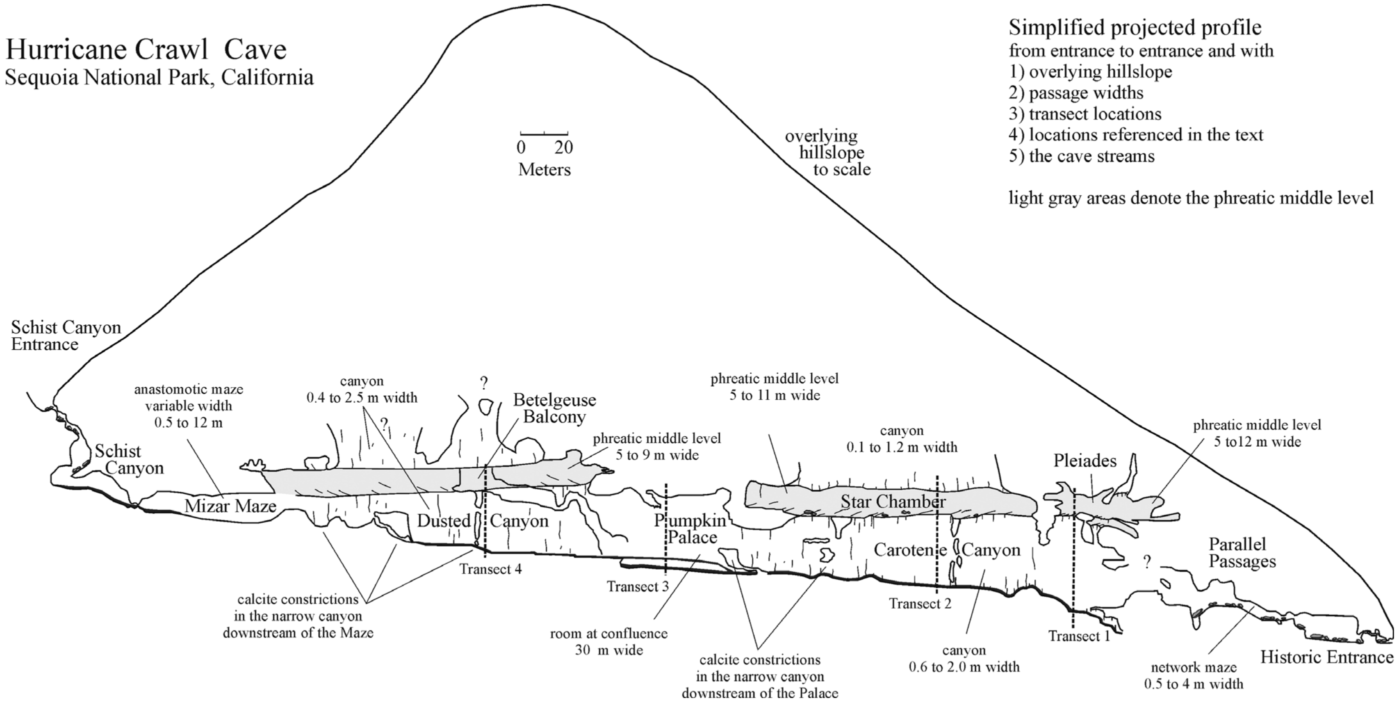

Figure 3. Profile view map of Hurricane Crawl Cave showing transects, locations referenced in the text, passage widths and types, the cave streams, and the overlying hillslope.

incision and the development of vadose canyons. This has been suggested for Crystal Cave (Despain and Stock, 2005), also in the North Fork of the Kaweah watershed.

Above the lowest canyons, the cave has two other well-defined levels. The first and primary one is a broad passage 6 to 14 m wide. It is accessible at four locations where vertical passages are not filled by speleothems deposits. Prominent passages at this level include the Star Chamber and the Pleiades. Above this level is another, higher canyon that can be accessed in only two locations due to its vertical orientation and prolific delicate speleothems found between narrow walls. From these two locations the canyon can be entered for a few tens of meters.

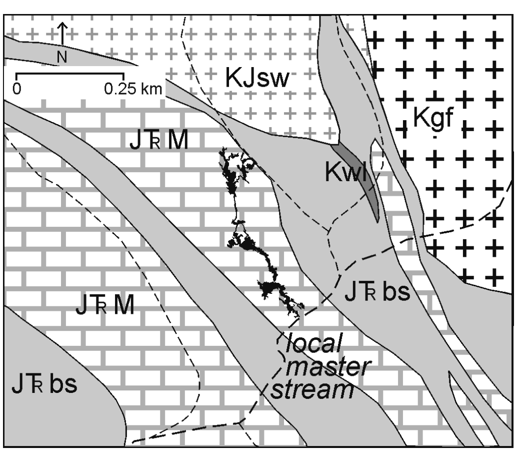

Figure 4. Geologic map with local surface streams (dashed lines) and the Hurricane Crawl Cave footprint in black (adapted from Sisson and Moore, 1994). JTR m marble, Jurassic and/or Triassic; JTR bs biotite-feldspar-quartz schist, Jurassic and/or Triassic; KJsw granite of Skagway Grove, Cretaceous or Jurassic; Kgf Giant Forest Granodiorite, Cretaceous; Kwl granite of Weaver Lake, Cretaceous. The name of the stream is omitted to protect the location of the cave.

Passages at all levels end in collapse, secondary calcite infill, or both where conduits approach the surface. These locations often have roots or organic soils and may act as entrances for small animals and airflow. Specific areas of collapse near the surface occur in the Parallel Passages, Pleiades, Mizar Maze, and Schist Canyon.

Granitic sediments derived from upstream watersheds are very common in sierran caves and vary from cobbles and gravels to silts and clays (Tinsley, et al., 1981; Stock et al., 2005b; Despain and Stock, 2005). Passages are sometimes completely filled by sediment or show evidence of being filled in the past, such as sediments in bedrock wall and ceiling notches. This implies a return to phreatic conditions and possible paragenetic cave development (Farrant and Smart, 2011) in Sierra Nevada caves. Sediment distribution within HCC varies because of the cave's varied morphology of rooms separated by narrow canyons. Steep-walled canyon passages have almost no storage capacity for fluvial sediments, while cave rooms have floors of sediments or speleothems that have been deposited on top of sediments. In addition to standard carbonic-acid dissolution in the development of cave

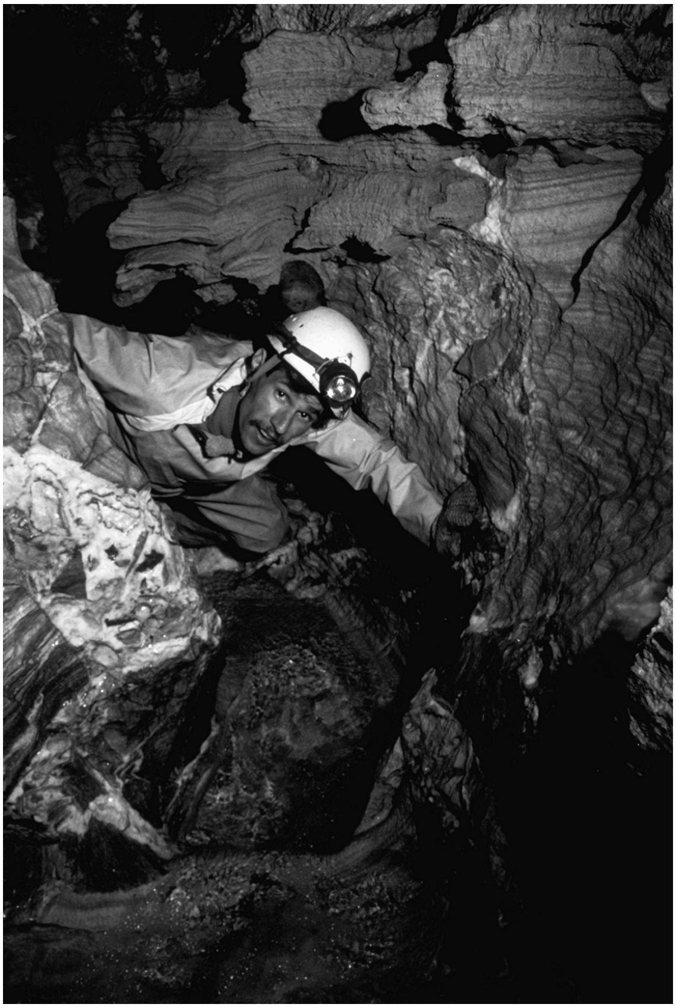

Figure 5. A caver moves through narrow stream passage in Carotene Canyon. This passage is 19 m tall and averages less than 1 m wide. Note brecciated marble bedrock and eroded speleothem deposits above the caver's head.

passages, prolific scallops in the cave give evidence for turbulent flow throughout the cave's history that would have entrained sediments, promoting mechanical erosion of marble surfaces.

HCC is known for its prolific and active speleothems, including large shields, rimstone pools, folia, spar crystals, curtains, and helictites. Many larger pool basins in the cave fill only seasonally, but some generate calcite deposits of up to 0.5 mm per annum. Cave speleothem deposition constricts and in-fills narrow canyon passages within HCC, creating upstream flooding and trapping sediments by reducing their movement downstream.

As attested by the name, HCC is breezy, with strong convection-generated air currents that reach 48 km h^{-1} at the lower entrance. Cave temperatures vary near the entrances in association with the strong airflow, but constant climatic conditions persist in the central regions of the cave, where temperatures varied less than 0.2 °C over

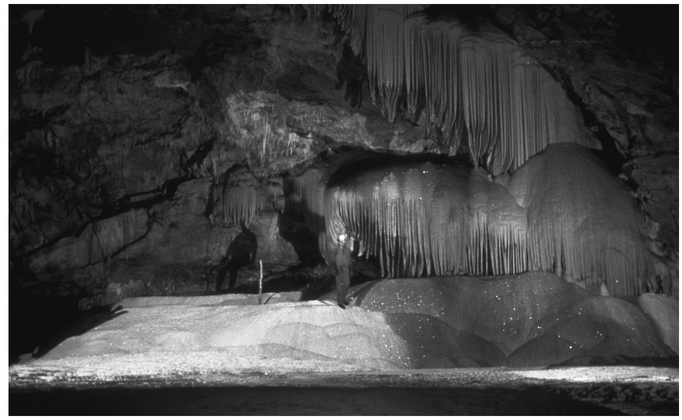

Figure 6. Pumpkin Palace, the largest room in Hurricane Crawl Cave with a maximum width of 38 m.

9 months with a mean of 10.9 °C in 2009. The presence of strong air currents apparently allowed soot from at least one wildfire above the cave to be drawn underground, as evidenced by thin black deposits that smear when touched. The deposits cover many areas of speleothems and sediments. In several locations, including the Mizar Rooms, a new growth of white calcite has covered some, but not all, speleothem surfaces, making for starkly contrasting patterns of black and white calcite (Fig. 7).

METHODS

Cave morphology, passage elevations, and basic hydrology were determined through a survey of the cave conducted from 1988 through 1995 using compasses, clinometers, and fiberglass measuring tapes or laser range-finders for high ceilings and tall passages. Data were processed using

Figure 7. Black stalagmites and flowstone apparently colored by soot and smoke that entered the cave during a surface fire. The single white spot atop of the rear stalagmite attests to recent calcite deposition post-fire.

Table 1. Transect locations.

Transect Number	Transect Location	Distance from Cave Terminus, m	Number of Measured Sites	Transect Height, m
1	Pleiades and Carotene Canyon	142	7 scallop 2 cobble	21.6
2	Star Chamber and Carotene Canyon	206	11 scallop 3 cobble	24.6
3	Pumpkin Palace, Sequin Balcony	367	6 cobble	19.9
4	Dusted Canyon and Betelgeuse Balcony	445	8 scallop 2 cobble	19.6

Compass Software (Fish, 2013) for reduction and display. A surface survey between the cave's two entrances, combined with a traverse through all of the cave's major passages, created a loop with a closure error of less than 1 %. This, combined with analysis of additional survey loops, produced a total survey error of less than 2 %. The initial mapping effort was supplemented through field checks of draft maps and tying the survey to prominent features in the cave (Despain and Fryer, 2002).

Two years after the cave's 1988 discovery, a sinking stream was noticed in a nearby canyon. This appeared to be an obvious source for Hurricane Crawl Cave's primary stream. We conducted two dye traces in the sinking stream. The first, in 1995, used fluorescein, coconut-husk charcoal receptors, and an eluent solution to complete a qualitative trace using an existing protocol (Smart and Brown, 1973). In 2012, we conducted a second dye trace in the same stream and in two adjacent sinking streams. Results of this trace were presented in Tobin (2013) and confirmed that the sinking stream discovered in 1988 was the only surface stream among those traced that flowed through the cave. However, observations suggest that the discharge differed greatly between the sinking stream's insurgence and the resurgence, implying a larger diffuse source feeding the cave stream. Under baseflow conditions, diffuse recharge sources also predominate in other karst in the North Fork of the Kaweah's watershed and other watersheds in the Kaweah area (Tobin, 2013).

We measured seasonal discharge values from 2010 to 2012 for comparison to paleodischarge, discussed below, using a pygmy meter and established methods (Shelton, 1994). We measured flow in a confined stretch of the main cave stream above Strawberry Falls twice per year, during high flow in June and in during baseflow conditions in October.

Geochronologic data from HCC were published in Stock et al. (2004, 2005a, 2005b). Paleomagnetic orientations of fine-grained sediments throughout the cave consistently indicated deposition during times of normal magnetic polarity. These include fine-grained sediment collected from an upper level passage in the Pleiades area, where an underlying granitic cobble yielded a cosmogenic $^{26}Al/^{10}Be$ burial age of 0.93 $\pm$ 0.24 Ma. Stock et al. (2005b) concluded that, given the stratigraphic relations in this area, either the fine sediment was deposited during one of the normal chrons prior to 0.93 Ma or the fine sediment was deposited stratigraphically above the coarse sediment by floodwaters entering the passage sometime after the Bruhes-Matuyama magnetochron boundary 0.78 Ma. A single cosmogenic burial-age sample was collected from HCC for the 2004 and 2005 papers, as the focus of that work was regional. Samples for the project were collected in caves in the southern and central Sierra Nevada and were processed at UC Santa Cruz and at the Lawrence Livermore National Laboratory's Center for Accelerator Mass Spectrometry.

Asymmetric bedrock scallops on cave surfaces can be used to infer both paleoflow direction and velocity. We use the method defined by Curl (1974) for determining paleoflow. As evidenced by bedrock features, turbulent flow that would entrain significant quantities of sediments, particularly during floods, was significant in the development of cave passages in Hurricane Crawl Cave. However, Curl does not consider kinematic viscosity in his calculations for determine flow velocity in caves from scallops. Thus velocity and discharge values presented here are likely to be over-estimated by this method and should be considered maximum possible values.

We examined 327 scallops at 27 locations and 157 cobbles at 13 locations along four vertical transects (Table 1) in locations chosen for their vertical extent and locations along the length of the cave (Fig. 2 and Fig. 3). We selected scallops for measurement based on their location, elevation, and abundance and the presence of distinct scallop margins needed for measurement. Scallop lengths were measured across their greatest lengths, and the widths were measured normal to the lengths.

Sampling transect 1 begins in Carotene Canyon where the cave stream flows over bedrock and extends 21.6 m straight up a narrow canyon. The transect ends on the margins of the larger Pleiades passages. Within the Pleiades, copious calcite deposits have covered most bedrock surfaces and sediments. Seven sets of scallops and two of cobbles were measured. Calculated paleodischarges for this and the other transects are given in Tables 2 and 3.

Transect 2 also begins at stream level in Carotene Canyon and extends 19 m upwards in the canyon, through the

Table 2. Cobble data and calculation values including velocity and discharge.

Transect Number	Transect Name	Mean Clast Size, m	Flow Width, m	Crit. Shear Stress (τ_c), N m^{-2}	Crit. Flow Depth (h_c), m	U_c After Manning's n, m s^{-1}	U_c After Friction Factor, m s^{-1}	Max. Discharge n, m^3 s^{-1}	Max. Discharge ff, m^3 s^{-1}
1	Pleiades	0.0492	2.1	44.6	0.04	3.20	2.67	0.30	0.25[b]
		0.0892	5.95	80.9	0.08	7.05	3.60	3.36	1.71[a]
2	Star Chamber	0.1228	13.16	111.3	0.35	13.19	4.22	61.56	19.69[a]
3	Pumpkin Palace	0.0745	2.3	67.5	0.07	3.63	3.29	0.56	0.51[b]
		0.0158	2.3	14.3	0.01	2.83	1.51	0.09	0.05[b]
		0.107	4.97	97.0	0.10	6.43	3.94	3.07	1.88[b]
		0.177	4.97	160.4	0.16	6.97	5.07	5.50	4.00[b]
4	Betelgeuse Balcony	0.0372	3.78	33.7	0.03	4.53	2.32	0.57	0.29[a]
		0.0422	2.2	38.3	0.04	3.22	2.47	0.27	0.21[b]

[a] Discharge calculated using passage cross section measurements.
[b] Discharge calculated assuming water depths equal to widths.

broad and wide Star Chamber level, and upward into another canyon, the highest passage in the cave, for a total height of 24.6 m. We measured 11 sets of scallops and three cobble locations in this transect.

Transect 3 lies in the large room at the center of the cave, Pumpkin Palace, and includes the adjacent ceiling alcove known as Sequin Balcony. No scallops were found in the room, the balcony, or immediately adjacent passages, but six cobble sites were measured. However, cobble locations were few, and we measured them in two different locations that do not constitute a vertical transect. We measured four sets of cobbles in Sequin Balcony and on the climb up to it. The highest is 19.9 m above the stream and the lowest 17.7. Two sets of cobbles were measured across the room where the entrance passage intersects. These cobbles are 1.5 m and 1.02 m above the stream.

Transect 4 is upstream of Pumpkin Palace and starts from the bottom of Dusted Canyon, extending to the upper level in this area known as Betelgeuse Balcony, reached by a roped ascent. We measured two cobble deposits and eight scallop sites along this transect encompassing a total height of 19.6 m.

Passage cross-sectional areas can be difficult to determine. In the well-defined passages of the Star Chamber, the Pleaides, and the Betelgeuse Balcony measurements were made directly for passage width and height, including wall irregularities and variations in floor elevations and ceiling heights. Some passage surfaces are obscured by deposits of sediments and calcite, adding uncertainty to the original cross-sectional area. Tall canyon passages in HCC are essentially ceiling-less. Here we assumed water depth equal to passage width. Collectively these data provide values for paleoflow velocities and discharges that help to illuminate the cave's hydrologic history. The two approaches for determining cross-sectional area, actual measurement or assumed equal height and width, are noted in the last columns in Tables 2 and 3. Discharge values are maximum possible flows since they assume pipe-full conditions, which would only occur during extreme floods, if ever, in larger passages.

Curl demonstrated a relation between mean scallop length, L, and the Reynolds number, Re_L, for scallops in both parallel-wall and circular conduits. We determined mean scallop lengths for each set of scallop populations and used Curl's predicted relation between the Reynolds number and the ratio of conduit width D to L, in parallel-wall conduits to determine Re_L values for each site. We then used the relation between L and Re_L to calculate mean flow velocity, v, through these conduits using the relation $v = \upsilon\ \mathrm{Re}_L / L$, where υ is the kinematic viscosity (~0.013 cm² s for fresh water at 10 °C; Curl, 1974).

Stream deposited cobbles were found to be in sorted and layered beds with varied sediment sizes ranging from sand to cobbles, to lie in flat-topped beds as opposed to slumped, sloped and angled piles of infill or collapse, to include rock types not found within the cave, predominantly granodiorite, to be consistently rounded on all axes, to be in immediate association with other evidence of fluvial action

Table 3. Scallop data and calculated values including velocity and discharge.

Transect							
Number	Name	Mean Scallop, m	Conduit Width, m	Re_L	Velocity (v), m^3 s^{-1}	Cross-sectional Area, m^2	Discharge, m^3 s^{-1}
1	Pleaides	0.037	0.41	0.0247	0.87	0.168	0.15[b]
		0.042	1.4	0.0309	0.96	1.96	1.89[b]
		0.0245	0.41	0.0270	1.44	0.168	0.24[b]
		0.019	0.41	0.0285	1.96	0.168	0.33[b]
		0.018	0.540	0.0303	2.21	0.292	0.64[b]
		0.0313	0.71	0.0287	1.20	0.504	0.61[b]
		0.0347	1.92	0.0338	1.28	3.686	4.70[b]
2	Star Chamber	0.0283	1.37	0.0331	1.53	1.877	2.87[b]
		0.0422	0.5	0.0250	0.78	0.25	0.19[b]
		0.0355	0.69	0.0279	1.03	0.476	0.49[b]
		0.029	2.6	0.0366	1.65	6.76	11.16[a]
		0.036	1.7	0.0329	1.20	2.89	3.46[b]
		0.0429	2.9	0.0350	1.07	8.41	8.97[a]
		0.0309	0.79	0.0294	1.27	0.624	0.78[b]
		0.025	1.8	0.0353	1.87	3.24	5.99[b]
		0.031	0.89	0.0301	1.27	0.792	1.01[b]
		0.0162	1.3	0.0359	2.91	1.69	4.91[b]
		0.0295	1.5	0.0333	1.48	2.25	3.337[b]
4	Betelgeuse Balcony	0.0301	4.72	0.0398	1.73	22.28	38.51[a]
		0.02	1.6	0.0359	2.35	2.56	6.02[b]
		0.03775	0.9	0.0290	1.03	0.81	0.81[b]
		0.0399	1.3	0.0308	1.01	1.69	1.71[b]
		0.032	1.7	0.0336	1.37	2.89	3.98[b]
		0.022	1.2	0.0337	2.01	1.44	2.90[b]
		0.044	1.6	0.0314	0.93	2.56	2.39[b]
		0.035	0.8	0.0288	1.08	0.64	0.69[b]

[a] Discharge calculated using passage cross section measurements.
[b] Discharge calculated assuming water depths equal to widths.

including scallops and eroded bedrock, to be common throughout the cave, and to occur tens to hundreds of meters below ground and far from evidence of collapse or infill from the surface.

Deposits of stream cobbles can be used to determine paleovelocity of cave streams through the critical shear stress required to entrain them in cave-stream flow (e.g., Despain and Stock, 2005). For spherical particles, such as fluvially deposited cobbles, the relationship between critical shear stress, τ_c, and particle size, D, is described by the Shields equation $\tau_c = \beta\ (\rho_p - \rho_f)\ g\ D$, where β is the Shields function (0.056 for typical gravel beds), ρ_p is the particle density (2700 kg m^{-3}), ρ_f is the fluid density (1000 kg m^{-3}), g is gravitational acceleration (9.81 m s^{-2}), and D is the sediment particle diameter in meters (Shields, 1936). We examined 157 sediment particles at 13 sites. At each site, we measured the population of largest spherical particles' diameters, which best represents the maximum discharge conditions before the basal shear stress of the flow fell below the critical shear stress necessary to transport the particles. We then used τ_c values to calculate the critical flow depths, h_c, required to entrain the particles, using an expression for basal shear stress $\tau_c = \rho_f\ g\ h_c\ S$, where S is the local passage slope (Bagnold, 1966). We determined passage slopes by dividing passage lengths by the change in elevation along the passage length. Lengths and slopes were 82 m and 3.2 % in the Star Chamber and 400 m and 10.3 % along the bedrock bottom of Carotene and Dusted canyons, respectively. We determined critical flow velocities, U_c, by combining the critical flow depths with two different methods for estimating the flow resistance. The first method uses a friction factor, f, which is a function of the Reynolds number and the relative conduit roughness: $U_c = (8\ g\ h_c\ S\ /\ f)^{0.5}$, where f is the friction factor, assumed to be 0.05, a value typical for turbulent flow in most cave conduits (Palmer, 1987). The second method of calculating the critical flow velocity utilizes a flow resistance based on hydraulic radius: $U_c = R_H^{0.66}\ S^{0.5}\ /\ n$, where R_H is the hydraulic radius, determined using passage width and the critical flow depth h_c. The variable n is Manning's roughness coefficient $0.32\ S^{0.38}\ h_c^{-0.16}$. We multiplied the critical flow velocities calculated by these two methods (friction factor f and Manning's n) by passage cross-sectional area to derive maximum paleodischarges.

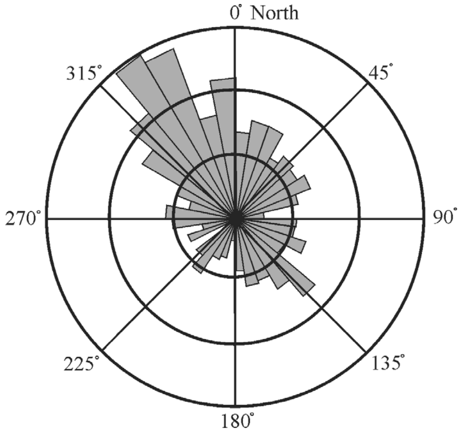

Figure 8. Rose diagram of Hurricane Crawl Cave (Fish, 2013) showing passage orientations as determined by the cave survey.

Results

HCC has three perennial and several seasonal streams. The primary stream pirated from Windy Canyon is seen in the Mizar Maze at the north end of the cave and downstream from Pumpkin Palace through Carotene Canyon, and it emerges at springs just downstream of the lower cave entrance along the local master stream. A tributary is found in Dusted Canyon, where a very low discharge stream originates from an area of dense secondary deposits near the Mizar Maze passages. The other perennial stream rises from another area of prolific secondary calcite in meandering Schist Canyon that has formed along an irregular schist contact.

Passage orientations reveal strong structural control on cave development. The overall trend of the cave is 330 to 150 degrees on strike across the near vertically bedded marble (Fig. 8). Passage development is also controlled by irregular contacts with schist bodies and significant sub-parallel fracture networks. Some of the length is due to the presence of anastomotic and network mazes (Palmer, 1975; 1991). Calcite-cemented marble breccia is found in lower Carotene Canyon, implying minor faulting and offset on strike in that area of cave development (Fig. 5).

Scalloped narrow canyons, such as at Transect 2 where the passage is 1 to 2 m wide and 17.5 m tall, and active streams point to vadose development by free-flowing streams and turbulent flow through at least 40 % of the cave's passages, including the network maze. As determined from the cave survey, the vadose passages have higher gradients compared to other levels (Table 4). Comparatively wide upper level passages with a lower gradient constitute about 10 % of surveyed cave passages and have fewer scallops. Other areas that lack scallops include the anastomotic Mizar Maze and Pumpkin Palace, the large room in the center of HCC.

Table 4. Overlying upper level and lower-level passage gradients.

Cave Passage	Elevation Range, m	Slope
Star Chamber, upper level	2.7	1.5
Carotene Canyon, lower level	7.9	10.7
All upper levels	9.5	1.6
All lower levels	18.0	10.3

The first dye trace, in 1995, showed that the water in the largest and longest stream inside HCC, and in the springs adjacent to the cave entrance, originates on the surface at a sinking stream draining a watershed of approximately 1.2 km^2. The straight-line distance through the karst from sink to spring is approximately 475 m. Transit time of the dye was less than three days. While the stream can be followed for hundreds of meters inside the cave, it is not possible to approach the sink point or the resurgence underground due to breakdown collapses. The other two perennial streams are likely related to diffuse inputs, as no other surface streams are found in the area or were traced to the cave in the 2012 dye trace.

Cave and surface streams show strong seasonal variation in discharge in the Sierra Nevada in accord with the Mediterranean climate. Thus baseflow and high-flow values are both of interest. Discharge measurements in the main cave stream from 2010 into 2012 ranged from 0.042 $m^3\ s^{-1}$ to 0.007 $m^3\ s^{-1}$ during high flow and 0.004 $m^3\ s^{-1}$ to 0.002 $m^3\ s^{-1}$ during baseflow conditions. The measurements missed the peak discharge of the cave stream during the sampling years.

Conditions during the cave's history limited cave-stream flow during certain periods. Insurgences in the unglaciated karst regions of the southern Sierra Nevada are frequently choked by granitic sediments, restricting and reducing discharge and additional sediment input into the cave systems. Current examples include the insurgences for Hurricane Crawl, Crystal, Lilburn, and other caves. Under these conditions, flow frequently bypasses the cave and continues in surface channels. When insurgence conduits are open, floods with high velocity flow move sediments deeper into cave passages and farther from entrances. Recent large flood events have been documented in park caves, including Wild Child (Despain and Stock, 2005) and Lilburn (Tinsley, et al., 1981; Despain and Stock, 2005) caves. This occurred most prominently on January 2, 1997, after a rain-on-snow event. Flooding occurred in both Lilburn and Wild Child that night, when the Kaweah had a peak flow of 1555 $m^3\ s^{-1}$ in Three Rivers below the park, compared to an average flow of 15 $m^3\ s^{-1}$ from 1959 to 1990.

Cosmogenic $^{26}Al/^{10}Be$ concentrations suggest that the granitic cobble from the Pleiades level of Hurricane Crawl was buried 0.93 $\pm$ 0.24 Ma (Stock et al., 2004; 2005a; 2005b). The vertical distance from this dated stream cobble to the active cave stream at the bottom of narrow Carotene Canyon (Transect 1) is 21.2 m, giving a cave stream down-cutting rate of approximately 0.02 mm y^{-1}. This rate is

Table 5. Summarized discharge results using results from the friction factor calculation method.

Transect				
Number	Name	Maximum, $m^3\ s^{-1}$	Minimum, $m^3\ s^{-1}$	Mean, $m^3\ s^{-1}$
1	Pleaides	4.7	0.15	1.17
2	Star Chamber	23.35	0.19	6.27
3	Pumpkin Palace	4.0	0.05	1.61
4	Betelgeuse	38.5	0.21	5.75
	Mean	17.64	0.15	3.7

similar to stream incision rates in other drainages of the southern Sierra Nevada (Stock et al., 2004; 2005a). The cave extends upward at least 12 m above the cobble sample location into the highest cave level, another narrow scalloped canyon. Assuming the same rate of cave passage development and down-cutting as lower in Carotene, the upper canyon would have developed over a minimum of 0.52 Ma. This would make the minimum potential age for the cave approximately 1.4 Ma, which is consistent with other measured cave ages in the southern Sierra Nevada (Stock et al., 2004; 2005a; 2005b).

Scallop orientations show that the present pattern of water flow through the cave persisted throughout the duration of cave development. This observation is corroborated by both ceiling and floor gradients of existing passages and by occasional imbrication of coarse sediments.

Cobbles sizes (Table 2) and scallop lengths (Table 3) indicate moderate to very high paleo-flow velocities. Scallop- and cobble-derived velocities vary little by transect or by elevation along the transects. The velocities depend less on passage morphology than the discharge values discussed below. Mean scallop velocity is 1.44 m s^{-1}, while cobbles show 3.23 m s^{-1} for the friction-factor velocities in Table 2. The cobble data include a few higher values from the Star Chamber, where calculated values range up to 13.9 m s^{-1} for two large rocks, according to Manning's method. Cobbles document higher flows and likely larger flood events compared to scallops.

Mean high-discharge data are more consistent, at 4.85 $m^3\ s^{-1}$ for cobbles based on the friction-factor formula and 4.18 $m^3\ s^{-1}$ for scallops. The data have a near-normal but positively skewed distribution reflecting a few very high discharge events that are orders of magnitude higher than current discharge values. Values range over four orders of magnitude from 0.05 $m^3\ s^{-1}$ to 66.1 $m^3\ s^{-1}$ for a cobble in the Star Chamber calculated using Manning's *n*. For comparison, modern calculated flood values for the watershed upstream of the cave insurgence produce values of 4.9 $m^3\ s^{-1}$ for 100-year events and 8.27 $m^3\ s^{-1}$ for 500-year events (USGS, 2015).

Mean discharge varies for the four transects; two results are a magnitude larger (Table 5). These transects include sample locations in the wide, phreatic upper levels, producing much larger discharge values due to much larger cross-sectional areas. Mean discharge from the larger passages is 27 $m^3\ s^{-1}$, while in the canyons the mean is 2.47 $m^3\ s^{-1}$. There is little variation in discharge values from each transect and thus there is little variation over elevation and time. Rather discharge values in this study are determined by passage morphology and size. Overall mean paleo-discharge is 3.7 $m^3\ s^{-1}$, far above current average or even high flow for the cave stream. Greater variations in paleo-discharge are seen in wider upper level passages that were subject to larger floods, as evidenced by the cobbles measured for this study.

As a first order approximation, overall scallop and cobble measurements imply extremely variable discharges, presumably due to these floods, a common occurrence in steep, mountainous catchments. This is supported by three discharge values in the Betelgeuse and Star Chamber transects that are approximately an order of magnitude larger than the transect means, skewing the transect discharge means to higher values. These values provide evidence for infrequent but very large discharge events in the dissolution and sedimentation of the cave.

Discussion

The hydrologic history of the cave is dominated by active vadose streams that created the narrow canyon at the cave's highest level and the 20 m tall current active stream passages of Carotene and Dusted canyons that make up much of the length of the cave. Also of vadose origin is the downstream maze, the Parallel Passages. This is a network of canyon passages developed on parallel beds in the vertically oriented marble. The maze in the downstream end of the cave is near an entrance and in an area subject to surface channel erosion, channel aggradation, and landslides; all of which can encourage the development of parallel conduits and hydrologic piracies when passages are blocked or constricted by sediment or collapse (Palmer, 1975). Headward migration of knickpoints in the steep surface canyon below the cave's spring and lower entrance drove vadose incision as the cave streams eroded downward toward base level.

An important exception to canyons are the scallop-less, wide, and broadly meandering level of the Pleiades, Star Chamber, Sequin Balcony, and Betelgeuse passages. We interpret these passages as forming under phreatic conditions because they exhibit low gradients and morphologies indicating low-velocity turbulent flow (Bogli, 1964). Why the active downcutting of the cave stream paused for thousands of years to create a broad low-gradient cave passage under different hydrologic conditions is unclear. Increased run off, rainfall, or sedimentation rates, the rapid migration of knickpoints through the marble unit (Despain and Stock, 2005), or local landslides that could bury cave entrances and effectively aggrade streams are all possibilities.

Other areas lacking scallops are the anastomotic Mizar Maze and Pumpkin Palace. Both lie at the junctions of tributary streams, allowing for mixing-zone chemistry to affect and possibly increase passage development (White, 1988; Bogli, 1964). Ceiling and wall surfaces of Pumpkin Palace and Mizar Maze, where they can be directly observed, are eroded bedrock, as opposed to collapses or fractured walls. However, this may reflect only current conditions, and evidence for earlier collapse may have eroded away. Both Pumpkin Palace and Mizar Maze are upstream of narrow canyons with prominent secondary speleothems that constrict cave passages. The active streams have only a small erosional effect on calcite deposition at passage constrictions. Evidence of erosion extends only 0.5 m above base flow. Both areas also contain voluminous quantities of granitic sediment deposited where stream velocities decreased behind the speleothem constrictions.

Seasonal flooding and storm discharges overwhelm conduits compromised by high sediment loads, which promotes the development of parallel conduits that bypass constrictions and create anastomotic mazes (Palmer, 1975; 1991). In the Mizar Maze, sediments aggraded behind constrictions, allowing the primary cave stream and the stream from Schist Canyon to meander, broadening passages and promoting curvilinear anastomotic maze development under little influence from prominent vertical bedding and joints (Palmer, 1975). In the Parallel Passages maze near the downstream terminus of the cave, fluvial sediments are sparse due to the filtering effects of constrictions earlier in the cave and the limited capacity of the present streams. The lack of sediments allowed multiple vadose piracies of the primary stream to form this network maze on strike, circumventing areas of collapse or infill at the nearby surface. Thus, sediment flux over time has determined passage morphology in the maze passages of HCC.

Pumpkin Palace, the cave's 35 m diameter central room, is anomalous, lying at the junction of two narrow vadose canyons and a complex of adjacent smaller rooms. The lack of scallops, even though they are prominent in adjacent passages, implies phreatic, low-velocity turbulent flow conditions during at least the last phases of room development. At the downstream end of the room, the stream sumps for a short distance where there are large deposits of secondary calcite in myriad forms. This includes the named formation areas of Pumpkin Palace itself, the north end of the Star Chamber, and the Dreamsicle. The size of the room may be partly due to mixing of the main stream, which rises near the room, with water from the small, perennial Dusted Canyon stream, generating more aggressive water (White, 1988). The presence of horizontal erosion planes etched into the bedrock above the rise of the stream does suggest chemically aggressive water. The downstream calcite restrictions promoted sediment deposition and stream meandering, contributing to the widening of the room. Ceiling breakdown was subsequently buried beneath sediments or removed by dissolution, increasing overall ceiling height.

Rooms in the Mizar Maze developed at passage intersections where frequent flooding and large sediment loads promoted passage bifurcation and stream widening due to meandering. The smaller rooms in the Parallel Passages occur at passage junctions.

Dusted Canyon, upstream of Pumpkin Palace, is approximately as large and deep as Carotene Canyon, but contains only a minor stream that currently deposits calcite along its entire length. It seems unlikely that the present low flow eroded this large, tall passage. The primary cave stream is seen both up and downstream of this passage, and the canyon likely contained the main flow for most of the cave's history. It was then pirated to lower, unexplored conduits within the last few tens of thousands of years, as judged by the volume of calcite deposits and the current stream and passage elevations.

There is evidence of hydrologic quiescence in cave passages that likely occurred when the primary water flow was diverted to parallel routes or the surface instead of sinking into the cave. This includes remnant bodies of secondary calcite in the phreatic Star Chamber level, where numerous rimstone dams up to 0.75 m tall are neatly bifurcated above narrow Carotene Canyon below. Calcite deposits are also prominent in Carotene Canyon approximately 1 m above the primary stream (Fig. 5) and within the modern stream, where speleothems are being actively eroded.

Scallops in canyons document little variation in discharge or velocity through elevation, and thus time, suggesting that the magnitude of scallop-forming flood events has not changed through time. This finding is in general accord with those of Despain and Stock (2005) from Crystal Cave, and also those of Lauritzen et al. (1983; 1985), who found that modern scallops in Norwegian caves preserved flood discharges three times larger than mean annual discharges.

Even though our methods produce maximum values for paleo-discharge, current high flow measurements three to five orders of magnitude lower than paleo-discharge calculations warrant discussion. Paleo-flow calculations are reasonable under the circumstances of the development of this cave in this environment. Clearly, clasts and the scallop measurements represent very large flood events. Past greater discharges likely reflect different climatic conditions; the present warm and dry Holocene climate of the Sierra Nevada differs markedly from the cooler, wetter climates of glacial times that dominated most of the past ~2 Myr (e.g., Benson and Thompson, 1987; Hostetler and Clark, 1997; Bartlein et al., 1998; Clark et al., 2003). Paleo-flows of similar magnitude are documented in Crystal Cave by both scallops and cobbles in three locations (Ensantina Passage, Entrance Passage, and Phosphorescent Room) and in HCC by both scallops and cobbles in the Star Chamber and Betelgeuse Balcony. Sediments in abandoned passages derive from the final fluvial inundation at that elevation

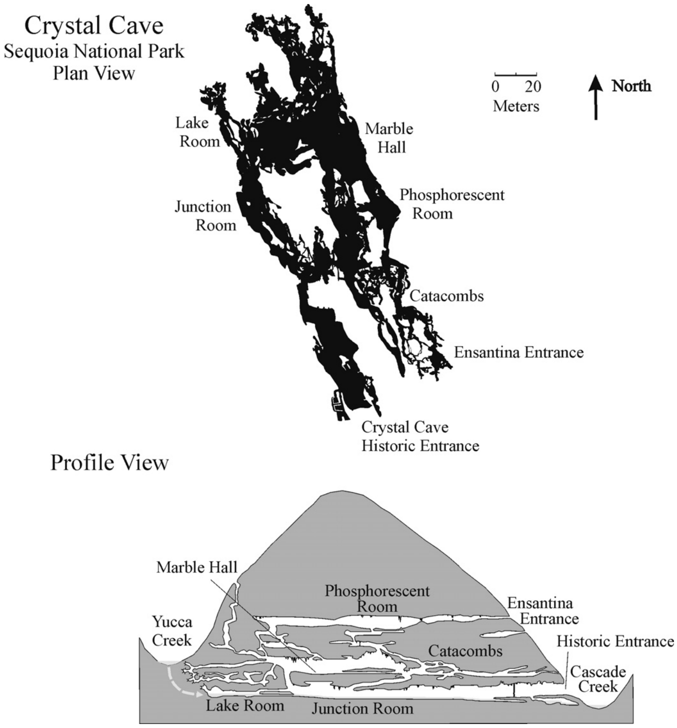

Figure 9. Plan and profile maps of Crystal Cave for comparison to Hurricane Crawl.

and so are likely to be produced by very large flood events that could carry large clasts. While paleo conduits and cave entrances of the size needed to transport such a flood event are not common in the southern Sierra, they do exist at caves such as Alto, Lilburn, and Panorama. Passages at the same elevation in maze complexes in Crystal, Lilburn, and White Chief caves have the collective capacity for floods of the size documented in HCC.

A western system parallel to the known cave passage is inferred from sink and rise points for the primary cave stream on the western margin of known cave passages upstream of Pumpkin Palace, a stream bifurcation to the west in Carotene Canyon below Pumpkin Palace, and the apparent continuation of a calcite-choked passage north from the Pleiades and west of known passages.

COMPARISON TO CRYSTAL CAVE

The basin of the North Fork of the Kaweah contains a number of large cave systems, including the longest in the state, Lilburn Cave (Tinsley, et al., 1981; Bosted, et al, 2003), as well as HCC, Crystal Cave, and many others. HCC and Crystal Cave are formed in vertically bedded host rock and are similar in length, depth, and age (Despain and Stock, 2005). However, they display different geomorphic features. Most of Crystal Cave is composed of anastomotic mazes with a few larger rooms, many passage junctions, and several distinct levels (Fig. 9). Crystal has no network mazes. Only a few canyons occur, and these are generally short (< 30 m) and steep ($12°$ to $25°$) and connect multiple low-gradient horizontal levels.

Both caves have numerous steep vadose passages developed when knickpoints migrated past downstream cave entrances, lowering the local base level and causing erosion and stream down-cutting inside the caves. Horizontal passages developed at several levels within Crystal Cave, while HCC contains one. These low-gradient passages would have developed once the cave stream had reached base level, before the next knickpoint migrated past. The smaller stream in Hurricane Crawl eroded to base level one time, while this happened at least four times in Crystal Cave (Despain and Stock, 2005).

Crystal Cave has copious granitic sediments with particle sizes that vary from large cobbles to clay. Sediments are seen on nearly all flat surfaces, including wall pockets, ledges, shelves, collapsed rocks, and ceiling and wall notches throughout the cave. Recharge conditions allowed large scale inundation by fluvial sediments throughout much of the cave's history. Crystal drains a basin 75 % larger than HCC and contains a larger stream that was likely even larger in the past. Both caves contain clasts and scallops that provide evidence for paleo-flows orders of magnitude larger than current discharges (Despain and Stock, 2005). Paleo-discharge and velocity data from both caves are similar in their range and mean (Table 6). Discharge values for both caves have a larger range than velocity, reflecting variations in conduit size and morphology. Both caves show paleo-discharge values from two to

Table 6. Comparison of Crystal and Hurricane Crawl paleo-velocity values, paleo-discharge values and means. Data were derived using the friction factor method.

		Velocity (v), $m^3\ s^{-1}$			Discharge, $m^3\ s^{-1}$		
Cave	Method	Min.	Max.	Mean	Min.	Max.	Mean
Crystal	Scallops	0.051	0.957	0.407	0.12	15.19	4.17
	Cobbles	0.85	5.32	2.65	0.01	39.06	8.36
	Mean	0.45	3.14	1.53	0.065	27.13	6.27
Hurricane	Scallops	0.78	2.91	1.44	0.15	38.51	4.18
	Cobbles	1.51	4.57	3.32	0.05	23.35	4.87
	Mean	1.15	3.74	2.38	0.1	30.93	4.53

five orders of magnitude above current discharge. Thus scallops and cobble in both caves reflect similar conditions for deposition of sediments and the formation of bedrock scallops—big floods.

Crystal Cave, while longer in surveyed passage length, developed as a shorter hydrologic system. The current transit of the cave stream through traversable cave passages is 225 m, while in HCC it is 475 m. More of Crystal is closer to its hydrologic input and more prone to seasonal flooding, a return to phreatic and paragenetic conditions, and large sediment loads and inundation that encourage widening of passages by meandering streams and parallel passage development as anastomotic mazes (Farrant and Smart, 2011; Palmer 1975; 1991). The HCC stream has a gradient of 10.3° and the Crystal Cave stream passage is 1.3°. The higher gradient has encouraged active stream downcutting and the development of vadose canyons continually throughout hundreds of thousands of years in HCC. The canyons contain almost no sediment storage capacity and are easily constricted and even completely blocked by calcite speleothems, which can form rapidly in HCC. Canyon calcite constrictions and areas of collapse reduce the throughput of sediment and starve downstream flows of sediment, further encouraging canyon development and more downcutting, provided base level has not been reached, in a positive feedback.

To summarize, HCC contains a wide variety of geomorphic forms and features developed over a minimum of 1.4 Ma. And although these features vary, they are well explained and understood by current theories of cave development, including the influences of hydrology, porosity, gradient, knickpoint migration, passage constrictions, and in particular, sediments. Flow conditions for scallop development agree with the results of other researchers (Lauritzen et al. 1983, 1985), and the cave's age correlates well with the age of other caves in the area (Despain and Stock, 2005). The varied morphologies of Hurricane Crawl and Crystal caves likely reflect different throughput capacities and budgets for sediment, but otherwise the caves share parallel geomorphic histories.

Acknowledgements

We wish to thank the many members of the National Speleological Society, Western Region, and the Cave Research Foundation, SEKI Operations Area, for volunteering their time to work on surveys, data collection, and photography in Hurricane Crawl and Crystal Caves. This paper would not have been possible without you. Photo in Figure 5 courtesy of Dick Laforge and photos in Figures 6 and 7 courtesy of Dave Bunnell.

References

Abu-Jaber, N., Hess, J.W., and Howcroft, W., 2001, Chemical erosion of the Lilburn Cave System, Kings Canyon National Park, California: Ground Water, v. 39, p. 223–229. doi:10.1111/j.1745-6584.2001.tb02303.x.

Bagnold, R.A., 1966, An approach to the sediment transport problem from general physics: U.S. Department of the Interior, U.S. Geological Survey Professional Paper 422-I, 37 p.

Bartlein, P.J., Anderson, P.M., Anderson, K.H., Edwards, M.E., Mock, C.J., Thompson, R.S., Webb, R.S., Webb III, T., and Whitlock, C., 1998, Paleoclimate simulations for North America for the past 21,000 years: features of the simulated climate and comparisons with paleoenvironmental data: Quaternary Science Reviews, v. 17, p. 549–585. doi:10.1016/S0277-3791(98)00012-2.

Bateman, P.C., and Clark, L.C., 1974, Stratigraphic and structural setting of the Sierra Nevada batholith, California: Pacific Geology, v. 8, p. 79–89.

Benson, L.V., and Thompson, R.S., 1987, The physical record of lakes in the Great Basin, *in* Ruddiman, W.F., and Wright, H.E., Jr., eds., North America and Adjacent Oceans during the Last Deglaciation: Boulder, Geological Society of America, Geology of North American series K-3, p. 241–259. doi:10.1130/DNAG-GNA-K3.241.

Bogli, Alfred, 1964, Corrosion par mélange des eaux: International Journal of Speleology, v.1, p. 61–70.

Bosted, P., Hacker, B., Despain, J., and Tinsley, J., 2003, Lilburn Cave Atlas, Tulare County, California: Cave Research Foundation, 90 p.

Clark, P.U., Weaver, A.J., and Mirovica, J.X., 2003, Ice sheet forcing of abrupt climate change: Lessons from the last deglaciation: Geophysical Research Abstracts, v. 5, #8091.

Curl, R.L., 1974, Deducing flow velocity in cave conduits from scallops: NSS Bulletin, v. 36, no. 2, p. 1–5.

Despain, J., 1999, A summer of discovery in Hurricane Crawl Cave: NSS News, v. 57, p. 170–173.

Despain, J., and Fryer, S., 2002, Hurricane Crawl Cave: A GIS-based cave management plan analysis and review: Journal of Cave and Karst Studies, v. 64, p. 71–76.

Despain, J.D., and Stock, G.M., 2005, Geomorphic history of Crystal Cave, Southern Sierra Nevada, California: Journal of Cave and Karst Studies, v. 67, p. 92–102.

Farrant, A.R., and Smart, P.L., 2011, Role of sediment in speleogenesis; sedimentation and paragenesis: Geomorphology, v. 134, p. 79–93. doi:10.1016/j.geomorph.2011.06.006.

Fish, L., 2013, Compass Caving Mapping Software Package by Fountain Computer: http://fountainware.com/compass/.

Hostetler, S.W., and Clark, P.U., 1997, Climatic controls of western U.S. glaciers at the last glacial maximum: Quaternary Science Reviews, v. 16. p. 505–511. doi:10.1016/S0277-3791(96)00116-3.

Lauritzen, S.-E., Ive, A., and Wilkinson, B., 1983, Mean annual runoff and the scallop flow regime in a subarctic environment: Preliminary Results from Svartisen, North Norway: Cave Science: The Transactions of the British Cave Research Association, v. 10, p. 97–102.

Lauritzen, S.-E., Abbott, J., Arnesen, R., Crossley, G., Grepperud, D., Ive, A, and Johnson, S., 1985, Morphology and hydraulics of an active phreatic conduit: Cave Science: The Transactions of the British Cave Research Association, v. 12, p. 139–146.

Nokleberg, W.J., 1983, Wallrocks of the Central Sierra Nevada Batholith, California: a Collage of Accreted Tectono-Stratigraphic Terranes: U.S. Department of the Interior, Geological Survey Professional Paper 1255, 28 p.

Palmer, A.N., 1975, The origin of maze caves: NSS Bulletin, v. 37, p. 56–76.

Palmer, A.N., 1987, Cave levels and their interpretation: NSS Bulletin, v. 49, p. 50–66.

Palmer, A.N., 1991, Origin and morphology of limestone caves, Geological Society of America Bulletin, v 103, p. 1–21. doi:10.1130/0016-606(1991)103<0001: OAMOLC>2.3.CO;2.

Saleeby, J.B., Goodin S.E., Sharp, W.D., and Busby, C.J., 1978, Early Mesozoic paleotectonic-paleogeographic reconstruction of the southern Sierra Nevada region, *in* Howell, D.G. and McDougal, K.A. eds., Mesozoic Paleogeography of the Western United States: Los Angeles, Society of Economic Paleontologists and Mineralogists, Pacific Section, Pacific Coast Paleogeography Symposium 2, p. 311–336.

Sasowsky, I.D., and White, W.B., 1994, The role of stress release fracturing in the development of cavernous porosity in carbonate aquifers: Water Resources Research, v. 30, p. 3523–3530. doi:10.1029/94WR01727.

Shelton, L.R., 1994, Field Guide for Collecting and Processing Stream-Water Samples for the National Water-Quality Assessment Program:

U.S. Department of the Interior, Geological Survey Open-File Report 94-455, 50 p.

Shields, A., 1936, Application of similarity mechanics and turbulence research to bedload movement: Pasadena, California Institute of Technology, Hydrodynamics Laboratory publication 167, 44 p. (translation by Ott, W.P., and van Uchelen, J.C., of Anwendung der Ähnlichkeitsmechanik und der Turbulenzforschung auf die Geschiebebewegung: Mitteilungen der Preußischen Versuchsanstalt für Wasserbau und Schiffbau, v. 26.)

Sisson, T.W. and Moore, J.G., 1994, Geologic map of the Giant Forest quadrangle, Tulare County, California: U.S. Geological Survey geologic quadrangle 1751, 1 sheet, scale 1:62,500.

Smart, P.L., and Brown, M.C., 1973, The use of activated carbon for the detection of the tracer dye Rhodamine WT: Proceedings of the Sixth International Speleological Congress, v. 4, p. 285–292.

Stock, G., 1999, Discovery of the Pleiades: NSS News, v. 57, p. 175–180.

Stock, G.M., Anderson, R.S., and Finkel, R.C., 2004, Pace of landscape evolution in the Sierra Nevada, California, revealed by cosmogenic dating of cave sediments: Geology, v. 32, p. 193–196. doi:10.1130/G20197.1.

Stock, G.M., Anderson, R.S., and Finkel, R.C., 2005a, Rates of erosion and topographic evolution of the Sierra Nevada, California, inferred from cosmogenic ^{26}Al and ^{10}Be concentrations: Earth Surface Processes and Landforms, v. 30, p. 985–1006. doi:10.1002/esp.1258.

Stock, G.M., Granger, D.E., Sasowsky, I.D., Anderson, R.S., and Finkel, R.C., 2005b, Comparison of U-Th, paleomagnetism, and cosmogenic burial methods for dating caves: Implications for landscape evolution studies: Earth and Planetary Science Letters, v. 236, p. 388–403. doi:10.1016/j.epsl.2005.04.024.

Tinsley, J.C., DesMarais, D.J., McCoy, G., Rogers, B.W., and Ulfeldt, S.R., 1981, Lilburn Cave's contribution to the natural history of Sequoia and Kings Canyon National Parks, California, USA, *in* Beck, B.F., ed., Proceedings of the Eighth International Congress of Speleology, volume 1, p. 287–290.

Tobin, B.W., and Schwartz, B.F., 2012, Quantifying concentrated and diffuse recharge in two marble karst aquifers: Big Spring and Tufa Spring, Sequoia and Kings Canyon National Parks, California, USA: Journal of Cave and Karst Studies v. 74, p. 186–196. doi:10.4311/2011 JCKS0210.

Tobin, B.W., 2013, Contributions of karst groundwater to water quality and quantity in a mountain river basin: the Kaweah River, Sequoia and Kings Canyon National Parks, California [PhD dissertation], San Marcos, Texas State University, 182 p.

USGS, 2015, USGS California StreamStats: United States Geological Survey, http://streamstatsags.cr.usgs.gov/ca_ss/default.aspx?stabbr=ca&dt=1428119007693 [accessed March 19, 2015].

Urzendowski, Linda, 1993, Spectral analysis of the flow behavior of Big Spring, Kings Canyon National Park, California [MS thesis], Las Vegas, University of Nevada, 122 p.

White, W.B., 1988, Geomorphology and Hydrology of Karst Terrains: New York, Oxford University Press, 464 p.

A.E. Edwards, E. Johnson, J.L. Coor, C.H. Jagoe, A. Sachi-Kocher, and W.F. Kenney – Historical record of atmospheric deposition of metals and $\delta^{15}N$ in an ombrotrophic karst sinkhole fen, South Carolina, USA. *Journal of Cave and Karst Studies*, v. 78, no. 2, p. 85–93. DOI: 10.4311/2014ES0109

HISTORICAL RECORD OF ATMOSPHERIC DEPOSITION OF METALS AND $\delta^{15}N$ IN AN OMBROTROPHIC KARST SINKHOLE FEN, SOUTH CAROLINA, USA

AMY E. EDWARDS[1]*, ELIJAH JOHNSON[2], JENNIFER L. COOR[3], CHARLES H. JAGOE[2], AFI SACHI-KOCHER[4], AND WILLIAM F. KENNEY[5]

Abstract: Radiometric ^{210}Pb dating, metal concentrations [As, Cd, Cr, Cu, Hg, Pb and Zn] and nitrogen-isotope ($\delta^{15}N$) analyses were conducted on a sediment core from an ombrotrophic karst sinkhole fen in South Carolina, USA, to obtain a historical record of nitrogen signatures and atmospherically deposited metals from increased anthropogenic emissions during the last several decades. Sinkhole fens in carbonate karst terrains are excellent environs for sediment core dating and metal analysis due to the low background metal concentrations in carbonates, as well as the alkaline nature of carbonates and the high organic-matter content in fens, both of which reduce mobility of metals in soils. Metal concentrations were found for the top twenty 1 cm intervals of the core and the bottom at 56 cm. Intervals 21–55 cm were analyzed only for Hg and organic-matter content due to financial constraints. The sinkhole fen in the study is ombrotrophic and receives metal inputs primarily through wet and dry atmospheric deposition, and the 20 cm deep sample had a ^{210}Pb CRS age of 1954. Metals with significant ($p < 0.05$) negative correlations with core depth were (negative correlation, sample size): Hg (−0.8948, n = 56), Pb (−0.9308, n = 21), Zn (−0.6299, n = 21), Cd (−0.5023, n = 21), and Cu (−0.5156, n = 21). In view of the low background concentrations of these five metals from limestone found in the sinkhole, atmospheric deposition from anthropogenic emissions is likely the predominant source for these increasing concentrations. As (+0.4431, n = 21) had a significant ($p < 0.05$) positive correlation with core depth, while Cr (+0.2761, n = 21) was the only metal with no significant correlation with core depth. Although $\delta^{15}N$ is shown in other studies to deplete upward in sediment cores due to increasing reactive nitrogen emissions, the sinkhole core in this study had no significant correlation (+0.2580, n = 21) between $\delta^{15}N$ and depth. Total carbon, total nitrogen, total phosphorus, and organic-matter content were also measured in intervals 1–20 and 56 cm and found to have several significant ($p < 0.05$) correlations with depth, metals, and $\delta^{15}N$.

INTRODUCTION

Anthropogenic activity has greatly impacted the regional and global cycling of trace metals in the soil, water, and atmosphere (Nriagu and Pacyna, 1988). Numerous industrial processes, such as coal and oil combustion, mining, cement production, refuse incineration, and phosphate application release metals (e.g., As, Cd, Cr, Cu, Hg, Pb, and Zn) into the environment, and fluxes of metals in the atmosphere have increased since the Industrial Revolution (Nriagu and Pacyna, 1988). Metals are capable of long distance atmospheric transport far away from emission sources, as they are found in the sediment record even in remote locations such as Antarctica (Wolff et al., 1999) and the Arctic (McConnell and Edwards, 2008).

Numerous studies have used radioactive isotopes such as ^{14}C, ^{210}Pb, and ^{137}Cs to find the historical concentrations of atmospherically deposited metals in various sediment types, including peats (Madsen, 1981; Shotyk et al., 1996; Marx et al., 2010), ice cores (Hong et al., 1994; Schuster et al., 2002), lacustrine sediment (Renberg et al., 2002), bat and bird guano deposits (Petit, 1977; Yan et al., 2011), and a sinkhole fen in karst terrane (Hettwer et al., 2003). The sinkhole fen in Eastern Europe (Hettwer et al., 2003) had enrichments of Pb, Zn, Cu, and Cd in a 13 m core of ~5000-years age that correlated with historical periods of smelting.

The majority of these studies used cores from peat bogs and lakes, but sinkhole fens have several characteristics that give them advantages over other sediment types (Hettwer et al., 2003): Carbonate terranes have low background concentrations of most elements. Limestone and dolomite terranes usually have neutral pH values between

* Corresponding author: aeedwards@hanovercounty.gov
[1] Hanover County Government, VA, 23116, USA
[2] Florida A&M University, School of the Environment, Tallahassee, FL, 32307, USA
[3] U.S. Army Corps of Engineers, Jacksonville, FL, 32207, USA
[4] The National High Magnetic Field Laboratory, Florida State University, Tallahassee, FL, 32306, USA
[5] Land Use and Environmental Change Institute, University of Florida, Gainesville, FL, 32611, USA

6.5 and 8.9 due to the alkaline nature of carbonates, and this inhibits the migration of cations (Ford and Williams, 1989), preserving the depth profile of heavy metals. The high organic matter content of fens also prevents the migration of heavy metal cations within the profile, since organic matter in soils is known to be a sorbent for metals, especially mercury (He et al., 2007; Nie et al., 2012), lead (Wang and Benoit, 1996; Shotky et al., 1996), and zinc (Dabkowska-Naskret, 2003). The ombrotrophic nature of a sinkhole ensures that most metal deposition is atmospherically derived, with minimal inputs from surface and groundwater. Metals transported from the bedrock into the sinkhole fen by groundwater can be determined from analysis of the bedrock.

Anthropogenic activity has also increased emissions of reactive nitrogen (Nr). Nr, comprising forms of nitrogen other than unreactive N_2 gas, such as NH_3, NH_4^+, NOx, HNO_3, N_2O, NO_3^-, urea, and proteins, in the atmosphere and biosphere has increased 120 % since 1970, mainly from agriculture and fossil fuel energy sources (Galloway et al., 2008). The additional Nr from increasing nitrogen and particle emissions is being distributed globally, predominantly by atmospheric transport and deposition (Galloway et al., 2008). Nr in the sediment record from anthropogenic sources has depleted concentrations of ^{15}N relative to ^{14}N ($\delta^{15}N$) compared to natural sources (Heaton et al., 2004). Research has shown the $\delta^{15}N$ values of dated sediment deposits to have decreased $\delta^{15}N$ values from the past to present, corresponding to a rise in Nr emissions. Holtgrieve et al. (2011) analyzed $\delta^{15}N$ in dated sediment cores from 25 lakes in the northern hemisphere. These lakes, in remote watersheds, were far from emission sources. Yet the isotopic signature of the lake sediment cores still showed a consistent decrease in $\delta^{15}N$ beginning in 1895 $\pm$ 10 years. Most literature on isotopes in cave and karst settings focuses on isotopes in springs and groundwater, not sediment. A study by Nold et al. (2013) used nitrogen-isotope analysis in sinkhole cores, but the core was from an underwater sinkhole in Lake Huron, and not an ombrotrophic, terrestrial sinkhole.

In this study, a sediment core from an ombrotrophic karst sinkhole fen in South Carolina, USA, was used to obtain a historical record of atmospheric deposition of metals and $\delta^{15}N$ associated with anthropogenic activity during the last several decades. The core was dated with ^{210}Pb and analyzed for $\delta^{15}N$, arsenic (As), cadmium (Cd), chromium (Cr), copper (Cu), mercury (Hg), lead (Pb), and zinc (Zn). Total carbon (TC), total nitrogen (TN), total phosphorus (TP), and organic matter content were analyzed for each interval to discern any relationship between these parameters with metal concentrations and $\delta^{15}N$ values.

The objectives of this study were to determine whether a sinkhole fen in South Carolina, having neutral pH values, high organic matter content, an ombrotrophic nature, and low lithogenic background concentrations, could preserve an archive of metal emissions from atmospheric sources and to compare changes in $\delta^{15}N$ with age and depth to results from other studies around the world.

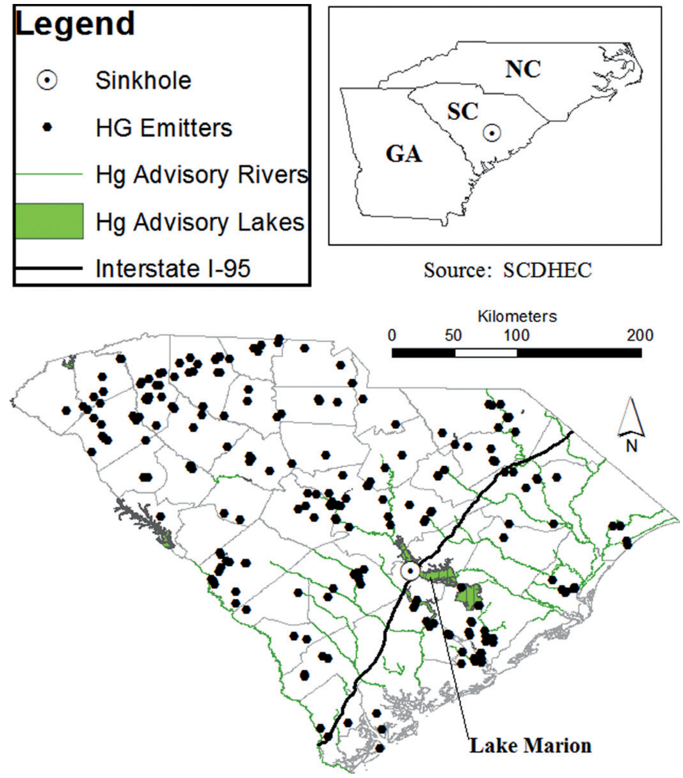

Figure 1. Location map for sinkhole in South Carolina, USA, displaying facilities with South Carolina Department of Health and Environmental Control permits under Title V for mercury emissions and lakes and streams with 2000–2006 fish advisories for mercury in South Carolina. (Source: SCDHEC, 2014; SCDHEC, 2013).

SITE DESCRIPTION

The core used in this study (N 33.49694°, W 80.47863°) was taken in a sinkhole located near Lake Marion in Santee State Park, Santee, South Carolina (Fig. 1). Karst topography in this region is developed in the carbonate Santee Limestone of Eocene age, with Holocene to Pleistocene sinkhole deposits consisting of quartz sands, clay, and humic matter in the Upper Duplin Formation, which overlies the Santee Limestone (Willoughby, 2002). The sinkhole is in a pine and hardwood forest, and the bottom of the sinkhole has experienced both dry and standing water conditions. The sinkhole fen karst feature has no surface drainage basin and is isolated from surface water other than precipitation. A 2009–2010 study of the watershed in which the sinkhole is contained measured pH values from surface and groundwater in the range of 6.6 to 7.6 (Edwards et al., 2013).

A long term sampling program measuring Hg from atmospheric deposition found high concentrations of the metal in the southeastern United States (NADP, 2014), representing the combined local, regional, and global sources of natural and anthropogenic Hg. Of the natural sources of mercury such as volcanoes, erosion, and forest fires, forest fires are likely the most common natural source to the sinkhole, as 67 % of the land area in South Carolina is forest (SCFC, 2015) and Santee State Park undergoes prescribed burns. Anthropogenic emissions in the region are predominantly from point sources, including coal-powered electric plants, cement plants, and paper and pulp mills, as well as from non-point sources such as open burning and mobile sources like roads and airports (SCHDEC, 2010). The major highway I-95, which passes about 2 miles from the sinkhole, was constructed in the 1960s and is a local anthropogenic source of emissions to the sinkhole. Figure 1 shows the sinkhole's location and the facilities regulated under Title V of the Clean Air Act by the South Carolina Department of Health and Environmental Control (SCDHEC) for mercury emissions (SCDHEC, 2014). Figure 1 also shows the streams and water bodies near the sinkhole where numerous 2000–2006 fish advisories were due to the bioaccumulation of anthropogenic Hg in aquatic systems.

Wind roses representing 52 years of weather data spanning the 1940s through the 1990s from two weather stations in the lower half of the state of South Carolina show the predominant wind speed and direction are 2 to 6 meters per second in the northeastern and southwestern directions (WSRC, 2002).

Materials and Methods

Core Collection and Sampling

The core used in this study was a 7.62 cm diameter, 56 cm long core (N 33.49694°, W 80.47863°) collected on November 24, 2012. A piece of limestone rock found in a second core (N 33.49694°, W 80.47862°) was analyzed for metal concentrations to estimate lithogenic background. The core sediment was fine and coarsening downwards, with root and plant fragments throughout. The Munsell color of the top 28 cm was 2/1 black, and the bottom 28 cm was 2.5 N black. The core was subsampled at 1 cm intervals for the whole length of the core. Interval 1 represented the top 1 cm of the core, and 56 represented the last interval at the bottom. Three-quarters of the bulk sample for each interval for intervals 1–20 and the last interval, 56, were oven dried overnight at 80 °C and used for analyses of the metals As, Cd, Cr, Cu, Pb, and Zn. Intervals 1–20 were also used for ^{210}Pb dating. The remaining bulk of each interval was later freeze-dried to a constant weight with the Labconco Freeze Dry System/Freezone 4.5 and used for analysis of total carbon, total nitrogen, total phosphorus, and δ^{15}N for intervals 1–20 and 56 and for organic matter and Hg for all intervals 1–56. Only Hg and organic matter content were analyzed for all 56 intervals due to financial constraints.

Analytical Methods

Core samples for radiometric ^{210}Pb dating were oven dried overnight at 80 °C and dated using ^{210}Pb by gamma spectrometric determination (Appleby, 2008). The software program CoreCal2 (Shukla, 2002) was used to find the ^{210}Pb date of each sample using the Constant Rate of Supply model. After oven drying, aliquots of 0.5 to 1.0 g of dry sample were packed and sealed in plastic vials and used for gamma-count measurement for ^{210}Pb, ^{137}Cs, and ^{226}Ra. Porosity for each interval was calculated by first using percent moisture and estimated grain density (2.45 g cm^{-3}) to find the bulk density (g cm^{-3}). Then the bulk density was subtracted from the estimated grain density and divided by the estimated grain density. The core interval, porosity, and excess ^{210}Pb in pCi g^{-1} were entered into the CoreDat2 program to find the CIC-Age (yr) and CRS-Age (yr). The Constant Rate of Supply (CRS) method was chosen to present radiometric results. This method lets the sediment supply vary while assuming a constant ^{210}Pb flux, which has remained constant over the last 100 years (Uottawa, 2013). The year for each interval was then calculated by subtracting the CRS age from the year 2012, the year the cores were obtained. (See supplemental material).

Total carbon and total nitrogen were analyzed on a Carlo Erba NA1500 CNHS Elemental Analyzer. Total phosphorus was measured with an Auto Analyzer for soluble reactive phosphorus by the methods in Schelske et al. (1986). All differences in replicate analyses for TC, TN, and TP were < 10 %. Nitrogen-isotope (^{15}N and ^{14}N, as δ^{15}N) analysis was conducted on a Thermo Electron Delta V Advantage isotope-ratio mass spectrometer coupled with a ConFlo II interface linked to a Carlo Erba NA 1500 CNS Elemental Analyzer. All nitrogen isotopic results are expressed in standard delta notation relative to air.

The metals As, Cd, Cr, Cu, Pb, and Zn underwent a series of acid digestions in the clean lab at the National High Magnetic Field Laboratory. Samples from each 1 cm interval from depths of 1–20 and 56 cm and from the limestone rock were analyzed for As, Cd, Cr, Cu, Pb and Zn using an Agilent 7500cs Quadrupole Inductively Coupled Plasma Mass Spectrometer (Q-ICP-MS) equipped with an Octopole Collision/Reaction Cell. Samples from each 1 cm interval for all core depths of 1–56 cm and the limestone sample were analyzed for total mercury, with blanks and duplicates (all within 10 %), and a standard (srm 1515 apple), using a Milestone DMA80 mercury analyzer that uses thermal decomposition, gold amalgamation, and atomic adsorption spectroscopy (EPA Test Methods SW-846 method 7473). All differences in replicate analyses for metals were < 10 %.

Organic matter was determined for each 1 cm interval from 1–56 and the limestone sample using ASTM D 2974 Standard Test Methods for Moisture, Ash and Organic

Table 1. Results for Pb-210 dating, nutrients, $\delta^{15}N$, organic-matter content, and trace metals in the sinkhole core and limestone (LS) rock sample.

Depth (cm)	Pb-210 (CRS-date)	$\delta^{15}N$ (%)	TN (Wt. %)	TP (mg g^{-1})	TC (Wt. %)	OM (%)	As (ppm)	Cu (ppm)	Cr (ppm)	Cd (ppm)	Hg (ppb)	Pb (ppm)	Zn (ppm)
1	2011	1.13	2.28	1.07	28.74	58	2.10	16.31	6.14	0.82	256.3	27.96	50.54
2	2007	0.60	2.32	0.97	29.98	59	1.87	14.14	5.87	0.52	257.5	25.47	46.70
3	2004	0.72	2.32	0.87	30.87	63	1.78	12.66	5.03	0.45	251.3	23.21	45.15
4	2002	0.58	2.29	0.84	31.17	60	1.63	12.47	4.67	0.44	258.1	22.05	45.53
5	1998	0.74	2.32	0.87	30.74	53	1.43	11.62	4.50	0.49	250.1	20.11	42.70
6	1994	0.36	2.13	0.82	33.88	68	1.56	12.03	5.47	0.51	238.2	21.69	43.52
7	1990	0.22	1.80	0.60	37.76	69	1.35	8.14	3.48	0.36	250.2	17.34	35.34
8	1987	0.51	1.97	0.58	32.63	57	1.85	9.62	4.88	0.47	221.5	19.61	42.83
9	1985	0.82	1.76	0.66	30.07	57	1.56	9.27	4.71	0.47	200.5	15.60	42.52
10	1983	0.81	1.75	0.68	27.36	51	1.53	8.58	4.76	0.45	213.5	14.33	35.73
11	1981	0.54	1.79	0.69	33.29	64	1.83	11.60	5.38	0.56	200.4	18.40	54.75
12	1980	0.56	1.90	0.80	30.84	61	2.15	12.49	5.82	0.46	233.9	18.40	48.51
13	1978	0.80	1.86	0.79	30.30	60	1.79	10.63	5.53	0.50	189.0	17.41	46.02
14	1977	0.74	1.89	0.85	29.69	57	2.18	11.23	5.26	0.52	209.9	15.67	41.38
15	1975	0.79	1.86	0.91	29.54	57	2.53	14.96	5.85	0.50	206.2	15.41	42.72
16	1971	0.81	1.79	0.97	28.73	56	2.61	12.00	5.92	0.36	198.0	14.62	41.07
17	1966	0.94	1.87	0.95	29.87	59	2.41	10.34	5.77	0.36	219.3	13.34	40.56
18	1963	0.83	1.76	0.78	30.70	57	2.42	10.13	6.93	0.44	193.7	13.92	40.00
19	1959	0.54	1.59	0.79	29.36	54	2.29	9.89	6.42	0.46	168.6	13.05	37.26
20	1954	0.65	1.50	0.86	30.48	59	2.29	9.19	5.85	0.33	126.5	11.23	31.52
56	...	0.89	0.73	1.06	27.38	53	0.54	5.63	4.40	0.23	26.9	3.30	12.66
LS	...	...	...	...	...	4	3.50	3.67	48.00	0.23	15.2	16.10	11.93

Notes: TN = total nitrogen, TP = total phosphorous, TC = total carbon, and OM = organic-matter content.

Matter of Peat and Organic Soils (ASTM, 2013), with the exception of using 430 °C instead of 550 °C. The temperature below the dissociation temperature of calcium carbonate was used, as by Hettwer et al. (2003), because the core came from a sinkhole in carbonate terrane. A few samples were also ashed at 530 °C, and a < 2.4 % change occurred. Blanks and duplicates, all within 4 %, were included. The distribution of the data was not normal, so multivariate correlations were calculated using the nonparametric Spearman's correlation coefficients using the SAS program JMP 11.

Results

Results of ^{210}Pb dating by the CRS method (Table 1) indicate that the 20 cm interval was deposited in 1954. The 20 cm interval still contained excess ^{210}Pb (excess lead in the 20 cm interval means that we could have gone deeper into the core and still found some ^{210}Pb).

Metal concentrations for the uppermost 20 cm and the interval at the bottom of the core (56 cm) varied with parameter and depth and ^{210}Pb dating (Table 1). Values in the core ranged: As (0.54 to 2.61 ppm), Cd (0.23 to 0.82 ppm), Cr (3.48 to 6.93 ppm), Cu (5.63 to 16.31 ppm), Pb (3.30 to 27.96 ppm), and Zn (12.66 to 54.75 ppm). Complete data for Hg and organic matter content, which were measured for all 56 1 cm intervals in the core, are shown in Table 2. Ranges were 11.0 to 258.1 ppb for mercury concentrations and 28 to 69 % for organic matter content. The metals As, Cr, and Pb had concentrations in the limestone sample that exceeded the highest values in the core (Table 1).

Results for total carbon, total nitrogen, and total phosphorus, as well as $\delta^{15}N$, are also shown in Table 1. Values in the core ranged: TC (27.36 to 37.76 wt. %), TN (0.73 to 2.32 wt. %), TP (0.58 to 1.07mg g^{-1}), and $\delta^{15}N$ (0.22 to 1.13 ‰). Although previous studies have shown $\delta^{15}N$ to decrease upward in sediment cores due to increasing reactive nitrogen emissions, this was not the case for this sinkhole core, which had a no significant ($p < 0.05$) (0.2580, n = 21) correlation with increasing depth (Table 3).

Data for all parameters as a function of depth in the core are shown in Figure 2. Five metals had significant ($p < 0.05$) negative correlations with depth, as shown in Table 3. These were Hg (−0.8948, n = 56), Pb (−0.9308 n = 21), Zn (−0.6299, n = 21), Cd (−0.5023, n = 21) and Cu (−0.5156, n = 21). As (+0.4431, n = 21) had a significant ($p < 0.05$) positive correlation with core depth, while Cr (+0.2761, n = 21) was the only metal with no significant correlation with core depth. Significant ($p < 0.05$) correlations occurred between total nitrogen and depth (−0.8018), TN

Table 2. Results for S1 core for mercury (Hg) and organic-matter content (OM).

Depth, cm	Hg, ppb	OM, %
1	256.3	58
2	257.5	59
3	251.3	63
4	258.1	60
5	250.1	53
6	238.2	68
7	250.2	69
8	221.5	57
9	200.5	57
10	213.5	51
11	200.4	64
12	233.9	61
13	189.0	60
14	209.9	57
15	206.2	57
16	198.0	56
17	219.3	59
18	193.7	57
19	168.6	54
20	126.5	59
21	159.6	53
22	153.7	55
23	121.5	54
24	122.5	53
25	104.2	53
26	74.3	46
27	74.0	28
28	55.7	33
29	39.9	34
30	53.4	38
31	48.7	41
32	46.3	43
33	44.3	41
34	46.4	42
35	41.9	41
36	43.4	41
37	40.0	40
38	42.9	42
39	37.7	43
40	39.4	44
41	31.9	43
42	31.2	42
43	36.1	47
44	33.9	45
45	35.1	46
46	27.0	48
47	25.0	45
48	11.0	47
49	16.1	48
50	14.6	49
51	12.8	40
52	18.3	40
53	22.0	41
54	22.5	43
55	20.8	40
56	26.9	38

and Hg (+0.8611), TN and Cd (+0.4760), TN and Cu (+0.7348), TN and Pb (+0.8877), and TN and Zn (+0.6847). Other significant ($p < 0.05$) correlations occurred between total carbon and $\delta^{15}N$ (−0.7117), TC and total phophorus (−0.4927), TC and organic matter content (+0.7490), TC and Pb (+0.4703), $\delta^{15}N$ and TP (+0.4785), $\delta^{15}N$ and organic-matter content (−0.5177), Pb and Zn (+0.8210), Pb and organic matter content (+0.4925), Pb and Hg (+0.8334), Pb and Cd (+0.6207), Pb and Cu (+0.6931), organic matter content and Zn (+0.4956), Zn and Hg (+0.5143), Zn and Cd (+0.7309), Zn and Cu (+0.7753), Hg and Cu (+0.5584), As and Cr (+0.8447), and Cd and Cu (+0.5603).

Discussion

Ombrotrophic Karst Fens

Results show that the sinkhole fen in South Carolina in this study, with its neutral pH values, high organic matter content, ombrotrophic nature, and low lithogenic background concentrations, was a suitable archive for recording the historical record of Hg, Pb, Zn, Cd, and Cr emissions from atmospheric sources. The metals with significant ($p \leq 0.05$) negative correlation with depth in the core (Hg, Pb, Zn, Cd, and Cu) had lithogenic concentrations that were low relative to the measured values for these metals in the top 20 cm of the core, suggesting that the major source is atmospheric and not lithogenic. Hg in the limestone sample was 15.2 ppb, which is 17 times less than the highest concentration (258.1 ppb) near the top of the core. Arguments for diagenetic processes and local geological sources have been made to explain Hg concentrations in lake and peat cores, but multiple studies around the world show increases in Hg flux that are consistent with local and global historical emissions and not with diagenetic or geologic processes (Fitzgerald et al., 1998). As had a significant ($p \leq 0.05$) positive correlation with depth and Cr had no significant correlation with depth. As and Cr, with higher lithogenic background concentrations than the highest values in the core, have sources that are more likely from bedrock and soil formation than atmospheric deposition. This suggests that the Hg, Pb, Zn, Cd, and Cu profiles reflect increasing emissions during the last several decades (longer for Hg) from local, regional, or global sources. The negative correlations between depth and metal concentrations show an overall increase up the core to present time,

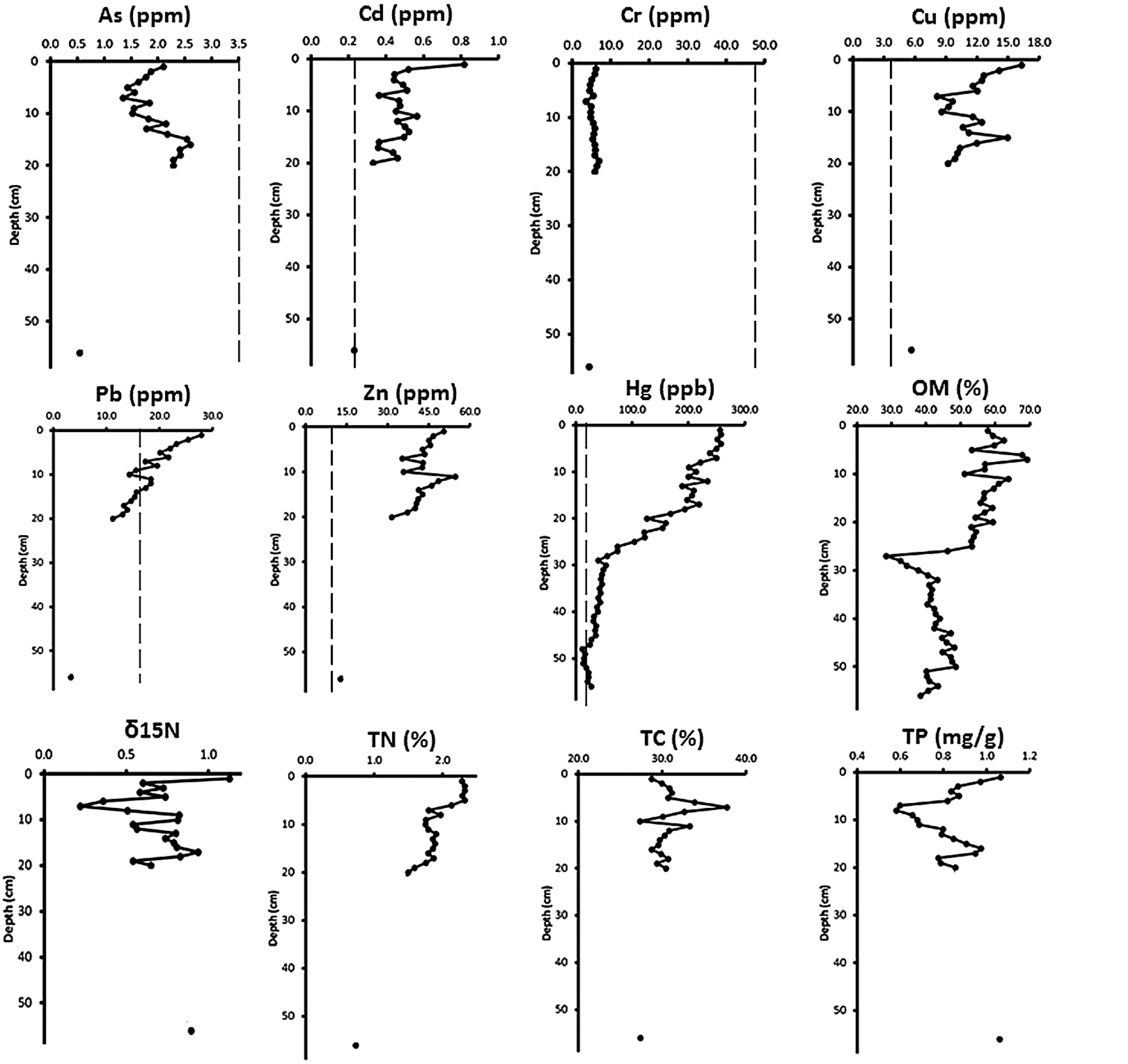

Figure 2. Relationships between analyzed parameters and depth. Dashed lines represent background concentrations in the limestone sample. Only Hg and organic matter content have complete data every centimeter of the 56 cm core; other parameters have uppermost centimeter intervals 1–20 and deepest interval at 56. Abbreviations, beside standard symbols for metal elements: OM, organic matter content; TN, total nitrogen; TC, total carbon; TP, total phosphorus.

with incremental concentrations affected by fluxes in emissions and variable wind speed, wind direction, temperature, and precipitation from year to year for the period of record in the core.

Although low background concentrations of metals and an alkaline pH were likely factors in limiting the downward migration of metals after atmospheric deposition, organic matter content was likely the most important factor in preventing migration of Hg, Pb, Zn, Cd, and Cu. Organic matter content in the core ranged from 28 to 69 %, which is much higher than the typical 0.3 to 10 % found in ombrotrophic peats (Allan et al., 2013). Organic matter content in soils has been shown to be a sorbent for Hg (Ravichandran, 2004; He et al., 2007; Nie et al., 2012). Although Hg and organic matter content in the core had no significant ($p \leq 0.05$) correlation, all five metals (Hg, Pb, Zn, Cd, Cu) with significant ($p \leq 0.05$) correlation with depth also had a significant correlation with total nitrogen. Organic matter is also known to be a sorbent for Pb (Wang and Benoit, 1996; Shotky et al., 1996), and Pb and organic matter content in the core had a significant ($p \leq$ 0.05) positive correlation. Studies also show complexation

Table 3. Spearman's Multivariate Correlations; bold indicates result is significant to $p < 0.05$; mercury (Hg) and organic–matter content (OM), n = 56; all other parameters, n = 21.

	Depth	$\delta^{15}N$	TN	TP	TC	OM	Hg	As	Cd	Cr	Cu	Pb	Zn
Depth	1.0000												
$\delta^{15}N$	0.2580	1.0000											
TN	**−0.8018**	−0.2215	1.0000										
TP	0.0130	**0.4785**	0.2606	1.0000									
TC	−0.3987	**−0.7117**	0.3957	**−0.4927**	1.0000								
OM	−0.3948	**−0.5177**	0.3855	−0.1884	**0.7490**	1.0000							
Hg	**−0.8948**	−0.2619	**0.8611**	0.1111	0.3857	0.4223	1.0000						
As	**0.4431**	0.1948	−0.1104	0.2644	−0.2891	−0.0898	−0.2794	1.0000					
Cd	**−0.5023**	−0.1477	**0.4760**	−0.0150	0.0938	0.1721	0.3062	0.0156	1.0000				
Cr	0.2761	0.1886	−0.0889	0.2958	−0.3144	−0.0347	−0.2332	**0.8447**	0.1874	1.0000			
Cu	**−0.5156**	−0.0195	**0.7348**	0.5050	0.0675	0.3090	**0.5584**	0.3255	**0.5603**	0.4001	1.0000		
Pb	**−0.9308**	−0.3202	**0.8877**	0.0735	**0.4703**	**0.4925**	**0.8334**	−0.2710	**0.6207**	−0.1144	**0.6931**	1.0000	
Zn	**−0.6299**	−0.1937	**0.6847**	0.0780	0.3416	**0.4956**	**0.5143**	0.0331	**0.7309**	0.1624	**0.7753**	**0.8210**	1.0000

Notes: TN = total nitrogen, TP = total phosphorous, TC = total carbon, and OM = organic-matter content.

between organic-matter content and Zn (Dabkowska-Naskret, 2003), and Zn in the core had a significant ($p \leq 0.05$) positive correlation. A hypothesis by Biester et al. (2012) suggested that disparities in Hg accumulation rates between lake and sediment cores could be due to peat decomposition and humification affecting trace metal concentrations. Metals may be redox sensitive, and mobility could increase with a change in redox conditions. However, many studies have shown that metal concentrations in dated cores correspond with historical emission records, indicating that biogeochemical processes are relatively insignificant, at least with respect to Pb (Biester et al., 2012) and Hg (Biester et al., 2012; Allen et al., 2013).

Mercury in South Carolina

The accumulation of Hg in the atmosphere, water, and soil is a health and environmental concern due to the metal's high toxicity and propensity to bioaccumulate in ecosystems. The southeastern United States, and South Carolina where the sinkhole is located, is an atmospheric mercury deposition hotspot (NADP, 2014) (Fig. 1), and 2000–2006 fish advisories cover rivers and lakes throughout the entire state, including Lake Marion near the sinkhole (SCDHEC, 2013). Figure 1 also shows mercury emitters under the Clean Air Act's Title V air permits in South Carolina (SCDHEC, 2014). Many emitters are in the coastal plain region, where the predominant wind directions carry atmospheric sources of Hg across the study site. Electric utilities are the dominant industrial point source of mercury in the state at 69 %, with steel mills, pulp and paper mills, cement kilns, and other sources also contributing (SCDHEC, 2010). Two recent studies of total mercury in surface sediments throughout South Carolina found concentrations ranged from 2 ppb to 162 ppb (Guentzel, 2009; Guentzel et al., 2012). The maximum total Hg in the sinkhole fen was 258.1 ppb. The higher values in the sinkhole are likely due to the ombrotrophic nature of the sinkhole, where the only loss of Hg would be volatilization. The sinkhole acts as an occasional wetland, as standing water has been observed in the sinkhole. Research in South Carolina has also shown that Hg tends to concentrate in watersheds with the highest percentage of wetlands (Guentzel, 2009), and fish with high levels of Hg are associated with areas with a high percentage of wetlands (Guentzel, 2009; Glover et al., 2010). The combination of elevated Hg in recent sediment in the sinkhole and fish advisories in Lake Marion supports the idea that Hg is an environmental concern in this region. Recent analysis of bat guano from Santee Cave, in close proximity to the sinkhole, gave values of 589.7 and 617.9 ppb (Edwards, unpublished data), and indicates that Hg bioaccumulation is also an issue in terrestrial wildlife.

$\delta^{15}N$ Signatures

Although other research (Holtgrieve et al., 2011) has shown the $\delta^{15}N$ values of dated sediment deposits to have a clear and continuous trend of decreasing $\delta^{15}N$ values since the beginning of the twentieth century corresponding to a rise in reactive nitrogen emissions, the sinkhole fen $\delta^{15}N$ does not show the expected positive correlation between $\delta^{15}N$ and depth since 1954. $\delta^{15}N$ values range randomly from 0.22 to 1.13 ‰ with a correlation with depth of only +0.2580. This could be due to the high organic matter content of the sinkhole fen versus the watersheds in the Holtgrieve et al. (2011) study, which dated sediment records from 25 oligotrophic (low organic content) lakes. They suggested that older sediments could have enriched $\delta^{15}N$ due to organic matter mineralization post-deposition. The same phenomenon may not occur to the same extent in the sinkhole fen as in the lakes. Interpreting nitrogen dynamics is complex, and many different processes affect the mobility and fractionation of nitrogen.

Conclusion

Hg, Pb, Zn, Cd, and Cu are negatively correlated with depth. This, in combination with low background lithogenic concentrations, indicates that concentrations of metals in the sinkhole due to atmospheric deposition has increased steadily over the past 60 years. These metals also have strong correlations with each other and total nitrogen. As and Cr are not correlated with depth. The $\delta^{15}N$ values did not deplete up the core as other studies have documented, and we found no correlation between $\delta^{15}N$ and depth.

In conclusion, this study shows that the ombrotrophic, alkaline, and high in organic matter nature of this sinkhole fen in karst terrane in South Carolina, with low metal background levels, is a suitable site to archive historical emissions of Hg, Pb, Zn, Cd, and Cu, but not As, Cr, or $\delta^{15}N$ signatures. As and Cr have higher lithogenic background metal concentrations and possible lower concentrations in emissions and subsequent atmospheric deposition from local, regional and global sources. $\delta^{15}N$ does not deplete upward in the core like other studies on lake sediments have found, possibly due to the different organic matter content of the sediments in the studies or the morphological and hydrological differences between lakes and sinkholes.

Sediments from sinkholes and other karst features are an underused resource that should be further studied to better understand the sources and distribution of atmospherically deposited pollutants; especially for the metals Hg, Pb, Zn, Cd, and Cu. Both Hg and Pb have several isotopes that can be used in environmental forensics to determine the local, regional, and global sources of natural and anthropogenic sources (Jackson, 2001; Jackson et al., 2004; Jackson, 2013). Future research could employ these methods to determine source contributions of these metals to the sinkhole in South Carolina. Determining which sources have contributed to increasing concentrations would be critical in developing policy using the Clean Air Act (1970) to combat atmospheric pollution in this and other regions.

Acknowledgements

Funding for the project was provided by the National Oceanic and Atmospheric Administration's Education Partnership Program through a cooperative agreement (NA60AAR4810164) with the Environmental Cooperative Science Center housed at Florida A&M University. The authors would like to thank Valerie-Carter Stone with the South Carolina Department of Parks, Recreation and Tourism for permit N-16-12 to sample the sinkhole in Santee State Park. We also thank Dan Phelps and Harvey Guy Means at the Florida Geological Survey; Steven Petrushak and Dr. Charlotte Sjunneskog at the Florida State University Antarctic Research Facility; Angela Dial at National High Magnetic Field Laboratory; William Burnett at Florida State University Department of Oceanography; Mark Malsick of South Carolina Department of Natural Resources; Henry Porter and Elzbieta Covington at South Carolina Department of Health and Environmental Control; and Christy Crandall at Florida A&M University. The authors would also like to thank Benjamin Schwartz and anonymous reviewers for improving the manuscript.

References

Allan, M., Le Roux, G., Sonke, J.E., Piotrowska, N., Streel, M. and Fagel, N., 2013, Reconstructing historical atmospheric mercury deposition in Western Europe using: Misten peat bog cores, Belgium: Science of the Total Environment, v. 442, p. 290–301. doi:10.1016 j.scitotenv.2012.10.044.

ASTM, 2013, ASTM D2974: Standard test methods for moisture, ash, and organic matter of peat and organic soils: West Conshohocken, PA, ASTM International.

Appleby, P.G., 2008, Three decades of dating recent sediments by fallout radionuclides: A review: Holocene, v. 18, no. 1, p. 83–93. doi:10.1177/0959683607085598.

Biester, H., Hermanns, Y.-M., and Martinez Cortizas, A., 2012, The influence of organic matter decay on the distribution of major and trace elements in ombrotrophic mires – A case study from the Harz Mountains: Geochimica et Cosmochimica Acta, v. 84, p. 126–136. doi:10.1016/ j.gca.2012.01.003.

Dabkowska-Naskret, H., 2003, The role of organic matter in association with zinc in selected arable soils from Kujawy Region, Poland: Organic Geochemistry, v. 34, p. 645–649. doi:10.1016/SO146-6380 (03)00019-6.

Edwards, A.E., Amatya, D.M., Williams, T.M., Hitchcock, D.R., and James, A.L., 2013, Flow characterization in the Santee Cave System in the Chapel Branch Creek Watershed, upper coastal plain of South Carolina, USA: Journal of Cave and Karst Studies, v. 75, no. 2, p. 136–145. doi:10.4311/2011/2011ES0262.

Fitzgerald, W.F., Engstrom, D.R., Mason, R.P., and Nater, E.A., 1998, The case for atmospheric mercury contamination in remote areas: Environmental Science and Technology, v. 32, no. 1, p. 1–7. doi:10.1021/es970284w.

Ford, D.C. and Williams, P.W., 1989, Karst Geomorphology and Hydrology: Unwin Hyman, London, 601 p.

Galloway, J.N., Townsend, A.R., Erisman, J.W., Bekunda, M., Cai, Zucong, Freney, J.R., Martinelli, L.A., Seitzinger, S.P., and Sutton, M.A., 2008, Transformation of the nitrogen cycle: Recent trends, questions, and potential solutions: Science, v. 320, p. 889–892. doi:10.1126/ science.1136674.

Glover, J.B., Domino, M.E., Altman, K.C., Dillman, J.W., Castleberry, W.S., Eidson, J.P., and Mattocks, M., 2010, Mercury in South Carolina Fishes, USA: Ecotoxicology, v. 19, p. 781–795. doi:10.1007/ s10646-009-0455-6.

Guentzel, J.L., 2009, Wetland influences on mercury transport and bioaccumulation in South Carolina: Science of the Total Environment, v. 407, no. 4, p. 1344–1353. doi:10.1016/j.scitotenv.2008.09.030.

Guentzel, J.L., Grave, D., and Glover, J., 2012, Total and methyl mercury in surface water and sediment from different ecoregions of South Carolina: 2012 South Carolina Water Resources Conference, Columbia, S.C.

He, Tianrong, Lu, Julia, Yang, Fan, and Feng, Xinbin, 2007, Horizontal and vertical variability of mercury species in pore water and sediments in small lakes in Ontario: Science of the Total Environment, v. 386, p. 53–64. doi:10.1016/j.scitotenv.2007.07.022.

Heaton, T.H.E., Wynn, P., and Tye, A.M., 2004, Low $^{15}N/^{14}N$ ratios for nitrate in snow in the high arctic (79°N): Atmospheric Environment, v. 38, p. 5611–5621. doi:10.1016/j.atmosenv.2004.06.028.

Hettwer, K., Deicke, M., and Ruppert, H., 2003, Fens in karst sinkholes – archives for long lasting 'immission' chronologies: Water, Air, and Soil Pollution, v. 149, p. 363–384. doi:10.1023/A:1025627218432.

Holtgrieve, G.W., Schindler, D.E., Hobbs, W.O., Leavitt, P.R., Ward, E.J., Bunting, L., Chen, Guangjie, Finney, B.P., Gregory-Eaves, I., Holmgren, S., Lisac, M.J., Lisi, P.J., Nydic, K., Roger, L.A., Saros, J.E., Selbie, D.T., Shapley, M.D., Walsh, P.B., and Wolfe, A.P., 2011, A coherent signature of anthropogenic nitrogen deposition to remote watersheds of the northern hemisphere: Science, v. 334, p. 1545–1548. doi:10.1126/science.1212267.

Hong, Sungmin, Candelone, J.-P., Patterson, C.C., and Boutron, C.F., 1994, Greenland ice evidence of hemispheric lead pollution two millenia ago by Greek and Roman civilizations: Science, v. 265, p. 1841–1843. doi:10.1126/science.265.5180.1841.

Jackson, T.A., 2001, Variations in the isotope composition of mercury in a freshwater sediment sequence and food web: Canadian Journal of Fisheries and Aquatic Sciences, v. 58, p. 185–196. doi:10.1139/f00-186.

Jackson, T.A., 2013, Mass-dependent and mass-independent variations in the isotope composition of mercury in a sediment core from Lake Ontario as related to pollution history and biogeochemical processes: Chemical Geology, v. 355, p. 88–102. doi:10.1016/j.chemgeo.2013.07.007.

Jackson, T.A., Muir, D.C.G., and Vincent, W.F., 2004, Historical variations in the stable isotope composition of mercury in arctic lake sediments: Environmental Science and Technology, v. 38, p. 2813–2821. doi:10.1021/es0306009.

Madsen P.P., 1981, Peat bog records of atmospheric mercury deposition: Nature, v. 293, p. 127–130. doi:10.1038/293127a0.

Marx, S.K., Kamber, B.S., McGowan, H.A., and Zawadzki, A., 2010, Atmospheric pollutants in alpine peat bogs record a detailed chronology of industrial and agricultural development on the Australian continent: Environmental Pollution, v. 158, p. 1615-1628, doi:10.1016/j.envpol.2009.12.009.

McConnell, J.R., and Edwards, R., 2008, Coal burning leaves toxic heavy metal legacy in the arctic: Proceedings of the National Academy of Sciences of the United States of America, v. 105, p. 12140–12144. doi:10.1073/pnas.0803564105.

NADP, 2014, National Atmospheric Deposition Program. http://nadp.sws.uiuc.edu/mdn/annualmdnmaps.aspx [accessed February 8, 2016].

Nie, Yaguang, Liu, Xiaodong, Sun, Liguang, and Emslie, S.D., 2012, Effect of penguin and seal excrement on mercury distribution in sediments from the Ross Sea region, East Antarctica: Science of the Total Environment, v. 433, p. 132–140. doi:10.1016/j.scitotenv.2012.06.022.

Nold, S.C., Bellecourt, M.J., Kendall, S.T., Ruberg, S.A., Sanders, T.G., Klump, J.V., and Biddanda, B.A., 2013, Underwater sinkhole sediments sequester Lake Huron's carbon: Biogeochemistry, v. 115, p. 235–250. doi:10.1007/s10533-013-9830-8.

Nriagu, J.O., and Pacyna, J.M., 1988, Quantitative assessment of worldwide contamination of air, water and soils by trace metals: Nature, v. 333, p. 134–139. doi:10.1038/333134a0.

Petit, M.G., 1977, A late Holocene chronology of atmospheric mercury: Environmental Research, v. 13, p. 94–101. doi:10.1016/0013-9351(77)90007-X.

Ravichandran, M., 2004, Interactions between mercury and dissolved organic matter – a review: Chemosphere, v. 55, p. 319–331. doi:10.1016/j.chemosphere.2003.11.011.

Renberg, I., Brännvall, M.-L., Bindler, R., and Emteryd, O., 2002, Stable lead isotopes and lake sediments – a useful combination for the study of atmospheric lead pollution history: Science of the Total Environment, v. 292, p. 45–54. doi:10.1016/S0048-9697(02)00032-3.

SCDHEC, 2014, South Carolina Department of Health and Environmental Control, Henry Porter and Elzbieta Covington, personal communication.

SCDHEC, 2013, South Carolina Department of Health and Environmental Control, GIS data clearinghouse; http://www.scdhec.gov/gis/GIS.aspx [Accessed December 19, 2013].

SCDHEC, 2010, South Carolina mercury assessment and reduction initiative, 98 p., pdf accessible at: http://www.dhec.sc.gov/HomeAndEnvironment/Mercury/MercuryinSC/

SCFC, 2015, South Carolina Forestry Commission, South Carolina's Forest Resource Assessment and Strategy, http://www.state.sc.us/forest/fra-cons.htm[Accessed 12/3/2015].

Schelske, C.L., Conley, D.J., Stoermer, E.F., Newberry, T.L., and Campbell, C.D., 1986, Biogenic silica and phosphorus accumulation in sediments as indices of eutrophication in the Laurentian Great Lakes: Hydrobiologia, v. 143, p. 79–86. doi:10.1007/BF00026648.

Schuster, P.F., Krabbenhoft, D.P., Naftz, D.L., Cecil, L.D., Olson, M.L., Dewild, J.F., Susong, D.D., Green, J.R., and Abbott, M.L., 2002, Atmospheric mercury deposition during the last 270 years: A glacial ice core record of natural and anthropogenic sources: Environmental Science and Technology, v. 36, p. 2303–2310. doi:10.1021/es0157503.

Shotyk, W., 1996, Peat bog archives of atmospheric metal deposition: geochemical evaluation of peat profiles, natural variations in metal concentrations, and metal enrichment factors: Environmental Reviews, v. 4, p. 149–183. doi:10.1139/a96-010.

Shukla, B.S., 2002, Sedimentation Rate through Environmental Radioactivity: Models and Applications: Hamilton, Ontario, Environmental Research & Publications, 192 p.

Uottawa, 2013, http://mysite.science.uottawa.ca/jblais/index_file/Page657.htm [accessed November 2013].

Wang, E.X., and Benoit, G., 1996, Mechanisms controlling the mobility of lead in the spodosols of a northern hardwood forest ecosystem: Environmental Science and Technology, v. 30, p. 2211–2219. doi:10.1021/es950590e.

Willoughby, R.H., 2002, Geologic map of the Saint Paul 7.5-minute quadrangle, Calhoun, Clarendon, and Orangeburg Counties, South Carolina: S.C. Geologic Quadrangle Map GQM-08, scale 1:24 000, 1 sheet.

Wolff, E.W., Suttie, E.D., and Peel, D.A., 1999, Antarctic snow record of cadmium, copper and zinc content during the twentieth century: Atmospheric Environment, v. 33, p. 1535–1541. doi:10.1016/S1352-2310(98)00276-3.

WSRC, 2002, Westinghouse Savannah River Company, Wind Climate Analyses for National Weather Service Stations in the Southeast: U.S. Department of Energy, WSRC-TR-2002-00515, 62 p.

Yan, Hong Wang, Yuhong, Chen, Wenhan, and Sun, Liguang, 2011, Millennial mercury records derived from ornithogenic sediment on Dongdao Island, South China Sea: Journal of Environmental Sciences, v. 23, no. 9, p. 1415-1423. doi:10.1016/S1001-0742(10)60603-1.

S. Zada, A.A. Naseem, S.-J. Lee, M. Rafiq, I. Khan, A.A. Shah, and F. Hasan – Geochemical and mineralogical analysis of Kashmir Cave (SMAST), Buner, Pakistan, and isolation and characterization of bacteria having antibacterial activity. *Journal of Cave and Karst Studies*, v. 78, no. 2, p. 94–109. DOI: 10.4311/2014MB0110

GEOCHEMICAL AND MINERALOGICAL ANALYSIS OF KASHMIR CAVE (SMAST), BUNER, PAKISTAN, AND ISOLATION AND CHARACTERIZATION OF BACTERIA HAVING ANTIBACTERIAL ACTIVITY

SAHIB ZADA[1], ABBAS ALI NASEEM[2], SEONG-JOO LEE[2], MUHAMMAD RAFIQ[1], IMRAN KHAN[1], AAMER ALI SHAH[1], AND FARIHA HASAN[1]*

Abstract: Bacterial strains having the ability to inhibit the growth of other bacteria were isolated from soil samples collected from Kashmir Smast (smast is Pushto for cave), Khyber Pakhtunkhwa, Pakistan. The study includes mineralogical and geochemical analyses of soil sample collected from the cave, so as to describe the habitat from which the microorganisms have been isolated. Total bacterial count of the soil sample was 5.25×10^4 CFU mL^{-1}. Four bacterial isolates having activity against test organisms *Micrococcus luteus*, *Klebsiella* sp., *Pseudomonas* sp., and *Staphylococcus aureus* were screened out for further study. Two of the isolates were found to be Gram-positive and the other two Gram-negative. The four isolates showing antibacterial activity were identified as *Serratia* sp. KC1-MRL, *Bacillus licheniformis* KC2-MRL, *Bacillus* sp. KC3-MRL, and *Stenotrophomonas* sp. KC4-MRL on the basis of 16S rRNA sequence analysis. Although all isolates showed antibacterial activity, only *Bacillus licheniformis* KC2-MRL was selected for further study due to its large zone of inhibition. Antibacterial activity of *B. licheniformis* KC2-MRL was optimum when grown in nutrient broth adjusted to pH 5 and after 24 hours of incubation at 35 °C. The extracted antibacterial compound was stable at pH 5–7 and 40 °C when incubated for 1 hour. The strain was found resistant against cefotaxime (ctx). Atomic-absorption analysis of the soil sample collected from the cave showed high concentrations of calcium (332.938 mg kg^{-1}) and magnesium (1.2576 mg kg^{-1}) compared to the control soil collected outside the cave. FTIR spectrum of the concentrated protein showed similarity to bacitracin. The antibacterial compound showed activity against both Gram-negative and positive test strains. Mineralogy of Kashmir Smast is diverse and noteworthy. Different geochemical classes identified by X-ray diffraction were nitrates, oxides, phosphates, silicates, and sulfates. Weathered cave limestone contributes notably to the formation of these minerals or compounds. FTIR spectroscopic analysis helped to identify minerals such as quartz, clinochlore, vermiculite, illite, calcite, and biotite.

INTRODUCTION

Caves are characterized as having very low nutrient availability, constant low temperatures, and high humidity. Caves can be either terrestrial or aquatic and are usually oligotrophic in nature (i.e., nutrient limited). Some may be rich in specific natural minerals or be exposed to different nutrient-containing sources, therefore, different caves will have different types of microorganisms inhabiting various ecological niches. Fauna, environmental factors, temperature, and organic matter dictate the caves' biotic activities, such as nutrient cycling and geomicrobiological activities, including formation or alteration of cave structures (Adetutu and Ball, 2014).

Cave organisms have evolved some extraordinary abilities to survive and live in this inhospitable environment (Engel et al., 2005; Simmons et al., 2008; Northup and Lavoie, 2004). Cave microbial flora is rich in different types of microorganisms having some diverse and unique characteristics (Groth et al., 1999). The most abundant organisms observed in caves are filamentous and belong to the Actinobacteria group, followed by coccoid and bacilli forms (Cuezva et al., 2009). Some pathogenic microorganisms have been reported from Altamira Cave (Jurado et al., 2006). Luong et al. (2010) for the first time reported the recovery of *Aurantimonas altamirensis* from human medical samples, rather than from a cave. The disease-causing bacteria E. coli and S. aureus have also been isolated from caves (Lavoie and Northup, 2005), as well as species of *Pseudomonas*, *Sphingomonas*, and *Alcaligenes* sp. (Ikner et al., 2007), and *Inquilinus* sp. (Laiz et al., 1999).

* Corresponding author: farihahasan@yahoo.com
[1] Department of Microbiology, Quaid-i-Azam University, Islamabad, Pakistan.
[2] Department of Geology, Kyungpook National University, Daegu 702 – 701, Korea

Caves can be a source of novel microorganisms and biomolecules, such as enzymes and antibiotics, that may be suitable for biotechnological purposes (Tomova et al., 2013). The influence of particular nutrients in antibiotic biosynthesis is caused by the chemical structures of antibiotic substances (Pereda et al., 1998). Rigali et al. (2008) provide evidence that certain substrates and oligotrophic conditions will lead to increased induction of secondary metabolites. Nitrogen from various sources may incorporate in antibiotic molecules as precursors, or their amino groups can transfer to specific intermediate products (Doull and Vining, 1990; Cheng et al., 1993). Nutrient deficiency is responsible for the onset of antibiotic biosynthesis (Demain et al., 1983; Doull and Vining, 1990; Sanchez and Demain, 2002). When carbon or nitrogen is a limiting factor, growth is rapidly reduced and antibiotic biosynthesis occurs in the stationary phase. In other cases, antibiotic production is associated with the growth phase. Due to the oligotrophic environment in cave ecosystems, microorganisms present in the cave compete for nutrients and produce antibiotics against other microbes. Wide-spectrum standard antibiotics, metabolic by-products (organic acids), lytic agents (lysozyme), and other biologically active compounds like exotoxins and bacteriocins are also produced by microbes (Riley and Wertz, 2002; Yeaman and Yount, 2003). The continuous job of scientists is to discover new antibiotics and new source microorganisms. Cave microorganisms can be used for the production of potential new antibiotics.

Antibiotic producing microbes mostly belong to the genera *Penicillium*, *Streptomyces*, *Cephalosporium*, *Micromonospora*, *Bacillus* (Park et al., 1998), and *Pseudomonas*, followed by the enterobacteria, lactobacilli, and streptococci (Bérdy, 2005). More than eight thousand antibiotics are known to exist and hundreds are discovered yearly (Brock and Madigan, 1991), but only a few prove to be commercially useful. About 17% of these antibiotics are produced by molds and 74% by actinomycetes (Zhang et al., 2008). *Bacillus* sp. mostly form peptides and phenazines, which are heterocyclic and derivatives of fatty acids, but the production of macrolactones is very rare (Bérdy, 2005). Gramicidins, polymixins, bacitracins, and some other antibiotics are formed non-ribosomally (Nissen-Meyer and Nes, 1997; Hancock and Chapple, 1999).

The number and species of microorganisms in soil vary in response to environmental conditions such as nutrient availability, soil texture, and type of vegetation cover (Atlas and Bartha, 1998). The soil composition and texture play important role in harboring microbes with unique characteristics. Thus it is important to know about the composition, type, structure, and texture of the soil from which the microorganisms are isolated for research or the production of metabolites such as antibiotics. A great number of antibiotics have been isolated from various microorganisms. Studies are still being conducted to isolate and identify novel antibiotics effective against pathogenic fungi and bacteria.

Microbial species adapt to caves by interacting with minerals there (Barton and Jurado, 2007). The geochemistry and metal content of the cave environment can influence the synthesis of antibiotics by cave bacteria, as metal ions are known to affect the synthesis of microbial metabolites *in vitro*. Tanaka et al. (2010) made a connection between the rare earth elements scandium and lanthanum and increased activation of the expression of nine genes belonging to nine secondary metabolite-biosynthetic gene clusters of *Streptomyces coelicolor* A3(2). Investigations on the effect of several metal ions indicated that Cu^{2+}, Mn^{2+}, and Fe^{2+} stimulated AK-111-81 biosynthesis by *Streptomyces hygroscopicus*, depending on their concentration (Gesheva et al., 2005). Divalent ions stimulated the production of polyenes (Georgieva-Borisova, 1974; Liu et al., 1975; Solivery et al., 1988; Park et al., 1998), and Fe^{2+} and Mn^{2+} have been found to favor niphimycin production. Soil texture and structure also strongly influence the activity of soil biota. For example, medium textured loam and clay soils enhance activity of microbes and earthworms, whereas fine textured sandy soils, with lower water retention potentials, are not very favorable. Alterations in pH of the soil can affect metabolism of species, enzyme activity, and availability of nutrients, and thus, are often lethal (Singh and Mishra, 2013).

The aim of the present study was to isolate microbes from the cave having antibacterial activity, identify them and their product, and investigate the geochemistry of the cave to understand the environmental conditions under which these microorganisms are living and producing compounds inhibitory for other microbes.

Materials and Methods

Sampling Site and Collection of Soil Samples

Two soil samples were collected from Kashmir Smast (*smast* in local language means cave), Nanser, Buner, Khyber Pakhtunkhwa (GPS coordinates 34°25′42.12″N 72°13′10.82″E) (Fig. 1). The cave is 188 m long, with average height and width about 28 m and 25 m, respectively. The Kashmir Smast is one of a series of natural caves in limestone, probably of marine origin, located in the Babozai Mountains between Mardan and Buner in northern Pakistan. According to study of a rare series of bronze coins and artifacts found in the region, the caves and their adjacent valley probably composed a sovereign kingdom in Gandhara, which maintained at least partial independence for almost 500 years, from the fourth to the ninth centuries AD (Ziad, 2006). It is a limestone cave with internal temperature around 10 °C. The interior of the cave was muddy due to dripping of water from the surface, the only source of water. Soil samples were collected from the cave wall (sample smast-7) and floor (sample smast-5) in sterile Falcon

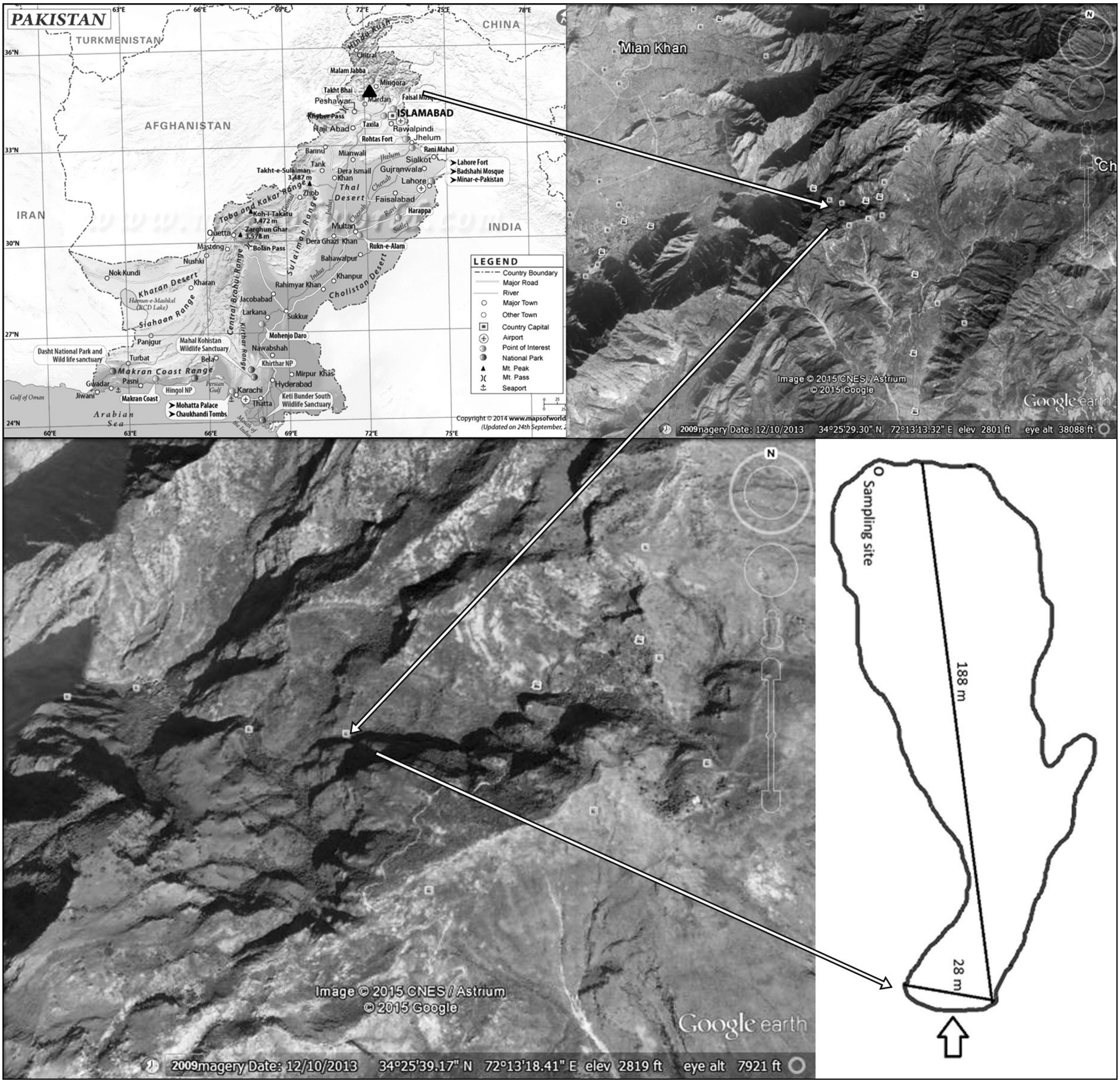

Figure 1. Location and plan map of Kashmir Smast (Cave), Nanseer Buner, Khyber Pakhtunkhwa, Pakistan. White arrows show location of the cave; large arrow shows entrance to the cave. (Pakistan full map from http://www.mapsofworld.com/pakistan/; aerial images Google Earth.)

tubes under aseptic conditions. The samples were collected from the dark end of the cave about 188 m from the entrance. This cave is located far away from human travel routes, so human intervention is negligible. The samples were then brought to the laboratory in an icebox and stored at 4 °C for further processing. These soil samples were screened for the antibiotic-producing isolates within 24 hours.

MINERALOGICAL ANALYSIS

For the quantitative analysis of elements (Ni, Cr, Co, Cu, Zn and Pb) in the soil sample, Atomic Absorption (AA240FS Fast Sequential Atomic Absorption Spectrophotometer) spectrophotometry was performed. To prepare the sample for this analysis, soil digestion was performed.

One gram each of soil from the cave floor and control soil from outside the cave were ground separately and were then mixed in 15 mL aqua regia, heated at 150 °C, and left overnight. Then 5 mL of $HClO_4$ was added and again heated at 150 °C. The solution almost became dry until brown fumes were produced. Whatman filter paper (No. 42) was used for filtration, and the volume was made up to 50 mL using double-distilled water (Jensen et al., 1983).

X-ray powder diffraction is a rapid analytical technique used for phase identification and characterization of unknown crystalline materials such as minerals and inorganic compounds and identification of fine-grained minerals such as clays and mixed-layer clays that are difficult to determine optically (Dutrow and Clark, n.d.). XRD patterns were obtained from the samples using X'Pert-APD (Philips, The Netherlands) with an X-ray generator (1.2 kW) and anode (LFF Cu). The Cu Kα radiation had a wavelength of 1.54 Å. The X-ray generator voltage and current were 40 kV and 30 mA, respectively. The step-scan data were continuously collected over the range of 5 to 80°2θ.

Mineral proportions were calculated using SIROQUANT, a commercially available MS-Windows program for standardless mineral quantification. Weight-percent mineral phase contents were estimated. Using calculated hkl mineral library files, refinement stages were optimized for the smallest possible χ^2 goodness-of-fit parameter for the associated Rietveld peak pattern match (Taylor, 1991; Taylor and Clapp, 1992).

Thermogravimetric analysis records change in mass from dehydration, decomposition, or oxidation of a sample as a function of heating time and temperature (Voitovich et al, 1994). TGA was performed on a high-resolution thermogravimetric analyzer (Staram TGA Instruments, series Q500) in a flowing nitrogen atmosphere (60 cm^3 min^{-1}). Approximately 35 mg of sample underwent thermal analysis, with a heating rate of 5 °C min^{-1} within the range of 25 to 1000 °C. With the isothermal, isobaric heating program of the instrument the furnace temperature was regulated precisely to provide a uniform rate of decomposition in the main decomposition stage.

The field-emission cathode in the electron gun of a scanning electron microscope provides narrower probing beams at low, as well as high, electron energy that results in improved spatial resolution and minimizes sample charging and damage (Stranks et al., 1970). FE-SEM with EDS analysis of the samples was performed for the determination of thickness, structure uniformity, and elemental composition, using S-4800 and EDX-350 (Horiba) FE-SEM (Hitachi, Tokyo, Japan). Samples were spread on a glass plate that was fixed onto a brass holder and coated with osmium tetraoxide (OsO_4) using a VD HPC-ISW osmium coater (Tokyo, Japan) prior to FE-SEM analysis

About 2 mg of the soil sample was mixed with 40 mg of KBr in ratio 1:20 using mortar and pestle. KBr powder had been dried at 120 °C in an oven to avoid the broad spectral peak. A 1 by13 mm pellet was prepared. The pellet was placed in a holder and introduced in the infrared beam for analysis through Fourier Transform Infrared Spectrometer (Jasco FT/ IR – 620).

Microbiological Studies

For isolation of bacteria from the cave soil, 1 g of each soil sample was serially diluted in normal saline and then was spread on nutrient-agar plates aseptically, and plates were incubated aerobically for 24 hrs at 35 °C. Viable cell count was calculated as CFU mL^{-1}.

The isolate *Bacillus licheniformis* KC2-MRL was incubated at 25, 35 and 45 °C. A growth curve was constructed by taking values of cell concentration on y-axis versus time along x-axis. Using a standard formula, growth rate and generation time was calculated from the graph.

Nutrient agar medium was used for isolation of antibiotic-producing bacteria. Lawns of susceptible test organisms *Micrococcus luteus* (ATCC 10240), *Klebsiella* sp., *Pseudomonas* sp., and *Staphylococcus aureus* (ATCC 6538) were made on nutrient agar plates (Gauthier, 1976) that were then sprinkled with 20 to 25 particles of soil. All the plates were gently shaken so that the soil particles spread uniformly. Plates were then incubated at 35 °C for 24 hours, lid side up so that the soil particles would not fall off the agar. After 24 hours of incubation, plates were checked for antibacterial activity shown by the formation of clear zone of inhibition around the KC2-MRL bacteria colony. Zone-producing isolates were purified and stored at 4 °C. Colony morphology, Gram-staining, and biochemical tests (citrate utilization, oxidase and catalase production, nitrate and sulfate reduction, H_2S production, and carbohydrate fermentation) were performed according to *Bergey's Manual of Determinative Bacteriology* (Holt, 2012).

The DNA extraction from bacteria was done by spinning 1 mL of culture at 10,000 rpm for about 3 min, after which the cells were pelleted out and rinsed twice in 400 µL TE buffer after removing the supernatant. Then the cells were centrifuged at 10,000 rpm for 3 min, and the pellets were resuspended in 200 µL TE buffer. Then 100 µL Tris-saturated phenols of pH 8.0 were added to these tubes, followed by a vortex-mixing step of 60 sec, to lyse the cells. To separate the aqueous and organic phases, the samples were centrifuged at 13,000 rpm at 4 °C for 5 minutes. Then 160 µL of upper aqueous phase was taken in a 1.5 mL Eppendorf. About 40 µL of TE buffer was added to make 200 µL, which was then mixed with 100 µL of 24:1 chloroform:isoamyl alcohol and centrifuged for 5 min at 13,000 rpm at 4 °C. Chloroform:isoamyl alcohol (24:1) extraction was used for the purification of lysate, until there was no longer a white interface, and the same method was repeated twice or thrice (Aitken, 2012). Purified DNA was present in the aqueous phase and was stored at −20 °C for further use. The purified DNA was analyzed through agarose gel 1.5 g in 1X TBE and staining with ethidium bromide.

Phylogenetic analysis was performed with a ClustalW program implemented in MEGA4.0 (Thompson et al., 1994). The similar sequences were downloaded from NCBI.

All sequences were aligned, and the phylogenetic tree was constructed using the neighbor-joining method. Bootstrap analysis with 1000 replicates was performed for the significance of the generated tree.

An inoculum of *B. licheniformis* KC2-MRL, selected after screening on the basis of its larger zone of inhibition against test strains, was prepared in nutrient broth. First about 50 mL of nutrient broth was prepared in 250 mL flask, autoclaved, and incubated at 35 °C overnight to check the sterility. The nutrient broth was taken in 100 mL flasks and its pH was adjusted to 5 (pH of sampling site was 5). Approximately 10% inoculum was added to each flask and incubated at 35 °C in orbital shaker at 150 rpm. After every 24 hrs, samples were collected and centrifuged at 10,000 rpm for 16 minutes, for a total of 96 hrs to obtain cell free supernatant that was checked for antibacterial activity by agar-well diffusion assay (Haque et al., 1995). About 80 µL of cell-free supernatant was added in the wells and the plates were incubated at 35 °C for 24 hours. After 24 hrs, the zones of inhibition were observed and the diameter of the zone of inhibition was measured.

Different media were used for the production of antibacterial compounds by *B. licheniformis* KC2-MRL, including Trypticase soya broth, nutrient broth and Luria Bertani broth. Inoculum (10%) was added and incubated at 37 °C and 150 rpm. The cell growth was measured by optical density at 600 nm, and antimicrobial activity was checked by agar-well diffusion assay.

To check the effect of time of incubation on the antimicrobial activity, the strain was incubated at 37 °C in orbital shaker at 150 rpm and samples were drawn after every 24 hours from 0 to 96 hours. The antimicrobial activity of all the collected cell-free supernatants was checked against *S. aureus*, *M. luteus*, *Klebsiella* sp., and *E. coli*.

The effect of temperature (15, 25, 35, and 45 °C) on optimum antibacterial activity was studied by inoculating *B. licheniformis* KC2-MRL in nutrient broth and incubating at 15, 25, 35 and 45 °C at 150 rpm. Samples were drawn every 24 hours from 0 to 96 hrs. Centrifuged cell-free supernatants were used for further analysis using *S. aureus*, *M. luteus*, *Klebsiella* sp., and *Pseudomonas* sp. as test strains.

The effect of pH (5, 6, 7, and 8) on the production of antibiotics was studied by inoculating *B. licheniformis* KC2-MRL in the growth medium adjusted to those values. Samples were drawn every 24 hours from 0 to 96 hours, and centrifuged and cell free supernatants were used for further analysis.

The standard Kirby-Bauer disk-diffusion assay (Koneman, 2006) was performed to check the sensitivity of the selected strains against various broad-spectrum antibiotics to check for the intrinsic ability of the microorganisms to resist antibiotics.

Cell-free supernatant of *B. licheniformis* KC2-MRL culture grown under optimized conditions was used for the precipitation of antibacterial compounds using increasing concentrations of 10 to 80% of ammonium sulfate. The pellet was kept at −20 °C in 10 mL of 0.1M phosphate buffer, pH 7. FTIR was performed to identify unknown compounds. Spectrum of the antibacterial compound produced by *Bacillus licheniformis* KC2-MRL was compared with that of bacitracin as a control. Samples were scanned from 4000-400 cm^{-1} at resolution of 6.0 cm^{-1}.

Results

Mineralogical Analysis

Observed X-ray diffraction patterns of samples smast-5 and smast-7 along with the Inorganic Crystal Structure Database reference data of different minerals are shown in Figures 2a and 2b. In Figure 2a, two prominent peaks at 2θ 26.624 and 29.420 were observed. The observed peaks match with the ICSD Reference codes 03-065-0466 Quartz and 01-086-1385 Muscovite-2M1. Along with these peaks, some other weak peaks matched with reference peaks of 01-075-8291 Chlorite-ll-4, 01-080-1108 Biotite, 01-075-1656 Dolomite, 01-077-0022 Vermiculite-2M, and 01-075-8291 Clinochlore-llb-4. Figure 2b indicates three prominent peaks at 2θ 26.661, 29.442, and 30.984. These matched with ICSD Reference codes 01-087-2096 Quartz, 01-072-4582 Calcite, and 01-076-6603 Vermiculite. Silicate minerals found in the cave were illite, muscovite, vermiculite, chlorite, clinochlore, and quartz. The chemical composition of the minerals is given in Table 1.

Weight-percent mineral phases were used to estimate the SIROQUANT (Fig. 3), considering 100% crystalline compound to calculate the quantitative analysis. Figure 3a shows that vermiculite, illite, and chlorite were the most abundant minerals in smast-5. Similarly, Figure 3b shows that the vermiculite-2M1, muscovite, and clinochlore-llb are the most abundant minerals in smast-7.

The Fourier-transform infrared absorption peaks from the cave were observed to determine the major and minor constituent minerals present in the sample smast-7 (Fig. 4). The samples analyzed were mixtures of minerals such as silicon oxide, calcite, quartz, muscovite, clinochlore, nimite, biotite, and vermiculite. Various peaks appeared indicating the presence of a variety of minerals.

Mass loss steps were observed from Figure 5 at 77, 200 and 280, 400 and 790 °C, with mass losses of 10.23, 21.55, 5.20 and 7.58% recorded due to carbonates.

Scanning electron microscope observations (Fig. 6) suggest that cave's clay particles are poorly crystallized clasts with angular, irregular outlines, and swirly texture with face-to-face arrangement of clay grains. Si, Al, and Fe were found enriched within the samples.

Soil Analysis

Atomic-absorption spectroscopy was performed to determine the concentration of elements in the cave soil sample smast-5. Ca was 332.938 mg kg^{-1} as compared to 121.65 mg kg^{-1} in control soil from the surface, Mg was

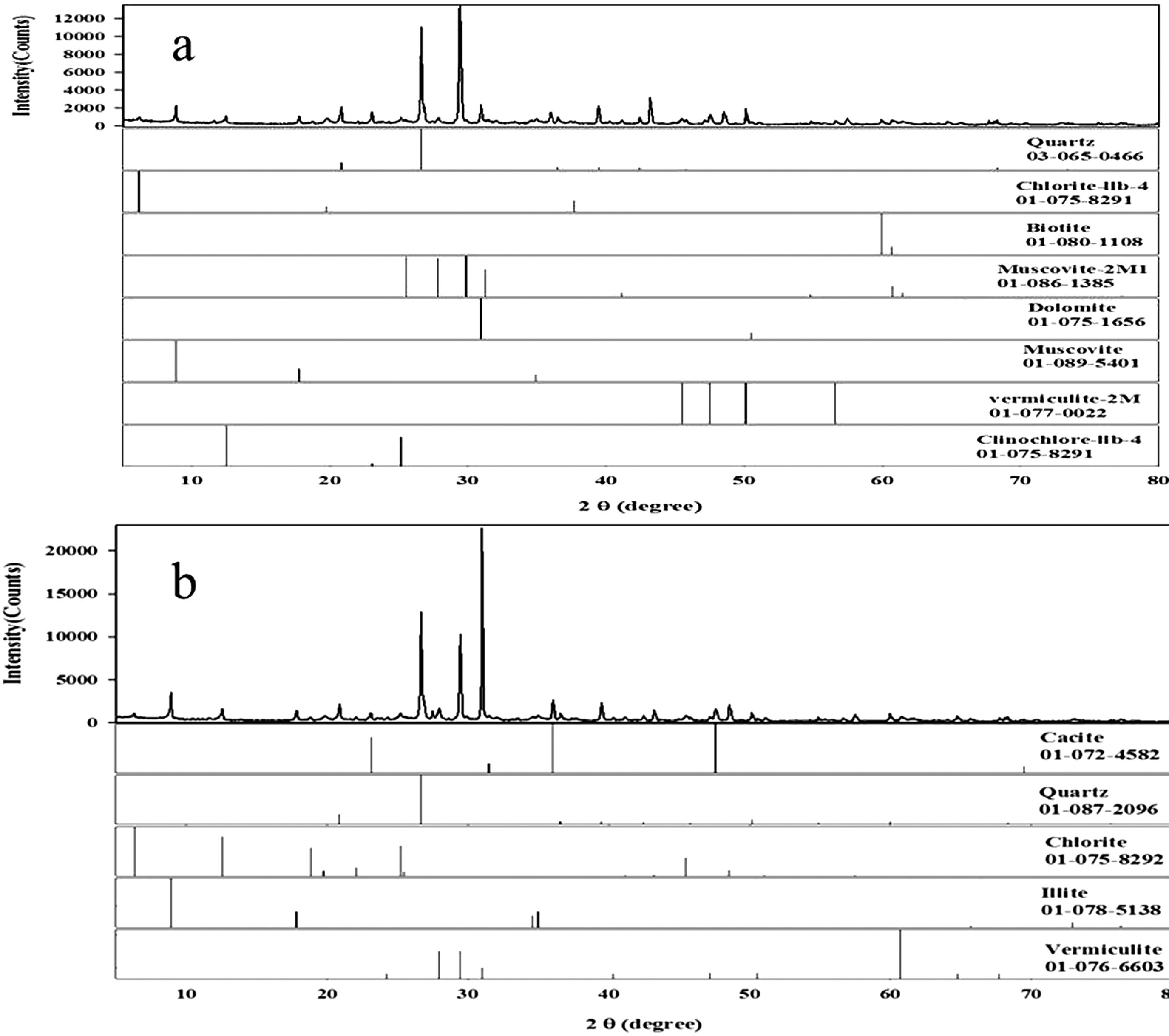

Figure 2. X-ray diffraction patterns of Kashmir Smast soil samples smast-5 from the floor (a) and smast-7 from the wall (b) with spectra from the Inorganic Crystal Structure Database for comparison and identification.

1.2576 mg kg^{-1} in cave soil and 1.023 mg kg^{-1} in control soil, and that of Ni, Cr, Co, Cu, Zn, and Pb were much lower than those found in the control soil (Table 2).

Microbiology Results

Numbers of viable cells per mL were calculated for the smast-7 floor-soil sample collected from Kashmir Cave. The bacterial count (CFU) was 5.25×10^4 mL^{-1}.

Initial screening resulted in isolation of four phenotypically distinct bacterial strains showing antimicrobial activity against four test organisms. Figure 7 shows a typical nutrient-agar plate with zones of inhibition. Of the four, the strain *B. licheniformis* KC2-MRL showed the largest zones of inhibition, 28 mm against *Micrococcus*, 20 mm against *E. coli*, 14 mm against *Staphylococcus aureus*, and 15 mm against *Klebsiella*). Therefore it was selected for further analysis.

The 16S rRNA gene sequences of the antibiotic-producing cave bacteria have been submitted to NCBI GenBank. The isolates KC1-MRL, KC2-MRL, KC3-MRL and KC4-MRL were identified as *Serratia* sp. KC1-MRL (Accession No. KC128829.1), *Bacillus licheniformis* KC2-MRL (Accession No. KC128830.1), *Bacillus* sp. KC3-MRL (Accession No. KC128831.1), and *Stenotrophomonas* sp. KC4-MRL (Accession No. KC128832.1) (Fig. 8).

Maximum antimicrobial activity was found when *B. licheniformis* KC2-MRL was cultured in nutrient broth

Table 1. List of minerals identified in samples from the wall and floor of Kashmir Smasta.

Mineral	Chemical Formula
Calcite	$CaCO_3$
Quartz	SiO_2
Dolomite	$CaMg(CO_3)_2$
Muscovite-2M1	$K_{0.86}Al_{1.94}(Al_{0.965}Si_{2.895}O_{10})((OH)_{1.744}F_{0.256})$
Muscovite	$KAl_{2.20}(Si_3Al)_{0.975}O_{10}((OH)_{1.72}O_{0.28})$
Clinochlore-llb	$(Mg_{4.715}Al_{0.394}Fe_{0.109}Cr_{0.128}Nl_{0.011})(Si_{3.056}A_{1.944})O_{10}(OH)_8$
Biotite	$KFeMg_2(AlSi_3O_{10})(OH)_2$
Vermicullite-2M	$(Mg_{2.36}Fe_{0.48}Al_{0.16})Mg_{0.32}(Al_{1.28}Si_{2.72})O_{10}(OH)_2(H_2O)_{4.32}Mg_{0.32}$
Vermicullite	$Mg_3((AlSi_3O_{10})(OH))(H_2O)$
Chlorite-llb-4	$(Mg_{11.06}Fe_{0.94})((Si_{5.22}Al_{2.78})O_{20}(OH)_{16})$
Illite	$(K_{0.71}Ca_{0.01}Na_{0.01})(Al_{1.86}Mg_{0.15}Fe_{0.04})((Si_{3.27}Al_{0.73})O_{10}(OH)_2)$

after 24 hours of incubation, with zone of inhibition of 28 mm against *M. luteus*, 20 mm against *S. aureus*, 11 mm against *Klebsiella* and 8 mm against *E. coli*. The antibacterial activity decreased with passage of time in all media except the nutrient broth.

Best antimicrobial activity (21 mm) of *B. licheniformis* KC2-MRL was observed against *M. luteus*, 14 mm against *S. aureus*, 12 mm against *Klebsiella*, and 8 mm against *E. coli* after 48 hours of incubation, while there was a decrease in the sizes of zones after 48 hours showing decrease in antimicrobial activity of *B. licheniformis* KC2-MRL (Fig. 9).

Maximum antibacterial activity of 28 mm and 22 mm was observed against *S. aureus* and *M. luteus*, respectively, with 17 mm against *E. coli* and 9 mm activity against *Klebsiella*, at 35 °C after 48 hrs of incubation. The activity in terms of zones of inhibition decreased with further increase in temperature (45 °C) (Fig. 9).

Effect of pH (5, 6, 7, and 8) on the production of antibiotics was studied. Activity in terms of zones of inhibition was measured against the same test organisms. Best activities were observed at pH 5, 23 mm against *S. aureus*, followed by *M. luteus*, *E. coli* and *Klebsiella* after 24 hrs of incubation. The second best activity was observed at pH 6, and a gradual decrease in activity was observed with increase in pH (Fig. 9).

To check the stability of antimicrobial compounds at different temperatures, the cell free supernatant was treated at 15, 25, 35, and 45 °C for 1 hour. Antibacterial activity (26 mm) was observed until 40 °C, but the activity decreased at a temperature above 40 °C and was totally lost with further rise in temperature. The antimicrobial compound produced by *B. licheniformis* KC2-MRL was stable at pH 5–8, although highest activity was observed at pH 5 and 6, whereas activity decreased at pH 7 and 8.

Vancomycin, nalidixic acid, cefotoxime, ampicillin, amoxicillin, imipenem, methicillin, cefotetan, and levofloxacin were tested to check the susceptibility of *Bacillus licheniformis* KC2-MRL. The organism was more susceptible to levofloxacin, which produced a 40 mm zone of inhibition (Fig. 10).

We used a solution of bacitracin as a standard. FTIR spectrum of *B. licheniformis* KC2-MRL's precipitated protein was compared with the standard. The FTIR spectrum

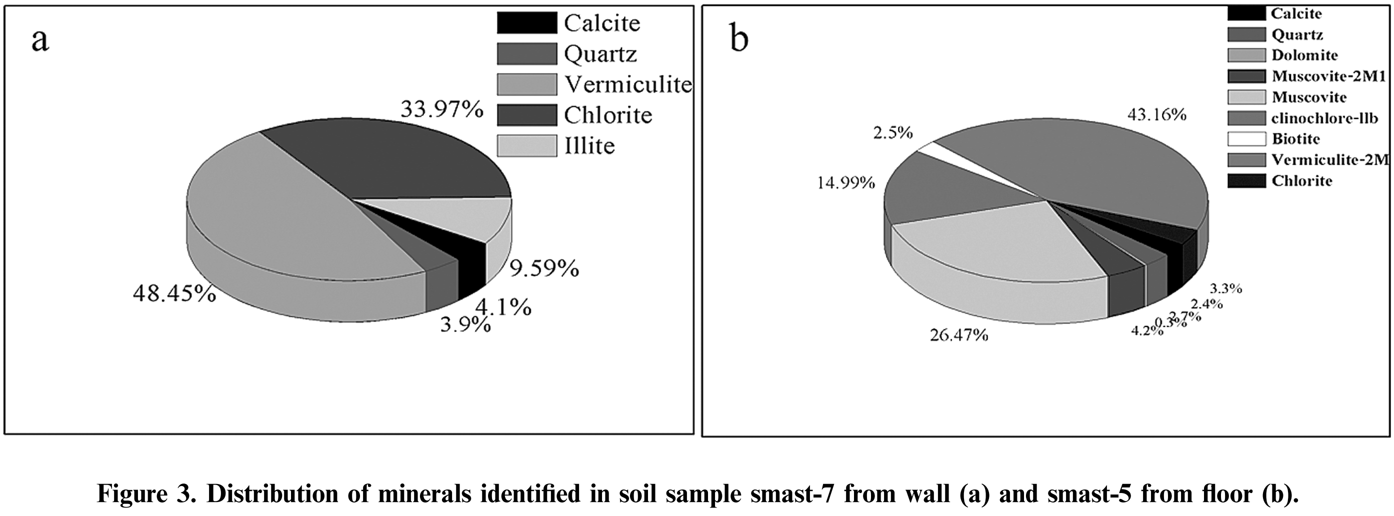

Figure 3. Distribution of minerals identified in soil sample smast-7 from wall (a) and smast-5 from floor (b).

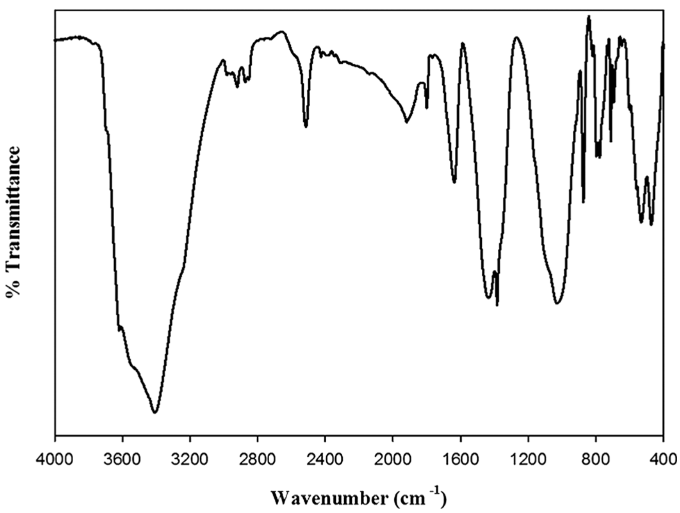

Figure 4. Fourier-transform infrared absorption spectrum of soil sample smast-7 from the cave wall.

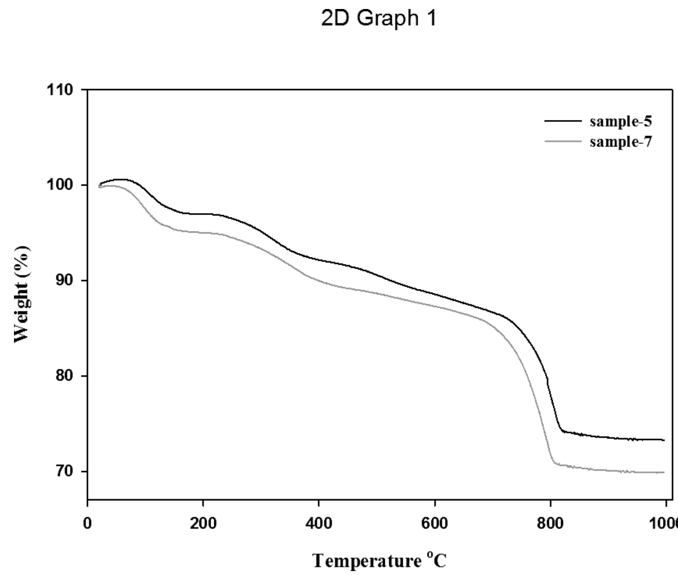

Figure 5. Thermogravimetric analysis plots of Kashmir Smast soil samples 5, cave soil, and 7, cave wall.

of bacitracin showed the absorption bands at 3295.63, 3016.9, 2133.64, and 1635 cm^{-1} that correspond to NH, CH, C–C, and C=C groups. Similarly, in the case of *B. licheniformis* KC2-MRL protein the absorption bands appeared at 3271.98, 3016.90, 2120.12, 1635.20 and 1076.22 cm^{-1} which were attributing to NH, CH, C=C and C–N (Fig. 11).

Discussion

Solution caves are formed in carbonate and sulfate rocks such as limestone, dolomite, marble, and gypsum by the action of slowly moving groundwater that dissolves the rock to form tunnels, irregular passages, and even large caverns along joints and bedding planes (Davies and Morgan, 2000). Caves usually have very low nutrient availability, but they still contain diverse, and often unique, microbial communities (Barton, 2006). Caves on other worlds such as Mars may provide protected sites for extraterrestrial life forms (Nelson, 1996). The subsurface of Earth is considered as the best possible site to look for microbial life and the characteristic lithologies that indicates the remnants of life (Boston et al., 2001). Microbial analysis of caves showed *Bacillus* as the most commonly detected microbial genus (Adetutu et al., 2012). It is important to understand how the ecosystems are operating and accommodating microbial diversity. The rock composition and mineralogy can be helpful to understand the geomicrobiology and potential metabolic capabilities of the microorganisms to use ions within the rock as nutrients and for chemolithotrophic energy production. Cave sediments can therefore act as reservoirs of microorganisms (Adetutu et al., 2012). The use of these ions may be supported by the formation of a corrosion residue, through microbial scavenging activities (Barton, 2006). Cave microorganisms also have potential to produce unique antibiotics and cancer treatment drugs (Onaga, 2001). Minerals have profound effect on the production of antibiotics by microorganisms. Basak and Majumdar (1975) reported that kanamycin production by *Streptomyces kanamyceticus* ATCC 12853 required magnesium sulfate and potassium phosphate (0.4 and 1.0 g L^{-1}, respectively) and Fe and Zn (0.25 and 0.575 µg mL^{-1}, respectively), amounts of Mn and Ca did not have any effect, and Cu, Co, Ni, and V have inhibitory effect. Divalent ions as Mn^{2+}, Cu^{2+}, Fe^{2+} stimulated AK-111-81 antibiotic biosynthesis by *Streptomyces hygroscopicus* 111-81 (Gesheva et al., 2005). The divalent metal ions (Mg, Fe and Mn) sodium dihydrogen phosphate were found essential for bacitracin production by *Bacillus licheniformis*,

Table 2. Concentrations of some metals from soil sample collected from the floor of Kashmir Smast and control sample from outside the cave, determined by atomic-absorption spectroscopy.

	Metals, mg kg^{-1}							
Soil Samples	Ni	Cr	Co	Cu	Zn	Ca	Mg	Pb
Cave Soil	0.965	0.571	0.266	1.824	12.7311	332.938	1.2576	1.31
Control Soil	10.4	8.74	0.810	4.7	36.41	121.65	1.023	8.14

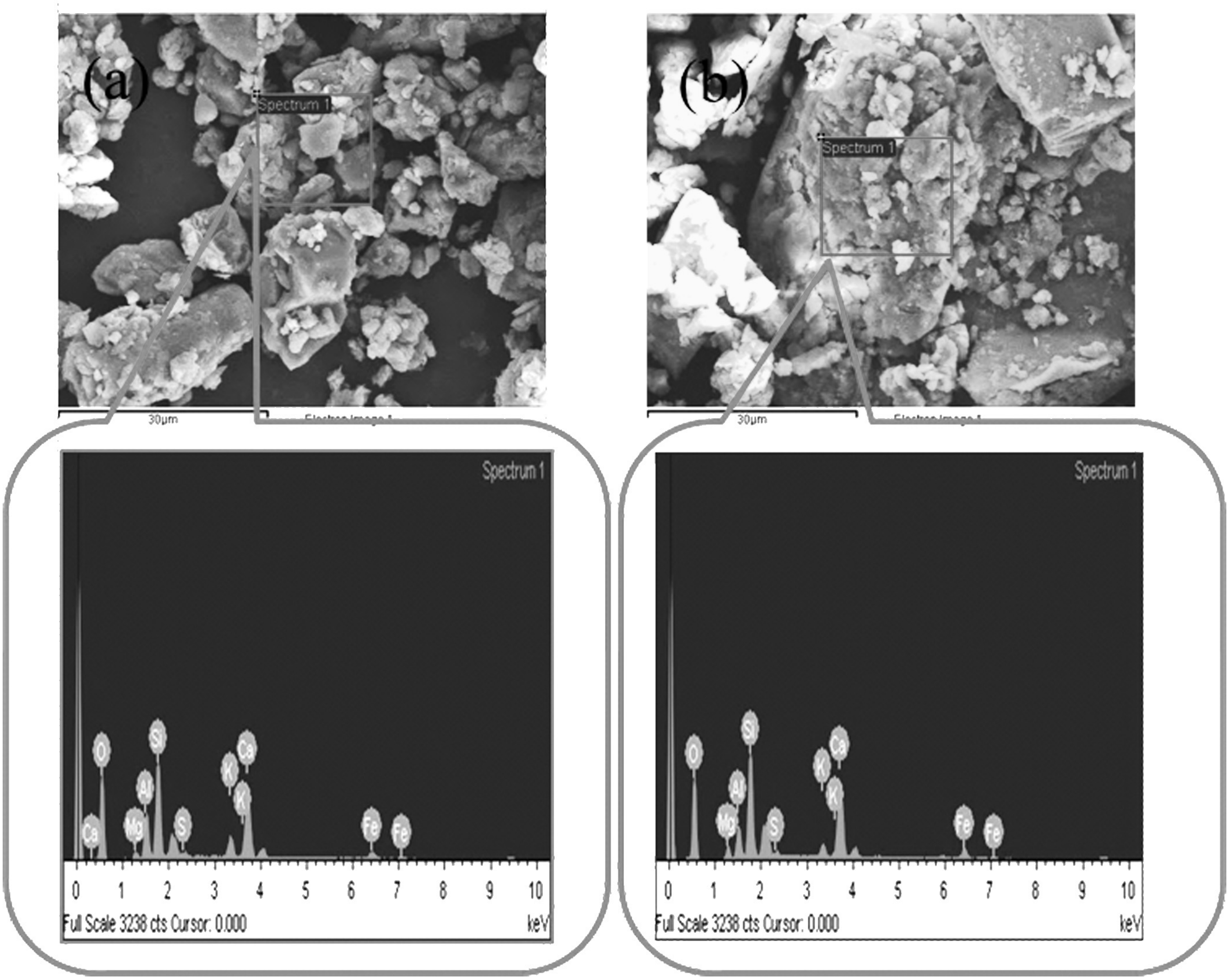

Figure 6. Scanning electron micrograph and energy-dispersive X-ray spectroscopy results for samples smast-7 from cave wall (a) and smast-5 from cave floor (b).

whereas Na_2SO_4 and $CaCl_2$ decreased the bacitracin yield (Yousaf, 1997).

The soil sample from which *B. licheniformis* KC2-MRL was isolated was reddish-brown in color. Brown soils are usually low in organic matter. Terra rossa is a soil that is heavy and clay-rich soil, strongly reddish, developed on limestone or dolomite, usually derived from the insoluble residue of the underlying rock. Following dissolution of calcium carbonate by rain, clay contained in limestone sediments, along with other insoluble substances or rock fragments, forms discontinuous residual layers variable in depth. Under oxidizing conditions iron oxides appear that produce the characteristic red color. According to this theory, terra rossa is usually considered a polygenetic relict soil, formed during the Tertiary and subjected to hot and humid periods during the Quaternary (Jordán, 2014).

X-ray diffraction analysis of the cave sample confirmed the presence of clay minerals, carbonates, and silicates (Hill, 1999). Minerals are produced as a result of intense chemical weathering on land under possibly tropical conditions, where abundant rainfall favored ionic transfer and pedogenic development (Millot, 1970).

Carbonates found in Kashmir Smast are predominantly calcite and traces of dolomite (Vogel et al., 1990; Schwabe et al., 1993). In caves, illite is found mostly in fault zones and also occurs as clay floor deposits (Hill, 1999). Illite is commonly present as little-altered, disintegrated particles (Weaver, 1989). Pedogenic clay minerals are derived from moderate chemical weathering and generally develop in poorly drained tropical to subtropical areas of low relief, marked by flooding during humid seasons and subsequent concentration of solutions in the soil during dry seasons.

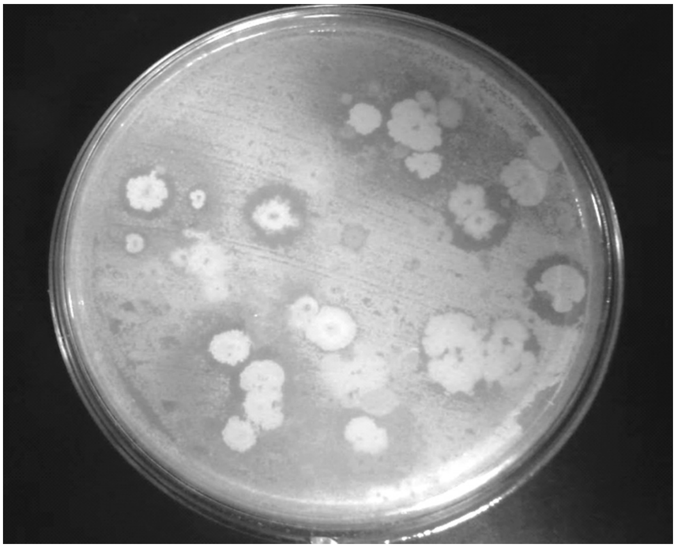

Figure 7. Nutrient-agar plate showing typical zones of inhibition due to antimicrobial activity against a test strain.

Al, Fe, and Si are transported by means of water saturation during wet seasons; concentration for mineral growth takes place during in dry seasons (ChamLey, 1989). During pedogenesis, chlorite transforms into kaolinite, and in intensely weathered laterite soils chlorite would be completely eliminated (Vicente et al., 1997). The accumulations of illite, kaolinite, chlorite, dolomite, and muscovite in Kashmir Smast are probably indicative of changes in degree of weathering, and thus reflect the changes in climatic conditions. The degree of weathering related to the presence of SiO_2 and Al_2O_3 shows a similar pattern to clay minerals (Tardy and Nahon, 1985; Zhao and Yang, 1995). The mineral assemblages investigated in the cave are diverse.

The quantitative mineral analysis technique SIROQUANT determined mineral compositions of rocks, including clay mineral content. Thermal analysis offers an important technique for the determination of thermal stability of minerals and roughly estimating organic content of samples. Importantly, the decomposition curves can be obtained and mechanism of decomposition of the mineral determined. Generally, the theoretical mass loss of water is 10.46%, and structural disorganization upon thermal treatment may occur in response to the loss of hydration water, which could provoke collapse of the crystalline structure (Doak et al., 1965). The two overlapping mass loss steps at 263 and 280 °C are attributed to the hydroxyl group (Palmer and Frost, 2010). The higher mass loss at 280 °C is believed to be due to the loss of both OH^- and CO_3^{2+}. The broad mass loss at 485 °C is ascribed to the loss of carbonate as carbon dioxide (CO_2) (Frost et al., 2009). The higher temperature mass loss at 828 °C is attributed to the Mg.

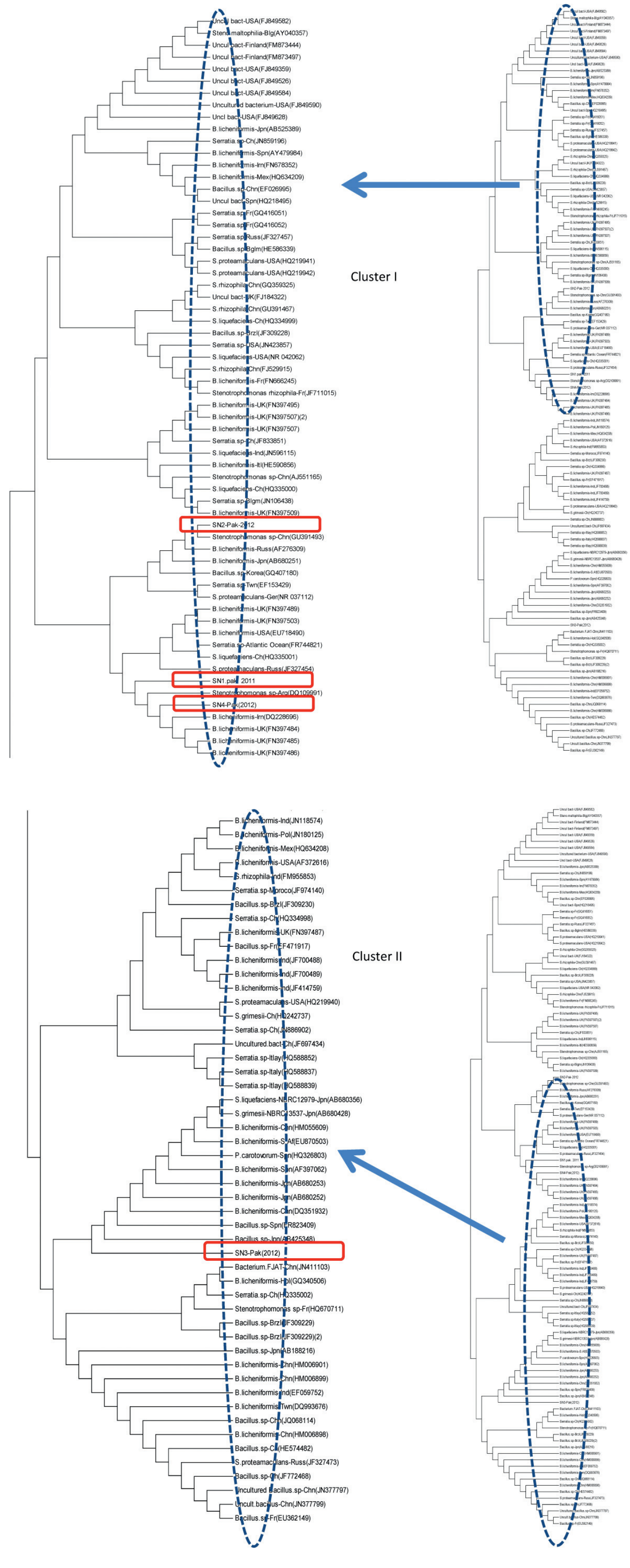

Figure 8. Phylogenetic tree showing all four isolates with related sequences in NCBI.

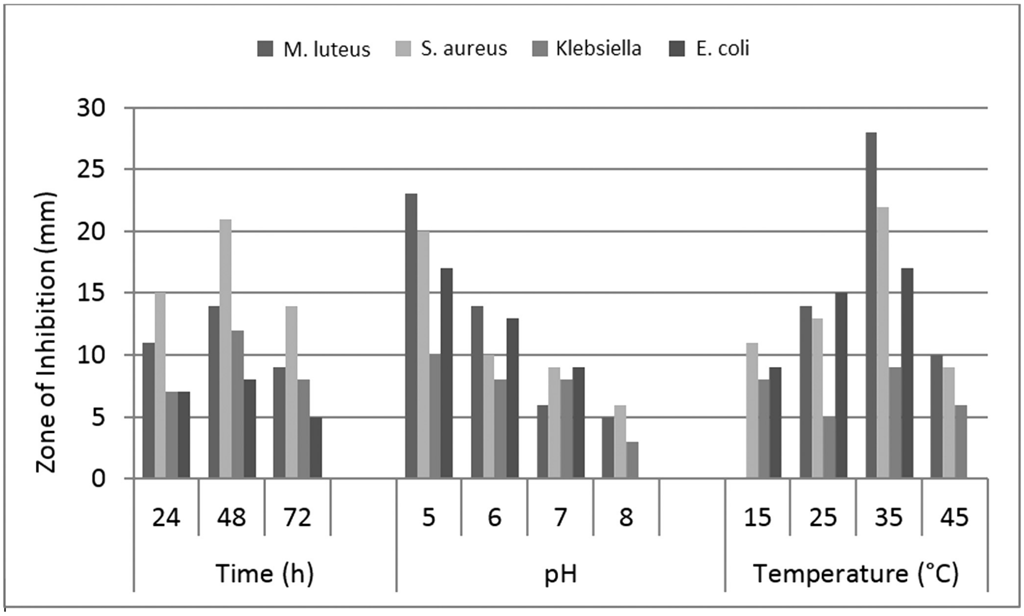

Figure 9. Effect of time of incubation, pH, and temperature on the growth and antimicrobial activity produced by growth of *Bacillus licheniformis* KC2-MRL against *Micrococcus luteus*, *Staphylococcus aureus*, *Klebsiella* sp., and *E. coli*.

Clay particles were observed to have poorly crystallized clasts with angular, irregular outlines, and swirly texture with face-to-face arrangement of clay grains, as also reported by Manju et al. (2001) in the Madayi kaolin deposit, North Kerala, India. Generally, intensely weathered clay flakes show ragged edges, exhibit a rounded outline or bay-shaped edges, and poor lateral dimension, with a particularly small platy thickness. Analysis shows that Si, Al, and Fe were enriched within the samples, which probably reflects minerals such as quartz, feldspar, clay minerals, and iron oxide (Jeong et al., 2003).

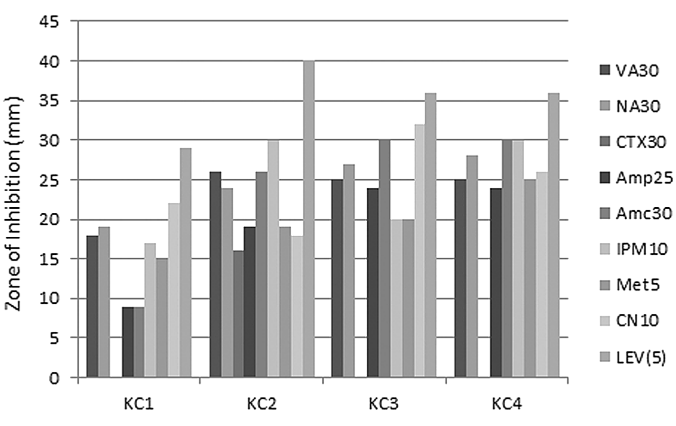

Figure 10. The results of disk-diffusion assay of the susceptability of our four antibiotic producing strains (*Serratia* sp. KC1-MRL, *Bacillus licheniformis* KC2-MRL, *Bacillus* sp. KC3-MRL and *Stenotrophomonas* sp. KC4-MRL) to selected antibiotics. Names of antibiotics can be found in the Results section of the text.

Fourier-transform infrared spectroscopy analysis showed peaks at 885 cm^{-1}, 746 cm^{-1}, and 715 cm^{-1} because of presence of dolomite (White, 1964; Van Der Marel and Beutelspacher, 1976). A wide band around 1020 cm^{-1} is assigned to quartz, SiO_2 (Russell, 1987; Ravisankar et al., 2012), and the peak at 1646 cm^{-1} is attributed to the bending vibration modes of water (Manoharan et al., 2007). Peaks in the region of 2800–3000 cm^{-1} are ascribed to the C–C stretching that is present in the form of organic matter in the mineral contribution (Maritan et al., 2005) or may be due to P–OH bond stretching around 2845 cm^{-1} and 2935 cm^{-1}. The sharp peak at 2513 cm^{-1} is due to the presence of silicate minerals like quartz, nimite, musciovite, and vermiculite (Vedder, 1964). The appearance of broad band in the region of 3000 cm^{-1} to 3700 cm^{-1} is attributed to the structural water present in the mineral vermiculite and to the moisture present in the sample (Zadrapa and Zykova, 2010). The hydroxyl and water-stretching region near 3200 cm^{-1} for most hydrated carbonates usually consists of one or two broad bands shifted somewhat to lower frequencies due to hydrogen bonding (Nakamoto, 2008; Schrader, 1995), but the appearance of the broad band is due to the interpretation OH^- and H_2O in a mineral in which some minerals were participating in hydrogen bonding and some were not involved, e.g., non-hydrogen-bonded Al-OH units (White, 1964; Van Der Marel and Beutelspacher, 1976). Atomic absorption spectroscopy was performed to determine the concentrations of the elements calcium, magnesium, chromium, cobalt, nickel, zinc, copper, and lead in the cave floor soil sample, and it was found that the soil contained very high amount of calcium compared to outside soil.

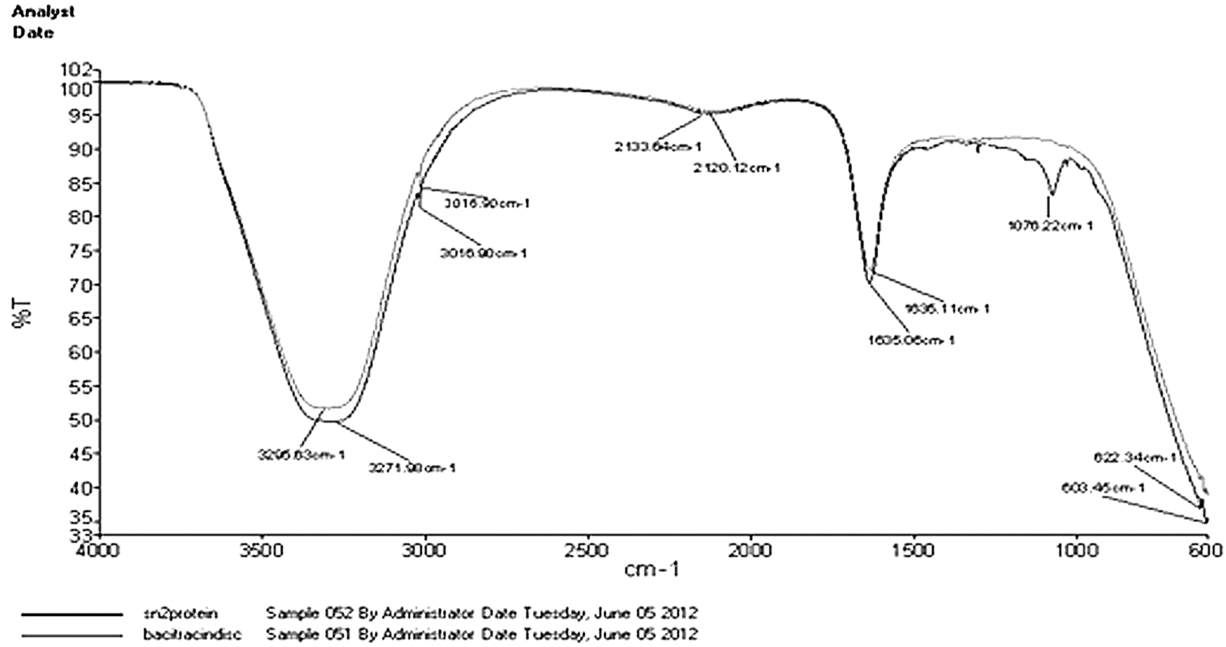

Figure 11. Comparison of Fourier-transform infrared spectra of bacitracin (lighter line) and the antibacterial compound produced by *Bacillus licheniformis* KC2-MRL (darker line).

Microbiology

The capacity of bacteria inhabiting karstic caves to produce valuable biologically active compounds has still not been investigated much (Tomova et al., 2013). Soil is a natural reservoir for microorganisms and their antimicrobial products (Dancer 2004). The four selected strains isolated from cave soil were screened for the production of antibiotics by using agar-well diffusion assay against *Staphylococcus aureus*, *Klebsiella*, *E. coli* and *Micrococcus luteus*. *B. licheniformis* KC2-MRL was selected for further analysis on the basis of the greatest zone of inhibition. In the present study, *B. licheniformis* KC2-MRL showed the best antimicrobial activity against *M. luteus*, followed by *S. aureus*, *Klebsiella* and *E. coli* after 48 hrs of incubation.

Studies show that caves are inhabited by different types of microorganisms having unique characteristics. A cave ecosystem has a deficiency of nutrients, which is why microorganisms present in the cave compete for the nutrients and fight for survival. Due to this struggle among microbes, they have the potential to produce antibiotics against other microbes. There are nine different groups of bacteria that have been reported to be present in caves, Proteobacteria, Acidobacteria, Planctomycetes, Chloroflexi, Bacteroidetes, Gemmatimonadetes, Nitrospirae, Actinobacteria and Firmicutes (Zhou et al., 2007; Porttillo et al., 2008). Proteobacteria are the dominant bacteria in caves (Zhou et al., 2007). The 16S rRNA gene sequences of our antibiotic producing cave bacteria have been submitted to NCBI GenBank. The isolates KC1-MRL, KC2-MRL, KC3-MRL and KC4-MRL were identified as *Serratia* sp. KC1-MRL (Accession No. KC128829.1), *Bacillus licheniformis* KC2-MRL (Accession No. KC128830.1), *Bacillus* sp. KC3-MRL (Accession No. KC128831.1), and *Stenotrophomonas* sp. KC4-MRL (Accession No. KC128832.1). In Magura Cave, Bulgaria, Tomonova et al. (2013) reported that Gram-positive bacteria were represented by the genera *Bacillus*, *Arthrobacter*, and *Micrococcus*.

Soil bacterial genera such as *Bacillus, Streptomyces*, and *Pseudomonas* synthesize a high proportion of agriculturally and medically important antibiotics (Hosoya et al., 1998; Sharga et al., 2004). Peptide antibiotics are the major group of antibiotics (Pinchuk et al., 2002). Antibiotic-producing microorganisms can be found in different habitats, but the majority are common inhabitants of soil. Caves contain abundant *Actinobacteria*, which are valuable sources of novel antibiotics that can replace currently ineffective antibiotics (Montano and Henderson, 2012). Molecular analysis of a sample from Kashmir cave showed the presence of different bacterial strains.

Isolated strains were screened for the production of antimicrobial compounds by using agar-well diffusion assay. Ducluzeau et al. (1978) isolated *Bacillus licheniformis* that was active against *Clostridium perfringens* or *Lactobacillus* sp. Muhammad et al. (2009) also observed that *Bacillus* metabolites showed activity against *M. luteus* and *S. aureus*. Bacitracin is a major polypeptide antibiotic produced by *Bacillus licheniformis* and *Bacillus subtilis*, based on using *M. luteus* as a test organism (Vieira et al., 2011). *B. licheniformis* isolated from marine sediments showed best antimicrobial activity against pathogenic test strains *S. aureus*, *E. coli* and *P. aeruginosa* (Hosny et al., 2011). Antibiotic production depends upon the composition of the medium, which is required for cell biomass and for its maintenance (Stanbury et al., 1995, chap. 4). Maximum activity was found when *Bacillus licheniformis* was grown in nutrient broth. Similarly, Vieira et al. (2011) used nutrient broth for the growth of *B. licheniformis* when incubated at 46 °C in a shaking incubator at 150 rpm. Al-Janabi (2006), Yilmaz et al. (2006), and Al-Ajlani and Hasnain. (2010) also reported maximum production of antimicrobial compound by *Bacillus* sp. in nutrient broth medium at varying temperatures.

External factors can also affect the growth of microorganisms and the production of antibiotics (Marwick et al., 1999). It has been reported that environmental factors such as temperature, pH, and incubation duration influence antibiotic production (Iwai et al., 1973). In our study, the optimum temperature for antimicrobial compound production was observed to be 30 to 35 °C. Béahdy (1974) and Haddar et al. (2007) observed production of bacitracin and other antibiotics by *B. licheniformis* (Zarei, 2012) at 37 °C, and it was also seen at 30 °C by Hosny et al. (2011).

We found that our selected organism showed optimum activity at pH 5–6. Flickinger and Perlman (1979) reported pH 6.5 for the optimum production of antibiotics by *B. licheniformis*. Haddar et al. (2007) found maximum bacitracin production rate (192 units/mL) at pH 7.5. A similar study was conducted by Gulahmadov et al. (2006) that found antimicrobial activity was best at the wide pH range of 6–8 by *Bacillus* sp. Newly emergent infectious diseases, re-emerging diseases, and multidrug-resistant bacteria mean that there is a persistent need to produce novel antimicrobial compounds (Uzair et al., 2009).

We performed an antibiotic susceptibility test in which *B. licheniformis* KC2-MRL was found resistant to cefotaxime, but was more susceptible to levofloxacin, which produces a 40 mm zone of inhibition. *B. thuringiensis* RSKK 380 was reported to be unaffected by cephazolin, cefoxitin, and cefamandole (Yilmaz et al., 2006).

Our results show that the antibacterial activity was stable up to 45 °C. A similar study by He et al. (2006) reported *B. licheniformis* to be stable at 25 °C for 6 hrs and inactivated above 40 °C. However, in some cases the antimicrobial compounds retained their activity even after autoclaving the sample at 121 °C (Fontoura et al., 2009; Tabbene et al., 2009; Uzair et al., 2009; Ebrahimipour et al., 2010). At the same time, sensitivity to different pH values was also evaluated in the present study, and the antimicrobial compound was found to be stable at pH 5–7. A similar study, in which antimicrobial activity was found to be stable at pH 7, was reported by He et al. (2006). The stability of antibacterial activity at pH 7 and after heat-treatment might be useful in several industrial applications (Tabbene et al., 2009). Our study showed best activity against *M. luteus*, *S. aureus*, and *E. coli* after 48 hours of incubation. A similar study by Aslim et al. (2002) showed the maximum zone of inhibition after 24 to 48 hrs.

Bacillus licheniformis KC2-MRL was further tested for antibiotic sensitivity by using the antibiotics vancomycin, nalidixic acid, cefotoxime, ampicillin, amoxicillin, imipenem, methicillin, Cefoten, and levofloxacin. It was found that the selected strain was more susceptible to levofloxacin, which produced a 40-mm zone of inhibition (Fig. 10).

Sirtori et al. (2006) reported clear absorption peaks at 3,500, 2,925, 1,639, and 1,546 cm^{-1} corresponding to the O–H, C–H, C–N and angular deformation of the N–H bond. Kong and Yu (2007) also detected bands at peaks of 3100, 1600–1690, 1480–1575 and 1229–1301 cm^{-1} that are assigned to N–H, C=O, C–N and N–H. Kumar et al. (2010) reported absorption bands at 1670, 1539, 1418, and 1488 cm^{-1} attributing to N–H, C=O, O–H and CO.

CONCLUSION

Our study explored the ability of cave microorganisms to produce antibiotics and characterized of the producing strain. Due to the internal acidic environment and high calcium concentration in the cave, *Bacillus licheniformis* KC2-MRL grew better under acidic conditions at temperatures higher than that in the cave. Caves of Pakistan had never been explored for the presence of bacteria with regards to diversity or having ability to produce novel antimicrobial metabolites. These metabolites, as well as those produced in other caves, can be further investigated to find bioactive compounds with unique characteristics.

REFERENCES

Adetutu, E.M., and Ball, A.S., 2014, Microbial diversity and activity in caves: Microbiology Australia, v. 35, p.192–194. doi:10.1071/MA14062.

Adetutu, E.M., Thorpe, K., Shahsavari, E., Bourne, S., Cao, Xiangsheng, Fard, R.M.N., Kirby, G., and Ball, A.S., 2012, Bacterial community survey of sediments at Naracoorte Caves, Australia: International Journal of Speleolology: v. 41, p. 137–147. doi:10.5038/1827-806X.41.2.2.

Aitken, M.A., 2012, Phenol: Chloroform: Isoamyl Alcohol (25:24:1). http://www.nhm.ac.uk/resources-rx/files/phenol-chloroform_aug12-118646.pdf. [Assessed March 23, 2014]

Al-Ajlani, M.M., and Hasnain, S., 2010, Bacteria exhibiting antimicrobial activities: Screening for antibiotics and the associated genetic studies: The Open Conference Proceedings Journal: v. 1, p. 230–238. doi:10.2174/2210289201001010230.

Al-Janabi, A.A.H.S., 2006, Identification of bacitracin produced by local isolate of *Bacillus licheniformis*: African Journal of Biotechnology, v. 5, p. 1600–1601.

Aslim, B., Sağlam, N., and Beyatali Y., 2002, Determination of some properties of *Bacillus* isolated from soil: Turkish Journal of Biology, v. 26, p. 41–48.

Atlas, R.M., and Bartha, R., 1998, Microbial Ecology: Fundamentals & Applications, fourth edition: San Francisco, Benjamin/Cummings, 640 p.

Barton, H.A., 2006, Introduction to cave microbiology: A review for the non-specialist: Journal of Cave and Karst Studies, v. 68, p. 43–54.

Barton, H.A., and Jurado, V., 2007, What's up down there? Microbial diversity in caves: Microbe, v. 2, no. 3, p. 132–138.

Basak, K., and Majumdar, S.K., 1975, Mineral nutrition of *Streptomyces kanamyceticus* for kanamycin formation: Antimicrobial Agents and Chemotherapy, v. 8, no. 4, p. 391–395. doi:10.1128/AAC.8.4.391.

Béahdy, J., 1974, Recent developments of antibiotic research and classification of antibiotics according to chemical structure: Advances in Applied Microbiology, v. 18, p. 309–406. doi:10.1016/S0065-2164(08)70573-2.

Bérdy, J., 2005, Bioactive microbial metabolites: The Journal of Antibiotics, v. 58, no. 1, p. 1–26. doi:10.1038/ja.2005.1.

Boston, P.J., Spilde, M.N., Northup, D.E., Melim, L.A., Soroka, D.S., Kleina, L.G., Lavoie, K.H., Hose, L.D., Mallory, L.M., Dahm, C. N., Crossey, L.J., and Schelble, R.T., 2001, Cave biosignature suites: Microbes, minerals and Mars: Astrobiology, v. 1, p. 25–55.

Brock, T.D., and Madigan, M.T., 1991, Biology of Microorganisms: Upper Saddle River, New Jersey, Prentice-Hall, 860 p.

ChamLey, H., 1989, Clay Sedimentology: New York, Springer-Verlag, 623 p.

Cheng, Xiaodong, Kumar, S., Posfai, J., Pflugrath, J.W., and Roberts, R.J., 1993, Crystal structure of the HhaI DNA methyltransferase complexed with S-adenosyl-L-methionine: Cell, v. 74, p. 299–307. doi:10.1016/0092-8674(93)90421-L.

Cuezva, S., Sanchez-Moral, S., Saiz-Jimenez, C., and Cañaveras, J.C., 2009, Microbial communities and associated mineral fabrics in Altamira Cave, Spain: International Journal of Speleology, v. 38, no. 1, p. 83–92.

Dancer, S.J., 2004, How antibiotics can make us sick: The less obvious adverse effects of antimicrobial chemotherapy: The Lancet Infectious Diseases, v. 4, p. 611–619. doi:10.1016/S1473-3099(04)01145-4.

Davies, W.E., and Morgan, I.M., 2000, Geology of Caves: U.S. Geological Survey, http://www.nature.nps.gov/geology/usgsnps/cave/cave.html. Last updated on May 9, 2000 [Accessed May 1, 2013]

Demain, A.L., Aharonowitz, Y., and Martin, J.F., 1983, Metabolite control of secondary biosynthetic pathways, *in* Vining, L.C., ed., Biochemistry and Genetic Regulation of Commercially Important Antibiotics: London, Addison-Wesley, Biotechnology Series 2, p. 49–67.

Doak, B.W., Gallagher, P.J., Evans, L., and Muller, F.B., 1965, Low-temperature calcination of "C"-grade phosphate from Christmas island —I. Growth and yield characteristics: New Zealand Journal of Agriculture Research, v. 8. p. 15–29. doi:10.1080/00288233.1965.10420020.

Doull, J.L., and Vining, L.C., 1990, Physiology of antibiotic production in actinomycetes and some underlying control mechanisms: Biotechnology Advances, v. 8, no. 1, p. 141–158. doi:10.1016/0734-9750(90)90010-9.

Ducluzeau, J.R., Dubos, F., Raibaud, P., and Abrams, G.D., 1978, Production of an antibiotic substance by *Bacillus licheniformis* with in the digestive tract of gnotobiotic mice: Antimicrobial Agents and Chemotherapy, v. 13. p. 97–103. doi:10.1128/AAC.13.1.97.

Dutrow, B.L., and Clark, C.M., n.d., X-Ray Powder Diffraction (XRD), http://serc.carleton.edu/research_education/geochemsheets/techniques/XRD.htmL.

Ebrahimipour, G., Moradi, A., Mehrdad, M., Marzban, A., and Alaee, H., 2010, Evaluation of antimicrobial substance produced by a bacterium isolated from *Parmacella iberica*: Jundishapur Journal of Microbiology, v. 4, p. 131–141.

Engel, A., Zondervan, I., Aerts, K., Beaufort, L., Benthien, A., Chou, L., Delille, B., Gattuso, J.-P., Harlay, J., Heemann, C., Hoffmann, L., Jacquet, S., Nejstgaard, J., Pizay, M.-D., Rochelle-Newall, E., Scheider, U., Terbrueggen, A., and Riebesell, U., 2005, Testing the direct effect of CO_2 concentration on a bloom of the coccolithophorid *Emiliania huxleyi* in mesocosm experiments: Limnology and Oceanography, v. 50, no. 2, p. 493–507. doi:10.4319/lo.2005.50.2.0493.

Flickinger, M.C., and Perlman, D., 1979, Application of oxygen-enriched aeration in the production of bacitracin by *Bacillus licheniformis*: Antimicrobial Agents and Chemotherapy, v. 15, p. 282–293. doi:10.1128/AAC.15.2.282.

Fontoura, R., Spada, J.C., Silverira, S.T., Tsai, S.M., and Brandelli, A., 2009, Purification and characterization of an antimicrobial peptide produced by *Pseudomonas* sp. strain 4B: World Journal of Microbial Biotechnology, v. 25, p. 205–213. doi:10.1007/s11274-008-9882-4.

Frost, R.L., Hales, M.C., and Martens, W.N., 2009, Thermogravimetric analysis of selected group (II) carbonate minerals—Implication for the geosequestration of greenhouse gases: Journal of Thermal Analysis and Calorimetry, v. 95, p. 999–1005. doi:10.1007/s10973-008-9196-7.

Gauthier, M.J., 1976, Modification of bacterial respiration by a macromolecular polyanionic antibiotic produced by a marine *Alteromonas*: Antimicrobial Agents and Chemotherapy, v. 9, p. 361–366. doi:10.1128/AAC.9.3.361.

Georgieva-Borisova, J.Ch., 1974, Taxonomic characteristics of strain *Actinomyces hygroscopicus* B-255 and conditions for its antibiotic production [PhD dissertation], University of Sofia, Bulgaria.

Gesheva, V., Ivanova, V., and Gesheva, R., 2005, Effects of nutrients on the production of AK-111-81 macrolide antibiotic by *Streptomyces hygroscopicus*: Microbiological Research, v. 160, no. 3, p. 243–248. doi:10.1016/j.micres.2004.06.005.

Groth, I., Vetterman, R., Schuetze, B., Schumann, P., and Saiz-Jimenez, C., 1999, Actinomycetes in karstic caves of northern Spain (Altamira and Tito Bustillo): Journal of Microbiological Methods, v. 36, p. 115–122. doi:10.1016/S0167-7012(99)00016-0.

Gulahmadov, S.G., Batdorj, B., Dalgalarrondo, M., Chobert, J.-M., Kuliev, A.A., and Haertlé, T., 2006, Characterization of bacteriocin-like inhibitory substances (BLIS) from lactic acid bacteria isolated from traditional Azerbaijani cheeses: European Food Research and Technology, v. 224, no. 2, p. 229–235. doi:10.1007/s00217-006-0338-5.

Haddar, H.O., Aziz, G.M., and Al-Gelawi, M.H., 2007, Optimization of bacitracin production by *Bacillus licheniformis* B5: Pakistan Journal of Biological Sciences, v. 10, p. 972–976. doi:10.3923/pjbs.2007.972.976.

Hancock, R.E., and Chapple, D.S., 1999, Peptide antibiotics: Antimicrobial Agents and Chemotherapy, v. 43, no. 6, p. 1317–1323.

Haque, S.F., Sen, S.K., and Pal, C.S., 1995, Nutrient optimization for the production of broad spectrum antibiotics by *Streptomyces*. Antibiotics Str. 15.4: Acta Microbiolgica et Immunologica Hungarica, v. 42, p. 155–162.

He, Lili, Chen, Weiliang, and Liu, Yang, 2006, Production and partial characterization of bacteriocin like pepitdes by *Bacillus licheniformis* ZJU12: Microbiological Research, v. 161, p. 321–326. doi:10.1016/j.micres.2005.12.002.

Hill, C.A., 1999, Mineralogy of Kartchner Caverns, Arizona: Journal of Cave and Karst Studies, v. 61, p. 73–78.

Holt, J.G., Bergey, D.H., and Krieg, N.R., 2012, Bergey's Manual of Determinative Bacteriology, 9th edition.

Hosny, M.S., Sheir, D.H., and Eldewany, A.I., 2011, Production of antimicrobial agent from marine bacteria isolated from Mediterranean: Australian Journal of Basic and Applied Sciences, v. 5, no. 5, p. 121–128.

Hosoya, Y., Okamoto, S., Muramatsu, H., and Ochi, K., 1998, Acquisition of certain streptomycin-resistant (*str*) mutations enhances antibiotic production in bacteria: Antimicrobial Agents and Chemotherapy, v. 42, p. 2041–2047.

Ikner, L.A., Toomey, R.S., Nolan, G., Neilson, J.W., Pryor, B.M., and Maier, R.M., 2007, Culturable microbial diversity and the impact of tourism in Kartchner Caverns, Arizona: Microbial Ecology, v. 53, no. 1, p. 30–42. doi:10.1007/s00248-006-9135-8.

Iwai, Y., Awaya, J., Kesado, T., Yamada, H., Ōmura, S., and Hata, T., 1973, Selective production of cerulenin by *Cephalosporium caerulens* KF-140: Journal of Fermentation Technology, v. 51, p. 575–581.

Jeong, Gi Young, Kim, Soo Jin, and Chang, Sae Jung, 2003, Black carbon pollution of speleothems by fine urban aerosols in tourist caves: American Mineralogist, v. 88, p. 1872–1878.

Jensen, S., Reutergård, L., and Jansson, B., 1983, Analytical methods for measuring organochlorines and methyl mercury by gas chromatography, *in* FAO/SIDA Manual of Methods in Aquatic Environmental Research, Part 9, Analysis of Metals and Organochlorines in Fish: FAO Fisheries Technical Paper 212, p. 21–33.

Jordán, A., 2014, Soils Going Red: Terra Rossa, blog of Soil System Sciences Division, European Geosciences Union, http://blogs.egu.eu/divisions/sss/2014/01/09/soils-going-red-terra-rossa. [Accessed January 3, 2015]

Jurado, V., Gonzalez, J.M., Laiz, L., and Saiz-Jimenez, C., 2006, *Aurantimonas altamirensis* sp. nov, a member of the order Rhizobiales isolated from Altamira Cave: International Journal of Systemic Evolutionary Microbiology, v. 56, p. 2583–2585. doi:10.1099/ijs.0.64397-0.

Koneman, E.W., 2006, Color Atlas and Textbook of Diagnostic Microbiology, sixth edition, Philadelphia, Lippincott Williams & Wilkins, 1736 p.

Kong, Jilie, and Yu, Shaoning, 2007, Fourier transform infrared spectroscopic analysis of protein secondary structures: Acta Biochimica Biophysica Sinica, v. 39, p. 549–559. doi:10.1111/j.1745-7270.2007.00320.x.

Kumar, S., Malhotra, R., and Kumar, D., 2010, Antihyperglycemic, antihyperlipidemic and antioxidant activities of *Euphorbia hirta* stem extract: International Research Journal of Pharmacy, v. 1, p. 150–156.

Laiz, L., Groth, I., Gonzalez, I., and Sáiz-Jiménez, C., 1999, Microbiological study of the dripping waters in Altamira cave (Santillana del Mar, Spain): Journal of Microbiological Methods, v. 36, no. 1, p. 129–138. doi:10.1016/S0167-7012(99)00018-4.

Lavoie, K.H., and Northup, D.E., 2005, Bacteria as indicators of human impact in caves, *in* Rea, G.T. ed., Proceedings of the 2005 National Cave and Karst Management Symposium: NCKMS Steering Committee, p. 40–47.

Liu, Chao-Min, McDaniel, L., and Schaffner, C.P., 1975, Factors affecting the production of candicidin: Antimicrobial Agents and Chemotherapy, v. 7, no. 2, p. 196–202. doi:10.1128/AAC.7.2.196.

Luong, P., Kinch, L.N., Brautigam, C.A., Grishin, N.V., Tomchick, D.R., and Orth, K., 2010, Kinetic and structural insights into the mechanism of AMPylation by VopS Fic domain: Journal of Biological Chemistry, v. 285, no. 26, p. 20155–20163. doi:10.1074/jbc.M110.114884.

Manju, C.S., Nair, V.N., and Lalithambika, M., 2001, Mineralogy, geochemistry and utilization study of the Madayi kaolin deposit, North Kerala, India: Clays and Clay Minerals, v. 49, p. 355–369.

Manoharan, C., Venkatachalapathy, R., Dhanapandian, S. and Deenadayalan, K., 2007, FTIR and Mössbauer spectroscopy applied to the study of archaeological artefacts from Maligaimedu, Tamil Nadu, India: Indian Journal of Pure and Applied Physics, v. 45, p. 860–865.

Maritan, L., Mazzoli, C., Nodari, L., and Russo, U., 2005, Second Iron Age grey pottery from Este (northeastern Italy): Study of provenance and technology: Applied Clay Science, v. 29, p. 31–44. doi:10.1016/j.clay.2004.09.003.

Marwick, J.D., Wright, P.C., and Burgess, J.G., 1999, Bioprocess intensification for production of novel marine bacterial antibiotics through bioreactor operation and design: Marine Biotechnology, v. 1, p. 495–507. doi:10.1007/PL00011806.

Millot, G., 1970, Geology of Clays: Weathering, Sedimentology, Geochemistry: Berlin, Springer Verlag, 430 p. doi:10.1007/978-3-662-41609-9.

Montano, E.T., and Henderson, L.O., 2012, Studies of antibiotic production by cave bacteria, *in* Cheeptham, N., ed., Cave Microbiomes: A Novel Resource for Drug Discovery: New York, Springer-Verlog, Springer Briefs in Microbiology 1, p. 109–130. doi:10.1007/978-1-4614-5206-5.

Muhammad, S.A., Ahmad, S., and Hameed, A., 2009, Antibiotic production by thermophilic *Bacillus specie* SAT-4: Pakistan Journal of Pharmaceutical Sciences, v. 22. p. 339–345.

Nakamoto, K., 2008, Infrared and Raman Spectra of Inorganic and Coordination Compounds, Part A: Theory and Applications in Inorganic Chemistry, sixth edition: New York, John Wiley and Sons, 419 p. doi:10.1002/9780470405840.

Nelson, A.P., 1996, What would real little green men tell us about evolution–and God? (Review of Davies, P., Are we alone? Philosophical Implications of the Discovery of Extraterrestrial Life: New York, Basic Books, 160 p.): Origens & Design, v. 17, no. 1.

Nissen-Meyer, J., and Nes, I.F., 1997, Ribosomally synthesized antimicrobial peptides: Their function, structure, biogenesis, and mechanism of action: Archives of Microbiology, v. 167, no. 2–3, p. 67–77. doi:10.1007/s002030050418.

Northup, D.E., and Lavoie K.H., 2004, Microorganisms in caves, *in* Gunn, J., ed., Encyclopedia of Caves and Karst Science: London, Taylor and Francis, p. 506–509.

Onaga, L., 2001, Cashing in on nature's pharmacy: EMBO Reports, v. 2, p. 263–265. doi:10.1093/embo-reports/kve077.

Palmer, S.J., and Frost, R.L., 2010, Thermal decomposition of Bayer precipitates formed at varying temperatures: Journal of Thermal Analysis and Calorimetry, v. 100, p. 27–32. doi:10.1007/s10973-009-0136-y.

Park Chang-Woong, Lee Hye-Sook, and Kim Yong-Sik, 1998, Mechanism of MPP^+-induced cytotoxicity in human neuroblastoma SH-SY5Y: Journal of Toxicological Sciences, v. 23, suppl., p. 184–188. doi:10.2131/jts.23.SupplementII_184.

Pereda, A., Summers, R.G., Stassi, D.L., Ruan, X., and Katz, L., 1998, The loading domain of the erythromycin polyketide synthase is not essential for erythromycin biosynthesis in *Saccharopolyspora erythraea*: Microbiology, v. 144, no. 2, p. 543–553. doi:10.1099/00221287-144-2-543.

Pinchuk, I.V., Bressollier, P., Sorokulova, I.B., Verneuil, B., and Urdaci, M.C., 2002, Amicoumacin antibiotic production and genetic diversity of *Bacillus subtilis* strains isolated from different habitats: Research in Microbiology, v. 153, p. 269–276. doi:10.1016/S0923-2508(02)01320-7.

Portillo, M.C., Gonzalez, J.M., and Saiz-Jimenez, C., 2008, Metabolically active microbial communities of yellow and grey colonizations on the walls of Altamira Cave, Spain: Journal of Applied Microbiology, v. 104, p. 681–691. doi:10.1111/j.1365-2672.2007.03594.x

Ravisankar, R., Eswaran, P., Rajalakshmi, A., Chandrasekaran, A., Thillaivelavan, K.K., and Dhinakaran, B., 2012, Beach rock from the south east Coast of Tamilnadu, India. A spectroscopic study: Advances in Applied Science Research, v. 3, p. 95–102.

Rigali, S., Titgemeyer, F., Barends, S., Mulder, S., Thomae, A.W., Hopwood, D.A., and van Wezel, G.P., 2008, Feast or famine: The global regulator DasR links nutrient stress to antibiotic production by *Streptomyces*: EMBO Reports, v. 9, no. 7, p. 670–675. doi:10.1038/embor.2008.83.

Riley, M.A., and Wertz, J.E., 2002, Bacteriocins: Evolution, ecology, and application: Annual Review of Microbiology, v. 56, p. 117–137. doi:10.1146/annurev.micro.56.012302.161024.

Russell, J.D., 1987, Infrared methods, *in* Wilson, M.J., ed., A Handbook of Determinative Methods in Clay Mineralogy: Glasgow, Blackie, p. 133–173.

Sanchez, S., and Demain, A.L., 2002, Metabolic regulation of fermentation processes: Enzyme and Microbial Technology, v. 31, no. 7, p. 895–906. doi:10.1016/S0141-0229(02)00172-2.

Schrader, B., ed., 1995, Infrared and Raman Spectroscopy: Methods and Applications: Weinheim, Wiley-VCH. doi:10.1002/9783527615438.

Schwabe, S.J., Carew, J.L., and Mylroie, J.E., 1993, The petrology of Bahamian Pleistocene eolianites and flank margin caves: Implications for late Quaternary island development, *in* White, B., ed., Proceedings of the Sixth Symposium on the Geology of the Bahamas: San Salvador, Bahamian Field Station, p. 149–164.

Sharga, B.M., Nikolaychuk, V.I., and Maga, M.I., 2004, Comparative IR spectrometry of antimicrobial substances derived antibiotic from *Bacillus*: Journal of the Uzhhorod National University, Series Biology, v. 15, p. 75–77.

Simmons, J.A., Currie, W.S., Eshleman, K.N., Kuers, K., Monteleone, S., Negley, T.L., Pohlad, B.R., and Thomas, C.L., 2008, Forest to reclaimed mine land use change leads to altered ecosystem structure and function: Ecological Applications, v. 18, no. 1, p. 104–118. doi:10.1890/07-1117.1.

Singh, Atul Pratap, and Mishra, S., 2013, Studies on antibiotic production by soil microflora and their biochemical characterization from different industrial waste polluted soil samples in (Uttar Pradesh and Uttarakhand) India: IOSR Journal of Pharmacy and Biological Science, v. 7, no. 4. p. 32–43. doi:10.9790/3008-0743243.

Sirtori, L.R., Cladera-Olivera, F., Lorenzini, D.M., Tsai, S., and Brandelli, A., 2006, Purification and partial characterization of an antimicrobial peptide produced by *Bacillus* sp. strain P45, a bacterium from the Amazon basin fish *Piaractus mesopotamicus*: Journal of General and Applied Microbiology, v. 52, p. 357–363. doi:0.2323/jgam.52.357

Solivery, S., Mendosa, A., and Arias, M.-E., 1988, Effect of different nutrients on the production of polyene antibiotics PA-5 and PA-7 by *Streptoverticillium* sp. 43/16 in chemically defined medium: Applied Microbiology and Biotechnology, v. 28, p. 254–257. doi:10.1007/BF00250450.

Stanbury, P.F., Whitaker, A., and Hall, S.J., 1995, Principles of Fermentation Technology, second edition: Oxford, Butterworth-Heinemann, 376 p.

Stranks, D.R., Heffernan, M.L., Lee Dow, K.C., McTigue, P.T., and Withers, G.R.A., 1970, Chemistry: A Structural View, second edition: Carlton, Victoria, Melbourne University Press, 516 p.

Tabbene, O., Karkouch, I., Elkahoui, S., Cosette, P., Mangoni, M.-L., Jouenne, T., and Limam, F., 2009, A new antibacterial and antioxidant S07-2 compound produced by *Bacillus subtilis* B38: FEMS Microbiology Letters, v. 303, p. 176–182. doi:10.1111/j.1574-6968.2009.01875.x.

Tanaka, Y., Hosaka, T., and Ochi, K., 2010, Rare earth elements activate the secondary metabolite–biosynthetic gene clusters in *Streptomyces coelicolor* A3(2): The Journal of Antibiotics, v. 63, p. 477–481. doi:10.1038/ja.2010.53.

Tardy, Y., and Nahon, D., 1985, Geochemistry of laterites, stability of Al-goethite, Al-hematite, and Fe (super 3+)-kaolinite in bauxites and ferricretes: An approach to the mechanism of concretion formation: American Journal of Science, v. 285, p. 865–903. doi:10.2475/ajs.285.10.865.

Taylor, J.C., 1991, Computer programs for standardless quantitative analysis of minerals using the full powder diffraction profile: Powder Diffraction, v. 6, p. 2–9. doi:10.1017/S0885715600016778.

Taylor, J.C., and Clapp, R.A., 1992, New features and advanced applications of SIROQUANT: A personal computer XRD full profile quantitative analysis software package: Advances in X-Ray Analysis, v. 35, p. 49–55.

Thompson, J.D., Higgins, D.G., and Gibson, T.J., 1994, CLUSTAL W: Improving the sensitivity of progressive multiple sequence alignment through sequence weighting, position-specific gap penalties and weight matrix choice: Nucleic Acids Research, v. 22, p. 4673–4680. doi:10.1093/nar/22.22.4673.

Tomova, I., Lazarkevich, I., Tomova, A., Kambourova, M., and Vasileva-Tonkova, E., 2013, Diversity and biosynthetic potential of culturable aerobic heterotrophic bacteria isolated from Magura Cave, Bulgaria: International Journal of Speleology, v. 42, no. 1, p. 65–76.

Uzair, M., Ahmed, M., and Nazim, K., 2009, Effect of industrial waste on seed bank and growth of wild plants in Dhabeji area, Karachi, Pakistan: Pakistan Journal of Botony, v. 41, p. 1659–1665.

Van Der Marel, H.W., and Beutelspacher, H., 1976, Atlas of Infrared Spectroscopy of Clay Minerals and Their Admixtures: Amsterdam, Elsevier Publishing Company, 396 p.

Vedder, W., 1964, Correlations between infrared spectrum and chemical composition of mica: American Mineralogist, v. 49, p. 736–768.

Vicente, M.A., Elsass, F., Molina, E., and Robert, M., 1997, Palaeoweathering in slates from the Iberian Hercynian Massif (Spain); investigation by TEM of clay mineral signatures: Clay Minerals, v. 32, p. 435–451.

Vieira, A.M., Alencar, A.A., and Alves Da Silva, C.A., 2011, Bacitracin produced by *Bacillus licheniformis* (UCP 1014) using economic medium formulated with milk serum [abstract]: Holos Environment, v. 11, suppl. 1 (Resumos apresentados no V Simpósio de Microbiologia Aplicada, Rio Claro), p. 20.

Vogel, P.N., Mylroie, J.E., and Carew, J.L., 1990, Limestone petrology and cave morphology on San Salvador Island, Bahamas: Cave Science, v. 17, p. 19–30.

Voitovich, V.B., Lavrenko, V.A., Voitovich, R.F., and Golovko, E.I., 1994, The effect of purity on high-temperature oxidation of zirconium: Oxidation of Metals, v. 42, p. 223–237. doi:10.1007/BF01052024.

Weaver, C.E., 1989, Clays, Muds, and Shales: Amsterdam, Elsevier, Scientific Publications, Development in Sedimentology 44, 819 p.

White, R.G., 1964, Handbook of Industrial Infrared Analysis: New York, Plenum Press, 440 p.

Yeaman, M.R., and Yount, N.Y., 2003, Mechanisms of antimicrobial peptide action and resistance: Pharmacological Reviews, v. 55, no. 1, p. 27–55. doi:10.1124/pr.55.1.2.

Yilmaz, M., Soran, H., and Beyatli, Y., 2006, Antimicrobial activities of some *Bacillus* spp. strains isolated from the soil: Microbiological Research, v. 161, p. 127–131. doi:10.1016/j.micres.2005.07.001.

Yousaf, M., 1997, Studies on the cultural conditions for the production of antibiotic bacitracin by *B. licheniformis* [Ph.D. dissertation], Islamia University, Bahawalpur.

Zadrapa, P., Zykova, J., Tripska, E., Malac, J., and Kovarova, L., 2010, Preparation of (ethylene-methacrylic acid) copolymer/vermiculite composites, *in* Frazao, O., ed., Advances in Sendsors, Signals and Materials: WSEAS Press, p. 75–78.

Zarei, I., 2012, Biosynthesis of bacitracin in stirred fermenter by *Bacillus licheniformis* using defatted oil seed cakes as substrate: Modern Applied Science, v. 6, no. 2, p. 30–36. doi:10.5539/mas.v6n2p30.

Zhang, Qin, Zhu, Bao-Quan, and Hu, Hai-Feng, 2008, Activated antibiotic production by inducing resistance to apreomycin, *Streptomyces lividans* and *Streptomyces coelicolor*: Chinese Journal of Natural Medicines, v. 6, no. 1, p. 57–62. doi:10.1016/S1875-5364(09)60006-6.

Zhao, Qiguo, and Yang, Hao, 1995, A preliminary study on red earth and changes of Quaternary environment in south China: Quaternary Sciences, v. 15, p. 107–116.

Zhou, Xin, Kjer, K.M., and Morse, J.C., 2007, Associating larvae and adults of Chinese Hydropsychidae caddisflies (Insecta: Trichoptera) using DNA sequences: Journal of the North American Benthological Society, v. 26, p. 719–742. doi:10.1899/06-089.1.

Ziad, W., 2006, A queen consort of the early Kidarite principality of Kashmir Smast:Oriental Numismatic Society Journal, no. 187.

Alireza Nassimi and Zargham Mohammadi – Comparison of the results of pumping and tracer tests in a karst terrain. *Journal of Cave and Karst Studies*, v. 78, no. 2, p. 110–118, DOI: 10.4311/2015ES0119

COMPARISON OF THE RESULTS OF PUMPING AND TRACER TESTS IN A KARST TERRAIN

ALIREZA NASSIMI AND ZARGHAM MOHAMMADI*

Department of Earth Sciences, Shiraz University, Faculty of Science, Adabiat Crossroads, 7146713565; Shiraz, Fars Province, Iran

Abstract: Pumping and tracer tests are commonly used to measure aquifer parameters such as hydraulic conductivity. Hydraulic conductivity is, however, difficult to characterize; especially in heterogeneous karst terrain. In this research, results of pumping and tracer tests are combined to determine hydraulic conductivities of the karst terrain at the Salman Farsi Dam Site. Pumping test data were analyzed by dual-porosity analytical models. The tracer tests were used to determine seepage velocities based on the assumption of Darcy's law, with calculated Reynolds numbers consistent with laminar flow. Geometric means of the hydraulic conductivities calculated from tracer tests were consistently higher than results derived from pumping tests. Movement of injected dye in a natural groundwater flow system is strongly controlled by preferential flow paths; therefore the estimated hydraulic conductivity is mainly affected by major dissolution openings. However, estimated hydraulic conductivity based on the pumping-test data is representative of the average hydraulic conductivity. In addition, Lugeon (or packer) tests were used to delineate the distribution of hydraulic conductivity within three boreholes.

INTRODUCTION

Aquifers in karst terrains are generally heterogeneous, anisotropic, and complex. These aquifers have an interconnected array of fractures and dissolution routes (Cacas et al., 1990; Hestir and Long, 1990). The dual-porosity model is an effective tool for modeling karst systems (Kovács and Sauter, 2007). The dual-porosity model was initially proposed by Barenblatt et al. (1960) and developed in detail by Streltsova-Adams (1978) and Gringarten (1982). The heterogeneity of karst aquifers, where solutional pathways have orders-of-magnitude higher hydraulic conductivity than the surrounding matrix porosity, requires careful application of analytical tools.

A pumping test induces a perturbation to an aquifer by pumping from a well, while at the same time measuring aquifer responses in the form of head variations (Renard et al., 2009). Selection of appropriate analytical and numerical models is a key part of calculating the hydraulic characteristics, such as hydraulic conductivity, transmissibility, and storage coefficient, of the aquifer (Renard et al., 2009). Hydrodynamic coefficients of aquifers in water resource studies vary of many orders of magnitude, and small errors in the calculation of these coefficients can produce errors of several orders of magnitude in budgets and numerical models of groundwater. Pumping tests do, however, directly produce results for transmissivity and storage, which are the key factors in groundwater studies (Drew and Goldscheider, 2007).

A simultaneous plot of the drawdown and the logarithmic derivative of the drawdown as a function of time in a log-log scale is called a diagnostic plot (Bourdet et al., 1983). A conceptual model for interpretation of the pumping test data is selected based on the diagnostic plot technique combined with knowledge of the local geology (Samani et al., 2006; Renard et al., 2009; Hammond and Field, 2014). The major advantage of diagnostic plots is that they provide a unified procedure to interpret pumping test data (Renard et al., 2009). The main limitation of the drawdown derivative approach to unsteady test analysis is the discrete measurements of drawdown data from individual times, because the rate of change of drawdown currently cannot be measured directly (Samani et al., 2006). Modern data loggers can produce much better temporal resolution than conventional hand measurements, as well as more consistent vertical resolution.

Tracer tests are a powerful tool for determining the origin, movement, and destination of groundwater in hydrogeological investigations, particularly in karst areas (Benischke et al., 2007). In hydrogeology, a tracer is any kind of substance in the water or some other measurable property of the water. It can be used to obtain information on the groundwater flow and impurity transport (Benischke et al., 2007). Through tracer testing, longitudinal and transverse dispersivity and the ratio of hydraulic conductivity and effective porosity can be determined (Lee et al., 2003).

Tracer tests have many advantages, allowing the direct determination of flow routes and velocities and the determination of the catchment area of springs (Drew and Goldscheider, 2007; Löfgren et al., 2007). Tracer tests do have limitations, especially where no tracer is recovered (negative traces), where tracers from other studies interfere

* Corresponding author: zmohammadi@shirazu.ac.ir

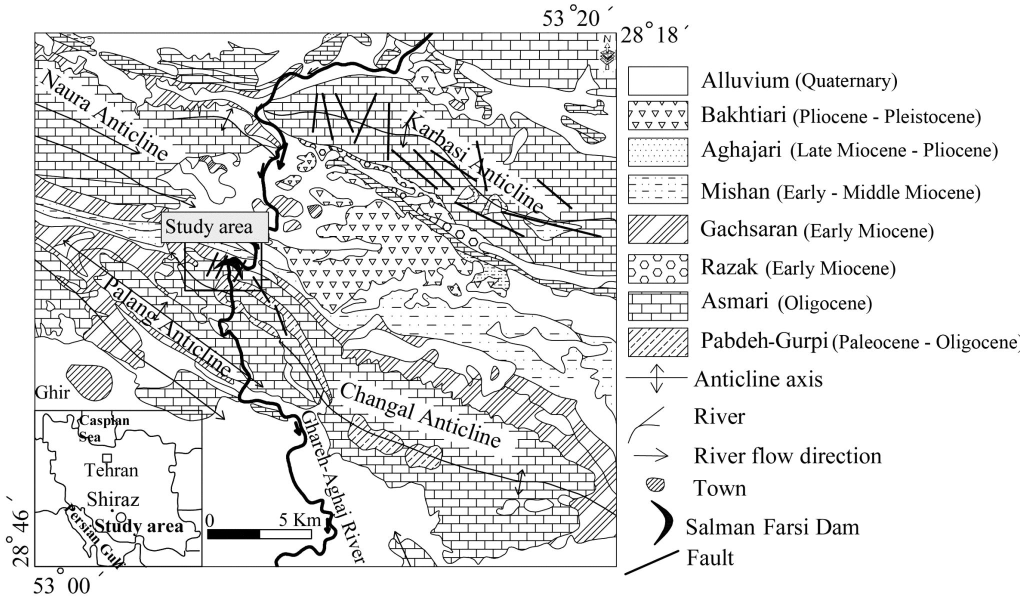

Figure 1. General geological map of the study area (modified from Mohammadi et al., 2010).

(false positives), where deep hydrogeological settings provide few monitoring points, and where high concentrations of tracer may impact potable water supplies (Drew and Goldscheider, 2007; Löfgren et al., 2007).

The combined application of pumping and tracer tests was conducted first by De Laguna (1970) in a two-layered sandy aquifer where a forced gradient tracer test was used to determine what proportion of the pumped water was coming from each sandy aquifer. Later applications of this dual method include Dann et al. (2008) in a channelized aquifer and Thorbjarnarson et al. (1998) in a stratified aquifer, who showed higher hydraulic conductivity values from tracer tests in comparison to pumping tests, though studies by Niemann and Rovey (2000) in an area of glacial outwash and by Rovey and Niemann (2005) under laboratory conditions in a sand tank have shown the opposite result. Vandenbohede and Lebbe (2003), in a phreatic coastal plain aquifer, found good agreement between pumping and tracer tests. Given the dual porosity common in karst terrains, a combined pumping and tracer tests allow evaluation of hydraulic conductivities in solutional conduits within the aquifer matrix. Tracer tests directly measure the groundwater flow velocity better by taking into account and compensating for heterogeneity (Vandenbohede and Lebbe, 2003; Drew and Goldscheider, 2007).

Technical projects in a karst terrain normally face crucial technical, managerial, and political challenges due to the complexity of the karst environment. Some engineering problems in karst environments are caused by the presence of caverns, sinkholes, shafts, and other preferential flow paths that influence groundwater hydraulics (Milanovic, 2002; Parise et al., 2008, 2015a; Gutiérrez et al., 2014).

The objectives of this research were the comparison of the hydraulic-conductivity values derived from pumping and tracer tests and the evaluation of the effect of karst development on the values obtained from selected tests at the Salman Farsi Dam Site (SFDS), Fars Province, southern Iran.

Materials and Methods

Geological Setting

The SFDS is located near Ghir city, 190 km from the city of Shiraz in Fars Province, in south Iran (Fig. 1). The Salman Farsi Dam is an arch-gravity dam with 125 m height and reservoir volume of 1,400 million cubic meters that was constructed on the Ghareh-Aghaj River in Fars Province.

The study area is situated at the Changal Anticline (Fig. 1) of the Zagros Folded Belt, which is 200 to 300 km wide and formed in the Upper Cenozoic. The SFDS is on the northern limb of the Changal Anticline, which trends NW-SE. The stratigraphy and structural framework of the study area were studied in detail by Fars Regional Water Authority (1990), Rahbari and Bagheri (1996), Vucković and Milanović (2001), and Fazeli (2007). In this region, the strata are from the Upper Cretaceous to the present time. Overburden includes slopewash deposits of angular rock fragments and alluvial terraces of cobbles, gravel, sand, and silt located along the rivers. The Bakhtiari Formation (Pliocene-Pleistocene) includes conglomerate of heterogeneous particles with calcareous cement and has a large extent within the Salman Farsi reservoir area. The Mishan Formation (early to mid-Miocene) includes gray to green marls, shaly limestone, and marly limestone outcropping in the bottom and the banks of the reservoir (Vucković and Milanović, 2001). The Razak Formation (Miocene) consists of gypsum, marl, siltstone, and shale with marly limestone.

Table 1. Summary of the tracer tests parameters at the SFDS (extracted from Khalaj Amirhosseini, 1997).

Injection Point	Sampling Points	Detection Points	Tracer Used
QR F	QR 8, QR 12, QR 25, QR 28, QR 32, QR 34, QR 55, P.W. 2, Springs diversion tunnel, The river at location the dam, QR 22, QR 26, G 6, The river at location bridge Abnema	No detection	Uranine
QR 51	QR 8, QR 12, QR 25, QR 28, QR 32, QR 34, QR 55, P.W. 2, Springs diversion tunnel, The river at location the dam, QR 22, QR 46, G 6, The river at location bridge Abnema	Springs diversion tunnel	Rhodamin B
QR 56	QR 53, QR 54, Spring Yargh, River upstream of the injection point, River downstream of the injection point	No detection	Uranine
QR 32	QR 8, QR 12, QR 25, QR 28, QR F, QR 34, QR 55, P.W. 2, Springs diversion tunnel, The river at location the dam, QR 22, QR 26, G 6, The river at location bridge Abnema	QR 28, The river at location the dam	KCl
QR 28	QR 8, QR 12, QR 25, QR F, QR 32, QR 34, QR 55, P.W. 2, Springs diversion tunnel, The river at location the dam, QR 22, QR 26, G 6, The river at location bridge Abnema	QR 8, QR 55	NaCl

Upstream of the dam site the dip of the Razak deposits varies from 55 to 65 degrees. This formation is widespread in the reservoir area. The Asmari Formation (Oligocene-Miocene) is dominated by limestones and is divided into Upper, Middle, and Lower units. The Upper Asmari, consisting of shelly limestone, marl, and marly limestone, outcrops upstream of the dam axis, forming the eastern and western reservoir banks (Fazeli, 2007). The Middle Asmari is about 180 m thick and composed of limestone calcarenite, cherty limestone, and nomolitic and oolitic limestones as well as a small number of marl and marly limestone interbeds. The dam and its appurtenances, including grouting curtain, are on the Middle Asmari, with its great lithological diversity and highly developed karst features such as conduits, big caverns, and chimneys. The Lower Asmari is found below the dam site and includes regularly bedded limestone alternating with marls at the top, and thin to very thin limestone and marly layers at the bottom (Fazeli, 2007). The relatively impermeable Pabdeh-Gurpi Formation (Paleocene to Oligocene) contains purple shale and marl with thin clayey and marly limestone interbeds. Outcrops of Pabdeh-Gurpi are found about 600 m downstream of the dam axis in the river bed section.

HYDROGEOLOGIC SETTING

The hydrogeology of the study site was described by Fars Regional Water Authority (1994), Aghili and Meidani (1998), Milanović et al. (2002), and Fazeli (2007). Tectonics are the major control of karst structure and speleogenesis of the karst massif. At the initial stage of karstification (fractured limestone aquifer), groundwater movement through the fractured limestone aquifer created dissolutional enlargement. Therefore, cave systems are composed of many segments of interconnected nets of discontinuities, such as bedding planes, joints and shear fractures, faults, and their intersections. These structural elements play a key role in the initial stage of karstification by directing the groundwater flows (Vucković and Milanović, 2001; De Waele et al., 2011; Parise et al., 2015b; Taheri et al., 2015). The Upper and Lower Asmari have low permeability due to the existence of some marly layers. The Middle Asmari contains a greater proportion of pure limestone than the Upper and Lower Asmari limestone. Brittle deformation is more predominant in the Middle Asmari, producing ample pathways for groundwater flow (Fazeli, 2007). The Middle Asmari constitutes the main aquifer system at the SFDS and is confined by the Upper Asmari at the SFDS (Aghili and Meidani, 1998; Vucković and Milanović, 2001). Temperature was 38 °C in the pumping well (QR 8) during the pumping test. Average temperature was 28.4 °C in the injection and detection points at the SFDS during the tracer test. Before the construction of the Salman Farsi Dam, several springs and boreholes were known to discharge into the Ghareh-Aghaj River from the Asmari Formation; the sum of discharge of these springs and boreholes was about 8 L s^{-1} (Milanović et al., 2002).

DATA USED

Five tracer tests were performed at the SFDS from November 1996 to February 1997 by the Water Research Center of the Ministry of Power. Table 1 lists the injection and sampling points and the detections, if any (Fig. 2).

One pumping test was conducted in well QR 8, and drawdowns were measured in the six observation wells QR 49, QR 47, QR 22, QR 28, QR 25 and QR 55 (Fig. 2) on November 1997 by the Mahab Ghodss Consulting Engineering Company. Table 2 shows the radial distance of the observation wells from the pumping well and some of their characteristics. Lugeon tests were done in three of the boreholes (QR 22, QR 28 and QR 32) that were also used in the pumping and tracer tests (Fars Regional Water Authority, 1995b).

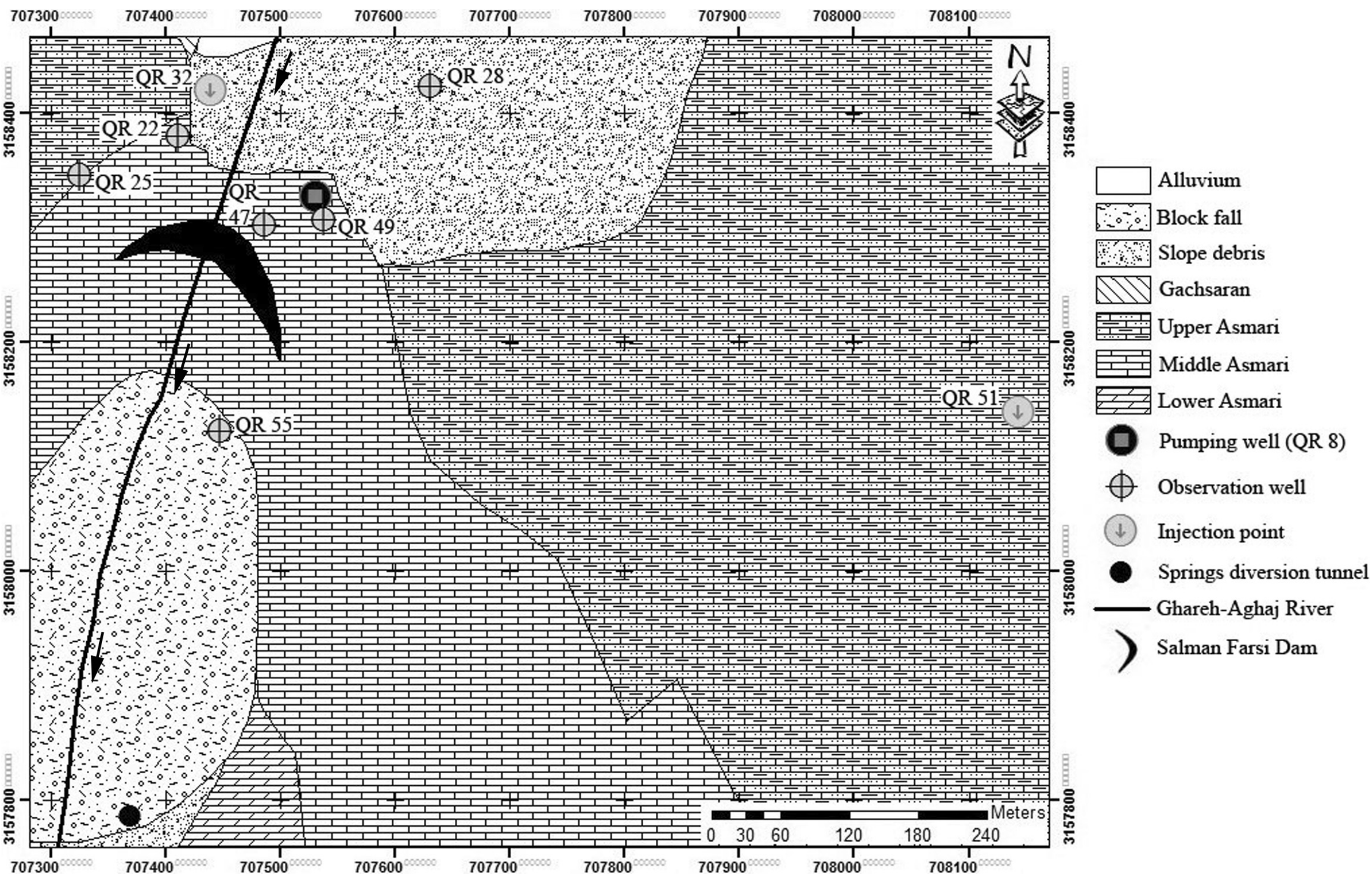

Figure 2. Locations of some of the wells used in the tracer tests, plus the springs diversion tunnel, and the wells used to measure the drawdown from pumping well QR 8.

Results

Natural Gradient Tracer Tests

Tracer tests directly measure groundwater flow velocities, providing a measure of range of velocities and a corresponding apparent hydraulic conductivity. Therefore tracer tests provide an important calibration of groundwater flow models in karst (Ghasemizadeh et al., 2012). Distance from the injection point to the detection point (x) and time of the center of tracer mass (t_c) were used for computation of mean groundwater velocity $v = x/t_c$ in Table 3. Time of the center of tracer mass was extracted from breakthrough curves (for example Fig. 3). Geometric means of porosity (n) and the diameter of the channels, fractures, and conduits (D) were assumed 10.55% and 0.1 m at the SFDS, respectively according to Fars Regional Water Authority (1995a) and Nazari (2008).

The Reynolds number (R_e) is a dimensionless parameter that determines the type of flow regime, laminar or turbulent, with formula $R_e = \rho v D/\mu$ appropriate for pipe of

Table 2. Some characteristics of the pumping well and observation wells at the SFDS (Aghili and Meidani, 1998).

Borehole	UTM (Zone 39 Datum) X	UTM (Zone 39 Datum) Y	Discharge ($m^3\ s^{-1}$)	Well Depth (m)	Depth to Water Table (m)	Thickness of the Aquifer (m)	Distance from the Pumping Well (m)
QR 8	707531.06	3158326.57	0.04	95	12.2	82.8	0.0
QR 49	707537.38	3158306.96	0.0	85	24.3	60.7	20.6
QR 47	707486.08	3158302.52	0.0	140	7.4	132.6	51.0
QR 22	707410.91	3158379.07	0.0	200	7.1	192.9	131.1
QR 28	707630.22	3158423.13	0.0	80	11.6	68.4	138.4
QR 25	707324.44	3158345.80	0.0	180	66.0	114.0	207.5
QR 55	707447.01	3158121.73	0.0	90	8.4	81.6	221.4

Table 3. Estimation of hydraulic conductivity from tracer tests analysis using formulas $v = x/t_c$ and $v = Ki/n$.

Tracer Test	x (m)	t_c (d)	v (m d^{-1})	i (m m^{-1})	Reynolds Number	K (m d^{-1})
QR 51 to Springs diversion tunnel	850	42	20.2	0.0330	28.0	64.7
QR 32 to QR 28	220	14	15.7	0.0052	21.8	319.0
QR 32 to The river at the location of the dam	160	7	22.9	0.0108	31.7	223.4
QR 28 to QR 8	140	60	2.3	0.0049	3.2	50.3
QR 28 to QR 55	230	62	3.7	0.0081	5.1	48.3
Geometric mean	249.3	–	–	–	–	102.3

diameter D, where ρ is the density of the fluid and μ is the dynamic viscosity of the fluid (Chanson, 2004). Laminar flow dominates when the Reynolds number is less than about 2,300, known as the critical Reynolds number, in pipe flow (Shaughnessy et al., 2005). However in karst terrains, laminar flow becomes unstable at Reynolds numbers in excess of 1,500 and transitions to turbulent flow at Reynolds numbers above 6,000 (Veress, 2010). Calculated groundwater flow Reynolds numbers were well within the laminar flow Reynolds numbers at the SFDS (Table 3). Application of the Darcian Flow Law $v = Ki\,n^{-1}$, where K is the hydraulic conductivity and i is the hydraulic gradient, is suitable only within the laminar flow regime.

The hydraulic conductivity was calculated for the five successful tracer paths tabulated in Table 3, one of which, QR 28 to QR 8 (Fig. 2), also provided pumping test data. Reynolds number ($\leq$ 30) were well within laminar flow limits, and hydraulic conductivity ranged from 50 to about 320 m d^{-1} (Table 3). The flow directions of the successful tracer tests (Table 3, Fig. 2) generally follow the topography (Fars Regional Water Authority, 1994); the tracers moved toward the dam site.

Pumping and Lugeon Tests

To calculate the hydrodynamic coefficients of the aquifer, the analytical models provided by Moench (1984) and Barker (1988) were applied in the study area. Dewandel et al. (2005) proposed that Moench's model for a dual-porosity

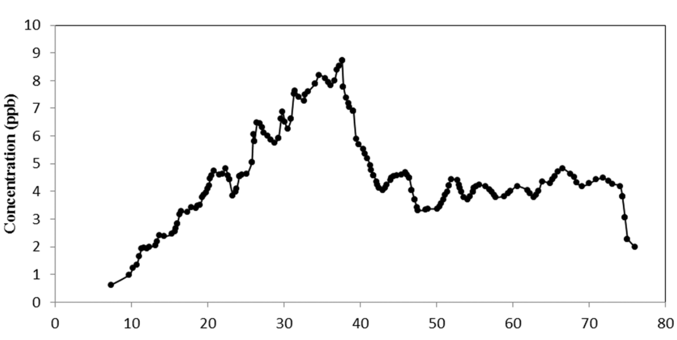

Figure 3. Breakthrough curve of Rhodamin B in the QR 51 to springs diversion tunnel dye trace (Khalaj Amirhosseini, 1997).

media is consistent with most of the pumping tests in karst aquifers.

The diagnostic plots showed that boundary interference was not evident in any of the test data at the SFDS. The diagnostic plots, such as those in Figures 4 and 5, of the observation wells suggested Moench's analytical model for the observation wells QR 49 and QR 47 and Barker's analytical model for the observation wells QR 22, QR 28, QR 25, and QR 55 (Fig. 2).

Hydraulic conductivity was calculated for the six monitoring wells based on the pumping test at QR 8. One path has data from both the tracer test and pumping test. Hydrodynamic coefficients of the aquifer were calculated using AQTESOLV (Duffield, 2007). Hydraulic conductivities from the pumping tests ranged from 8 to 160 m d^{-1} with a geometric mean of 30 m d^{-1} (Table 4).

Hydraulic conductivity was also determined from three Lugeon, or packer, tests. Results were reported in Lugeon unit (L_u) around the boreholes QR 22, QR 28, and QR 32. Approximately 1 L_u is 0.1 m d^{-1} in fractured rocks (Kovács, 1981). Hydraulic conductivities from the Lugeon tests ranged from 0.02 to 75 m d^{-1} (Table 5).

Discussion

The results of the estimated hydraulic conductivity are presented in Tables 3, 4, and 5. The wide range of hydraulic conductivity is representative of the notable local heterogeneity in the karst aquifer at the Salman Farsi Dam Site. The geometric means of the hydraulic conductivity were 100 and 30 m d^{-1} for tracer and pumping tests, respectively. From the Lugeon tests, the mean hydraulic conductivity was 3.8 m d^{-1}. The Lugeon tests are important because they are much more sensitive to the rock matrix, in great contrast to the tracer tests, which are dominated by flow in conduits and fractures. The geometric mean of the hydraulic conductivity obtained by the tracer tests was three and a half times greater than the pumping test results. Greater values for the geometric mean of the hydraulic conductivity in the tracer tests may be due to the scale effect (Király, 1975), because the geometric mean of the distances in the tracer tests (249.3 m) is more than the geometric mean of the distances in the pumping test (97.8 m) and Lugeon tests (30 m according to Bliss and Rushton, 1984). In other words, on a longer distance scale, the role of macrofractures and dissolution openings increases in

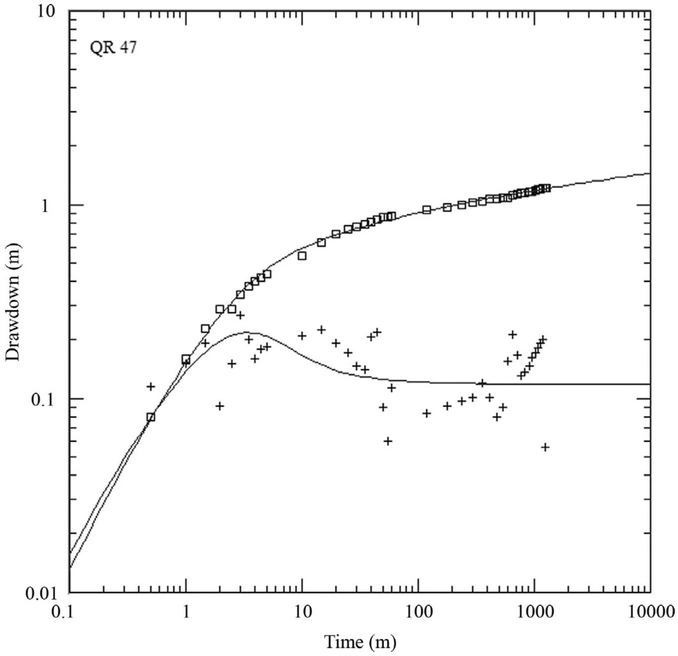

Figure 4. Moench (1984) analytical model is suggested for the observation well QR 47 based on this diagnostic plot from the pumping test (□ amount of drawdown; + derivative of drawdown).

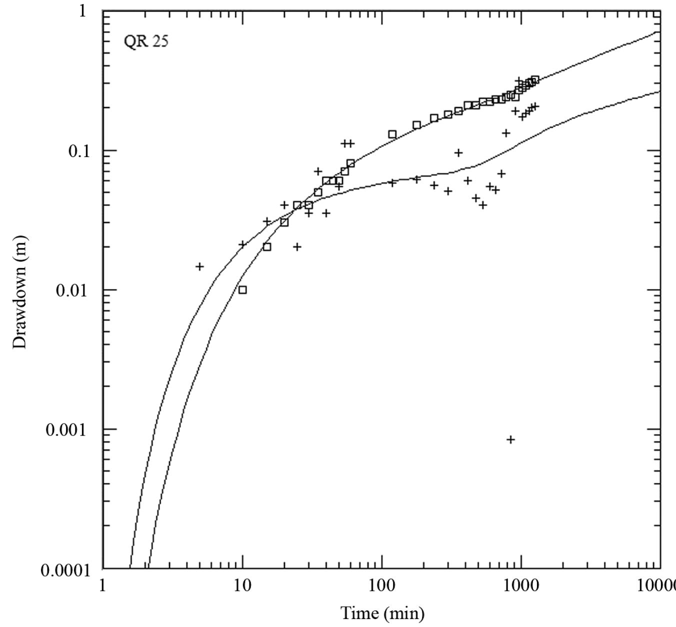

Figure 5. Barker (1988) analytical model is suggested for the observation well QR 25 based on this diagnostic plot from the pumping test (□ amount of drawdown; + derivative of drawdown).

karst terrain, so it is expected that the hydraulic conductivity should increase, too. In the path QR 28 to QR 8 common to both tests, the hydraulic conductivities were 50 and 30 m d^{-1} based on the tracer and pumping tests, respectively. Different values for hydraulic conductivity in one path may be due to the different hydraulic behavior of groundwater flow in the karst terrain during tracer and pumping tests. In a pumping test, groundwater mainly flows from the both macrofractures and matrix (Moench, 1984; Maréchal et al., 2008), while in a tracer test groundwater and dissolved dye mainly flow via the macrofracture and dissolution openings routes toward the observation points (Gouzie et al., 2010). In other words, transmission of dye in anisotropic media in tracer test is mainly via routes with minimum head loss (Salgado-Castro, 1988; Nassimi, 2011) such as dissolution-created channel and conduit (macrofracture) routes, while in a pumped well that taps anisotropic media, groundwater flows through both macrofractures and matrices in the cone of depression (Moench, 1984). The heterogeneous karst terrain at the SFDS is composed of many dissolution openings including caves, channels, and shafts that have been enlarged along geological discontinuities such as bedding planes, joints, and shear fractures. These structural elements developed as conduit routes play a major role for groundwater flow.

In the Burnham field site, near Christchurch on the South Island of New Zealand, "the combined use of pumping and tracer test data enabled the derivation of equivalent average hydraulic conductivities (K_{avg}) for each test in a heterogeneous channelized alluvial aquifer, whereas K values of the preferential flow paths were two orders of magnitude higher" (Dann et al., 2008). Also K estimated from tracer test was six times greater than the K_{avg} estimated from a pumping test in a stratified aquifer at the Bonita, California, field site (Thorbjarnarson et al., 1998).

Table 4. Estimation of hydraulic conductivity from analysis of pumping test using Moench (1984) and Barker (1988) analytical models.

Borehole	Distance from the Pumping Well (m)	Analytical Model	Transmissivity (m^2 d^{-1})	K_{ave} (m^2 d^{-1})
QR 49	20.6	Moench (1984)	522.0	8.6
QR 47	51.0	Moench (1984)	2,347.0	17.7
QR 22	131.1	Barker (1988)	3,723.0	19.3
QR 28	138.4	Barker (1988)	1,976.8	28.9
QR 25	207.5	Barker (1988)	6,748.8	59.2
QR 55	221.4	Barker (1988)	13,105.0	160.6
Geometric mean	97.8	–	–	30.5

Table 5. Estimation of hydraulic conductivity from Lugeon test.

Borehole	Depth, m	Hydraulic Conductivity, L_u	Hydraulic Conductivity, m d^{-1}
QR 22	13-18	31.8	3.2
	18-23	748.2	74.8
	23-28	4.2	0.4
	28-33	1.7	0.2
	33-38	1.3	0.1
	38-43	0.8	0.1
	43-48	2.1	0.2
	48-53	17.0	1.7
	53-58	0.6	0.1
	58-63	22.9	2.3
	63-68	0.5	0.1
	68-73	5.0	0.5
	73-78	10.6	1.1
	78-83	14.9	1.5
	83-88	30.8	3.1
	88-93	35.9	3.6
	93-98	11.8	1.2
	98-103	2.1	0.2
	103-108	11.2	1.1
	108-113	8.9	0.9
	113-118	13.9	1.4
	118-123	2.0	0.2
	123-128	1.9	0.2
	128-133	1.3	0.1
	133-138	1.8	0.2
	138-143	25.3	2.5
	143-148	0.6	0.1
	148-153	0.7	0.1
QR 28	33-37	12.8	1.3
	37-40	11.9	1.2
	40-45	0.2	0.02
	45-50	10.3	1.0
	50-55	13.5	1.4
	55-60	22.3	2.2
	60-65	77.2	7.7
	65-70	2.3	0.2
	75-80	2.7	0.3
QR 32	5.7-10.7	111.6	11.2
	10.7-15.7	28.3	2.8
	15.7-20.7	127.9	12.8
	20.7-25.7	75.4	7.5
	25.7-30.7	75.7	7.6
Mean	–	–	3.8

Hydraulic conductivity is dominated by the development of karst features in a karst terrain. Different approaches are introduced to overcome the wide range of hydraulic conductivity in karst terrains. At the SFDS, with notable conduit and joint systems, the data received from the tracer test demonstrate the dual porosity with preferential flow paths, while the data obtained by the pumping test would cause considerable underestimation of hydraulic conductivity due to the effects of preferential flow paths in the tracer test and solute transport.

Conclusions

Hydraulic conductivity was estimated as about 100, 30, and 3.8 m d^{-1} based on the tracer, pumping and Lugeon tests, respectively, in the study area. The K estimated from tracer tests was approximately three and half times greater than the K_{avg} estimated from the pumping test. In a karst terrain, the estimated value of K based on a tracer test is more representative of groundwater flow velocities than those based on the pumping and Lugeon tests, due to the dominant role of preferential flow paths in the tracer test in comparison to the pumping test. The observed results are consistent with a dual porosity continuum and are not unexpected in a karst system. Assuming transmission of tracer by preferential flow paths in the scale of basins in the heterogeneous karst terrain, the value of hydraulic conductivity based on the tracer test is greater than that given by dual porosity analysis of pumping tests. The development of karst features played a major role in the hydraulic conductivity in the study area. As a result, for areas with preferential flow paths, such as karst aquifers, the hydraulic conductivity obtained from tracer tests are greater than the hydraulic conductivity obtained from pumping test.

Acknowledgements

The authors thank the University of Shiraz for their support of this work. Also some of hydrogeology data of the study area was supplied by Fars Regional Water Authority in Shiraz. The authors thank the *Journal of Cave and Karst Studies* Associate Editors and Advisory Board for their encouragement and constructive criticism.

References

Aghili, B., and Meidani, A., 1998, Report of pumping test of karstic wells at the Salman Farsi Dam Site: Mahab Ghodss consulting engineering company, Fars regional water authority, 62 p. (in Persian).

Barenblatt, G.I., Zheltov, Iu.P., and Kocina, I.N., 1960, Basic concepts in the theory of seepage of homogeneous liquids in fissured rocks [strata]: Journal of Applied Mathematics and Mechanics, v. 24, no. 5, p. 1286–1303. doi:10.1016/0021-8928(60)90107-6.

Barker, J.A., 1988, A generalized radial flow model for hydraulic tests in fractured rock: Water Resources Research, v. 24, no. 10, p. 1796–1804. doi:10.1029/WR024i010p01796.

Benischke, R., Goldscheider, N., and Smart, C., 2007, Tracer techniques, *in* Goldscheider, N., and Drew, D., eds., Methods in Karst Hydrogeology: London, Taylor & Francis, IAH International Contributions to Hydrogeology 26, p. 147–170.

Bliss, J.C., and Rushton, K.R., 1984, The reliability of packer tests for estimating the hydraulic conductivity of aquifers: Quarterly Journal of Engineering Geology and Hydrogeology, v. 17, no. 1, p. 81–91. doi:10.1144/GSL.QJEG.1984.017.01.10.

Bourdet, D., Whittle, T.M., Douglas, A.A., and Pirard, Y.M., 1983, A new set of type curves simplifies well test analysis: World Oil, v. 196, p. 95–106.

Cacas, M.C., Ledoux, E., de Marsily, G., Tillie, B., Barbreau, A., Durand, B., Feuga, B. and Peadecerf, P., 1990, Modeling fracture flow with a stochastic discrete fracture network: Calibration and validation: 1. The flow model: Water Resources Research, v. 26, no. 3, p. 479–489. doi:10.1029/WR026i003p00479.

Chanson, H., 2004, The Hydraulics of Open Channel Flow: An Introduction: Basic Principles, Sediment Motion, Hydraulic Modelling, Design of Hydraulic Structures, second edition: Oxford, Butterworth-Heinemann, 634 p.

Dann, R.L., Close, M.E., Pang, L., Flintoft, M.J., and Hector, R.P., 2008, Complementary use of tracer and pumping tests to characterize a heterogeneous channelized aquifer system in New Zealand: Hydrogeology Journal, v. 16, no. 6, p. 1177–1191. doi:10.1007/s10040-008-0291-4.

De Laguna, W., 1970, Tracer aids interpretation of pumping test: Water Resources Research, v. 6, no. 1, p. 172–184. doi:10.1029/WR006i001p00172.

De Waele J., Gutiérrez F., Parise M., and Plan, L., 2011, Geomorphology and natural hazards in karst areas: A review: Geomorphology, v. 134, no. 1-2, p. 1–8. doi:10.1016/j.geomorph.2011.08.001.

Dewandel, B., Lachassagne, P., Boudier, F., Al-Hattali, S., Ladouche, B., Pinault, J.-L., and Al-Suleimani, Z., 2005, A conceptual hydrogeological model of ophiolite hard-rock aquifers in Oman based on a multiscale and a multidisciplinary approach: Hydrogeology Journal, v. 13, no. 5-6, p. 708–726. doi:10.1007/s10040-005-0449-2.

Drew, D., and Goldscheider, N., 2007, Combined use of methods, *in* Goldscheider, N., and Drew, D., eds., Methods in Karst Hydrogeology: London, Taylor & Francis, p. 223–228.

Duffield, G.M., 2007, AQTESOLV (pumping tests, constant-head tests and slug tests) Software for Windows. Version 4.5, User's Guide: Reston, Virginia, HydroSOLVE Inc., 530 p.

Fars Regional Water Authority, 1990, Report of geology at the Salman Farsi Dam Site: Mahab Ghodss consulting engineering company, 71 p. (in Persian).

Fars Regional Water Authority, 1994, Report of studies at the Salman Farsi Dam Site: Mahab Ghodss consulting engineering company, 869 p.

Fars Regional Water Authority, 1995a, Report the results of experiments on rock samples of the Salman Farsi Dam Site: Khak & Sang civil work contractor & geotechnical consultant company, 274 p. (in Persian).

Fars Regional Water Authority, 1995b, Report of the results of Lugeon tests at the Salman Farsi Dam Site: Khak & Sang civil work contractor & geotechnical consultant company, 243 p. (in Persian).

Fazeli, M.A., 2007, Construction of grout curtain in karstic environment case study: Salman Farsi Dam: Environmental Geology, v. 51, no. 5, p. 791–796. doi:10.1007/s00254-006-0397-8.

Ghasemizadeh, R., Hellweger, F., Butscher, C., Padilla, I., Vesper, D., Field, M., and Alshawabkeh, A., 2012, Review: Groundwater flow and transport modeling of karst aquifers, with particular reference to the North Coast Limestone aquifer system of Puerto Rico: Hydrogeology Journal, v. 20, no. 8, p. 1441–1461. doi:10.1007/s10040-012-0897-4.

Gouzie, D., Dodd, R.P., and White, D.M., 2010, Dye-tracing studies in southwestern Missouri, USA: Indication of stratigraphic flow control in the Burlington Limestone: Hydrogeology Journal, v. 18, no. 4, p. 1043–1052. doi:10.1007/s10040-010-0581-5.

Gringarten, A.C., 1982, Flow test evaluation of fractured reservoirs, *in* Narasimhan, T.N., ed., Recent Trends in Hydrogeology: Geological Society of America special paper 189, p. 237–263. doi:10.1130/SPE189-p237.

Gutiérrez, F., Parise, M., De Waele, J., and Jourde, H., 2014, A review on natural and human-induced geohazards and impacts in karst: Earth Science Reviews, v. 138, p. 61–88. doi:10.1016/j.earscirev.2014.08.002.

Hammond, P.A., and Field, M.S., 2014, A reinterpretation of historic aquifer tests of two hydraulically fractured wells by application of inverse analysis, derivative analysis, and diagnostic plots: Journal of Water Resource and Protection, v. 6, no. 5, p. 481–506. doi:10.4236/jwarp.2014.65048.

Hestir, K., and Long, J.C.S., 1990, Analytical expressions for the permeability of random two-dimensional Poisson fracture networks based on regular lattice percolation and equivalent media theories: Journal of Geophysical Research: Solid Earth, v. 95, no. B13, p. 21565–21581. doi:10.1029/JB095iB13p21565.

Khalaj Amirhosseini, Y., 1997, Report of tracer tests at the Salman Farsi Dam Site: Water Research Center of the Ministry of Power, Fars Regional Water Authority, 68 p. (in Persian).

Király, L., 1975, Rapport sur l'état actuel des connaissances dans le domaine des caracteres physique des roches karstique, *in* Burger, A., and Dubertet, L., eds., Hydrogeology of Karstic Terrains: Paris, International Union of Geological Sciences, series B, number 3, p. 53–67.

Kovács, G., 1981, Seepage Hydraulics: Amsterdam, Elsevier, Developments in Water Science 10, 730 p.

Kovács, A., and Sauter, M., 2007, Modelling karst hydrodynamics, *in* Goldscheider, N., and Drew, D., eds., Methods in Karst Hydrogeology: London, Taylor & Francis, p. 201–222.

Lee, Jin-Yong, Kim, Jung-Woo, Cheon, Jeong-Yong, Yi, Myeong-Jae, and Lee, Kang-Kim, 2003, Combined performance of pumping and tracer tests: A case study: Geosciences Journal, v. 7, no. 3, p. 237–241. doi:10.1007/BF02910290.

Löfgren, M., Crawford, J., and Elert, M., 2007, Tracer Tests - Possibilities and Limitations. Experience from SKB Fieldwork: 1977-2007: Swedish Nuclear Fuel and Waste Management Co., SKB report R-07-39, 121 p.

Maréchal, J.C., Ladouche, B., Dörfliger, N., Lachassagne, P., 2008, Interpretation of pumping tests in a mixed flow karst system: Water Resources Research, v. 44, no. 5, paper W05401. doi:10.1029/2007WR006288.

Milanovic, P., 2002, The environmental impacts of human activities and engineering constructions in karst regions: Episodes, v. 25, no. 1, p. 13–21.

Milanović, P., Kreuzer, H., Dolder, T., 2002, Report on design of the Grout Curtain, Salman Farsi Dam Project in Iran: Mahab Ghodss consulting engineering company, Fars Regional Water Authority, 202 p.

Moench, A.F., 1984, Double-porosity models for a fissured groundwater reservoir with fracture skin: Water Resources Research, v. 20, no. 7, p. 831–846. doi:10.1029/WR020i007p00831.

Mohammadi, Z., Bagheri, R., Jahanshahi, R., 2010, Hydrogeochemistry and geothermometry of Changal thermal springs, Zagros region, Iran: Geothermics, v. 39, no. 3, p. 242–249. doi:10.1016/j.geothermics.2010.06.007.

Nassimi, A., 2011, Groundwater: Tehran, Dibagaran Tehran, 300 p. (in Persian).

Nazari, M.H., 2008, Sealing the karst cavity base on the scale at the Salman Farsi Dam Site, *in* Proceedings of 2nd National Conference on Dam and Hydropower, May 14-15, Tehran, Ministry of Power, p. 1–9 (in Persian).

Niemann, W.L., and Rovey, II, C.W., 2000, Comparison of hydraulic conductivity values obtained from aquifer pumping tests and conservative tracer tests: Groundwater Monitoring & Remediation, v. 20, no. 3, p. 122–128. doi: 10.1111/j.1745-6592.2000.tb00278.x.

Parise, M., De Waele, J., and Gutierrez, F., 2008, Engineering and environmental problems in karst – An introduction: Engineering Geology, v. 99, no. 3-4, p. 91–94. doi:10.1016/j.enggeo.2007.11.009.

Parise, M., Closson, D., Gutiérrez, F., and Stevanović, Z., 2015a, Anticipating and managing engineering problems in the complex karst environment: Environmental Earth Sciences, v. 74, no. 12, p. 7823–7835. doi:10.1007/s12665-015-4647-5.

Parise, M., Ravbar, N., Živanović, V., Mikszewski, A., Kresic, N., Mádl-Szőnyi, J., and Kukurić, N., 2015b, Hazards in karst and managing water resources quality, *in* Stevanovic, Z., ed., Karst Aquifers – Characterization and Engineering: Cham, Switzerland, Springer, p. 601–687. doi:10.1007/978-3-319-12850-4_17.

Rahbari, A., and Bagheri, S., 1996, Report on the geology and geomorphology in the Salman Farsi Dam Catchment: Jihad Engineering Services Co. and Parsab Consulting Engineers, Ministry of Agriculture Jihad, 225 p. (in Persian).

Renard, P., Glenz, D., and Mejias, M., 2009, Understanding diagnostic plots for well-test interpretation: Hydrogeology Journal, v. 17, no. 3, p. 589–600. doi:10.1007/s10040-008-0392-0.

Rovey, II, C.W., and Niemann, W.L., 2005, Do conservative solutes migrate at average pore-water velocity?: Groundwater, v. 43, no. 1, p. 52–62. doi:10.1111/j.1745-6584.2005.tb02285.x.

Salgado-Castro, R.O., 1988, Computer modelling of water supply distribution networks using the gradient method [Ph.D. thesis]: Newcastle upon Tyne, Newcastle University, 419 p.

Samani, N., Pasandi, M., and Barry, D.A., 2006, Characterizing a heterogeneous aquifer by derivative analysis of pumping and recovery test data: Journal of Geological Society of Iran, v. 1, p. 29–41.

Shaughnessy, E.J., Jr., Katz, I.M., and Schaffer, J.P., 2005, Introduction to Fluid Mechanics: New York, Oxford University Press, 1057 p.

Streltsova-Adams, T.D., 1978, Well hydraulics in heterogeneous aquifer formations: Advances in Hydroscience, v. 11, p. 357–423. doi:10.1016/B978-0-12-021811-0.50011-5.

Taheri, K., Taheri, M., and Parise, M., 2015, Unprotected karst resources in western Iran: the environmental impacts of intensive agricultural pumping on the covered karstic aquifer, a case in Kermanshah province: Geophysical Research Abstracts, v. 17, p. 1640.

Thorbjarnarson, K.W., Huntley, D., and McCarty, J.J., 1998, Absolute hydraulic conductivity estimates from aquifer pumping and tracer tests in a stratified aquifer: Groundwater, v. 36, no. 1, p. 87–97. doi:10.1111/j.1745-6584.1998.tb01068.x.

Vandenbohede, A., and Lebbe, L., 2003, Combined interpretation of pumping and tracer tests: theoretical considerations and illustration with a field test: Journal of Hydrology, v. 277, p. 134–149. doi:10.1016/S0022-1694(03)00090-8.

Veress, M., 2010, Karst Environments: Karren Formation in High Mountains: Dortrecht, Springer, 238 p. doi:10.1007/978-90-481-3550-9.

Vucković, D., and Milanović, S., 2001, Report on the speleological investigation (mission report) at the Salman Farsi Dam Site: Mahab Ghodss consulting engineering company, Fars Regional Water Authority, 35 p.

R. Ogórek, M. Dyląg, Z. Višňovská, D. Tančinová, and D. Zalewski – Speleomycology of air and rock surfaces in Driny Cave (Lesser Carpathians, Slovakia). *Journal of Cave and Karst Studies*, v. 78, no. 2, p. 119–127. DOI: 10.4311/2015MB0128

SPELEOMYCOLOGY OF AIR AND ROCK SURFACES IN DRINY CAVE (LESSER CARPATHIANS, SLOVAKIA)

Rafał Ogórek[1]*, Mariusz Dyląg[1], Zuzana Višňovská[2], Dana Tančinová[3], and Dariusz Zalewski[4]

Abstract: This paper is a speleomycological report from Driny Cave in the Lesser Carpathian Mountains, Slovakia. The samples were collected in July 2014 from one location outside and five locations inside the cave. To examine the air, the Air Ideal 3P sampler was used. Samples from the rock surfaces were collected using sterile swabs wetted in physiological saline (0.85% NaCl). The density of filamentous fungi isolated from the air inside and outside the cave ranged from 89.6 to 1284.7 colony-forming units per 1 m^3 of air and from 38.3 to 588.5 CFU per m^2 of the rock surface. Six species of filamentous fungi were isolated from the external air samples, and eleven species of filamentous fungi and three species of yeast-like fungi from the internal air samples. Fungi belonging to the *Cladosporium* genus were the most frequently isolated species from the internal and the external air. Six species of filamentous fungi and two species of yeast-like fungi were isolated from the surface of the rocks inside the cave and only two species from the samples collected outside the cave. Among the fungi isolated from the rock surfaces most frequently were *Penicillium chrysogenum*, *P. granulatum*, and *Trichoderma harzianum*. The concentration of airborne fungi inside the cave did not exceed official limits and norms stated as safe for health of tourists. However, the species found here can cause degradation of rock surfaces.

Introduction

Mycological research on caves and underground facilities has been conducted since the 1960s (Balabanoff, 1967; Brashear et al., 1966; Al-Doory and Rhoades, 1968). However, the term *speleomycology* was first introduced by Polish scientists in 2014 as a name for all kinds of investigations that focus on exploration of caves and their underground mycobiota (Pusz et al., 2014).

Ecosystems such as caves or underground facilities created by man have stable, low temperatures and very restricted nutrients during the year (Poulson and White, 1969). Therefore, the majority of fungi underground are present as spores or conidia carried by water, air currents, animals such as bats and arthropods, or humans (Kubátová and Dvořák, 2005; Jurado et al., 2010; Chelius et al., 2009; Vanderwolf et al., 2013; Griffin et al., 2014).

As shown previously (Ogórek et al., 2014a, 2014b, 2014c), bioaerosols from the external environment most strongly influence the percentage composition of fungi in caves and other underground sites. Tourist activities are also very important, because they may have a serious impact on the hypogean system (Taylor et al., 2013). Visitors can enrich the environment with organic and inorganic matter, compact soil, and change the pristine climate through, inter alia, an increase in temperature and the concentration of carbon dioxide (Pulido-Bosch et al., 1997; Barton, 2006; Barton and Northup, 2007). Tourist activities may also favor the dispersion and import of new microbes, even those that are potentially pathogenic for humans and animals (Barton, 2006; Cury et al., 2001).

Each underground site may be divided into three zones: the twilight zone, the middle zone and the dark zone (Karkun et al., 2012). The area most susceptible to external conditions is the twilight zone, which is located at the entrance or exit and the vicinity of ventilation shafts (Poulson and White, 1969; Koilraj and Marimuthu, 1998). The most fungi typically are isolated from this zone (Ogórek et al., 2014a, 2014b, 2014c). In the middle zone relative darkness prevails, with fluctuating temperature. In the dark zone, in which total darkness and constant temperature prevail, the least fungi are usually isolated (Poulson and White, 1969; Koilraj and Marimuthu, 1998; Pusz et al., 2015).

Fungi and their secondary metabolites present in the atmosphere play a significant role in air pollution (Papuas et al., 2000). Thus this type of bioaerosol can affect the health of humans or animals. Moreover, the cave mycobiota are very important for underground ecology, because fungi and bacteria probably constitute the major source of

*Corresponding author: rafal-ogorek@wp.pl
[1] University of Wroclaw, Institute of Genetics and Microbiology, Department of Genetics, Przybyszewskiego Street 63/77, 51-148 Wroclaw, Poland
[2] State Nature Conservancy of the Slovak Republic, Slovak Caves Administration, Hodžova 11, 031-01 Liptovský Mikuláš, Slovakia
[3] Slovak University of Agriculture in Nitra, Department of Microbiology, Tr. Hlinku 2, 949-76 Nitra, Slovakia
[4] Wrocław University of Environmental and Life Sciences, Department of Genetics, Plant Breeding and Seed Production, pl. Grunwaldzki 24a, 50-363 Wrocław, Poland

food for other organisms (Sustr et al., 2005; Walochnik and Mulec, 2009; Bastian et al., 2010). Fungi can also cause biodeterioration of rocks through biochemical and mechanical activities (Kalogerakis et al., 2005; Ogórek et al., 2014c; Sterflinger, 2000). Biochemical activities based on secondary metabolites of fungi that act on rocks, such as acids and other metabolites with metal-chelating properties or pigments, can cause foxing on the surface of rocks (Sterflinger, 2000; Gu 2003; Barton and Northup, 2007; Cwalina, 2008; Li et al., 2008). The biomechanical impact of fungi on rocks is less important than biochemical, and it can occur, for example, through penetration by fungal hyphae into decayed limestone and by burrowing into otherwise intact minerals (Scheerer et al., 2009; Sterflinger, 2000).

This study aimed to carry out speleomycological research in Driny Cave, and our research focused on two goals, the mycological analysis of species composition of the fungi found in the air and the rock surface inside and outside of Driny Cave and quantifying their concentrations.

Materials and Methods

Driny Cave is located in the Smolenice Karst in the Lesser Carpathian Mountains, southwest from Smolenice, in the Trnava district and near the recreation resort Jahodník. Geographic coordinates of the cave are 48°50′04″ N, 17°40′20″ E. It was formed in brown-grey Lower Cretaceous chert limestones of the Vysocký Nappe by corrosion by atmospheric waters penetrating along tectonic faults. Its entrance is situated on the western slope of Driny Hill and lies at an elevation of 399 m a.s.l. Its length is 680 m and its vertical span 40 m. It consists of narrow fissure passages, from one to three meters wide, and a medium-size room, Slovak Speleological Society Hall, formed mostly at the intersection of tectonic faults. The discovery chimney descends to 36 m depth from the upper opening to the intersection of the Entrance Passage. A rich sinter fill decorates underground fissures. Flowstone draperies with indented facing are typical for this cave. Flowstone waterfalls and structures, pagoda-like stalagmites, and various forms of stalactites commonly occur here. Also small flowstone pools, supplied with water by percolating rainfall, can be found. The cave was opened to the public in 1935 with provisional electric lighting for 175 m. Currently the length of the tourist path is 410 m (Bella et al., 2001; Bella, 2003). This cave is one of the most important underground localities for bats in Slovakia, and the dominant species is the lesser horseshoe bat *Rhinolophus hipposideros*, with 100 to 150 individuals (Lehotská and Lehotský, 2009). In 2014 Driny Cave was visited by 31,859 people (Nudziková, 2014).

The samples were taken before the tourists arrived on July 25, 2014 from an outdoor location about 3 m in front of the entrance to the cave and from five locations inside (Fig. 1). The air temperature and relative humidity were measured using a thermohygrometer (LB-522, LAB-EL) six times in each location.

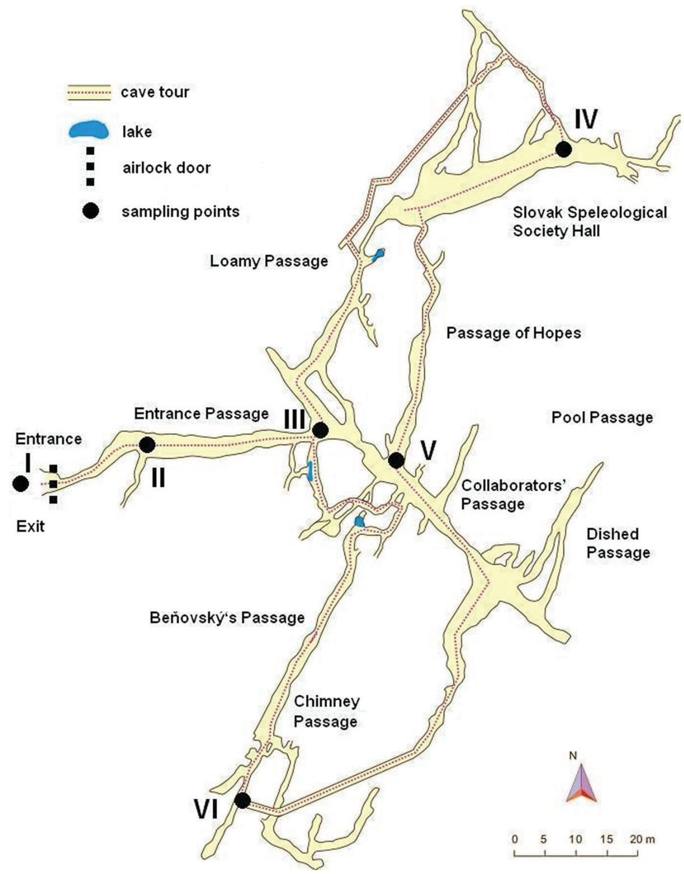

Figure 1. Map of the tourist route and the sampling locations in Driny Cave.

Potato Dextrose Agar medium (PDA, Biocorp) was used for the isolation of fungi from the air, the rock surface, and for the identification of some species. Czapek-Dox Agar medium (1.2% agar, Biocorp) and Malt Extract Agar medium (MEA, Biocorp) were used for the identification of species belonging to *Penicillium* and *Aspergillus* genera. Sabouraud Agar medium (4% dextrose, 2% agar, 1% peptone, A&A Biotechnology) was used for identification of yeast-like fungi.

The air sampler (Air Ideal 3P) was programmed for the air sample volumes of 100 L and 150 L. Six replicates of air were collected at each location. The sampler was positioned 1.5 m above the level of the cave floor.

Swabs of the rock surface were made using sterile swabs wetted in physiological saline (0.85% NaCl) stored in transport tubes (plastic applicator, viscose swab, of 15 cm length). Every location was sampled with three swabs from a surface area of 1.0 cm^2 at a height of 1 m and 2 m above the floor. The samples from each collection point were put together into one 50 mL Erlenmeyer flask containing 10 mL of sterile distilled water, and they were shaken for 20 minutes. After shaking, the samples were placed in a Petri dish, on the solidified PDA medium, using serial dilution technique in three replicates for the three incubation temperatures.

Table 1. Filamentous fungi and yeast-like fungi isolated from the air and the rock surfaces inside and outside Driny Cave on July 25, 2014. A "+" indicates that the species was found.

	Air		Rock Surface	
Species	Outside	Inside	Outside	Inside
Alternaria alternata (Fr.) Keissl.	+	+		
Aspergillus fumigatus Fresen.		+	+	+
Aspergillus niger Tiegh	+			
Candida albicans (C.P. Robin) Berkhout		+		+
Cladosporium cladosporioides (Fresen.) G.A. de Vries	+	+		
Cladosporium herbarum (Pers.) Link	+	+		
Epicoccum nigrum Link	+	+		
Fusarium equiseti (Corda) Sacc.		+		
Mucor hiemalis Wehmer		+		+
Penicillium chrysogenum Thom		+	+	+
Penicillium granulatum Rainier		+		+
Penicillium urticae Rainier	+	+		
Phoma fimeti Brunaud		+		
Rhizopus stolonifer (Ehrenb.) Vuill.				+
Rhodotorula glutinis (Fresen.) F.C. Harrison		+		
Rhodotorula rubra (Schimon) F.C. Harrison		+		+
Trichoderma harzianum Rifai				+
Total Species	6	14	2	8

After incubation at 15, 20, or 25 °C for 4 to 14 days in darkness, fungal colonies were counted as averages from the replicates at all incubation temperatures and identified. The species identification was based on macro- and microscopic observations of the morphology of hyphae, conidia, and sporangia of the colonies that had grown on culture media. The filamentous fungi were identified using diagnostic keys and descriptions by Pitt and Hocking (2009) and Watanabe (2010). The yeast-like fungi were identified by diagnostic key and descriptions by Kurtzman and Fell (1998) and Barnett et al. (2000).

The results were analyzed by ANOVA, using Statistica 12.0 package. Means were compared using Tukey Honest Significant Differences test at $\alpha \leq 0.05$.

Results

More species of fungi (12 filamentous fungi and 3 yeast-like fungi) were isolated from the air samples than from the rock surfaces (respectively 6 and 2). Species *Rhizopus stolonifer* and *Trichoderma harzianum* were cultured only from the rock, whereas *Alternaria alternata*, *Aspergillus niger*, *Cladosporium* spp., *Epicoccum nigrum*, *Fusarium equiseti*, *Penicillium urticae*, *Phoma fimeti*, and *Rhodotorula glutinis* were cultured only from the sampled air (Table 1).

Six species of filamentous fungi were isolated from the air sampled outside the cave, whereas from the inside air eleven species of filamentous fungi and three species of yeast-like fungi were cultured. *Aspergillus fumigatus*, *Fusarium equiseti*, *Mucor hiemalis*, *Penicillium chrysogenum*, *P. granulatum*, *Phoma fimeti*, and yeast-like fungi were present only in the indoor air compared to the outside air, and *A. niger* was isolated only from the outside air. From the rock surfaces inside the cave, six species of filamentous fungi and two yeast-like fungi were isolated, but only two species were isolated from the samples collected outside the cave. Species such as *Candida albicans*, *M. hiemalis*, *P. granulatum*, *Rhizopus stolonifer*, *Rhodotorula rubra*, and *Trichoderma harzianum* were isolated only from the surfaces inside the cave (Table 1).

We detected an association between the air temperature and the content of fungi in the air and, to some extent, on the rocks. The temperature of the air outside Driny Cave (25.5 °C) was higher than inside (7.6–8.6 °C), whereas the air humidity was higher inside the cave (92.0–93.3%) than outside (52.6%). The concentration of fungi increased with the increase in the air temperature (Fig. 2).

The density of airborne fungi isolated from the air samples was 1284.7 $\pm$ 405.8 colony-forming units (CFU) per m^3 of outside air and from 89.6 $\pm$ 25.4 to 217.5 $\pm$ 34.7 CFU per m^3 for the indoor air samples, and it varied significantly between studied locations. The majority of fungi were isolated from the air outside the cave; $P_{I,V}$ = 0.0000001. The highest number of species isolated from the indoor air was noted for Location V, the Passage of Hopes, and the smallest number was noted for Location III, the Entrance Passage; $P_{III,V}$ = 0.0000001 (Table 2, Figs. 1 and 2). The number of CFU obtained from the rock surfaces inside and outside the cave ranged from 38.3 $\pm$ 13.3 to 588.5 $\pm$ 134.5 CFU per cm^2. The highest number

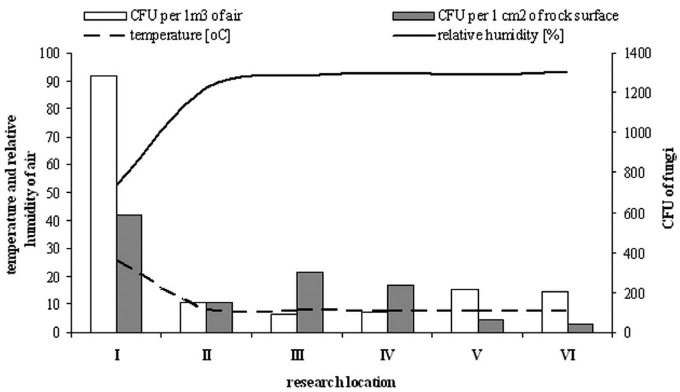

Figure 2. The climate parameters and measured concentrations of fungal spores at the sampled locations in Driny Cave on July 25, 2014. Location I is outside the cave entrance.

of fungal propagules isolated from the rock surface was found outside the cave at Location I, whereas the smallest number was observed from Location VI, the Chimney Passage; $P_{I, VI}$ = 0.0000001 (Table 3, Figs. 1 and 2).

The fungus most frequently isolated from the air outside and inside of Driny Cave was *Cladosporium cladosporioides*. The exception was Location VI, the Chimney Passage, where the most frequently isolated species was *Penicillium urticae*. All other fungi were much less common in the outside air ($P_{C. cladosporioides, E. nigrum}$ = 0.0000001). The same was true for fungi isolated from Location III, Entrance Passage ($P_{C. cladosporioides, P. urticae}$ = 0.0000001) and from Location IV, the Slovak Speleological Society Hall ($P_{C. cladosporioides, P. urticae}$ = 0.0000001). On the other hand, *Rhodotorula* spp. were the least frequently isolated species from Location II, also in the Entrance Passage ($P_{C. albicans, R. glutinis}$= 0.0081021). *Aspergillus fumigatus*, *Candida albicans*, *Penicillium granulatum* and *Rhodotorula rubra* ($P_{P. urticae, A. fumigatus}$ = 0.0149291) were rarest the Passage of Hopesand *Alternaria alternata*, *C. albicans*, *P. chrysogenum* and *R. rubra* ($P_{C. cladosporioides, A. alternata}$ = 0.0000002) were rarest at Location VI, the Chimney Passage (Table 2, Fig. 1, 3).

The species that most frequently occurred on the rock surface in three of seven tested locations was *Penicillium chrysogenum*, whereas the least frequent were *Rhizopus stolonifer*, *Rhodotorula rubra*, and *Trichoderma harzianum*, all of which were found only at Location II. *Penicillium chrysogenum* was the most numerous species isolated from Location I outside the cave ($P_{P. chrysogenum, A. fumigatus}$ = 0.0000001), Location III in the Entrance Passage ($P_{P. chrysogenum, A. fumigatus}$ = 0.0000001), and Location VI in the Chimney Passage ($P_{P. chrysogenum, C. albicans}$ = 0.0000002). The same was true for *T. harzianum* from Location II in the Entrance Passage ($P_{R. rubra, T. harzianum}$= 0.0000001) and for *P. granulatum* from Location IV, the Slovak Speleological Society Hall ($P_{P. granulatum, P. chrysogenum}$ = 0.0000001) and Location V, the Passage of Hopes ($P_{M. hiemalis, P. granulatum}$ = 0.0000001) (Table 3, Fig. 1 and 3).

DISCUSSION

Mycological evaluation of the air was performed according to the collision method using the Air Ideal 3P sampler and Petri dishes with appropriate solidified culture medium. In this method, the suction force ensures adherence of all the fungal propagules to the surface of a suitable culture medium. Furthermore, we can accurately determine their number per volume of the sucked air. This method is also suitable for evaluation of air for the concentration of bacteria and viruses (Kaiser and Wolski, 2007; Wiejak, 2011). It is very fast and easy to take a large number of samples during one day. Moreover, air samplers, such as the Air Ideal 3P sampler, are small in size, so they are useful for application in difficult conditions such as underground sites (Ogórek and Lejman, 2015).

Ogórek et al. (2014a, 2014b, 2014c) and Pusz et al. (2014, 2015), who studied fungi from air in underground sites, reported that higher levels of fungi were isolated from outside sites than from inside, as found in our study. Ecosystems such as underground sites, when compared to the external environment, are very unfavorable for survival and development of fungi due to the relatively stable low temperatures and very restricted availability of organic matter (Poulson and White, 1969; Barton and Northup, 2007). The concentration of fungal propagules in the air of Driny Cave did not exceed official limits and norms, and it is not dangerous for the health of tourists. According to the World Health Organization, the air is not contaminated by fungi if it contains no more than 1500 CFU per m^3 of air and if there is a mixture of fungal species (WHO, 1988). In the present study, the observed CFU values, 1284.7 per m^3 for outdoor and 89.6 to 217.5 CFU per m^3 for indoor air, were similar or lower than those reported by other researchers for cave air or other underground sites (Ogórek et al., 2013, 2014b; Pusz et al., 2014).

The indoor air samples collected inside Driny Cave contained more species of fungi than the outdoor air. This situation may be connected with the limitations of the method of sample collection or may be associated with specific conditions prevailing outside the entrance to the cave, such as temperature and humidity of the air, the vegetation present, the elevation, and the season of the year. It was also stated in the previous reports by Ogórek et al. (2014a, 2014b, 2014c) and Pusz et al. (2014) that most fungal species are transferred to underground sites by air currents from the external environment, which is why *Cladosporium* spp. dominated in the air both inside and outside of Driny Cave. Moreover, favorable conditions probably caused the domination of species of fungi that are cosmopolitan organisms and produce many spores, such as *C. cladosporioides*. However, Ogórek et al. (2016), who studied fungi cultured

Table 2. Filamentous fungi and yeast-like fungi isolated from the indoor and outdoor air of Driny Cave, with means of CFU per m^3 for six replicated air samples at each location on July 25, 2014.

Sampling Location[a]	Species	Air ± S.D., CFU per m^3	Effect of Location on Fungal Species Isolates[b]	Percent, %
I	*Alternaria alternata*	26.7 ± 6.8	b	2.1
I	*Aspergillus niger*	3.0 ± 1.1	b	0.2
I	*Cladosporium cladosporioides*	1000.0 ± 488.1	a	77.8
I	*Cladosporium herbarum*	15.0 ± 4.1	b	1.2
I	*Epicoccum nigrum*	140.0 ± 43.9	b	10.9
I	*Penicillium urticae*	100.0 ± 30.8	b	7.8
I	Total	1284.7 ± 405.8	A	100
II	*Candida albicans*	20.0 ± 4.6	c	13.4
II	*Cladosporium cladosporioides*	60.0 ± 16.7	a	40.2
II	*Cladosporium herbarum*	10.0 ± 4.2	cd	6.7
II	*Penicillium chrysogenum*	13.3 ± 4.0	cd	8.9
II	*Penicillium urticae*	33.4 ± 9.9	b	22.4
II	*Rhodotorula glutinis*	6.7 ± 3.0	d	4.5
II	*Rhodotorula rubra*	5.9 ± 3.7	d	4.0
II	Total	149.3 ± 19.8	C	100
III	*Aspergillus fumigatus*	0.2 ± 0.4	b	0.2
III	*Cladosporium cladosporioides*	71.1 ± 21.7	a	79.4
III	*Epicoccum nigrum*	5.6 ± 3.9	b	6.3
III	*Fusarium equiseti*	1.2 ± 1.0	b	1.3
III	*Penicillium granulatum*	0.8 ± 0.4	b	0.9
III	*Penicillium urticae*	6.7 ± 2.5	b	7.5
III	*Phoma fimeti*	4.0 ± 1.9	b	4.5
III	Total	89.6 ± 25.4	E	100
IV	*Alternaria alternata*	1.1 ± 1.1	b	1.1
IV	*Cladosporium cladosporioides*	80.9 ± 24.1	a	77.3
IV	*Epicoccum nigrum*	7.3 ± 2.6	b	7.0
IV	*Fusarium equiseti*	0.2 ± 0.4	b	0.2
IV	*Penicillium chrysogenum*	1.7 ± 1.2	b	1.6
IV	*Penicillium granulatum*	2.1 ± 1.3	b	2.0
IV	*Penicillium urticae*	10.4 ± 3.4	b	9.9
IV	*Phoma fimeti*	0.9 ± 0.3	b	0.9
IV	Total	104.6 ± 27.3	D	100
V	*Alternaria alternata*	16.7 ± 2.3	bc	7.7
V	*Aspergillus fumigatus*	3.0 ± 0.9	c	1.4
V	*Candida albicans*	0.3 ± 0.5	c	0.1
V	*Cladosporium cladosporioides*	115.0 ± 39.2	a	52.9
V	*Epicoccum nigrum*	26.7 ± 4.6	b	12.3
V	*Mucor hiemalis*	14.1 ± 3.0	bc	6.5
V	*Penicillium chrysogenum*	13.2 ± 3.2	bc	6.1
V	*Penicillium granulatum*	1.8 ± 1.1	c	0.8
V	*Penicillium urticae*	25.0 ± 5.3	b	11.5
V	*Rhodotorula rubra*	1.7 ± 1.5	c	0.8
V	Total	217.5 ± 34.7	B	100
VI	*Alternaria alternata*	15.0 ± 4.1	c	7.2
VI	*Candida albicans*	5.0 ± 1.9	c	2.4

Table 2. Continued.

Sampling Location[a]	Species	Air ± S.D., CFU per m^3	Effect of Location on Fungal Species Isolates[b]	Percent, %
VI	*Cladosporium cladosporioides*	70.0 ± 24.4	b	33.8
VI	*Penicillium chrysogenum*	8.0 ± 3.2	c	3.9
VI	*Penicillium urticae*	99.0 ± 32.7	a	47.8
VI	*Rhodotorula rubra*	10.0 ± 4.4	c	4.8
VI	Total	207.0 ± 40.2	B	100

[a] Sampling Station I = Outside the cave; Sampling Stations II–VI = Inside the cave.
[b] For each location, fungi concentrations (CFU per m^3) followed by the same letter are not statistically different at the $\alpha \leq 0.05$ level according to Tukey HSD test; others are. Small letters indicate the effect of location on fungal species isolates. Capital letters indicate the effect of a particular location on total fungal isolates.

from bat guano and air around it in Driny Cave on the same day, reported that the fungus most frequently isolated from the Slovak Speleological Society Hall (Location IV in this paper) was *P. granulatum*. Furthermore, the air around the bat guano contained more species and a higher concentration of airborne fungi than we report here.

According to Domsch et al. (1980), *Cladosporium cladosporioides* is common in many parts of the world, and its spores can be found in air, soil, and water. Moreover, studies of atmospheric air of various regions in Europe similarly show that the spores of *Cladosporium* spp. similarly dominate as 80% of caught spores. The level of concentrations of *Cladosporium* spores in the air shows a very large variation

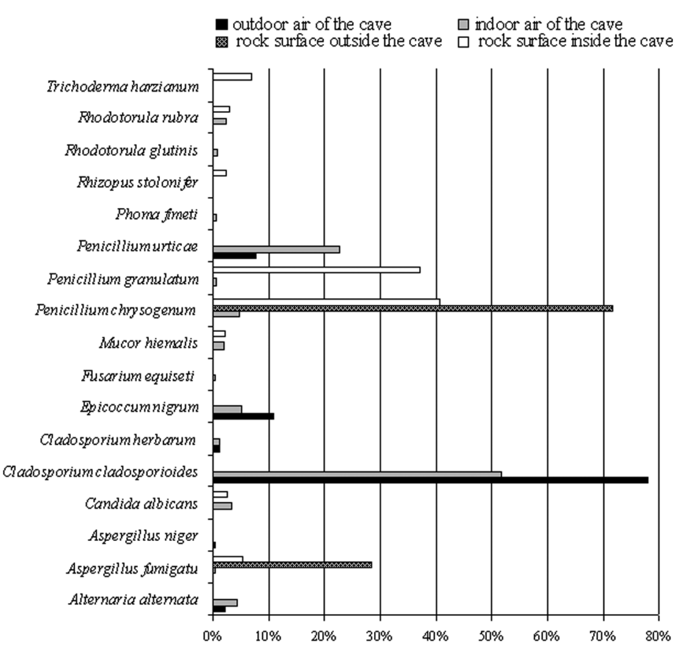

Figure 3. The percentage each species of filamentous and yeast-like fungi isolated contributed to the totals for the air and rock samples taken inside and outside Driny Cave on July 25, 2014.

over the year, from zero to several thousand spores per cubic meter, reaching its peak is in the months from June to September (D'Amato and Spieksma, 1995; Lipiec et al., 2000). Our research was conducted during this period, which is particularly conducive for fungal development, due, for example, to the high availability of plant material. Moreover, *Cladosporium* spp. are classified as inducers of IgE-mediated sensitization and sources of allergic rhinitis or asthma (Douwes et al., 2003; Eduard, 2009). About 2800 spores per liter are necessary to induce symptoms of allergic respiratory system disease in most patients with hypersensitivity to these allergens (Rapiejko et al., 2004). Thus the level of fungi we found does not constitute a significant allergic risk to visitors. However, *Cladosporium* spp. can be isolated from rocks, and they can cause mineralization of birnessite (Burford et al., 2003). These fungi may secrete acids such as formic, fumaric, gluconic, and lactic and pigments such as melanin, light to dark brown, or gray, and they may cause oxidation of Fe(II), reduction of Fe(III) and of Mn(IV), adsorption of Cu^{2+}, and corrosion of Al (Grote, 1986; Wainwright, 1993; Sterflinger, 2000).

Our results showed that higher numbers of fungi were isolated from the rock surfaces outside the cave (588.5 CFU/cm^2) than from the surfaces inside the cave (from 38.3 to 301.7). However, the samples collected inside the cave contained more fungal species than those collected from surfaces located outside the cave. The mean values of CFU per cm^2 found in the present study were higher than those noted by other researchers for surfaces located inside different underground sites or caves. During the previous studies, Ogórek et al. (2014b) isolated 113.5 to 185.0 CFU per cm^2 from the rock surfaces located inside the underground Rzeczka complex. For comparison, Pusz et al. (2014) collected 24 to 54.9 CFU per cm^2 in the case of the Osówka underground complex, and 102.2 to 178.0 CFU per cm^2 were isolated by Ogórek et al. (2014a) from the Włodarz underground complex.

According to other authors, the most abundant fungi isolated from rocks belong to such genera as *Aspergillus*, *Aureobasidium*, *Mucor*, *Penicillium*, *Phoma*, and *Trichoderma* (Hirsch et al., 1995; Burford et al., 2003; Ogórek et al., 2014a, 2014b). Our results showed statistically

Table 3. Filamentous fungi and yeast-like fungi isolated from the rock surfaces at each location in Driny Cave, with means of CFU per cm^2 for nine replicated samples taken on July 25, 2014.

Sampling Location[a]	Species	Air ± S.D., CFU per m^3	Effect of Location on Fungal Species Isolates[b]	Percent, %
I	*Aspergillus fumigatus*	166.8 ± 29.2	b	28.3
I	*Penicillium chrysogenum*	421.7 ± 32.0	a	71.7
I	Total	588.5 ± 134.5	A	100
II	*Aspergillus fumigatus*	19.1 ± 4.7	bc	26.9
II	*Candida albicans*	15.0 ± 3.3	cd	21.1
II	*Mucor hiemalis*	3.3 ± 2.0	f	4.6
II	*Penicillium chrysogenum*	10.2 ± 2.9	de	14.3
II	*Penicillium granulatum*	5.2 ± 2.2	e, f	7.3
II	*Rhizopus stolonifer*	18.3 ± 4.7	bc	25.7
II	*Rhodotorula rubra*	23.2 ± 3.5	b	29.7
II	*Trichoderma harzianum*	54.9 ± 4.5	a	70.3
II	Total	149.2 ± 15.6	D	100
III	*Aspergillus fumigatus*	23.8 ± 3.3	b	7.9
III	*Penicillium chrysogenum*	265.1 ± 66.4	a	87.9
III	*Penicillium granulatum*	12.8 ± 4.0	b	4.2
III	Total	301.7 ± 124.2	B	
IV	*Penicillium chrysogenum*	12.4 ± 3.6	b	5.2
IV	*Penicillium granulatum*	228.0 ± 41.5	a	94.8
IV	Total	240.4 ± 114.5	C	100
V	*Candida albicans*	0.6 ± 0.5	c	1.0
V	*Mucor hiemalis*	12.7 ± 2.7	b	20.8
V	*Penicillium granulatum*	47.8 ± 4.4	a	78.2
V	Total	61.1 ± 20.6	E	100
VI	*Candida albicans*	4.9 ± 1.8	b	12.8
VI	*Penicillium chrysogenum*	33.4 ± 7.9	a	87.2
VI	Total	38.3 ± 13.3	F	100

[a] Sampling Station I = Outside the cave; Sampling Stations II–VI = Inside the cave.
[b] For each location, fungi concentrations (CFU per m^3) followed by the same letter are not statistically different at the $\alpha \leq 0.05$ level according to Tukey HSD test; others are. Small letters indicate the effect of location on fungal species isolates. Capital letters indicate the effect of a particular location on total fungal isolates.

significant differences in the numbers of fungi isolated from the rocks and differences in the species composition of the fungi most frequently isolated from the rock surfaces. In our study, the most abundant fungi cultured from the rock surfaces were *Penicillium chrysogenum*, *P. granulatum* and *Trichoderma harzianum*. These fungi are able to grow in a wide range of temperatures (Rippel-Baldes, 1955; Pusz et al., 2014). It is known that they can degrade a wide range of rocks and minerals (Sterflinger, 2000). They may degrade sandstone, marble, and granite, secrete acids and pigments, and some of them even cause bioconversion of coal. They are also able to solubilize minerals and accumulate metals. For example, *Penicillium* spp. may secrete acids (citric, 2-oxogluconic, acetic, formic, fumaric, gluconic, glyoxylic, kojic, lactic, malonic, orsellinic, oxalic and tartaric) or different pigments of various colors (grey, orange, purple, red, white, yellow), and they may cause oxidation of Fe(II) and Mn(II), adsorption of Al, Zn, Cd, U, Th, Pb, Sn, solubilization of rock phosphate and coal, and reduction of Fe(III) (Sterflinger, 2000; Cwalina, 2008). In addition, these fungi can cause mineralization of materials such as halloysite ($Al_2Si_2O_5(OH)_4 \cdot 2H_2O$) and montmorillonite ($(Na,Ca)_{0.33}(Al,Mg)_2(Si_4O_{10})(OH)_2 \cdot nH_2O$) or todorokite ($(Mn,Ca,Mg)Mn_3O_{12} \cdot 3H_2O$) (Burford et al., 2003). *Trichoderma* spp. may secrete acids, such as acetic, citric, formic, gluconic, glyoxylic, and oxalic, and green pigments. This species is able to oxidize sulfide groups, solubilize coal, and accumulate Cd, Cu, and even uranium (Sterflinger, 2000).

Conclusions

Our results show that the external environment around the cave directly affects the concentration of fungal propagules and their species composition inside the studied area. The mean number of fungi was higher outside than inside Driny Cave, but the samples collected from inside contained a higher number of fungal species than samples collected outside the cave. The widely recognized and accepted standards for airborne fungi are not exceeded in Driny Cave; therefore, this place does not constitute a health risk to visiting tourists. The most frequently isolated fungus from the indoor and outdoor air was *Cladosporium cladosporioides*, a cosmopolitan organism predominant in the atmosphere, especially during the summertime. The fungi most frequently isolated from the rock surfaces were *Penicillium chrysogenum*, *P. granulatum*, and *Trichoderma harzianum*. It should be noted that the species of fungi isolated from the rock surfaces can cause their slow degradation. We believe that this type of research allows people to better understand the cave ecosystems, in particular to characterize the underground mycobiota and their role in the occupied ecological niche.

Acknowledgements

We thank Dr. Ján Zuskin, director of Slovak Caves Administration, for his help in the study. This work was co-financed by the Ministry of Science and Higher Education carried out by the University of Wroclaw "Grant to Young Researchers". Grant number: 0420/1398/16.

References

Al-Doory, Y., and Rhoades, E.R., 1968, Isolation of *Histoplasma capsulatum* from a Texas cave: Mycopathologia et Mycologia Applicata, v. 35, no. 3, p. 201–207. doi:10.1007/BF02050730.

Balabanoff, V.A., 1967, Etudes comparées des Dermatophytes isolés de grottes et d'étables en Bulgarie: Mycopathologia et Mycologia Applicata, v. 32, no. 3, p. 237–248. doi:10.1007/BF02049801.

Barnett, J.A., Payne, R.W., and Yarrow, D., 2000, Yeasts: Characteristics and Identification, third edition: Cambridge, Cambridge University Press, 1150 p.

Barton, H.A., 2006, Introduction to cave microbiology: A review for the non-specialist: Journal of Cave and Karst Studies, v. 68, no. 2, p. 43–54.

Barton, H.A., and Northup, D.E., 2007, Geomicrobiology in cave environments: Past, current, and future perspectives: Journal of Cave and Karst Studies, v. 69, no. 1, p. 163–178.

Bastian, F., Jurado, V., Nováková, A., Alabouvette, C., and Saiz-Jimenez, C., 2010, The microbiology of Lascaux Cave: Microbiology, v. 156, no. 3, p. 644–652. doi:10.1099/mic.0.036160-0.

Bella, P., 2003, Slovensko – Sprístupnené Jaskyne (Slovakia Show Caves): Liptovský Mikuláš, Grafon, 64 p.

Bella, P., Hlavac, J., and Gazik, P., 2001, Protection and management of show caves in Slovakia: 13th International Congress of Speleology, 4th Speleological Congress of Latin América and the Caribbean, 26th Brazilian Congress of Speleology, Brasília, 15–22, July, 2001, p. 287–290.

Brashear, D., Wiseman R.F., and Barr Jr., T.C., 1966, A psychrophilic yeast from Mammoth Cave, Kentucky: International Journal of Speleology, v. 2, no. 4, p. 403–404. doi:10.5038/1827-806X.2.4.12.

Burford, E.P., Kierans M., and Gadd, G.M., 2003, Geomycology: Fungi in mineral substrata: Mycologist, v. 17, no. 3, p. 98–107. doi:10.1017/S0269915X03003112.

Chelius, M.K, Beresford, G., Horton, H., Quirk, M., Selby, G., Simpson, R.T., Horrocks, R., and Moore, J.C., 2009: Impacts of alterations of organic inputs on the bacterial community within the sediments of Wind Cave, South Dakota, USA. International Journal of Speleology, v. 38, no. 1, p. 1–10. doi: 10.5038/1827-806X.38.1.1.

Cury, G.C., Dinez Filho, A., Cruz, A.G.C., and Hobaika, A.B.S., 2001. Surto de histoplasmose em Pedro Leopoldo, Minas Gerais, Brasil. (Outbreak of histoplasmosis in Pedro Leopoldo, Minas Gerais, Brazil): Revista Sociedade Brasileira de Medicina Tropical, v. 34, no. 5, p. 483–486. doi:10.1590/S0037-86822001000500013.

Cwalina, B., 2008, Biodeterioration of concrete: Architecture Civil Engineering Environment, v.1, no. 4, p. 133–140.

D'Amato, G., and Spieksma, F.Th.M., 1995, Aerobiologic and clinical aspects of mould allergy in Europe: Allergy, v. 50, no. 11, p. 870–877. doi:10.1111/j.1398-9995.1995.tb02492.x.

Domsch, K.H., Games, W., and Anderson, T.H., 1980, Compendium of Soil Fungi: London, Academic Press, 1264 p.

Douwes, J., Thorne, P., Pearce N., and Heederik, D., 2003, Bioaerosol health effects and exposure assessment: Progress and prospects: The Annals of Occupational Hygiene, v. 47, no. 3, p. 187–200. doi:10.1093/annhyg/meg032.

Eduard, W., 2009, Fungal spores: A critical review of the toxicological and epidemiological evidence as a basis for occupational exposure limit setting: Critical Reviews in Toxicology, v. 39, no. 10, p. 799–864. doi:10.3109/10408440903307333.

Griffin, D.W., Gray, M.A., Lyles, M.B., and Northup, D.E., 2014, The transport of nonindigenous microorganisms into caves by human visitation: A case study at Carlsbad Caverns National Park: Geomicrobiology Journal, v. 31, no. 3, p. 175–185. doi:10.1080/01490451.2013.815294.

Grote, G., 1986, Mikrobieller Mangan- und Eisentransfer an Rock Varnish und Petroglyphen arider Gebiete [PhD thesis]: University of Oldenburg, Germany, 335 p.

Gu, Ji-Dong, 2003, Microbiological deterioration and degradation of synthetic polymeric materials: Recent research advances: International Biodeterioration & Biodegradation, v. 52, no. 2, p. 69–91. doi:10.1016/S0964-8305(02)00177-4.

Hirsch, P., Eckhardt, F.E.W., and Palmer, R.J., Jr., 1995, Fungi active in weathering of rock and stone monuments: Canadian Journal of Botany, v. 73, no. S1, p. 1384–1390. doi:10.1139/b95-401.

Jurado, V., Laiz, L., Rodriguez-Nava, V., Boiron, P., Hermosin, B., Sanchez-Moral, S., and Saiz-Jimenez, C., 2010, Pathogenic and opportunistic microorganisms in caves: International Journal of Speleology, v. 39, no. 1, p. 15–24. doi:10.5038/1827-806X.39.1.2.

Kaiser, K., and Wolski, A., 2007, Kontrola czystości mikrobiologicznej powietrza (Control of microbiological purity of air): Technika Chłodnicza i Klimatyzacyjna, no. 135, p. 158–162.

Kalogerakis, N., Paschali, D., Lekaditis, V.,Pantidou, A., Elefheriadis, K., and Lazarides, M., 2005, Indoor air quality—bioaerosol measurements in domestic and office premises: Journal of Aerosol Science, v. 36, no. 5-6, p. 751–761. doi:10.1016/j.jaerosci.2005.02.004.

Karkun, A., Tiwari, K.L., and Jadav, S.K., 2012, Fungal diversity of Mandeepkhol Cave in Chhattisgarh, India: Advances in Bioresearch, v. 3, no. 2, p. 119–123.

Koilraj, A.J., and Marimuthu, G., 1998, Algal flora in the cave soils: Current Science, v. 75, no. 11, p. 1111–1113.

Kubátová, A., and Dvořák, L., 2005, Entomopathogenic fungi associated with insect hibernating in underground shelters: Czech Mycology, v. 57, no. 3-4, p. 221–237.

Kurtzman, C.P., and Fell, W., eds., 1998, The Yeasts, a Taxonomic Study, fourth edition: Amsterdam, Elsevier, 1076 p.

Lehotská, B., and Lehotský, R., 2009, 15 rokov zimného monitoringu netopierov v jaskyni Driny (15 years of winter monitoring of bats in the Driny Cave): Aragonit, v. 14, no. 2, p. 171–172.

Li, Xianshu, Arai, H., Shimoda, I., Kuraishi, H., and Katayama, Y., 2008, Enumeration of sulfur-oxidizing microorganisms on deteriorating stone of the Angkor monuments, Cambodia: Microbes and Environments, v. 23, no. 4, p. 293–298. doi:10.1264/jsme2.ME08521.

Lipiec, A., Jurklewicz, D., and Rapiejko, P., 2000, Mould hypersensitivity in allergic rhinitis patients: International Review of Allergology and Clinical Immunology, v. 6, p. 57–63.

Nudziková, Ľ., 2014, Vývoj návštevnosti sprístupnených jaskýň na Slovensku od roku 2009 (Course of show caves attendance in Slovakia since 2009): Aragonit, v. 19, no. 1-2, p. 35–38.

Ogórek, R., Lejman, A., and Matkowski, K., 2013, Fungi isolated from the Niedźwiedzia Cave in Kletno (Lower Silesia, Poland): International

Journal of Speleology, v. 42, no. 2, p. 161–166. doi: 10.5038/1827-806X.42.2.9.

Ogórek, R., Pusz, W., Lejman, A., and Uklańska-Pusz, C., 2014a, Microclimate effects on number and distribution of fungi in the underground comlex in the Owl mountains (Góry Sowie), Poland: Journal of Cave and Karst Studies, v. 76, no. 2, p. 146–153. doi:10.4311/2013MB0123.

Ogórek, R., Pusz, W., Matkowski, K., and Pląskowska, E., 2014b, Assessment of abundance and species composition of filamentous fungi in the underground Rzeczka complex in Sowie Mountains (Lower Silesia, Poland): Geomicrobiology Journal, v. 31, no. 10, p. 900–906. doi:10.1080/01490451.2014.907380.

Ogórek, R., Lejman, A., and Matkowski, K., 2014c, Influence of the external environment on airborne fungi isolated from a cave: Polish Journal of Environmental Studies, v. 23, no. 2, p. 435–440.

Ogórek, R., and Lejman, A., 2015, Badania speleomikologiczne w wybranych obiektach podziemnego kompleksu Riese (Góry Sowie, Dolny Śląsk, Polska) / (Speleomycological research in the selected objects of underground Riese complex (Sowie Mountains, Lower Silesia, Poland)): Postępy Mikrobiologii, v. 54, no. 4, p. 344–353.

Ogórek, R., Pląskowska, E., Dyląg, M., Višňovská, Z., Tančinová, D., and Lejman, A., Fungi isolated and quantified from bat guano and air in Harmanecká and Driny Caves (Slovakia): Journal of Cave and Karst Studies, v. 78, no. 1, p. 41–49. doi:10.4311/2015MB0108.

Papuas, G.P., Herbert, R.J., Henderson, W., Koenig, J., Stover, B., and Barnhart, S., 2000, The respiratory effects of volatile organic compounds: International Journal of Occupational and Environmental Health, v. 6, no. 1, p. 1–8. doi:10.1179/oeh.2000.6.1.1.

Pitt, J.I., and Hocking, A.D., 2009, Fungi and Food Spoilage, third edition: Dordrecht, Springer, 519 p.

Poulson, T.L., and White, W.B., 1969, The cave environment: Science, v. 165, no. 3897, p. 971–981. doi:10.1126/science.165.3897.971.

Pulido-Bosch, A., Martín-Rosales, W., López-Chicano, M., Rodríquez-Navarro, C.M., and Vallejos, A., 1997, Human impact in a tourist karstic cave (Aracena, Spain): Environmental Geology, v. 31, no. 3-4, p. 142–149. doi:10.1007/s002540050173.

Pusz, W., Ogórek, R., Knapik, R., Kozak, B., and Bujak, H., 2015, The occurrence of fungi in the recently discovered Jarkowicka cave in the Karkonosze Mts. (Poland): Geomicrobiology Journal, v. 32, no. 1, p. 59–67. doi:10.1080/01490451.2014.925010.

Pusz, W., Ogórek, R., Uklańska-Pusz, C.M., and Zagożdżon, P., 2014, Speleomycological research in underground Osówka complex in Sowie Mountains (Lower Silesia, Poland): International Journal of Speleology, v. 43, no. 1, p. 27–34. doi: 10.5038/1827-806X.43.1.3.

Rapiejko, P., Lipiec, A., Wojdas, A., and Jurkiewicz, D., 2004, Threshold pollen concentration necessary to evoke allergic symptoms: International Review of Allergology and Clinical Immunology, v. 10, p. 91–94.

Rippel-Baldes, A., 1955, Grundzüge der Mikrobiologie, third edition: Berlin, Springer, 418 p. doi: 10.1007/978-3-662-01454-7.

Scheerer, S., Ortega-Morales, O., and Gaylarde, C., 2009, Microbial deterioration of stone monuments: An updated overview: Advances in Applied Microbiology, v. 66, p. 97–139. doi:10.1016/S0065-2164(08)00805-8.

Sterflinger, K., 2000, Fungi as geologic agents: Geomicrobiology Journal, v. 17, no. 2, p. 97–124. doi:10.1080/01490450050023791.

Šustr, V., Elhottová, D., Krištůfek, V., Lukešova, A., Nováková, A., Tajovský, K., and Tříska, J., 2005, Ecophysiology of the cave isopod *Mesoniscus graniger* (Frivaldszky 1865) (Crustacea: Isopoda): European Journal of Soil Biology, v. 41, no. 3-4, p. 69–75. doi:10.1016/j.ejsobi.2005.09.008.

Taylor, E.L.S., Resende-Stoianoff, M.A.R., and Lopes Ferreira, R., 2013, Mycological study for a management plan of a neotropical show cave (Brazil): International Journal of Speleology, v. 42, no. 3, p. 267–277. doi: 10.5038/1827-806X.42.3.10.

Vanderwolf, K.J., Malloch, D., McAlpine, D.F., and Forbes, G.J., 2013, A world review of fungi, yeasts, and slime molds in caves: International Journal of Speleology, v. 42, no. 1, p. 77–96. doi: 10.5038/1827-806X.42.1.9.

Wainwright, M., 1993, Oligotrophic growth of fungi—stress or natural state? *in* Jennings, D.H., ed., Stress Tolerance of Fungi: New York, Marcel Dekker, Mycology Series 10, p. 127–144.

Walochnik, J., and Mulec, J., 2009, Free-living amoebae in carbonate precipitating microhabitats of karst caves and a new vahlkampfiid amoeba, *Allovahlkampfia spelaea* gen. nov., sp. nov.: Acta Protozoologica, v. 48, no. 1, p. 25–33.

Watanabe, T., 2010, Pictorial Atlas of Soil and Seed Fungi: Morphologies of Cultured Fungi and Key to Species, third edition: Boca Raton, Florida, CRC Press, 426 p.

Wiejak, A., 2011, Ocena stopnia skażenia powietrza zarodnikami grzybów pleśniowych jako czynnik ekspertyzy mikologicznej (The assessment of air contamination with the mould fungi spores as an Essentials factor of mycological report): Prace Instytutu Techniki Budowlanej, v. 3, no. 159, p. 3–12.

WHO (World Health Organization), 1988, Indoor Air Quality: Biological Contaminants, Report on a WHO Meeting, Rautavaara, 29 August–2 September 1988: Copenhagan, WHO Regional Office for Europe, WHO Regional Publications, European Series no. 31, 67 p.

T.K. Philips, C.S. DeWildt, H. Davis, and R.S. Anderson – Survey of the terrestrial arthropods found in the caves of Ghana. *Journal of Cave and Karst Studies*, v. 78, no. 2, p. 128–137. DOI: 10.4311/2015LSC0120

SURVEY OF THE TERRESTRIAL ARTHROPODS FOUND IN THE CAVES OF GHANA

T. Keith Philips[1]*, Chris S. DeWildt[1,2], Henry Davis[3], and Roger S. Anderson[3]

Abstract: The first biological inventory of the caves of Ghana was conducted during January 2006 with some subsequent work in June 2007 and July 2008. Seventy species or morphospecies of insects, as well as amblypigids, phalangids, and diplopods were discovered in sixteen caves. All taxa appear to be either troglophilic or accidental and the most abundant and richest insect faunas were found in caves with resident bat populations. Insect diversity in caves consists mainly of species of cockroaches, cave crickets, tenebrionid beetles, reduviid assassin bugs, and ants. All caves surveyed are briefly described, coordinates documented, and a list of all the arthropods discovered is also given.

Introduction

The caves of Ghana have never been sampled for their biodiversity; no faunal survey, list of taxa, or other scientific publication on any aspect of the invertebrate cave fauna of this country exists. In stark contrast and surprisingly, cave research has been conducted in every one of the surrounding countries, including Burkina Faso, Togo, and Côte d'Ivoire, as well as Guinea (Juberthie and Decu, 2001), and has resulted in novel discoveries. For example, a cave in Burkina Faso produced a new species of dytiscid beetle (Bourgies and Juberthie, 2001). In a Guinean cave, a new genus and species of blaberid cockroach was discovered and described (Roth and Naskrecki, 2004). Outside of West Africa, several publications by Villers (1953, 1973, 1976) described the Reduviidae fauna of African caves, including one new genus, in the Belgian Congo (Democratic Republic of the Congo), Kenya, and South West Africa (Namibia).

The apparent lack of research on Ghana caves was the incentive for conducting this study as a contribution to the knowledge of cave biodiversity found worldwide. This research is also part of an effort in surveying the threatened insect fauna found in the Upper Guinean Forests of West Africa (Critical Ecosystem Partnership Fund, n.d.; Conservation International, n.d.), as well as that found in the drier savannah bush in the central and northern regions. The Guinean forests of West Africa are one of approximately 35 regions that have been recognized as global biodiversity hotspots. These hotspots make up only 2.3 % of the total land area on the planet but hold an estimated 44 % of plants and 35 % of the land-vertebrate species (Harrison and Pearce, 2001). In contrast, the invertebrate fauna is poorly known. Hence, as part of an overall insect fauna survey of this country and the larger hotspot and to support conservation efforts, all of the known caves of Ghana were sampled for their insect faunas, as well as other arthropods.

One should note that the caves of this region are not extensive in length or depth, and none of the invertebrate fauna collected are likely either cave-limited or cave-adapted species known as troglobites; all appear to be either troglophiles or accidentals (Howarth, 1983), and it is possible that all species we report can be found outside of cave habitats. Further, no maps for any of these caves are known to exist. Regardless, this list is a first effort to put on record the insects found in Ghanaian caves and to more broadly encourage research on the relatively neglected and highly threatened insect fauna of this region.

Materials and Methods

Some of the caves sampled for study were known to scientific contacts in Ghana. Other caves were discovered by asking villagers in many locations about the possible presence of any caves in the vicinity and by searching the World Wide Web. Insects and other arthropods were collected throughout the various subterranean habitats in the caves by searching and hand-collecting using various tools, including aspirators and forceps. The four co-authors continued their investigation in each cave until available habitats, such as under rocks and wood or on walls or in crevices, were gleaned and no additional species could be found. On two occasions pitfalls baited with peanut butter were set in caves for about 24 hours to further sample the fauna. Fieldwork took place during an extensive three-week survey in January 2006, with smaller surveys in June 2007 (a repeat of the Shai Hills, Sayu Cave) and July 2008 (never-before-sampled Tengzu Caves). Throughout most of Ghana, June–July and September–October are the rainy seasons, with the former the wettest. In the north, the rainfall increases from January through to a peak in September, with a steep decline through the rest of the year. In Ghana, January is a period of low seasonal rainfall throughout the country, and in some areas sampled in 2006 several species of deciduous trees had lost their leaves. Cave descriptions

* Corresponding author: keith.philips@wku.edu
[1] Systematics and Evolution Laboratory, Department of Biology, Western Kentucky University, Bowling Green KY 42101-3576, USA
[2] Current Address: 5762 S. Lady Slippery Pl., Tucson AZ 85747, USA
[3] Department of Animal Biology and Conservation Science, University of Ghana, P.O. Box 67, Legon, Accra, GHANA

Table 1. List of caves in which collections were made, their coordinates, elevation, and number of taxa collected.

Cave	Region	Coordinates		Elevation, m	No. of Taxa Collected
		Latitude	Longitude		
Kaese	Eastern	~N 6°38.383′	W 1°24.674′	580	7
Kyireabe	Eastern	~N 6°38.383′	W 1°24.674′	580	4
Wiafe	Eastern	~N 6°38.383′	W 1°24.674′	580	3
Mframaboum	Ashanti	N 7°0.217′	W 1°18.016′	413	14
Mprisi	Ashanti	N 7°43.417′	W 1°59.282′	420	9
Water	Ashanti	N 7°43.845′	W 1°59.261′	425	9
Akpomu Falls	Volta	N 6°53.068′	E 0°27.936′	480	4
Kokosiaba, dry	Volta	N 6°48.510′	E 0°23.153′	430	12
Kokosiaba, moist	Volta	N 6°48.510′	E 0°23.153′	430	7
Likpe Cave 3	Volta	N 7°9.850′	E 0°36.491′	626	16
Likpe Cave 5	Volta	N 7°9.892′	E 0°36.537′	615	7
Obom	Volta	N 5°59.815′	W 0°11.015′	246	12
Sayu (Bat/Chief)	Greater Accra	N 5°55.793′	E 0° 03.431′	160	13

and only approximate size estimations are given, as precise mapping of the caves was not a goal of this project.

Specimen identifications were made by the first two authors to as low a level as accurately possible using literature and websites such as AntWiki (http://www.antwiki.org/wiki/Ghana). Attempts were made to procure more specific and accurate determinations from specialists as much as possible. It is our hope that this paper may interest insect systematists in studying specimens that were collected during this project. Hence all vouchers collected are available for study and are currently deposited in the T. K. Philips Collection (Western Kentucky University), with the exception of the Reduviidae that are in the B. D. Gill Collection (Ottawa, Canada). It is hoped that the eventual depository for most of the specimens from this study and from other collections will be the developing National Insect Collection at the Department of Animal Biology and Conservation Science at the University of Ghana, currently located in the African Regional Postgraduate Program in Insect Science (ARPPIS) on the main campus in Legon.

As the cave faunas of Ghana do not seem to be characterized morphologically as troglobites (species restricted to cave habitats with morphological features such as loss of eyes and pigmentation) and there are no collection records outside of the caves to determine if most of the species are either trogloxenes (species that regularly enter caves but leave periodically for certain living requirements) or accidentals (species rarely found in caves and not making any real use of the habitat), we have left off these designations as defined by Romero (2009). Notes are given for caves that appear to be well known as such, but actually are only caves by the broadest definition possible, such as Abutia Cave and Kpando Blue Uzs Grotto, and where no particular fauna were observed. They are reported in order to save time and effort for those wishing to further explore and sample the faunas of the true caves found in Ghana.

One should be aware that typically permission is first needed from the nearest village chief or the village elders before one can gain cave entry. While the caves at Likpe are commercial, at the other caves a local person can serve as a guide for some monetary compensation, usually negotiated in advance, for his services. Once at the cave entrance, it may also be necessary to perform a ceremony, referred to as *libations,* in which alcohol, typically schnapps, is poured onto the ground while prayers are recited in a short ceremony of ancestor worship. The true caves from which taxa were collected and their locations are listed in Table 1. All sites investigated are described in the following section.

Cave Descriptions

Eastern Region

Caves explored in this region are all situated near the town of Abesua (N 6°38.383′ W 1°24.674′; 583 m). A short drive from the main road was taken to an area near the base of a hill, and one must hike to visit the four caves. The entire process of surveying all the sites took about six hours.

Kyireabe Cave. This rock shelter consists of an overhang that protects a small cavity in the rock face that extends in approximately 3.5 m. The cavity is high enough to stand up in. Accumulated seeds that had been carried in by rodents and eaten were observed. There did not seem to be an associated cave fauna, and the cavity was very dry.

Kaasi Cave. This cave is located on a steep hill with an entrance about 2 m high and 1 m wide. The cave extends in approximately 10 to 15 m. The floor at the entrance immediately begins to slope down for three-quarters of the length. The walls angle in and meet at the ceiling, which in some places is about 5 m high. There is also a second, smaller passage about 2 m up near the end of the main passage. Bats are present, and this was the only cave of the four in this area with cave crickets (*Phaeophilacris* sp.).

Figure 1. Cave crickets (*Phaeophilacris* sp.) on a wall in Mframaboum Cave.

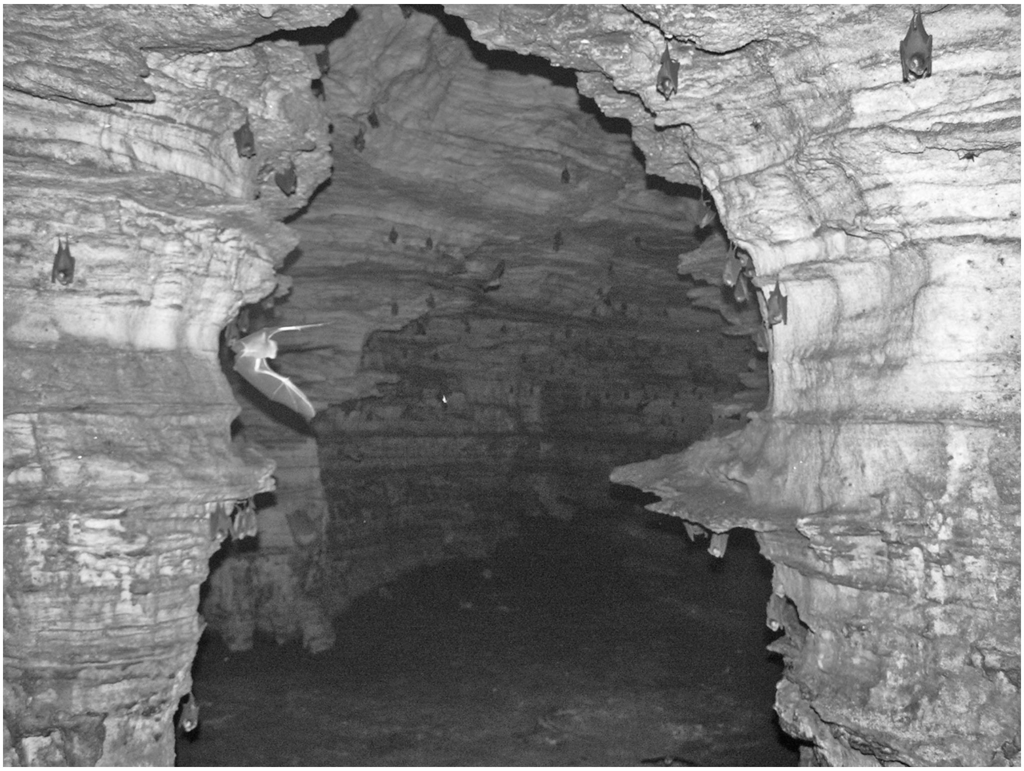

Figure 2. The main passage in Mframaboum Cave.

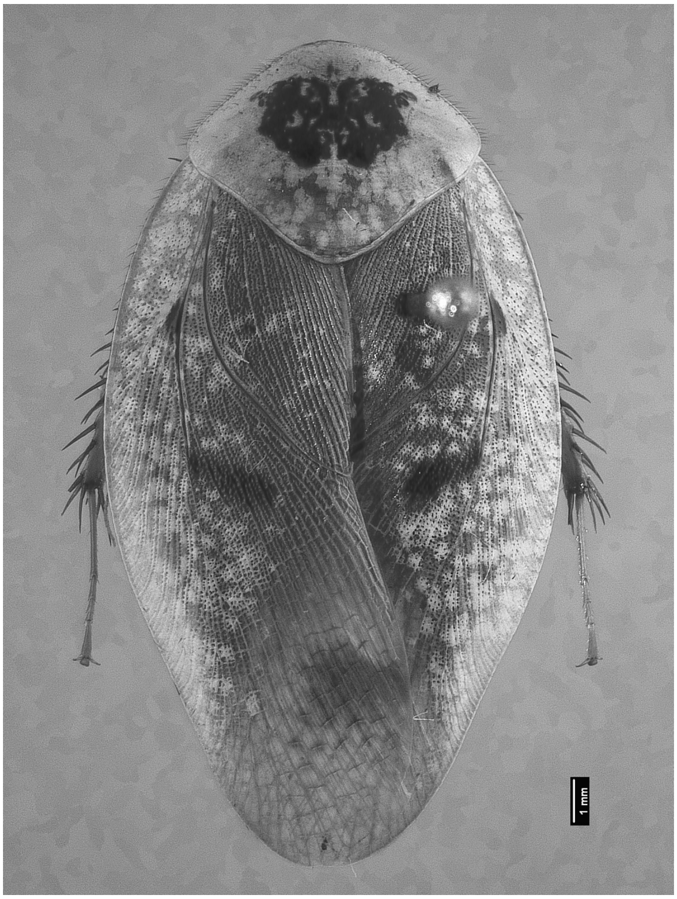

Figure 3. Dorsal habitus of a cockroach belonging to the *Gyna maculipennis* group collected in Mframaboum Cave.

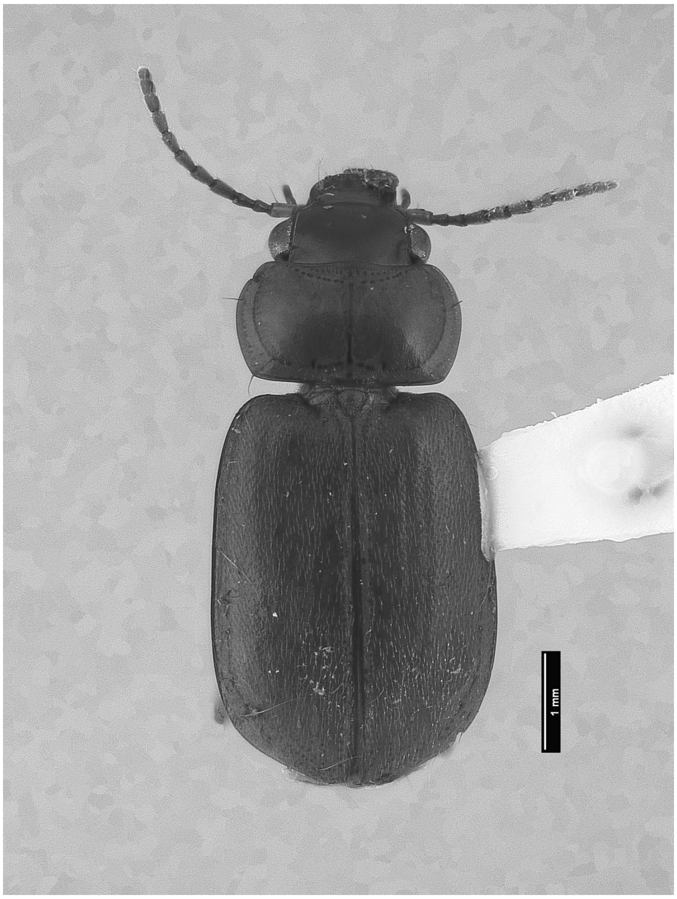

Figure 4. Dorsal habitus of an undetermined species of ground beetle (Carabidae, Masoreini) found in Mframaboum Cave, Water Cave, Ancestral Caves at Likpe Todome #3, and both the Kokosiaba Dry and Moist Caves.

Prati Cave. This is only a small rock shelter without a cave fauna.

Wiafe Cave. Reaching this cave entails a steep climb, including passing over large rocks. The entrance is in a vertical rock face, is about 0.75 m wide and over 4 m in height, and leads to about 5 m of passage to a drop about 2.75 m onto a wet muddy floor.

Ashanti Region

Mframaboum Cave (N 7°0.217′, W 1°18.016′; 413 m). This cave is accessed via a short hike of about 200 m from a road. The cave consists of a main chamber that intersects several additional secondary chambers. The air inside the cave was extremely humid, and bats were abundant with one small chamber that contained more than 90 bats (Fig. 1 and Fig. 2). There was a large chamber immediately behind the main chamber, and there was a shallow stream running the entire length (7 m). Platyhelminth flatworms were present and common in the stream detritus. This stream continued through several sub-chambers and through a passage in the wall of the cave, emerging outside to the right side of the cave entrance as a small waterfall. Twenty pitfall traps were set in the silt of the cave, 5 in small passage and 15 in the main chamber. Rodent disturbance of the 5 small-passage traps made collection impossible. Several other traps were found filled with dry, powdery detritus, common in these caves. Its presence was most likely due to activity of "dust or guano swimmers," a group of cave cockroaches (Fig. 3 and Fig. 4) that engage in an interesting ambulatory "swimming" movement through guano dust and detritus. Traps did not result in the collection of any additional species.

Water Cave (N 7°43.845′ W 1°59.261′; 425 m; near Buoyem). The cave entrance is about 20 m wide and more than 4 m in height and arches down towards the sides. A large termite mound approximately 7 m in diameter at the base currently divides the entrance almost directly in the center. The interior can be divided into two separate regions. Initially inside is a very large, dry room. A stream runs from the back of the cave, exiting out the left side of the entrance. The ceiling of this first room gradually slopes down the length of the room, leveling off at about 1 m high some 6.5 m into the cave. This lower section continues about 5 m to where the ceiling abruptly rises into the second, slightly smaller chamber. Water running into this second chamber from the ceiling is the source of the stream in the cave.

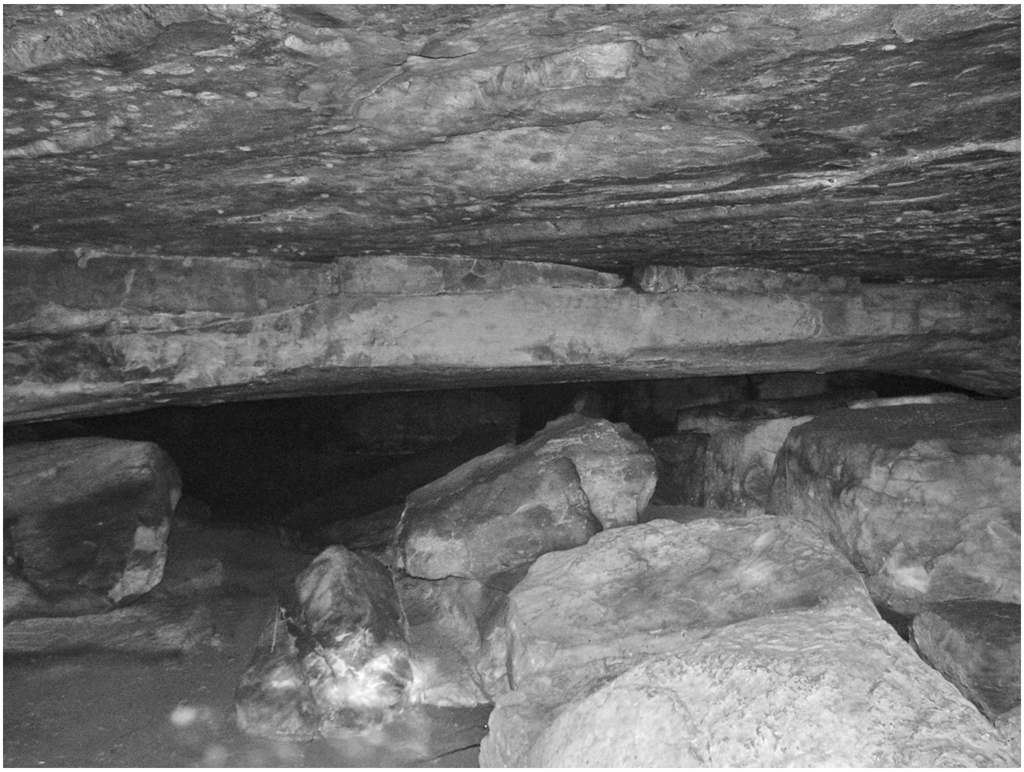

Figure 5. Mprisi Cave near the entrance.

Mprisi Cave (N 7°43.417′ W 1°59.282′; 420 m; near Buoyem; also known as the "Don't rush and enter cave"). This cave is mostly dry at the entrance, with much powdery detritus at least 5 cm deep covering the floor (Fig. 5). The rear of the cave is very moist, with a small waterfall flowing from the ceiling. Guano accumulations in this area are as deep as 0.75 m (Fig. 6). Many megachiropterans and microchiropterans utilize this cave, and a pungent and somewhat overwhelming odor of ammonia is present.

Abutia Cave (N 6°58.881′ W 1°16.446′; 475 m). This is not a cave, but consists only of a water seep at the base of a cliff face. This spring is used as a water source for the people in the town of Kwamang.

VOLTA REGION

Ancestral Caves at Likpe Todome. This set of caves is located 14 km east of Hohoe-Likpe Mate Road at the western foot of Todome Hill. This hill is part of the Akwapin-Togo Mountain Range. These caves appear to be formed within dolomite. *Caves #1 and #2* are both small, elongate caves and no arthropods were detected in either one. Village elders used the first cave for meetings during regional wars, while the second cave was used as a watchtower. *Cave #3* (N 7°9.850′ E 0°36.491′; 626 m) is a slightly larger cave with a relatively large fauna, likely due to high numbers of accidentals as well as the presence of bats. This cave was once used as a hideout during times of tribal war. *Cave #4* consists of a single chamber with a chimney that angles steeply upward. This cave is said to have been used for private consultations with elders. The chimney could serve as a passage for the king to escape in the event of an ambush. No biota was observed. *Cave #5* (N 7°9.892′ E 0°36.537′; 615 m) consists of a relatively narrow tunnel, with a side chamber, that is approximately 5 m in length. This cave previously has been used as a holding cell for criminals.

Akpomu Falls (Eagle Pool) (N 6° 53.068′ E 0° 27.936′; 480 m). The cave is in the vicinity of a 25 m high waterfall and large pool. The cave is a small cavity to the left of waterfall. A chimney near the entrance extends about 6 m vertically. Though it is rich in moisture, no cave fauna was discovered.

Kokosiaba Caves (N 6°48.510′ E 0°23.153′; 430 m; near Nyagbo Konda) are two caves without separate local names, but they are easily distinguished by the level of moisture present and can be referred to as Dry Cave (the first cave reached) and Moist Cave. These caves are accessible via the town of Agodome (N 6°48.597′ E 0°23.339′; 460 m). A hike of about 280 m up to the top of the ridge leads to village of Nyagbo Konda. An additional short hike south of the village, skirting the hillside leads to the caves. Both caves are located about 600 m from the village. Dry Cave was completely dry during our visit, and it is notable for the presence of an unidentified purple-colored mineral. The cave entrance is accessible via a 2.5 m climb up a vertical rock face and is large, round in shape, and easily accessible. The cave consists of a tubular passage about 8 m in depth. At the end of the passage on left is a crevice that

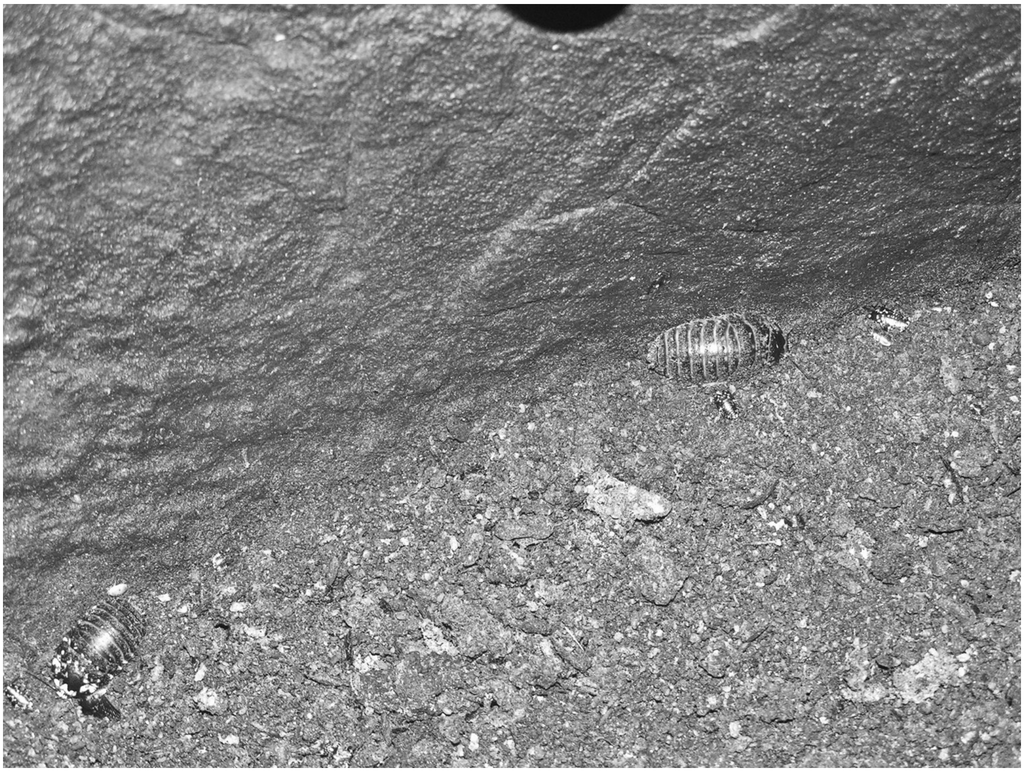

Figure 6. Cockroaches belonging to the *Gyna maculipennis* group in the cave floor litter composed of dry bat guano in Mprisi Cave.

opens to the opposite side near the access trail. Moist Cave is short walk farther down the trail. The cave is circular, with a round entrance approximately 2 m in diameter, and is very moist inside, no doubt in part from bat urine. It extends at least 25 m in depth, with the height gradually decreasing and becoming difficult and then impossible to access any farther. The passage also extends laterally 10 m or more and varies in height from as much as 0.5 m to as little as several 5 to 10 cm. The cave floor is composed of a layer of firm and likely very deep guano covered by a 5 to 10 cm layer of loose detritus.

Obom Cave (N 5°59.815′ W 0°11.015′; 246 m). This cave is 500 m from Obom village. The opening is very wide, approximately 13 m across. The ceiling is low, approximately 1.3 m at the entrance, rapidly drops to less than 1 m, and lowers toward the rear of cave. The total length of the cave is greater than 14 m in some areas, although much of the area is relatively inaccessible due to low ceiling height unless one crawls in a prone position. The cave is quite dry, although it has some moisture toward the rear.

Greater Accra Region (Shai Hills Resource Reserve)

Sayu Cave (also known as Bat Cave or Chief Cave; N 5°55.793′ E 0°3.431′; 160 m). This cave is located near the top of a hill. The first part of the cave is relatively open and airy with plenty of natural light. Continuing through a crevice leads one into a second chamber composed of a 15 m tall slanting wall on the right side and a more vertical wall on the left, with the passage width averaging 1 to 2 m. The slanting wall catches falling urine and guano deposited by numerous bats hanging above the floor. That wall, on the right facing in, was wet with urine, and the loose guano deposits on the floor were more than 0.5 m deep in some areas. In both January 2006 and June 2007, a cetoniine (*Pachnoda marginata aurantia* Herbst; see Orozco and Philips, 2012) and one species of tenebrionid (*Tenebrio c.f. guineensis* Imhoff) were numerous. In January 2006, no streblid flies (*Brachytarsina* spp.) were observed, while in June, they were numerous along the relatively dry left wall of the cave.

Adwuku Cave (N 5°55.783′, E 0°4.992′, 144 m). This cave is also near the top of a hill and is composed of a pile of large, loose rocks possibly consisting of iron-rich basalt. There is no evidence of any specific cave fauna. In January 2006 the cave was extremely arid due to the *harmatan* winds blowing from the north that are present during the dry season in Ghana.

Oboniten Caves (also called Hioweyo Caves; N 5°54. 028′, E 0°03.992′, 230 m). There is a large cave above and a much smaller cave near the trail. The latter cave is very open. The former cave consists of a passage some 10 m long. Both caves were very dry, and we did not observe any cave fauna. These caves are similar to those found in Tengzu in the Upper East Region.

Kpando Blue Uzs Grotto (N 6°58.300′, E °17.171′, 127 m). This is part of a Catholic Church shrine. This is not a true cave, but only a rock pile about 4 to 5 m in height

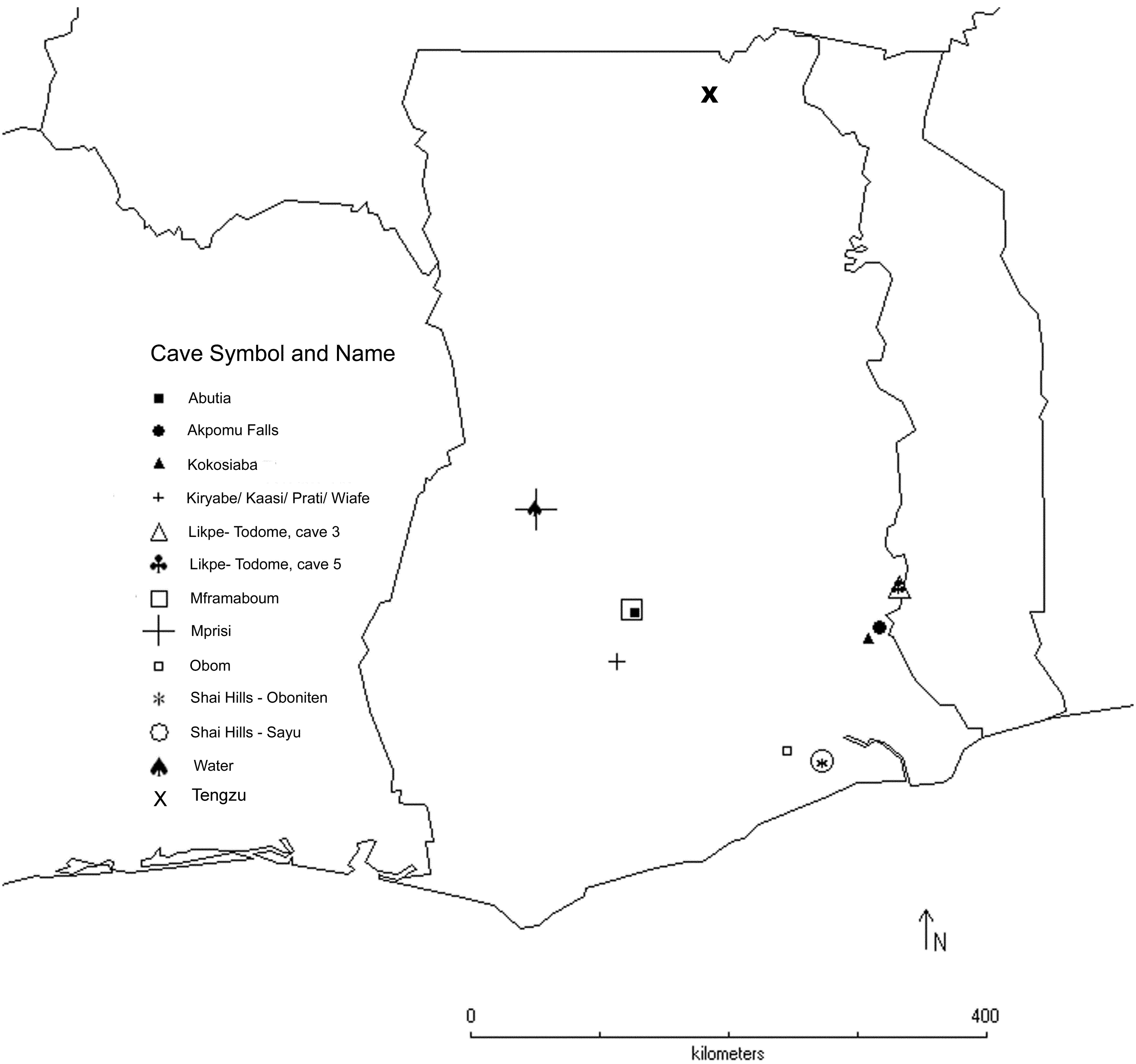

Figure 7. Location of the caves sampled in Ghana.

with a cavity that drops down vertically approximately 1 m and extends horizontally roughly 0.7 m.

Upper East Region

Tengzu caves (Kpenlinne Caves, Hyena, School, Donkey, and Shrine Caves (N 10°41′ 05″, W 0°48′ 30″, 300 m**)**. These caves are perhaps better referred to as rock shelters. They are near the village of Tongo and were explored during July 2008. They consist mainly of large balanced boulders with crevices, and they lack what one would consider a true cave fauna. These caves are similar to some of those found Shai Hills in the Greater Accra Region. Of note is the presence of an undetermined and likely undescribed species of spider beetle (Ptinidae) in the genus *Dignomus* Wollaston that was found breeding in goat pellets within some of the shelters.

Discussion

This work is the first study on the cave fauna of Ghana. All caves known, publicized, and that we could discover were investigated for their cave faunas (Fig. 7). It is quite

Table 2. List of taxa collected or observed in the caves of Ghana.

Organism	Cave
Vertebrata	
Chiroptera	Mframaboum Cave, Mprisi Cave, Ancestral Caves at Likpe Todome Cave #3, Ancestral Caves at Likpe Todome #5, Sayu Cave (Bat Cave or Chief Cave)
Invertebrata	
Amblypigida sp. (only observed)	Kaasi Cave, Wiafe Cave Ancestral Caves at Likpe Todome #5
Phalangida sp.	Kaasi Cave
Diplopoda sp.	Kyireabe Cave (Eastern region), Kokosiaba Dry Cave
Thysanura sp. 1 & 2	Obom Cave
Blattodea	
Blaberidae: *Gyna maculipennis* group	Kyireabe Cave (Eastern Region), Mframaboum Cave, Water Cave, Mprisi Cave Ancestral Caves at Likpe Todome #3, Ancestral Caves at Likpe Todome #5, Kokosiaba Dry Cave, Obom Cave, Sayu Cave (Bat Cave or Chief Cave)
Blaberidae: *Rhabdoblatta* sp.	Akpomu Falls
Polyphagidae: *Tivia* sp.	Sayu Cave (Bat Cave or Chief Cave)
Polyphagidae: *Euthyrrhapha* sp.	Kokosiaba Moist Cave
Coleoptera	
Anthicidae sp.	Ancestral Caves at Likpe Todome #3, Ancestral Caves at Likpe Todome #5, Kokosiaba Moist Cave
Buprestidae sp.	Kokosiaba Dry Cave
Carabidae, Masoreini sp.	Mframaboum Cave, Water Cave, Ancestral Caves at Likpe Todome #3, Kokosiaba Dry Cave, Kokosiaba Moist Cave
Cetoniidae: *Pachnoda marginata aurantia* Herbst	Sayu Cave (Bat Cave or Chief Cave)
Chrysomelidae sp. 1	Water Cave
Chrysomelidae sp. 2	Kokosiaba Dry Cave
Dermestidae sp.	Ancestral Caves at Likpe Todome #3, Obom Cave
Elateridae sp.	Mframaboum Cave, Kokosiaba Dry Cave
Euglenidae sp.	Ancestral Caves at Likpe Todome #3, Kokosiaba Moist Cave
Histeridae sp. 1, 2 and 3	Mframaboum Cave
Histeridae sp. 4	Mprisi Cave
Hydrophilidae sp. 1	Mframaboum Cave, Sayu Cave (Bat Cave or Chief Cave)
Hydrophilidae sp. 2 and 3	Akpomu Falls
Hydrophilidae sp. 4	Mframaboum Cave
Hydrophilidae sp. 5	Sayu Cave (Bat Cave or Chief Cave)
Lampyridae sp.	Mprisi Cave
Scymaenidae sp.	Kaasi Cave
Staphylinidae: Scaphidiinae sp.	Kaasi Cave, Wiafe Cave
Tenebrionidae: *Tenebrio c.f. guineensis* Imhoff	Mprisi Cave, Sayu Cave (Bat Cave or Chief Cave)
Tenebrionidae sp. 2	Sayu Cave (Bat Cave or Chief Cave)
Throscidae sp.	Ancestral Caves at Likpe Todome #3
Diptera	
Calypterate Diptera sp.	Sayu Cave (Bat Cave or Chief Cave)
Chironomidae sp.	Water Cave, Mprisi Cave, Ancestral Caves at Likpe Todome #5
Psychodidae sp.	Mframaboum Cave, Water Cave, Mprisi Cave
Streblidae: *Brachtarsina* sp.	Ancestral Caves at Likpe Todome #3, Obom Cave, Sayu Cave (Bat Cave or Chief Cave)
Tipulidae or near sp.	Water Cave, Obom Cave
Hemiptera	
Gerridae sp.	Mframaboum Cave

Table 2. Continued.

Organism	Cave
Lygaeidae sp.	Kaasi Cave
Naucoridae sp.	Mframaboum Cave
Anthocoridae? nymph	Kaasi Cave
Reduviidae sp. (nymph)	Wiafe Cave
Reduviidae: *Hermillus geniculatus* (Sign.)	Ancestral Caves at Likpe Todome #3
Reduviidae sp. (nymph)	Ancestral Caves at Likpe Todome #5
Reduviidae: *Cethera cornifrons* Villiers	Kyireabe Cave (Eastern Region)
Reduviidae: Stenopodainae (missing head)	Mframaboum Cave
Reduviidae: *Ectrichodia lucida* (L. & S.)	Obom Cave
Reduviidae: *Lhostella congoensis* (Lhoste)	Obom Cave
Reduviidae: *Myiophanes leleupi* Villiers ?	Ancestral Caves at Likpe Todome #3
Reduviidae *Hermillus* sp.	Kokosiaba Moist Cave
Reduviidae: Emesinae sp.	Mprisi Cave
Hymenoptera	
Apidae: Meloponinae sp.	Kokosiaba Dry Cave
Formicidae: *Tetramorium* sp.	Mframaboum Cave, Water Cave, Sayu Cave (Bat Cave or Chief Cave)
Formicidae: *Messor* sp.	Sayu Cave (Bat Cave or Chief Cave)
Formicidae: *Camponotus* sp. 1	Ancestral Caves at Likpe Todome #3
Formicidae: *Cematogaster* sp.	Kokosiaba Dry Cave
Formicidae: *Camponotus* sp. 2	Kokosiaba Dry Cave, Obom Cave
Formicidae: Ponerinae?	Ancestral Caves at Likpe Todome #3
Formicidae: *Cardiocondyla* sp.	Ancestral Caves at Likpe Todome #5
Formicidae: *Dorylus* sp.	Mprisi Cave
Formicidae: *Polyrhachis* sp.	Kokosiaba Dry Cave
Formicidae: *Megaponera* sp.	Sayu Cave (Bat Cave or Chief Cave)
Formicidae: *Camponotus* sp. 3	Kokosiaba Moist Cave
Formicidae: *Bothroponera* sp.	Ancestral Caves at Likpe Todome #3
Scoliidae sp.	Sayu Cave (Bat Cave or Chief Cave)
Chalcidoidea sp.	Ancestral Caves at Likpe Todome #3
Lepidoptera	
Tineidae sp.	Mframaboum Cave, Water Cave, Ancestral Caves at Likpe Todome #3, Obom Cave, Sayu Cave (Bat Cave or Chief Cave)
Orthoptera	
Phalangopsidae: *Phaeophilacris* spp.	Kyireabe Cave, Kaasi Cave, Water Cave, Mprisi Cave, Ancestral Caves at Likpe Todome #3, Ancestral Caves at Likpe Todome #5, Akpomu Falls, Kokosiaba Dry Cave, Kokosiaba Moist Cave, Obom Cave
Gryllidae sp.	Kokosiaba Dry Cave, Obom Cave
Psocoptera sp.	Sayu Cave (Bat Cave or Chief Cave)
Trichoptera (family undetermined, 2 spp.)	Water Cave

possible that there are additional caves that are well known by the local population but not yet surveyed. Current evidence suggests, however, that it is doubtful that a much more extensive fauna exists than has been documented in this report. Further, it is likely that all the species we collected (Table 2) are either troglophiles or accidentals. No species discovered have some of the typical morphological characteristics of true troglobites, such as lack of eyes, eye pigment, or unusually long setae or antennae. Candidates for caves containing true troglobites are Mframaboum and Water Caves, as these have smaller, deeper passages that could be thoroughly explored.

As might be expected, the highest diversity was typically found in caves with good bat populations, including Mframaboum, Likpe Cave #3, and Sayu, with 14, 16, and 13 species, respectively. Two other caves with relatively high diversity of 12 species in each were Kokosiaba Dry Cave and Obom Cave (Table 1).

The cave fauna, unsurprisingly, is very similar to that found in the surrounding countries (Juberthie and Bourgies, 2001). For example, some of the caves have dense populations of cockroaches that move in dry detritus mainly composed of bat dung in a manner best described as swimming, often diving below the surface to avoid detection. These have been described by others as "guanobies," a group of guano swimming cockroach species (Roth and Naskrecki, 2004).

Of specific interest was the relatively large number (12) of assassin-bug species (Reduviidae) found within caves that may be opportunistically feeding on large populations of cockroaches, other insects, or perhaps millipedes. Also, the record of a daytime-active cetoniine scarab beetle, a taxon that has never been reported from cave or rock shelter habitats, is unusual, as both adults and larvae were found deep inside Sayu Cave in the Shai Hills (Orozco and Philips, 2012).

In summary, it is likely that many of the insects we recorded can be found outside of these cave habitats. Hence the invertebrate cave fauna of Ghana may not be extremely unusual or exhibit endemicity to any great degree, and they may be found in additional caves or other non-cave environments. In regard to cave conservation, many of the village elders and chiefs discussed with us the tourism potential of caves in the vicinity of their villages as a possible source of revenue. Unfortunately, many of the caves are small, difficult to access, often quite malodorous, and only esoterically interesting to a few people. Nevertheless, some caves, in addition to those at Likpe, do have potential for the adventure-tourism niche. Regardless, the biodiversity of these caves, including the vertebrates, is a part of the natural heritage of Ghana, and care should be taken to ensure that the fauna is protected and disturbance is minimized.

Acknowledgements

We first and foremost thank the assistance of the following cave guides: Kwasi Kumnipa, Benjamin Nyarko, Benjamin Tachie-Menson, Nanatakyi-Abiam, Justice (Ameyaw) Konadu, Johnson Tulasi, Koku "Frank" Asibe, Joshua K. Sokpah, Godwin K. Sokpah, Christian Adae, Rebecca Okuara, Godson Asigbedse, Nestor Kpordzih, A.K. Marfo, and Goldan David. We also thank Kingsley Osei (Shai Hills Reserve director) for his hospitality and for generously providing lodging during our visit to the reserve. A research permit from Cletus K. Nateg, Director of the Forestry Commission and Mike Adu-Asiah, Senior Wildlife Officer with the Forestry Commission, Wildlife Division, as well as permission from many village chiefs and elders, enabled us to visit these caves. We also appreciate the following individuals with their help at identifying species: Kipling Will (University of California, Berkeley); Darren Mann (Hope Entomological Collections at the Oxford University Museum of Natural History); Laure Desutter-Grandcolas (Muséum National d'Histoire naturelle); Kurt Helf (National Park Service Cumberland Piedmont Network, Mammoth Cave, KY) and Bruce Gill (Agriculture Canada, Ottawa). We also appreciate the useful comments from Kurt Helf and one anonymous reviewer. Lastly, this work also would not have been possible without the support of a National Science Foundation Biological Surveys and Inventories grant (DEB- 0430132) for which we are extremely grateful. This research was part of a Master's of Science thesis by the second author.

References

Bourgies, F. and Juberthie, C., 2001, Burkina Faso, *in* Juberthie, C. and Decu, V., eds., Encyclopaedia Biospeologia, Tome III: Moulis and Bucarest, Société Internationale de Biospéologie, p. 1505–1506.

Conservation International, n.d., The Biodiversity Hotspots: http://www.conservation.org/How/Pages/Hotspots.aspx [accessed June 20, 2015].

Critical Ecosystem Partnership Fund, n.d., Guinean Forests of West Africa: http://www.cepf.net/resources/hotspots/africa/Pages/Guinean-Forests-of-West-Africa.aspx [accessed June 20, 2015].

Harrison, P., and Pearce, F., 2001, AAAS Atlas of Population and Environment: Berkeley, California, University of California Press, 215 p.

Howarth, F.G., 1983, Ecology of cave arthropods: Annual Review of Entomology, v. 28, p. 365–389. doi:10.1146/annurev.en.28.010183.002053.

Juberthie, C., and Decu V., eds., 2001, Encyclopaedia Biospeologia, Tome III: Moulis and Bucarest,Société Internationale de Biospéologie, p. 1381–2294.

Orozco, J. and Philips, T. K. 2012, *Pachnoda marginata* (Drury) (Coleoptera: Scarabaeidae: Cetoniinae) developing in bat guano in a West African Cave: Coleopterists Bulletin, v. 66, 378–379. doi:10.1649/072.066.0417.

Romero, A., 2009, Cave Biology, Life in Darkness: New York, Cambridge University Press, 291 p.

Roth, L.M., and Naskrecki, P., 2004, A new genus and species of cave cockroach (Blaberidae: Oxyhaloinae) from Guinea, West Africa: Journal of Orthoptera Research, v. 13, p. 57–61. doi:10.1665/1082-6467(2004)013[0057:ANGASO]2.0.CO;2.

Villiers, A., 1953, Emesinae cavernicoles du Congo belge (Hemiptera Reduviidae): Revue de zoologie et de botanique africaines, v. 47, p. 31–33.

Villiers, A., 1973, Hémiptères réduviides cavernicoles du Sud-Ouest africain: Revue Suisse de Zoologie, v. 80, p. 573–576.

Villiers, A., 1976, Hémiptères Reduviidae des grottes du Kenya (Mission V. Aellen et P. Strinati): Revue Suisse de Zoologie, v. 83, p. 765–768.

GUIDE TO AUTHORS

The *Journal of Cave and Karst Studies* is a multidisciplinary journal devoted to cave and karst research. The *Journal* is seeking original, unpublished manuscripts concerning the scientific study of caves or other karst features. Authors do not need to be members of the National Speleological Society, but preference is given to manuscripts of importance to North American speleology.

LANGUAGES: The *Journal of Cave and Karst Studies* uses American-style English as its standard language and spelling style, with the exception of allowing a second abstract in another language when room allows. In the case of proper names, the *Journal* tries to accommodate other spellings and punctuation styles. In cases where the Editor-in-Chief finds it appropriate to use non-English words outside of proper names (generally where no equivalent English word exists), the *Journal* italicizes them. However, the common abbreviations i.e., e.g., et al., and etc. should appear in roman text. Authors are encouraged to write for our combined professional and amateur readerships.

CONTENT: Each paper will contain a title with the authors' names and addresses, an abstract, and the text of the paper, including a summary or conclusions section. Acknowledgments and references follow the text.

ABSTRACTS: An abstract stating the essential points and results must accompany all articles. An abstract is a summary, not a promise of what topics are covered in the paper.

STYLE: The *Journal* consults The Chicago Manual of Style on most general style issues.

REFERENCES: In the text, references to previously published work should be followed by the relevant author's name and date (and page number, when appropriate) in parentheses. All cited references are alphabetical at the end of the manuscript with senior author's last name first, followed by date of publication, title, publisher, volume, and page numbers. Geological Society of America format should be used (see http://www.geosociety.org/pubs/geoguid5.htm). Please do not abbreviate periodical titles. Web references are acceptable when deemed appropriate. The references should follow the style of: Author (or publisher), year, Webpage title: Publisher (if a specific author is available), full URL (e.g., http://www.usgs.gov/citguide.html) and date when the web site was accessed in brackets; for example [accessed July 16, 2002]. If there are specific authors given, use their name and list the responsible organization as publisher. Because of the ephemeral nature of websites, please provide the specific date. Citations within the text should read: (Author, Year).

SUBMISSION: Effective February 2011, all manuscripts are to be submitted via Peertrack, a web-based system for online submission. The web address is http://www.edmgr.com/jcks. Instructions are provided at that address. At your first visit, you will be prompted to establish a login and password, after which you will enter information about your manuscript (e.g., authors and addresses, manuscript title, abstract, etc.). You will then enter your manuscript, tables, and figure files separately or all together as part of the manuscript. Manuscript files can be uploaded as DOC, WPD, RTF, TXT, or LaTeX. A DOC template with additional manuscript specifications may be downloaded. (Note: LaTeX files should not use any unusual style files; a LaTeX template and BiBTeX file for the *Journal* may be downloaded or obtained from the Editor-in-Chief.) Table files can be uploaded as DOC, WPD, RTF, TXT, or LaTeX files, and figure files can be uploaded as TIFF, EPS, AI, or CDR files. Alternatively, authors may submit manuscripts as PDF or HTML files, but if the manuscript is accepted for publication, the manuscript will need to be submitted as one of the accepted file types listed above. Manuscripts must be typed, double spaced, and single-sided. Manuscripts should be no longer than 6,000 words plus tables and figures, but exceptions are permitted on a case-by-case basis. Authors of accepted papers exceeding this limit may have to pay a current page charge for the extra pages unless decided otherwise by the Editor-in-Chief. Extensive supporting data will be placed on the *Journal*'s website with a paper copy placed in the NSS archives and library. The data that are used within a paper must be made available. Authors may be required to provide supporting data in a fundamental format, such as ASCII for text data or comma-delimited ASCII for tabular data.

DISCUSSIONS: Critical discussions of papers previously published in the *Journal* are welcome. Authors will be given an opportunity to reply. Discussions and replies must be limited to a maximum of 1000 words and discussions will be subject to review before publication. Discussions must be within 6 months after the original article appears.

MEASUREMENTS: All measurements will be in Systeme Internationale (metric) except when quoting historical references. Other units will be allowed where necessary if placed in parentheses and following the SI units.

FIGURES: Figures and lettering must be neat and legible. Figure captions should be on a separate sheet of paper and not within the figure. Figures should be numbered in sequence and referred to in the text by inserting (Fig. x). Most figures will be reduced, hence the lettering should be large. Photographs must be sharp and high contrast. Color will generally only be printed at author's expense.

TABLES: See http://www.caves.org/pub/journal/PDF/Tables.pdf to get guidelines for table layout.

COPYRIGHT AND AUTHOR'S RESPONSIBILITIES: It is the author's responsibility to clear any copyright or acknowledgement matters concerning text, tables, or figures used. Authors should also ensure adequate attention to sensitive or legal issues such as land owner and land manager concerns or policies.

PROCESS: All submitted manuscripts are sent out to at least two experts in the field. Reviewed manuscripts are then returned to the author for consideration of the referees' remarks and revision, where appropriate. Revised manuscripts are returned to the appropriate Associate Editor who then recommends acceptance or rejection. The Editor-in-Chief makes final decisions regarding publication. Upon acceptance, the senior author will be sent one set of PDF proofs for review. Examine the current issue for more information about the format used.

ELECTRONIC FILES: The *Journal* is printed at high resolution. Illustrations must be a minimum of 300 dpi for acceptance.

Journal of Cave and Karst Studies

Volume 78 Number 2 August 2016

Journal of Cave and Karst Studies **Distribution Changes**

During the November 9, 2013, Board of Governors meeting, the BOG voted to change the *Journal* to electronic distribution for all levels of membership beginning with the April 2014 issue. Upon publication, electronic files (as PDFs) for each issue will be available for immediate viewing and download through the Member Portal at www.caves.org/pub/journal. For those individuals that wish to continue to receive the *Journal* in a printed format, it will be available by subscription for an additional fee. Online subscription and payment options will be made available through the website in the near future. Until then, you can arrange to receive a print subscription of the *Journal* by contacting the NSS office at (256) 852-1300.